A PROTEOGENOMICS FRAMEWORK FOR DISCOVERY OF TRANSLATED MICROPEPTIDES IN MOUSE BRAIN AND OTHER SYSTEMS

by

Ravi Tharakan

A dissertation submitted to Johns Hopkins University in conformity with the requirements for the degree of Doctor of Philosophy

Baltimore, Maryland

March 2017

Abstract

In this thesis, we developed methods for micropeptide discovery and applied these methods to several biological systems to find evidence of novel translated micropeptides. Micropeptides are small proteins translated from open reading frames shorter than 100 codons, and have historically been understudied in genome annotations. This framework allows discovery of these peptides, by an approach called proteogenomics, which combines mass spectrometry-based proteomics with deep sequencing-based transcriptomics in order to study the genome. We developed a bioinformatics framework for micropeptide discovery experiments, and also developed and validated an LC-MS/MS platform for micropeptide discovery. Finally, to show these methods are broadly applicable, we used these methods to analyze the liver proteome, the HIV-1 virion proteome, and the mouse cerebellum proteome, finding evidence of novel micropeptides in each case.

Micropeptides are thought to be low-abundance, and therefore difficult to detect by biochemical methods. A lack of sensitivity in proteomics is often due to suppression effects of high abundance molecules which co-elute with low abundance molecules. We developed a two dimensional chromatography platform, in which a strong cation exchange column is coupled in series with two hydrophobicity columns all coupled to a tandem mass spectrometer, allowing online fractionation of peptides. Applying this system to micropeptidomics, we have shown that sensitivity for micropeptides greatly increases as well. This system is applied in to discover novel micropeptides in human liver.

The framework was applied to several biological systems with varying degrees of genome complexity: the HepG2 liver cell line, to study the human liver proteome, purified HIV-1 virions, to study the packaged virion proteome, and the mouse brain. The three experiments represent a large range of genomic complexity: HIV-1 has a very small genome, the human genome is much larger, and the mammalian CNS genome is believed to be highly complex due to alternative splicing.

The human liver HepG2 cell line was subjected to proteogenomics analysis. A transcriptome assembly was translated *in silico* and used to search for peptide products from all possible open reading frames shorter than 100 codons. Two novel peptides were found with high confidence. Next, HIV-1 virions were subjected to proteogenomics. The HIV-1 genome is very small, so the whole genome was translated. In order to capture strain-specific differences, three biological replicates were genomically sequenced, and the resulting HIV-1 genome assemblies translated *in silico*. One novel peptide was observed in each replicate with high confidence.

Finally, the mouse brain was subjected to proteogenomics in order to find novel secreted peptides. The soluble fraction of mouse brain was used to generate proteomics data. As the mammalian CNS proteome is believed to be very complex due to alternative splicing we utilized ribosome profiling data, which allows reading frame and translation start sites to be determined. A translatome was assembled from the frame determination and used to generate the database for proteomics analysis. Several micropeptides were again found, and in particular one highly expressed peptide was found to be enriched in behavior regulating regions of the brain.

Thus, applying the framework to several different biological systems shows that it is robust against various genomes so that micropeptides can be discovered in various experimental contexts. The results also suggest the ubiquity of micropeptide expression in all organisms.

Acknowledgements

If the reader will indulge me, I want here to thank some of the people who have helped me along the way to this thesis.

First, my mentor for the last two years, Akira Sawa, who has supported me tremendously and generously in my own intellectual development.

Second, the many other scientific mentors I have had along the way, including David Graham, Lennart Martens, Allen Everett, Gerhard Thallinger, Juergen Hartler, Alexey Lyashkov, Julia Drewes, Kelly Meulendyke, M. Christine Zink, Janice Clements, Lucio Gama, David Colquhoun, Shinichi Kano, Takahiro Kato, Graham Diering, Richard Huganir, Lindsay Hayes, Koko Ishizuka, Leslie Nucifora, Minae Niwa, Kyongman An, Rhoel Dinglasan, Julian Bess, Gerben Menschaert, and Robert Cole. Most importantly, I have to thank Dingyin Tao, Nicholas Ingolia and Rachel Green for their tireless support.

Finally, I have to thank my family, without whom this would never have been possible; my parents, Soma and George Tharakan, who made me believe this was possible, and my brothers, Raj and Anuj Tharakan. The debt I owe to Ceereena Ubaida-Mohien and Immanuel Tharakan is beyond words.

Some material presented in Chapter 2 has been previously printed in Journal of Proteome Research (Tharakan et al. 2015).

Table of Contents

List of Tables

List of Figures.

Chapter 1: Introduction

The sequencing and publication of complete genomic sequences of many organisms has aided the medical sciences greatly, allowing advances in both the genetics and biology of human disease and greater understanding of the biology of human pathogens. In particular, the human genome sequence has advanced human disease genetics by allowing genome-wide association studies (GWAS), and knowledge of gene sequences and their chromosomal loci has produced deeper understanding of the biology of all organisms whose genomes have been sequenced, including human pathogens such as HIV. Crucial to all of these efforts is genome annotation, which uses genomic, genetic, epigenetic, and other information to find loci in the genome which code functional genes. While genome annotation has been performed alongside efforts to sequence genomes, the continuing pace of novel gene discovery, aided by advancing technology in molecular biology and biochemistry, shows that annotation is often incomplete.

During the early stages of genome annotation, when genomes such as the human genome were first sequenced, a lower limit was placed upon the length of an open reading frame (ORF) that could be considered a possible gene(Bissette, Nemeroff, & MacKay, 1986; Dujon et al., 1994). These limits were set by modeling a biochemically equivalent random genome, and determining the ORF length distribution over that random genome, thus showing the length distribution of 'random' ORFs. In the case of the human genome, in order to exclude such random ORFs, the minimum ORF length was set to be 100 codons by reasoning about the size distribution of random ORFs. However, while a high proportion of ORFs below these limits may be spurious, there are also a substantial number which are real genes, and these are missed by such a filtering step(Basrai, Hieter, & Boeke, 1997). Furthermore, while gene discovery can be accomplished by means other than genome annotation, it appears that these original

genome annotation decisions continue to be reflected in our current understanding of genomes, since there is a disproportionately low number of genes annotated for the human genome below the 100 codon cutoff(Frith et al., 2006).

Recently, evidence has emerged that many of these short (<100 codons) open reading frames may indeed be protein-coding genes, whose gene products have been named 'micropeptides.' Evidence for functionality of these short peptides has come from several sources, including bioinformatics, through novel conservation analyses(Crowe, Wang, & Rothnagel, 2006), and biochemical approaches, such as expressed sequence tag experiments(Frith et al., 2006), deep sequencing based-experiments such RNA sequencing(Kageyama, Kondo, & Hashimoto, 2011) and ribosome profiling(Ingolia, Lareau, & Weissman, 2011). These micropeptides have been found in studies of many model organisms, suggesting that micropeptide genes indeed exist throughout all genomes. Nevertheless, it has been controversial how many micropeptide genes there are, and general estimates have varied by orders of magnitude. In particular, since all techniques have biases and false positives, there has been continued debate on the extent to which evidence for micropeptides is artifact of the techniques used for discovery(Guttman, Russell, Ingolia, Weissman, & Lander, 2013; Ingolia et al., 2014). Furthermore, the mechanisms by which micropeptides perform their functions in the cell is often difficult to define exactly; in particular, it is still not clear whether micropeptides as a class of protein share a general cellular role, or whether they have diverse functions in the same way large well-annotated proteins do.

In prokaryotes, annotation of short open reading frame (sORF)-encoded micropeptides has been of increasing interest. In the bacterium *Mycoplasma pneumoniae*, micropeptides translated from non-coding RNA (ncRNA) were discovered by mass spectrometry, defining the total complement of micropeptides in that organism's genome at 67, approximately 5% of all coding genes(Lluch-Senar et al., 2015). A

transposon-based essentiality screen found that 53% of these micropeptides were essential for the bacterium's growth, indicating that many micropeptides are not only functional but essential for bacterial growth. Since *M. pneumoniae* has a relatively small genome of 816 kb which is likely to be well annotated, such an essentiality study also suggests that many micropeptides are proteins essential for a minimal organism and thus essential for life(Lluch-Senar et al., 2015). Similarly, in the bacterial strains *Synechocystis* 6803 and *Synechocystis* 6714, and bioinformatics screen using BLAST searches found 293 transcriptional units putatively encoding micropeptides, of which 5 could be functionally characterized, showing structural features such as transmembrane helices and regulated expression during environmental perturbation and bacterial stress responses(Baumgartner, Kopf, Klahn, Steglich, & Hess, 2016; Hemm et al., 2010). Finally, in the widely used model bacterium *Escherichia coli*, 44 micropeptides have been found, many of which also perform basic functions in the cell(Hemm, Paul, Schneider, Storz, & Rudd, 2008).

Micropeptide discovery has also continued apace in eukaryotic model systems. A study in *Saccharomyces cerevisiae* by ribosome profiling found many cases of translation of micropeptides, which appear to serve some purpose during the meiotic process(Brar et al., 2012). During meiosis, translation of some 9,989 unannotated ORFs was found, with a mean lengths of the novel ORFs of 46.8 codons, much shorter than the average of known genes of 484.9, and substantially under the 80 to 100 codon cutoff which was used to annotate the yeast genome. These novel genes appeared to have their translation increased in a regulated fashion during meiosis, indicating once again that they are functional, although the functions of these many putative novel genes have not been defined yet(Brar et al., 2012). A bioinformatics screen of the yeast genome searching for micropeptides similarly yielded 184 yeast sORFs conserved across many species, suggesting that they may be functional(Kastenmayer et al., 2006). These novel

genes were then validated as to function by development of deletion strains for 140 of them, of which 9 gave clearly observable phenotypes. The latter study provides a model of how novel micropeptide genes can be validated as to function; furthermore, the large increase in the number of micropeptides observed between the two studies demonstrates the role of advancing technology in the rapid advance of micropeptide annotation.

Studies in higher-order animals have also found several significant novel micropeptides. Perhaps most relevantly for human health, a screen in *Danio rerio* discovered a novel micropeptide translated from a transcript annotated as a long non-coding transcript (lncRNA), christening the micropeptide *Toddler*(Pauli et al., 2014). This micropeptide was discovered by a series of screens, in which developing zebrafish were subjected to RNA sequencing to discover novel lncRNAs(Chew et al., 2013), and the same material was used for a ribosome profiling study(Pauli et al., 2012). The latter ribosome profiling study showed that 399 of the putative lncRNAs were indeed translated, of which one produced a micropeptide which was confirmed by mass spectrometry. GFP-tagging of the novel micropeptide to find tissue distribution and production of a knockout animal showed that the micropeptide appeared to function as an extracellular secreted ligand for the Apelin receptor, essential for cell migration during embryonic development(Pauli et al., 2014). Importantly, the same micropeptide was found to be essential for regulation of the human cardiovascular system, again functioning as a ligand for the Apelin receptor(Yang et al., 2017). As GPCRs are very frequently targeted by drugs, the discovery of this novel ligand could eventually produce a novel cardiovascular therapy, as has been recently proposed. This series of studies thus shows that discoveries of micropeptides in animals can not only be relevant for human biology, they can also almost immediately lead to novel therapies.

In another animal model system, *Drosophila melanogaster*, progress in annotation of micropeptides has been even more rapid. Several screens of this system have produced a number of novel micropeptides which regulate the cardiovascular system(Magny et al., 2013), developmental regulation through proteasomal function(Zanet et al., 2015), and control of RNA polymerase(Hanyu-Nakamura, Sonobe-Nojima, Tanigawa, Lasko, & Nakamura, 2008). In the cardiovascular system, the micropeptides Sarcolamban A and B were initially found in a search for functional sORFs among the set of putative ncRNAs, a screen which found two possible micropeptides of 28 and 29 amino acids long on a single transcript(Magny et al., 2013). *In vivo* translation and GFP tagging confirmed translation localized to the sarcoplasmic reticulum, and a null mutant showed a cardiac arrhythmia phenotype with dysregulated calcium transients, suggesting a novel micropeptide involved in regulation of the Sarcoplasmic-endoplasmic reticulum calcium (SERCA) pump. Strikingly, the micropeptides were found to be highly evolutionarily conserved throughout evolution, including in humans(Magny et al., 2013). In *Drosophila* development, the *mlpt/tal/pri* gene, discovered independently by several groups, contains four sORFs which appear to code for peptides(Zanet, Chanut-Delalande, Plaza, & Payre, 2016). Null mutants of this gene show dramatically dysregulated development, apparently due to disruption of a transcription factor(Zanet et al., 2015). In this case, the micropeptides appear in some fashion to regulate the ubiquitination and proteasomal degradation of the transcription factor. Finally, in the regulation of transcription, the micropeptide *pgc* was postulated to be a coding transcript by investigation of the Kozak sequence surrounding a translation start site(Hanyu-Nakamura et al., 2008). Synthesis and injection of the micropeptide into the embryo showed that it directly regulated phosphorylation of the CTD of Pol II, and immunoprecipitation showed that this was mediated by an interaction with P-TEFb. These three examples, unlike the above *Toddler* example above, show cases of

intracellular micropeptides regulating protein-protein interactions, in the case of *Sarcolamban* hydrophobic micropeptides regulating a membrane bound ion channel, and in the latter two cases soluble micropeptides regulating cytosolic interaction. Further, a recent genome-wide study by ribosome profiling has increased the number of candidate micropeptides in that genome to ~285, although most of these are of unknown function(Aspden et al., 2014; Zanet et al., 2016).

In mouse and human, finally, there has also been progress in identifying biologically relevant micropeptides, including the case of the *Toddler* peptide described above. Next, and also significantly, is the *Myoregulin* micropeptide, which followed on from the discovery of *Sarcolamban* in *Drosophila* already described(Anderson et al., 2015). Like *Sarcolamban*, the *Myoregulin* micropeptide regulates activity of the SERCA pump and thereby calcium transients, and similarly, it was found by bioinformatically screening newly discovered non-coding RNA transcripts for sORFs which could encode putative micropeptides. In this case, the screening was done by evolutionary conservation, and found a 46 amino acid peptide in a skeletal muscle-specific transcript. The peptide was found by labeling experiments to interact with the SERCA pump and have some homology to *Sarcolamban*, as well as to the human peptides *Phospholamban* and *Sarcolipin*(Anderson et al., 2015). Remarkably, the *Phospholamban* and *Sarcolipin* micropeptides have been known for some time as regulators of SERCA activity, but their tissue expression is limited to slow skeletal muscle and cardiac muscle, leaving a long-standing mystery as to how SERCA is regulated in other tissues; the *Myoregulin* peptide begins to solve this mystery. Further, extending work on the *Myoregulin* micropeptide, three more micropeptide members of the same family were found by screening the peptide binding motif of the family, discovering the micropeptides *Dworf*(B. R. Nelson et al., 2016)*, Endoregulin* and *Another-regulin*(Anderson et al., 2016). These peptides all regulate SERCA, and their

tissue distribution is substantially different, including tissues beyond muscle(Anderson et al., 2016), indicating that micropeptide-SERCA interactions are a widespread and perhaps fundamental system for regulating calcium transients in mouse and human.

Beyond bioinformatics screens of ORFs in ncRNAs, the human and mouse systems have also been substantially probed for micropeptides by ribosome profiling. A recent study in mouse embryonic stem cells found that many sORFs are indeed translated in these cells, and the majority of lincRNAs have translation levels comparable to annotated protein-coding genes, suggesting that many lincRNAs in fact encode micropeptides(Ingolia et al., 2011). The same study also observed widespread translation in upstream ORFs (uORFs) of known coding genes, which translation was downregulated during embryoid body formation. However, these latter observations cannot necessarily be taken to indicate functional micropeptides, since ribosome presence on a transcript means at most that a peptide is produced, but not that it is functional. For example, ribosome presence on upstream ORFs has canonically been interpreted as a regulatory process by which the ribosome's access to the main coding ORF is blocked, thus impeding translation of the main ORF(Hinnebusch, 2014). These uORF peptides, however, have been recently found to presented on MHC molecules, indicating at least a potential function in human immunity in some cases(Starck et al., 2016). Similarly, in human HEK293 cells, a recent ribosome profiling study found evidence of widespread translation in both uORFs and ncRNA-sORFs, and found evolutionary conservation of these translated ORFs(S. Lee et al., 2012). Once again, however, this cannot be taken to be definitive evidence of functional micropeptides.

In the human genome, annotation of micropeptides as to function has been somewhat limited, possibly by the complexity of the system; however, two functional micropeptides have been found, both in the human mitochondrial genome. The *Humanin* peptide, encoded by a short ORF from the mitochondrial DNA, was discovered some

years ago by a purely functional cDNA library screen for genes inhibiting apoptosis(Hashimoto et al., 2001). The cDNA was then confirmed to produce a peptide by discovery of its interaction with a cell-death regulator by a yeast 2-hybrid screen(Guo et al., 2003). More recently, the MOTS-c peptide, which regulates metabolism in some fashion, has been discovered in an sORF on the 12s rRNA gene in the mitochondrial genome by a bioinformatics screen of sORFs in mtDNA, showing a conserved 51 nt ORF with a strong Kozak context(C. Lee et al., 2015). Treatment of HEK293 cells with a synthetic peptide substantially regulated gene expression of enzymes involved in cellular metabolism, and treatment of mice fed a high fat diet prevented obesity, suggesting that the peptide is an extracellular signaling molecule.

Finally, substantial probing of viral genomes for micropeptides has also yielded some interesting results. Due to the small size of many their genomes, historically, viral genomes were not usually annotated with the explicit lower limits on the lengths of open reading frames, although the vaccinia virus, which has a large genome, had a lower limit of 65 codons for its original annotation(Goebel et al., 1990). Even without explicit minima during annotation, many viral micropeptides were simply overlooked because of systematic assumptions of how large genes should be, as genomes were annotated in an *ad hoc* fashion(Ratner et al., 1985). Micropeptides in viral genomes have been discovered in a similarly *ad hoc* manner, with several micropeptides found in influenza virus, human immunodeficiency virus, papillomavirus, poxviruses and paramyxoviruses(DiMaio, 2014). These micropeptides are often dominated by a single alpha-helical transmembrane domain, which allows them to be inserted into lipid bilayers, in which context they can interact with and regulate host cell proteins (i.e., HIV-1 Vpu), form ion-selective pores (i.e., influenza M2), allow binding and entry into host cells (i.e., poxvirus (O3L), or perform other functions crucial for the viral life cycle(DiMaio, 2014). These micropeptides are short genes which have been discovered

in genomes with many reading frames of such a size, and indeed, a recent genome-wide screen of human cytomegalovirus by ribosome profiling and mass spectrometry found ~484 novel ORFs shorter than 80 codons, including 245 shorter than 20 codons which were actively translated by the ribosome(Stern-Ginossar et al., 2012). These latter micropeptides must be validated by functional studies, but the high number identified here shows that there may be a substantial number of micropeptides produced by viruses.

It has been widely shown by a variety of methods, therefore, that despite underrepresentation in genome annotations, sORFs encode functional micropeptides in nearly all genomes studied, thus suggesting that there may be many micropeptides produced both from the human genome and from human pathogens that may be of relevance to human health. However, how many micropeptides there may be in genomes is still controversial. Many types of genome-wide approaches have given a wide range for how many coding micropeptides there are in the human genome, from tens of thousands to a few dozen(Andrews & Rothnagel, 2014). These problems reflect issues identifying sORFs which caused them to be overlooked in all genomes. In particular, it is difficult to detect evolutionary conservation of these ORFs, because their small size disrupts the statistical assumptions of homology detection algorithms such as BLAST or PhyloCSF(Couso, 2015). Thus, genome wide searches for conservation of sORFs incorrectly showed them to be unconserved. Secondly, very short peptides were thought to not have stable secondary structure, and thus, if biological function is assumed to be entirely dependent on the structure of the protein, short peptides could be assumed not to have a function(Ingolia et al., 2014; Wright & Dyson, 2015). This lack of secondary structure can also cause difficulties for genome-wide description of sORF-encoded micropeptides, for example by a biochemical method such as mass

spectrometry, since peptides without stable conformations may be rapidly degraded when cell are lysed for extraction(Hackett et al., 1986).

If these are reasons for micropeptide numbers to be underestimated historically, questions of artifact in newer methods may cause the number of functional micropeptides to be overestimated. In particular, each genome-wide method for micropeptide discovery can be prone to false positives for various reasons. Central methods which have been used to discover micropeptides genome-wide are ribosome profiling, mass spectrometry, RNA sequencing, and direct searches for conservation. In ribosome profiling, polysomes are extracted from cells, then treated with RNase to destroy RNA which is unprotected by ribosomes(Ingolia, Ghaemmaghami, Newman, & Weissman, 2009). The ribosome footprints are then sequenced, and these are used to map the positions of the ribosomes. These studies were some of the first to find translation of sORFs in the genome, and indeed found many ORFs translated from alternative start codons, which, if correct, would exponentially increase even the estimates of the number of potential sORFs in the genome(Ingolia et al., 2011). However, failure of RNase to digest a given section of the genome may be due factors besides ribosome content; in particular, RNA secondary structure may also block digestion, and RNA may also be underdigested due to sub-optimal reaction conditions. RNA-binding proteins may also block digestion. Furthermore, the mere presence of ribosomes in a given ORF does not necessarily demonstrate translation of that ORF. Certain features of ribosome profiling datasets, such as codon periodicity, can be used to determine ‘genuine’ translation, this continues to be controversial and as yet there is no definitive metric by which ORFs can be determined to be translated(Calviello et al., 2016; Guttman et al., 2013; Ingolia et al., 2014).

In RNA sequencing, the length of the transcript is sequenced, and the high sensitivity of this method has allowed many novel transcripts to be discovered. In

particular, RNA sequencing has recently discovered a large set of novel RNAs called long non-coding RNAs(Hart & Goff, 2016; Sun et al., 2013; Ulitsky & Bartel, 2013). These RNAs were originally believed to be non-coding because they contain no long ORF, but subsequent conservation analyses of short ORFs have revealed several of these lncRNAs to indeed be micropeptide-encoding(Anderson et al., 2015; Pauli et al., 2014). Thus, lncRNAs, which continue to be discovered by improved deep sequencing methods, may therefore be a large source of novel micropeptides. However, for the reasons mentioned above, most mainstream conservation analyses cannot be well applied to short ORFs, and thus, screening for conserved sORFs in lncRNAs to search for micropeptides likely underestimates the total number of sORFs, and indeed may account for why some lncRNAs were originally misclassified as non-coding. A recent attempt to address this problem, in which a novel conservation detection method was developed using an SVM classifier, some 2000 novel ORFs were found in the genome(Mackowiak et al., 2015). However, only a small percentage of these could be identified by mass spectrometry or ribosomal profiling data, raising the possibility that this paper overestimates the number of conserved sORFs. Thus, the number of micropeptides produced by newly discovered lncRNAs continues to be an open question. For these kinds of reasons, RNA sequencing experiments have not been able to provide a clear picture of how many micropeptides there may be in genomes.

Mass spectrometry for discovery of micropeptides also seems to run afoul of the underestimation problem. Firstly, as mentioned above, mass spectrometry attempts to directly detect micropeptides, and if it is correct that micropeptides are rapidly degraded by proteolytic enzymes after cell lysis, mass spectrometry thus may have problems with the speed of degradation of micropeptides after cell lysis. Secondly, lncRNAs are now known to be very low abundance in any given tissue(Cabili et al., 2015). Thus, detecting micropeptides translated from lncRNAs by mass spectrometry may have problems with

sufficient sensitivity. Indeed, across the literature one finds a mismatch between deep-sequencing based results and mass spectrometry, with deep-sequencing based results generally producing much higher numbers of micropeptides detected than mass spectrometry. There are two possible explanations for the latter phenomenon; first, mass spectrometry may underestimate, or deep sequencing may overestimate, the number of micropeptides in the genome, or both; second, ribosomes may bind to many ORFs promiscuously, but these peptides are either not translated or quickly degraded and non-functional. The former model implies that there are an undetermined number of micropeptides in the genome to discover, but the latter implies that there is no clear evidence that there is any substantial number of micropeptides in the genome.

Considering these issues, we propose that micropeptide discovery can be well-approached by the new technique of proteogenomics bioinformatics(Nesvizhskii, 2014), in which deep-sequencing data is used to generated candidate sequences to analyze mass spectrometry proteomics data. Mass spectrometry data must be searched against a database of candidate proteins in order to match experimental spectra to peptide sequences, and these databases have historically been lists of all annotated proteins from a genome(Eng, McCormack, & Yates, 1994); in proteogenomics, the database is produced by *in vitro* translation of a set of candidate sequences, from genomic or transcriptomic data. This allows mass spectrometry to orthogonally confirm ribosome profiling data indicating translation of micropeptides, and thus addresses the problem of the specific artifacts of each technical method to search for micropeptides genome-wide. Furthermore, we propose that since micropeptides are very low abundance, the sensitivity of mass spectrometry must be improved in order to discover them. We therefore here present a set of methods to discover micropeptides by mass spectrometry-based proteogenomics methods. In Chapter 2, we develop a novel method for online fractionation to improve sensitivity. This method can also be applied to

metabolomic profiling of cells and tissues, an application which we describe. In Chapter 3, these mass spectrometry methods are used to find micropeptides in HepG2 cells and HIV-1 purified virions, by combining mass spectrometry data with RNA sequencing data. Finally in Chapter 4, the proteogenomics approach is used to combine mass spectrometry and ribosome profiling data, to find a novel signaling micropeptide in the mouse CNS.

Chapter 2: Integrated Microfluidic Chip and Online SCX Separation Allows Untargeted Nanoscale Metabolomic and Peptidomic Profiling

Abstract

In order to study micropeptides, mass spectrometry methods must be developed in order to capture them for analysis. We have here developed a two-dimensional LC-MS/MS system, which allows high-sensitivity detection of micropeptides in tissues. This was accomplished by liquid-liquid extraction of peptides and metabolites from tissue samples and online SCX separation to allow characterization of each population individually. The platform was validated both by a mixed set of purified standards for synthetic peptide sequences and by an analysis of splenic tissue from SIV-infected macaques, showing both good reproducibility in chromatography, with RSD of hold time less than 0.4%, and clear separation of charge states, with ~95% of molecular features in SCX separated runs at expected charge states. The system can indeed be used to detect micropeptides as short as a few amino acids. Secondarily, we find that we can apply this system to perform metabolomics and micropeptidomics. These two molecular populations, metabolites and peptides, can be extracted from tissues in a similar fashion, and we therefore have here developed an integrated platform for their extraction and characterization. Finally, we used this platform to analyze the physiological response to infection in the spleen, showing that the spleen contains an abundance of hemoglobin-derived peptides, which do not appear to change in response to infection, and that there appears to be a large and variable metabolic response to infection. We therefore present a method for micropeptidomic and metabolomic profiling which is simple and robust.

Introduction

In recent years, the study of endogenous small molecule metabolites and endogenous peptides have both been greatly advanced by the application of high-throughput methods. These fields, now called “metabolomics” and “peptidomics” involve the study of a broad swath of the metabolite and peptide molecular content of cells or tissues.(Milne, Mathews, Myers, Ivanova, & Brown, 2013; Oliver, Winson, Kell, & Baganz, 1998; Patti, Yanes, & Siuzdak, 2012; Schulz-Knappe, Schrader, & Zucht, 2005; Tautenhahn et al., 2012) The results from these kinds of analyses can support “systems” analyses of cells or tissues under perturbed or pathological conditions, in which the integration of data on several molecular species allows a holistic picture of a biological response. Systems analyses therefore require methods by which several molecular species can be surveyed simultaneously. Furthermore, so-called micropeptides, which are produced by short open reading frames in genomes, can be discovered by mass spectrometry; however, since they are very low abundance, a high-sensitivity method for mass spectrometry must be used. Online fractionation can allow higher sensitivity for these low abundance analytes.

The metabolome consists of all small molecule intermediates of metabolism in a cell, and thus includes amino acids, nucleotides, fatty acids, lipids, and each of their various metabolites. It can thus be considered the molecular component of a cell which is not under the direct control of the genome.(Milne et al., 2013) The peptidome, similarly, is the complement of peptide species produced by a cell. Peptides and metabolites together perform significant biological functions, and thus their levels can be used for direct phenotyping of a biological system. For example, in the nervous system, peptides and small molecule metabolites of amino acids both function as neurotransmitters. Finally, study of the small molecule complement of tissues allows the

characterization of exogenous molecules, such as drugs and environmental exposures; the so-called “exposome.”(Wild, 2012) Therefore, since a profile of these species, micropeptides and metabolites, provides a useful molecular picture of a cell or tissue, we sought to develop a simple and robust means of simultaneously extracting and then analyzing them, by means of a single sample preparation and then an online LC-MS separation.

Here, we report the development of an HPLC-MS platform for simultaneous metabolomics and micropeptidomics. This was accomplished by integration of an online SCX separation into a nanoRPLC-MS/MS system. The platform was validated by a mixed set of small molecule and peptide standards, which showed separation into SCX fractions with good reproducibility. Applying our method to a tissue sample, we found that endogenous peptides seem to preferentially ionize in nanoESI, suppressing small molecule metabolite detection; these two molecular populations could be separated by our online SCX method, allowing both populations to be characterized. Finally, we used our platform to analyze the metabolome and peptidome of tissue samples in two biological conditions. Our platform thus provides an integrated workflow for fast and robust metabolite and peptide profiling in nanoLC systems already adapted for proteomics experiments, all in a combined MS analysis.

Methods

Reagents and Materials

Ascorbic acid, ammonium hydroxide, dithiothreitol, sodium chloride and HPLC-grade acetic acid, formic acid, methanol, and acetonitrile were acquired from Sigma-Aldrich (St. Louis, MO). Amicon 50,000 MWCO filters were obtained from Millipore (Bedford, MA). SDS sample buffer was obtained from Life Technologies (Carlsbad, California).

Atenolol, serotonin creatinine sulfate monohydrate, and 9-anthracene carboxylic acid were used at 100 µM, 100 µM, and 10 µM, respectively, and were obtained from Sigma-Aldrich (St. Louis, MO). Peptide standards were used at 150 pM and obtained from Biognosys AG (Zurich, Switzerland).

Nanoflow HPLC-MS/MS System Profiling Method

For the online SCX method, we integrated one SCX column (150 µm i.d. 2 cm length, Polysulfoethyl A, 5 µm 300 Å, PolyLC) into the Agilent HPLC-MS system, which is comprised of a 1200 Infinity HPLC system coupled to an Agilent 6520 QTOF via an HPLC Chip Cube interface. The HPLC Chip contains an enrichment column to capture compounds and then a C18 analytical column, with rotor microvalve switching to bring the enrichment column in line with the analytical column for separation and injection.(Buckenmaier, Vollmer, Trojer, & Emotte, 2008) Thus, the whole sample metabolite extract was loaded onto the SCX column at 1.8 µL/min and the flowthrough compounds captured by the enrichment column, prior to further separation by the C18 HPLC analytical column and MS detection. The SCX-captured compounds were eluted off the SCX column by injecting 6 µL of 500 mM NaCl in 2% ACN/0.1% FA using the autosampler. The salt elution was captured by a C18 enrichment column integrated in the Agilent ultra-high capacity small molecule HPLC-Chip, (500 nL, 80 Å C18 trap with a 75 µm i.d., 150 mm length, 80 Å C18 analytical column).

For both fraction injections (flowthrough and salt elution), desalting was done on the enrichment column in the HPLC Chip by washing with 6 µL 3% ACN/0.1% FA. The rotor valve was then switched and HPLC gradient started at nanoflow, eluting the analyte from the enrichment column and separating it on the C18 analytical column. Elution of both fractions from the analytical column was performed using a gradient starting at 98% A, 2% B (A: 99.9% water, 0.1% FA; B: 89.9% ACN, 10% water and 0.1% FA) at 300

nL/min. The mobile phase gradient for both fractions was 2-98% B for 13 min, maintained at 98% B for 6 min, followed by re-equilibration of column with 2% B for 5 min.

Nanoflow HPLC-MS/MS System Shotgun Method

An online SCX column fractionation method was used as described for the profiling method. Data dependent acquisition mode was used for MS acquisition by an Agilent 6520 QTOF. Precursor MS spectra were acquired within the *m/z* range 315 to 1700 and the top 4 peaks were selected for MS/MS analysis. Product scans were acquired within the *m/z* range 50 to 1700 at a scan rate of 1.5/second. A medium isolation width (~4 amu) was used, and a collision energy of slope 3.9 V/100 Da with a 2.9 V offset was applied for fragmentation for peptide acquisition, while a fixed collision energy of 10 and 20 V was applied for metabolite acquisition. A dynamic exclusion list was applied, with precursor exclusion of 0.50 min after two MS/MS spectrum was acquired.

Bioinformatics Analysis

Molecular Feature Extraction was performed using the Agilent MassHunter Qualitative Analysis program, version B.04.00. Centroided peaks were filtered at 5,000 counts and the chromatographic small molecules extraction algorithm was used. Allowed adducts were H+ and Na+. Charge state determination was unrestricted to avoid improper charge state assignment. For isotope grouping, peak spacing tolerance was 0.0025 *m/z* plus 7 ppm, and an isotope model of common organic molecules was used. For peptide identifications, Mascot (version 2.2) was used with variable modifications of oxidation of methionine and carbamylation of cysteine. Database was constructed in-house with sequences from SwissProt with a Mammals taxonomy limitation and HIV and SIV sequences (66,813 sequences). The search results were filtered and annotated in

MASPECTRAS 2.0;(Ubaida Mohien et al., 2010) filtering was done with a minimum of two peptides per protein. For metabolite identifications, the METLIN database was searched using the MassHunter Qualitative Analysis program (Agilent Technologies, version B.04.00) with precursor and product *m/z* expansion of 10 ppm ± 2 mDa and 20 ppm ± 2 mDa, respectively, relative height of 0.5%, no collision energy limitation, and minimum reverse score of 80. For quantitative profiling, Mass Profiler (Agilent Technologies, version B.03.00) with default settings of minimum relative frequency of 70% in at least one group and minimum differential score of 85% was then used to align runs, and all features, along with annotations for number of runs aligned, were exported to spreadsheets for further analysis.

Results and Discussion

We sought to develop a method for profiling both metabolite and micropeptide species simultaneously. We noted, firstly, that peptide species and small molecules can be made to co-partition in a Bligh-Dyer extraction.(Sana & Fischer, 2007) Secondly, peptide species become more highly charged in acidic conditions (i.e., pH < 3) than smaller metabolites. We hypothesized, therefore, that peptides and metabolites could be extracted together in a modified Bligh-Dyer reaction and then separated by an online SCX column. Therefore, we integrated a short SCX column into the HPLC Chip Cube system, in line with the autosampler. In this platform, the biosample extract can be injected and loaded onto the SCX column, while the SCX flowthrough is captured by the enrichment column on the HPLC Chip. We have developed a similar method for online multidimensional proteomics.(Tao et al., 2014) The captured flowthrough is then eluted from the enrichment column to the analytical column and analyzed by MS. As the loading buffer is acidic, the SCX flowthrough should contain small molecule metabolites, as these collect less charge in acidic conditions. The captured peptides are then eluted

by an injection of high salt buffer and loaded onto the enrichment column for desalting, then in turn eluted and analyzed by MS and MS/MS (Figure 1).

We first tested our platform for separation and reproducibility with a mix of purified standards. In order to apply the platform to a range of possible analytes, we used one bioactive endogenous small molecule, serotonin, one exogenous pharmacological compound, atenolol, and one polycyclic aromatic hydrocarbon, anthracene carboxylic acid, as an environmental compound. These were combined with three synthetic peptides (Table 1). The small molecule and peptide species were well separated by the SCX column, and chromatography was highly reproducible, with RSD of reproducibility at hold time of no greater than 0.4% (Figure 1, Table 1).

We next applied our LC-MS platform to the analysis of tissue sample extracts containing both peptides and metabolites. Mammalian spleen tissue is a mix of both liquid and solid biological matrix, since the spleen contains an open blood circulation which is filtered through sinusoids composed of structural and immune cells.(Mebius & Kraal, 2005) As such it provides a useful test sample for a profiling method such as ours. Four spleen homogenates from rhesus macaques were suspended in methanol and chloroform to precipitate proteins, and the aqueous (upper) phase collected to remove lipids. The resulting peptide and metabolite extracts MS runs were run in triplicate. The MS results show a significant change in the charge state distribution of the SCX flowthrough fractions vs. the high salt elution, with the vast majority (~95%) of molecular features in the flowthrough at +1 or +2, while the high salt elution produced a large range of charge states in a distribution centered around +4, with ~76% at charge states >2 (Figure 2b). By contrast, when the same samples were run without SCX fractionation, we observed only the broad charge state distribution (Figure 2a). We thus show that the SCX system reproducibly separates analytes by charge state.

The charge state distributions thus suggested that, when samples were run without SCX separation, peptide species preferentially ionized and suppressed detection of small molecule metabolites. Indeed, when MS/MS was performed on both peptides and metabolites in a “shotgun proteomics-like” manner, in which masses were acquired and fragmented with a rolling exclusion window, peptide suppression was reflected in a high percentage of features identified as peptides by a Mascot search, with a correspondingly low level of identifications of metabolites by a METLIN search (Figure 2c). In this experiment our SCX platform produced an improvement of 2- to 5-fold in metabolite identification (Figure 2d). We also found that the peptide population was shifted into the high-salt elution fractions (Figure 2e), showing that the high charge state features were accounted for by peptide. Peptide identifications were derived from degradation products of hemoglobin (Table S1), which was not unexpected from aqueous phase extractions from spleen, in which red blood cells are reprocessed and hemoglobin catabolized.

The overall metabolite identification results from the HPLC-MS metabolomics and HPLC-MS/MS “shotgun” metabolomics experiments are shown in Table S2 (identified by both accurate mass and MS/MS spectra), Table S3 (identified by MS/MS spectra), and Table S4 (identified by accurate mass alone). Metabolites identified by both MS and MS/MS spectra were primarily single amino acids, and identifications only by MS/MS spectra also contain many single amino acids. Finally, by accurate mass (AM) alone we find a large number of candidate small molecules. As these identifications are only by AM, they should not considered absolute identifications, and it would be necessary to confirm by running purified standards. Nevertheless, we show here that we can profile small molecules and peptides by our nanoflow-SCX system, especially, in this case, bioactive amino acids. Our SCX-nanoRPLC-MS system, therefore, allows

metabolomics and peptidomics profiling experiments for qualitative metabolite identification.

Finally, in order to test whether our system could be used to discover pathological differences in the metabolome and peptidome in tissues in a disease state, we applied the system to find metabolomic and peptidomic changes in SIV-infected spleen tissues compared with healthy controls. This macaque model of SIV is well characterized and contains clear peripheral inflammation during the acute phase of infection.(Clements, Mankowski, Gama, & Zink, 2008; Dinoso et al., 2009; Mankowski, Clements, & Zink, 2002) Here, metabolites and peptides were extracted as above, with 6 spleens derived from SIV-infected macaques and 6 derived from uninfected control macaques. In order to maximize metabolite yield, extractions were performed at three different pH levels and the extracts combined. Metabolite and peptide species were analyzed by the platform as described above. LC-MS runs were aligned and features that aligned in greater than 80% percent of runs were quantified. Although we find no significant differences in particular metabolite features, possibly reflecting a large variability in the response to infection in particular biochemical pathways, we find differences in clustering by PCA in features derived from the SCX flowthrough fractions (Figure 3). In particular, while control uninfected animal tissues clustered closely together, the metabolomes of the infected tissue were spread widely, suggesting a response to infection which was variable at the level of particular metabolites. No significant differences were observed in peptide levels (Table S5). We speculate that while there may be no changes in the hemoglobin content of the spleen during acute infection, the infected spleens are undergoing tissue-level and cellular population changes which cause these metabolomic differences. However, we cannot rule out that there may be significant changes in particular metabolites or peptides which are not

being detected by our platform, and it is possible more sensitive metabolomic methods may detect differences in particular metabolites. Finally, we must note that biopsies were taken without any knowledge of the local anatomy of the frozen spleen tissue, which may mean that some biopsies from infected samples may have included splenic zones such as germinal centers, while some did not, and this may account for some of the variability we see in the metabolic response. Nevertheless, the data shows that the SCX-nanoRPLC-MS method can provide reproducible chromatography and allows metabolomic and peptidomic profiling which detects biological differences across treatment conditions.

Conclusion

In this work, we present a method for profiling of metabolite and peptide extracts from whole tissue samples. We find that nanoflow metabolomic profiling of tissue may be substantially suppressed by peptide ionization and this suppression may be avoided by a simple and robust system whereby peptides and metabolites are separated by online SCX fractionation. Thus, our system allows extraction of a large range of metabolites and peptides from tissue samples and their simultaneous characterization in a single sample injection. While offline SCX separation has previously been used to purify metabolites before analysis, we know of no other integrated online separation system such as ours, which allows immediate analysis of both species. Furthermore, we show that the SCX-nanoRPLC-MS method produces chromatography which is sufficiently reproducible for quantitative profiling. Most importantly, this method is easy to implement, as it requires only the addition of an SCX column, and it utilizes the same chromatography buffers as most proteomics experiments. We believe this will make metabolomics more accessible to labs already using nanoHPLC for protein identification. Finally, although we have not attempted this here, we speculate that if protein samples

were to be digested and then precipitated in our modified Bligh-Dyer, this method could be used for simultaneous metabolomics and proteomics in the same analysis run. We therefore believe that this method may be useful for the development of integrated systems biology approaches combining metabolomics and peptidomics.

Figures.

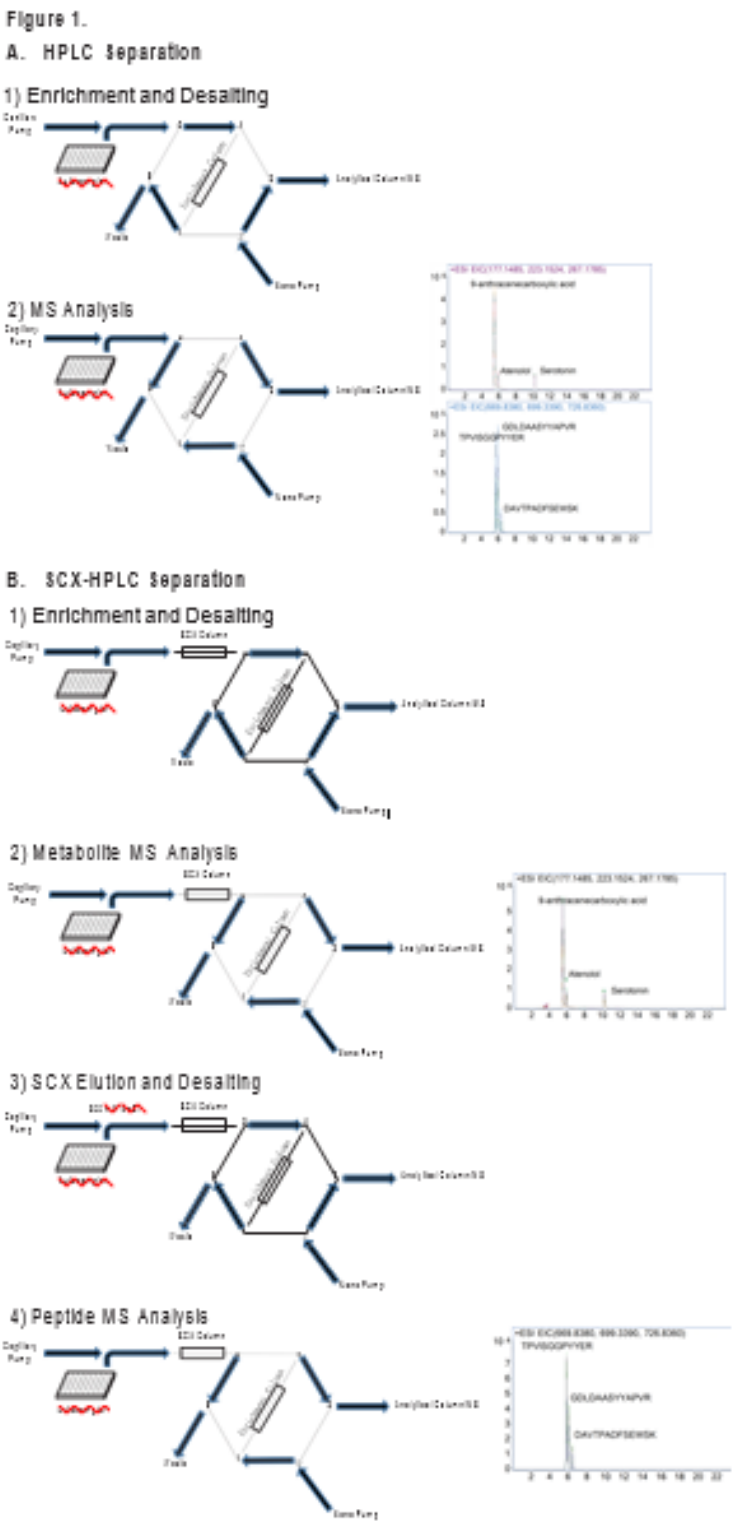

Figure 1. Schema and EIC of online SCX separated metabolite and peptide standard mixtures. Three metabolite standards, Atenolol (100 μM), Serotonin (100 μM)

and 9-anthracenecarboxylic acid (10 μM), and purified peptides TPVISGGPYYER, GDLDAASYYAPVR and DAVTPADFSEWSK (150 pM). Mix of three small molecule standards and three peptide standards were run in replicate injections, with HPLC separation only and with SCX separation online with HPLC separation. *A*, small molecule (top) and peptide (bottom) signals for replicate runs separated by HPLC alone. Metabolite and peptide mix is first desalted on an enrichment column and then eluted by an acetonitrile gradient into the MS. *B*, small molecule (top) and peptide (bottom) signal for SCX flowthrough of replicate runs separated online by both SCX and HPLC. Peptides are captured on an SCX column, and the metabolites are desalted on an enrichment column, then eluted and analyzed by MS. The peptides are then eluted from the SCX column by a 500 mM NaCl injection, then desalted on the enrichment column, and then eluted and analyzed by MS. Each replicate sample run is coded by color, y-axes are ion counts and x-axes are retention times in minutes. See text for chromatographic workflow.

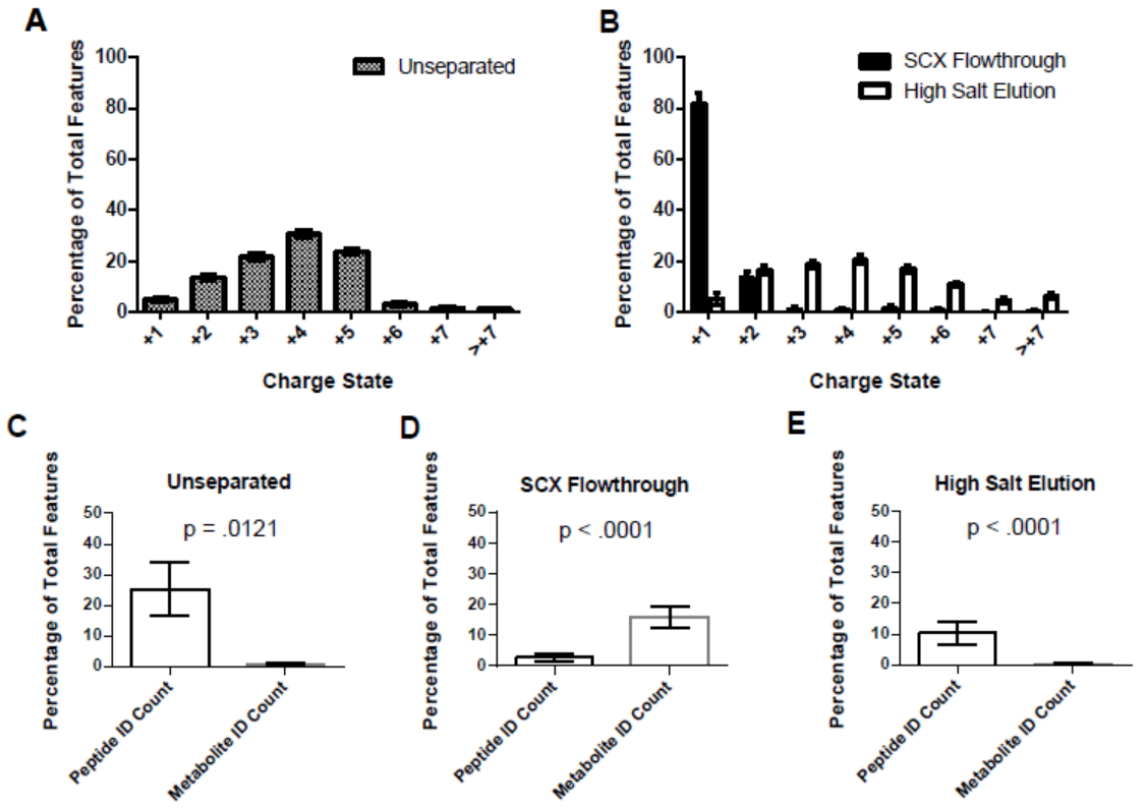

Figure 2. SCX separation alleviates peptide contamination of nanoflow metabolomic profiling experiments and allows characterization of both species. (***A***) Charge state distribution as a percentage of total features for an unseparated sample. 4 spleen homogenates were analyzed in triplicate by MS and molecular features extracted, percentages were averaged over all 12 runs. Charge states greater than +1 suggest peptide species. (***B***) Charge state distribution as a percentage of total features for SCX separated sample. 12 spleen homogenates were analyzed by MS with an SCX column placed inline with the autosampler, and high salt washes run after each sample run. Molecular features were extracted and percentages were averaged over all 12 runs. (***C-E***) Number of peptides identified by Mascot and number of metabolites identified by METLIN search, as percentage of total features extracted, from (***C***) unseparated sample, (***D***) SCX flowthrough runs, and (***E***) high salt elutions. Error bars are 95% CI, p-values are by two-tailed Mann-Whitney U Test.

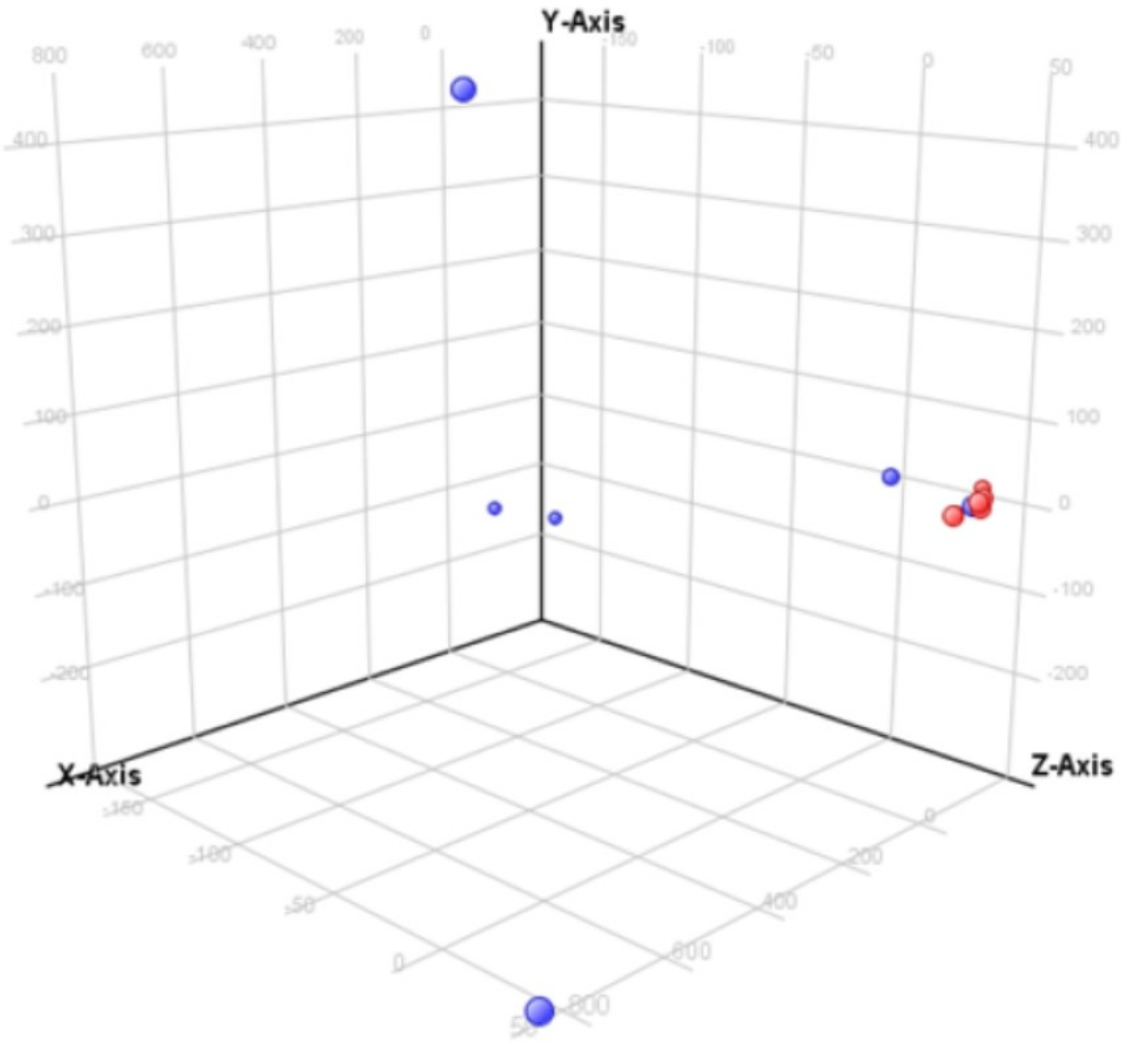

Figure 3. Principal Components Analysis for control and infected metabolite samples analyzed by online SCX system. PCA shows differences between control and infected samples. Control animals are clustered together (Red, n=6) and show a clear separation from infected (Blue, n=6), which are widely spread, showing strong but variable response to infection. The PCA components are represented as X, Y and Z, where X axis is PCA component 1 (accounts for 48.73%), Y axis PCA component 2 (24.86%) and Z axis PCA component 3 (10.99%) according to their decreasing significance.

HPLC Separated Only

	Reproducibility at hold time			Reproducibility in peak area		
	Average (min)	Standard Deviation (min)	Relative Standard Deviation (min)	Average (µV*sec)	Standard Deviation (µV*sec)	Relative Standard Deviation (µV*sec)
9-Anthracene carboxylic acid	5.45	0.00	0.00	3.20E+07	6.95E+05	2.17
Atenolol	5.92	0.01	0.10	4.32E+06	1.29E+05	2.97
Serotonin	10.23	0.00	0.00	6.45E+06	2.56E+05	3.96
Peptide TPVISGGPYYER	5.67	0.01	0.20	1.10E+06	1.27E+05	11.50
Peptide GDLDAASYYAPVR	5.95	0.01	0.10	1.09E+06	2.25E+05	20.61
Peptide DAVTPADFSEWSK	6.33	0.01	0.18	2.68E+05	5.68E+04	21.21

SCX Flowthrough – HPLC Separated

	Reproducibility at hold time			Reproducibility in peak area		
	Average (min)	Standard Deviation (min)	Relative Standard Deviation (min)	Average (µV*sec)	Standard Deviation (µV*sec)	Relative Standard Deviation (µV*sec)
9-Anthracene carboxylic acid	5.52	0.01	0.10	2.79E+07	6.38E+06	22.92
Atenolol	5.93	0.00	0.00	4.24E+06	9.26E+05	21.83
Serotonin	10.24	0.02	0.15	6.14E+06	1.89E+06	30.78

SCX High Salt Elution – HPLC Separated

	Reproducibility at hold time			Reproducibility in peak area		
	Average (min)	Standard Deviation (min)	Relative Standard Deviation (min)	Average (µV*sec)	Standard Deviation (µV*sec)	Relative Standard Deviation (µV*sec)
Peptide TPVISGGPYYER	5.79	0.02	0.40	3.49E+05	9.41E+04	26.93
Peptide GDLDAASYYAPVR	6.03	0.02	0.35	1.66E+05	3.42E+04	20.60
Peptide DAVTPADFSEWSK	6.42	0.02	0.27	7.96E+04	1.62E+04	20.40

Table 1. Retention time reproducibility and abundance reproducibility of peptide and metabolite standards with and without online SCX fractionation. Top, without SCX fractionation, bottom, with SCX fractionation.

Supplemental Figures.

Peptide identifications in SCX elution runs and assigned proteins.										
Peptide Score	Sequence	# Spectra	Mass	Number of Ions	Parent Charge	Protein Accession Number	Parent Ion Mass	# Spectra Combined Controls	# Spectra Combined Infected Samples	P-value
95.16	.WGKVNVDEVGGEA.	8	1359.65	12	2	HBB_TALEU	680.34	2	8	0.209383
95.16	.WGKVNVXEVGGEA.	4	1359.65	12	2	HBB_TALEU	680.34	1	4	0.209383
79.5	.WGKVNVEDVGGEA.	4	1359.65	12	2	HBB_TALEU	680.34	1	4	0.209383
76.75	.JSKQEYDESGPSIVHRK.	1	1359.65	12	2	HBB_CALTO	680.34	6	1	0.021872
68.11	.HLPAEFTPAVHASLDK.	18	1732.90	13	3	HBA1_OTOCR	578.31	14	18	0.54128
65.85	.AAHLPAEFTPAVHASLDK.	2	1874.98	14	4	HBA_MACFA	469.51	0	2	0.144928
63.42	.HLPAEFTPAVHASLDKFLASVSTVLTSKYR.	2	3285.76	10	5	HBA_MACFA	657.97	1	2	0.549014
63.28	.WGKVNVXEVGGEALG.	3	1529.76	11	2	HBB_CALTO	765.39	1	3	0.259573
63.28	.WGKVNVDEVGGEALG.	6	1529.76	11	2	HBB_TALEU	765.39	2	6	0.259573
62.1	.VLSPADKTNVKAAWGKVGGHAGEYGAEALER.	0	3181.64	16	5	HBA_MACFA	637.14	1	0	0.340893
59.07	.PADKTNVK*DAWGKVGGHAGEYGAEALER.	5	2969.45	9	5	HBA_MACSI	594.70	1	5	0.085638
59.07	.PADKTNVKDAWGK*VGGHAGEYGAEALER.	4	2969.45	9	5	HBA_MACSI	594.70	1	4	0.209383
58.28	.WGKVNVDEVGGEALGRL.	0	1798.95	8	2	HBB_TALEU	899.98	4	0	0.144928
58.28	.WGKVNVXEVGGEALGRL.	0	1798.95	8	2	HBB_CALTO	899.98	2	0	0.144928
55.91	.VHLTPEEKNAVT.	4	1337.71	7	3	HBB_PAPAN	446.58	0	4	0.340893
55.39	*.PADKTNVKDAWGKVGGHAGEYGAEALER.	3	2969.45	9	5	HBA_MACSI	594.70	1	3	0.259573
55.39	.PADK*TNVKDAWGKVGGHAGEYGAEALER.	4	2969.45	9	5	HBA_MACSI	594.70	1	4	0.092436
55.18	.AAHLPAEFTPAVHASLDKFLASVSTVLTSKYR.	1	3427.84	15	6	HBA_MACFA	572.16	0	1	0.340893
54.78	.AHLPAEFTPAVHASLDK.	0	1803.94	11	3	HBA_MACFA	601.99	1	0	0.340893
54.75	.SPADKTNVKAAWGKVGGHAGEYGAEALER.	3	2969.49	9	5	HBA_MACFA	594.70	2	3	0.686744
54.3	.HLPAEFTPAVHASLDKF.	2	1879.97	13	3	HBA1_OTOCR	627.33	4	2	0.549014
53.93	*.LSPADK*TNVK*AAWGKVGGHAGEYGAEALER	1	3211.59	10	5	HBA_MACFA	643.14	0	1	0.340893
53.93	*.LSPADKTNVK*AAWGK*VGGHAGEYGAEALER	1	3211.59	10	5	HBA_MACFA	643.14	0	1	0.340893
53.93	*.LSPADK*TNVKAAWGK*VGGHAGEYGAEALER	1	3211.59	10	5	HBA_MACFA	643.14	0	1	0.340893
53.93	.LSPADK*TNVK*AAWGK*VGGHAGEYGAEALER	1	3211.59	10	5	HBA_MACFA	643.14	0	1	0.340893
52.93	.QEYDESGPSIVHRK.	0	1644.80	10	3	ACTBM_HUMAN	548.94	1	0	0.340893
51.36	.LPAEFTPAVHASLDK.	1	1595.84	12	2	HBA_MACNE	798.43	0	1	0.340893
50.82	.DESGPSIVHRK.	0	1224.63	8	2	PDTEF_HUMAN	612.82	1	0	0.340893

Table S1. Peptide identifications in SCX elution runs and assigned proteins.

Name	Diff (ppm)	m/z	Max Z	Height	RT	Score
Lysine	-1.2	147.1129	2	90347	0.785	98.86
Histidine	-1.29	156.077	1	31454	0.812	93.18
Glutamic Acid	3.72	148.0599	1	34331	0.839	93.96
Proline	1.93	116.0704	1	20162	0.844	98.66
Valine	3.23	118.0859	1	35557	0.854	93.9
Glutamic Acid	2.18	148.0601	1	22997	0.859	93.66
Glutamic Acid	-0.78	148.0605	1	28662	0.877	95.2
Phenylalanine	2.42	166.0859	1	18551	0.889	94.31
Phenylalanine	0.87	166.0861	1	26964	1.111	96.36
Isoleucine	3.21	132.1015	1	817179	1.18	96.35
Serotonin	-1.37	177.1025	1	123370	1.188	95.61
Phenylalanine	-1.89	166.0866	1	537654	1.341	99.29
ALANYL-dl-LEUCINE	-1.9	203.1394	1	33200	2.675	92.35
Ile Val	-3.1	231.171	1	28451	3.628	94.64
Tryptophan	-3	205.0978	1	71304	4.324	94.57
ALANYL-dl-PHENYLALANINE	-3.7	237.1242	1	37393	4.418	95.07
Met Ile	-2.65	263.1431	1	107960	5.584	91.53
Val Phe	-3.95	265.1557	1	238602	5.691	91.47
Phe Phe	-4.9	313.1562	1	24608	5.872	91.6
Phe Phe	-3.04	313.1556	1	9563	6.157	93.53
Leu Leu	-4.69	245.1871	1	66097	6.783	91.51
URAPIDIL	3.02	388.2331	1	15552	8.936	93.15
ALPRENOLOL	4.24	250.1791	1	19272	10.678	89.76
ALPRENOLOL	0.87	250.1799	1	21869	10.688	94.16
ALPRENOLOL	4.48	250.179	1	21294	10.691	89.24
ALPRENOLOL	-0.9	250.1804	1	37392	10.697	94.15
ALPRENOLOL	0.78	250.18	1	27664	10.726	94.21
1-Octadecanamine	-4.76	270.3168	1	33166	13.843	90.13

Table S2. Putative metabolite identifications by accurate mass and MS/MS with METLIN search. Nanoflow-SCX runs were extracted by Agilent MFE and searched for matching MS1 and MS2 in METLIN.

Name	Mass Diff (ppm)	m/z	Max Z	Height	RT	Score
Asymmetric dimethylarginine	-5.45	203.1514	1	159161	0.818	44.98
Isoleucine	17.18	132.0997	1	51595	0.973	42.97
Isoleucine	7.97	132.1009	1	64163	1	45.16
Leucine	9.08	132.1007	1	40917	1.008	44.49
Isoleucine	20.54	132.0992	1	49822	1.01	41.78
Ile Thr	-7.72	233.1514	1	27306	1.059	42.74
Serotonin	-9.26	177.1039	1	28174	1.071	50
Met Phe	6774.52	295.1342	1	20791	1.101	42.66
Mebendazole metabolite (2-Amino-5-benzoylbenzimidazole)	-16.97	238.1015	1	29616	1.192	44.1
Mebendazole metabolite (2-Amino-5-benzoylbenzimidazole)	-14.81	238.101	1	43679	1.195	44.1
Mebendazole metabolite (2-Amino-5-benzoylbenzimidazole)	-16.01	238.1013	1	35378	1.201	49.37
Mebendazole metabolite (2-Amino-5-benzoylbenzimidazole)	-18.37	238.1018	1	127672	1.202	44.1
Mebendazole metabolite (2-Amino-5-benzoylbenzimidazole)	-18.23	238.1018	1	53776	1.205	44.1
Phe Ile	-11.78	279.1736	1	64760	1.209	47.05
Phe Ile	-10.21	279.1732	1	67324	1.213	48
Phe Ile	-9.07	279.1728	1	184410	1.215	48.91
Mebendazole metabolite (2-Amino-5-benzoylbenzimidazole)	-14.31	238.1009	1	15926	1.221	44.1
Phe Ile	-7.2	279.1723	1	60471	1.225	46.6
Phe Ile	-8.61	279.1727	1	85743	1.232	48.44
Phe Leu	-6.35	279.1721	1	19918	1.246	45.38
Mebendazole metabolite (2-Amino-5-benzoylbenzimidazole)	-11.99	238.1003	1	76179	1.306	49.37
Phe Phe	9.04	313.1518	1	26984	1.331	46.56
Phe Ile	-8.69	279.1727	1	11677	5.474	44.93
Phe Tyr	-5.5	329.1514	1	58218	5.615	48.81
Phe Phe	-5.33	313.1563	1	52690	5.961	49.97
Tyr Phe	-6.1	329.1516	1	66741	6.097	46.84
Val Trp	-9.11	304.1683	1	71197	6.12	48.11
Mebendazole	-13.74	238.1007	1	35127	6.157	44.1

metabolite (2-Amino-5-benzoylbenzimidazole)						
Met Phe	-7.45	297.1289	1	549774	6.241	44.04
Mebendazole metabolite (2-Amino-5-benzoylbenzimidazole)	-16.4	238.1014	1	31601	6.338	44.1
Mebendazole metabolite (2-Amino-5-benzoylbenzimidazole)	-14.17	238.1008	1	14023	6.339	49.37
Mebendazole metabolite (2-Amino-5-benzoylbenzimidazole)	-13.26	238.1006	1	1748413	6.387	44.1
Mebendazole metabolite (2-Amino-5-benzoylbenzimidazole)	-13.08	238.1006	1	27841	6.425	49.37
Phe Ile	-8.92	279.1728	1	50416	6.468	47.37
Phe Leu	-6.96	279.1723	1	16295	6.481	44.86
Phe Ile	-9.38	279.1729	1	53411	6.516	48.28
Phe Ile	-8.03	279.1726	1	119162	6.517	48.43
Phe Ile	-6.57	279.1722	1	3532588	6.589	48.94
Phe Phe	-6.3	313.1566	1	96348	7.008	49.97
1-(2-(allyloxy)phenoxy)-3-(isopropylamino)propan-2-ol	7.07	266.1732	1	13735	9.635	41.12
Decanoyl-L-carnitine	3191.78	316.2499	1	21616	10.506	48.29
Decanoyl-L-carnitine	3190.26	316.2504	1	71348	10.545	49.74
ALPRENOLOL	6.03	250.1787	1	24692	10.721	44.37
1-Monopalmitin	-5.66	331.2862	1	1863084	17.625	41.56

Table S3. Putative metabolite identifications by MS/MS with METLIN search.

Nanoflow-SCX runs were extracted by Agilent MFE and searched for matching MS2 in METLIN.

Name	**Diff (DB, ppm)**	**m/z**	**Max Z**	**Height**	**RT**	**Score**
Ser Ile	-1.79	219.1343	1	23489	0.788	98.55
Ser Ile	-0.23	219.134	1	10758	0.865	99.97
N,N-Didemethylchlorpromazine	-0.92	291.072	1	78284	0.944	99.46

Ser Ile	-3.86	219.1348	1	19403	0.946	93.41
Val Val	-3.29	217.1554	1	18595	0.991	95.2
1-Ethylcarbamyl-4-methylpiperazine	1.57	172.1442	1	32535	1.037	99.17
Moclobemide	2.39	269.1045	1	9432	1.06	96.7
Leu Val	-2.63	231.1709	1	40257	1.068	48.33
Tyrosine	-2.71	182.0817	1	20845	1.077	97.39
2-Ketogulonolactone	-4.81	177.0402	1	29004	1.078	46.13
Cys Ile	-2.95	235.1118	1	11845	1.078	95.73
Cimetidine	4.05	253.122	1	12195	1.089	91.43
2-amino-4'-hydroxy-Propiophenone	-3.95	166.0869	1	17215	1.09	95.16
Leu Val	-4.71	231.1714	1	132846	1.092	44.84
2-Ketogulonolactone	-0.08	177.0394	1	64306	1.098	50
HELENINE	4.92	233.1525	1	20916	1.099	88.7
Leu Val	-4.98	231.1715	1	28289	1.105	44.29
Leu Val	-4.3	231.1713	1	69649	1.111	45.67
Thr Ile Val	-3.6	332.2192	1	9646	1.112	90.89
Dienestrol	3.63	267.137	1	13056	1.116	92.63
Phe Thr	-4.9	267.1352	1	10626	1.116	86.99
TIAPRIDE	4.17	329.1516	1	8617	1.124	88.05
Phe Met	-4.51	297.1281	1	6069	1.128	87.53
Leu Val	-3.95	231.1712	1	116805	1.135	46.33
TIAPRIDE	0.42	329.1528	1	7153	1.138	99.87
TIAPRIDE	2.78	329.152	1	9916	1.139	94.51
TIAPRIDE	3	329.152	1	7554	1.14	46.81
Phe Tyr	-4.67	329.1511	1	5923	1.143	85.28

2H-Indol-2-one, 1,3-dihydro-4-[2-hydroxy-3-[(1-methylethyl)amino]propoxy]-	-2.43	265.1553	1	6915	1.143	96.66
2H-Indol-2-one, 1,3-dihydro-4-[2-hydroxy-3-[(1-methylethyl)amino]propoxy]-	-3.66	265.1556	1	11002	1.145	92.58
2H-Indol-2-one, 1,3-dihydro-4-[2-hydroxy-3-[(1-methylethyl)amino]propoxy]-	-3.89	265.1557	1	8918	1.153	91.65
Gly Leu	-3.35	189.124	1	82908	1.17	47.91
Tyr Ala	-1.74	253.1187	1	37806	1.177	98.35
Indoleacetaldehyde	0.02	160.0757	1	44807	1.192	100
Warfarin alcohol	0.44	311.1277	1	32231	1.212	99.87
Val Val	-4.23	217.1556	1	293546	1.257	46.11
6-Hydroxymelatonin	-4.34	249.1244	1	15791	1.331	90.42
albendazole (IV) 1H-Benzimidazol-2-amine	2.12	240.0796	1	59904	1.333	48.86
Tyr Ala	-3.79	253.1192	1	9340	3.426	46.22
Thr Ala Val	-3.61	290.1721	1	7577	4.165	92.03
Thr Ile Val	-0.49	332.2182	1	17930	4.189	99.82
5'-Methylthioadenosine	-3.94	298.098	1	9507	4.312	90.29
Indoleacrylic acid	-2.14	188.071	1	9499	4.337	98.29
albendazole (IV) 1H-Benzimidazol-2-amine	1.47	240.0798	1	66411	4.37	49.45
Phe Thr	-4.6	267.1352	1	55208	4.428	44.21
Leu Pro	-3.51	229.1555	1	36112	4.46	47.09
Ala Thr Phe	-3.22	338.1721	1	5844	4.53	92.48
Leu Val	-4.66	231.1714	1	1455590	4.727	44.96
Phe Ser Thr	-4.58	354.1676	1	9466	4.888	84.75
Pro Val Tyr	1.25	378.2019	1	6703	5.047	98.7
Cys Phe	-4.68	269.0967	1	31400	5.097	43.97
Leu Val	-1.8	231.17	1	30938	5.19	49.2

		07			6	1
Leu Val	-4.59	231.1714	1	21159	5.204	45.1
Leu Val	-2.43	231.1709	1	18218	5.246	48.57
2H-Indol-2-one, 1,3-dihydro-4-[2-hydroxy-3-[(1-methylethyl)amino]propoxy]-	-2.63	265.1554	1	43806	5.28	48.05
Thr Ile Phe	-4.98	380.2199	1	72670	5.375	40.53
Cys Val Met	0.61	352.1357	1	10052	5.657	49.86
Ala Tyr Leu	-4.65	366.204	1	41113	5.739	41.93
Ile Ser Val	-1.86	318.2029	1	10743	5.753	97.59
Val Val	1.93	217.1543	1	8029	5.943	98.33
Ipecac (Emetamine)	2.89	477.2734	1	128586	5.983	45.84
Leu Ile Asp	-4.38	360.2145	1	35203	6.046	42.88
Ser Pro Pro	2.88	300.1545	1	36319	6.348	94.65
Phe Phe Leu	4.91	426.2366	1	14996	6.381	79.7
Phe Phe Leu	0.56	426.2385	1	18242	6.418	99.71
Thr Ser Glu	0.29	336.14	1	32480	6.498	49.97
MYCOPHENOLIC ACID	-1.68	321.1338	1	21637	6.6	98.01
Pro Tyr Trp	-3.94	465.2151	1	9838	6.608	85.4
MYCOPHENOLIC ACID	0.12	321.1332	1	22179	6.63	49.99
MYCOPHENOLIC ACID	1.04	321.1329	1	18346	6.637	99.24
2-Deoxyglucose	-3.67	165.0764	1	26508	6.639	47.92
Phenylmethyl methyl ketone	-2.48	135.0808	1	19251	6.655	98.54
2-Deoxyglucose	-2.06	165.0761	1	33876	6.666	98.66
Thr Leu Trp	-4.98	419.231	1	15390	6.667	79.41
Phenylmethyl methyl ketone	-2.09	135.0807	1	24666	6.669	98.97
2-Deoxyglucose	-0.81	165.0759	1	17446	6.675	49.9

Phenylmethyl methyl ketone	0.71	135.0803	1	20270	6.679	99.88
2-Deoxyglucose	-3.68	165.0764	1	54351	6.704	95.81
MYCOPHENOLIC ACID	-3.24	321.1343	1	22981	6.71	92.79
Thr Leu Trp	-3.64	419.2304	1	9979	6.774	88.43
Leu Leu	-1.94	245.1864	1	8722	6.811	98.03
Phe Phe Leu	4.5	426.2368	1	39170	6.878	82.6
Met His Lys	-3.36	415.2136	1	38431	6.886	45.08
4-Hydroxyestrone	3.43	287.1632	1	10350	6.9	92.85
N-HISTIDYL-2-AMINONAPHTHALENE (betaNA)	-2.93	281.1405	1	11485	6.941	94.86
4-Hydroxyestrone	4.28	287.1629	1	12741	6.945	89.09
Met Cys Thr	-0.14	354.1152	1	9960	6.96	99.98
Met His Lys	-3.18	415.2135	1	41446	6.962	91.14
Phenylmethyl methyl ketone	3.26	135.08	1	29865	6.972	97.51
N-HISTIDYL-2-AMINONAPHTHALENE (betaNA)	-4.53	281.141	1	7537	6.977	88.12
Phe Leu	-3.3	279.1712	1	11033	6.989	93.57
2-Deoxyglucose	-1.25	165.076	1	70412	6.992	49.75
N-HISTIDYL-2-AMINONAPHTHALENE (betaNA)	0.53	281.1395	1	6874	6.997	99.83
MYCOPHENOLIC ACID	0.62	321.1331	1	19677	7.006	49.87
2-Deoxyglucose	0.09	165.0757	1	63017	7.024	50
Ipecac (Methylpsychotrine)	2.7	479.2891	1	10180	7.031	92.66
Phenylmethyl methyl ketone	4.91	135.0798	1	27302	7.041	94.43
Met His Lys	-2.87	415.2134	1	39617	7.048	92.72
Ipecac (Methylpsychotrine)	1.36	479.2898	1	5459	7.051	98.09
N-HISTIDYL-2-	-2.91	281.14	1	9773	7.05	94.9

AMINONAPHTHALENE (betaNA)		05			4	2
MYCOPHENOLIC ACID	1.56	321.1328	1	18276	7.095	98.28
Ipecac (Methylpsychotrine)	2.59	479.2892	1	7533	7.131	93.24
2-Deoxyglucose	-0.37	165.0758	1	69360	7.131	49.98
Phenylmethyl methyl ketone	3	135.08	1	27213	7.148	97.88
MYCOPHENOLIC ACID	0.14	321.1332	1	15226	7.16	99.99
MYCOPHENOLIC ACID	-3.77	321.1345	1	17111	7.161	90.38
N-HISTIDYL-2-AMINONAPHTHALENE (betaNA)	-3.41	281.1406	1	8359	7.167	93.09
Phenylmethyl methyl ketone	2.78	135.0801	1	10491	7.184	98.18
MYCOPHENOLIC ACID	-3.76	321.1345	1	17468	7.195	90.43
MYCOPHENOLIC ACID	2.98	321.1323	1	24878	7.223	46.93
ENOXACIN	3.25	321.1347	1	16843	7.229	92.76
Ser Gly Arg	4.39	319.171	1	12343	7.308	87.23
3-Methylsuberic acid	-0.18	189.1122	1	10108	7.308	99.99
Phe Phe Leu	3.15	426.2374	1	113085	7.318	45.54
Ser Gly Arg	1.02	319.1721	1	6077	7.406	99.26
Met His Lys	-4.82	415.2142	1	143076	7.477	80.74
Phenylmethyl methyl ketone	3.12	135.08	1	53881	7.511	97.72
2-Deoxyglucose	-0.48	165.0758	1	120124	7.531	49.96
Ipecac (Methylpsychotrine)	4.61	479.2882	1	26895	7.595	80.07
MYCOPHENOLIC ACID	-1.03	321.1336	1	23340	7.637	99.24
CDP-DG(18:1(9Z)/18:1(9Z))	3.96	1006.549	1	125352	7.7	76.21
Carteolol	-3.45	293.187	1	14976	7.796	46.31
17-Epiestriol	4.15	289.1786	1	45829	7.832	44.82
Avermectin B2b	3.67	877.49	2	14493	7.83	40.2

		04		5	2	4
Gabapentin	-1.47	172.1335	1	16373	7.854	49.64
Avermectin B2b	4.12	877.4898	2	180599	7.859	38.04
17-Epiestriol	3.6	289.1788	1	121526	7.866	46.05
Avermectin B2b	4.34	877.4898	2	43730	7.867	36.91
17-Epiestriol	4.76	289.1784	1	176033	7.875	43.29
Avermectin B2b	4.52	877.4898	2	316504	7.889	35.96
CAPSAICIN	0.73	306.2061	1	11443	7.891	99.64
17-Epiestriol	3.02	289.179	1	163515	7.904	47.18
Carteolol	-3.24	293.1869	1	55708	7.988	46.73
3-(a-Naphthoxy)lactic acid	4.55	233.0798	1	18528	8.089	45.14
p-HYDROXYCINNAMALDEHYDE	3.64	149.0592	1	13247	8.096	96.45
3-(2,5-dimethoxyphenyl)propanoic acid	-2.87	211.0971	1	80995	8.098	48.23
Val Arg Gly	-0.23	331.2089	1	13774	8.107	49.98
Dimethylimidazole	-4.83	99.0558	1	40344	8.111	48.3
Ciglitazone	-3.13	334.1482	1	6839	8.15	92.97
Arg Val Asn	3.87	388.2288	1	19461	8.211	87.85
Carteolol	-4.8	293.1874	1	12770	8.281	86.16
DL-2-Aminooctanoic acid	-4.16	160.1339	1	20987	8.308	94.9
Biliverdin IX	-2.14	583.2564	1	57158	8.313	47.28
2-ethyl-3E-hexenoic acid	-3.91	143.1072	1	70437	8.314	48.07
2-ethyl-3E-hexenoic acid	0.94	143.1065	1	43888	8.315	49.89
2-ethyl-3E-hexenoic acid	-1.67	143.1069	1	70277	8.316	49.64
2-ethyl-3E-hexenoic acid	-3.67	143.1072	1	15689	8.319	48.29
Biliverdin IX	-4.17	583.2575	1	56797	8.319	40.39

MUCRONULATOL((+/-))	-0.12	303.1227	1	19161	8.32	99.99
MUCRONULATOL((+/-))	-3.7	303.1238	1	19967	8.323	91.24
Biliverdin IX	-0.41	583.2554	1	30269	8.324	49.9
Biliverdin IX	0.55	583.2548	1	33058	8.325	49.82
MUCRONULATOL((+/-))	-1.85	303.1233	1	13334	8.332	97.74
Biliverdin IX	-3.53	583.2572	1	48701	8.333	42.92
Biliverdin IX	1.08	583.2545	1	35132	8.337	49.29
DL-2-Aminooctanoic acid	-0.31	160.1333	1	10297	8.339	99.97
MUCRONULATOL((+/-))	-3.26	303.1237	1	18149	8.34	93.13
2-ethyl-3E-hexenoic acid	0.84	143.1065	1	35708	8.344	49.91
N-HISTIDYL-2-AMINONAPHTHALENE (betaNA)	-4.62	281.141	1	145994	8.349	43.84
MUCRONULATOL((+/-))	-3.08	303.1236	1	16976	8.35	93.84
DL-2-Aminooctanoic acid	-1.72	160.1335	1	17228	8.352	99.11
2-ethyl-3E-hexenoic acid	1.08	143.1065	1	65847	8.354	49.85
MUCRONULATOL((+/-))	2.12	303.1221	1	13376	8.355	97.04
N-HISTIDYL-2-AMINONAPHTHALENE (betaNA)	-2.66	281.1404	1	54342	8.358	47.86
N-HISTIDYL-2-AMINONAPHTHALENE (betaNA)	-2.38	281.1404	1	95229	8.364	48.28
N-HISTIDYL-2-AMINONAPHTHALENE (betaNA)	-3.29	281.1406	1	101897	8.368	46.77
3-(2,5-dimethoxyphenyl)propanoic acid	-3.61	211.0972	1	68931	8.368	47.23
Biliverdin IX	-1.34	583.2559	1	57760	8.37	48.9
2-ethyl-3E-hexenoic acid	-4.69	143.1073	1	31709	8.388	94.47
MUCRONULATOL((+/-))	0.85	303.1224	1	19691	8.391	49.76
Phenylmethyl methyl ketone	2.83	135.0801	1	8500	8.405	98.12

Phenylmethyl methyl ketone	-2.27	135.0807	1	18602	8.414	98.78
N-HISTIDYL-2-AMINONAPHTHALENE (betaNA)	-3.54	281.1407	1	108294	8.421	46.29
2-ethyl-3E-hexenoic acid	-0.5	143.1067	1	34981	8.427	49.97
Phenylmethyl methyl ketone	-2.99	135.0808	1	13307	8.433	97.89
3-Hydroxydodecanedioic acid	-4.31	247.1551	1	13947	8.466	90.6
FISSINOLIDE	-4.96	513.2508	1	8244	8.469	76.18
Biliverdin IX	0.14	583.255	1	57049	8.47	49.99
FISSINOLIDE	-2.99	513.2498	1	20148	8.472	90.58
FISSINOLIDE	-2.21	513.2494	1	12061	8.477	94.74
FISSINOLIDE	-2.04	513.2493	1	12646	8.483	95.51
MUCRONULATOL((+/-))	-0.41	303.1228	1	18886	8.484	49.94
N-methyl-Gabapentin	-3.07	186.1494	1	7435	8.486	96.57
FISSINOLIDE	-3.53	513.2501	1	15380	8.487	87.12
Biliverdin IX	1.38	583.2543	1	46056	8.493	48.85
FISSINOLIDE	-4.75	513.2507	1	17526	8.5	77.9
N-HISTIDYL-2-AMINONAPHTHALENE (betaNA)	-1.59	281.1401	1	159539	8.501	49.23
4-(2-Hydroxy-3-isopropylaminoproxy)-benzyloxy acetic acid	-3.54	298.166	1	49623	8.517	46.05
FISSINOLIDE	-1.52	513.2491	1	16806	8.518	97.47
N-HISTIDYL-2-AMINONAPHTHALENE (betaNA)	-1.74	281.1402	1	89722	8.518	49.08
MUCRONULATOL((+/-))	3.27	303.1217	1	21288	8.519	46.54
Biliverdin IX	3.14	583.2533	1	37520	8.52	44.3
2Z,6E-decadienoic acid	-4.25	169.123	1	23257	8.521	47.13
MUCRONULATOL((+/-))	0.86	303.1224	1	14627	8.539	99.51

Phenylmethyl methyl ketone	3.31	135.08	1	18950	8.554	97.43
N-HISTIDYL-2-AMINONAPHTHALENE (betaNA)	-0.63	281.1399	1	93764	8.554	49.88
N-methyl-Gabapentin	-4.38	186.1497	1	20627	8.556	46.55
2Z,6E-decadienoic acid	-3.17	169.1228	1	11127	8.558	96.78
2Z,6E-decadienoic acid	-2.67	169.1228	1	18473	8.571	48.85
2Z,6E-decadienoic acid	-4.96	169.1231	1	10926	8.582	46.15
tetranor-PGEM	-4.7	327.1454	1	37392	8.596	42.58
2-ethyl-3E-hexenoic acid	3.73	143.1061	1	50317	8.637	48.24
FISSINOLIDE	-1.98	513.2493	1	17899	8.642	95.76
3,5-hexadienoic acid	-3.77	225.1133	1	26073	8.655	97.44
FISSINOLIDE	-1.21	513.2489	1	18000	8.663	98.38
Biliverdin IX	3.06	583.2533	1	36434	8.668	44.57
MUCRONULATOL((+/-))	0.31	303.1226	1	15872	8.673	49.97
N-HISTIDYL-2-AMINONAPHTHALENE (betaNA)	-0.55	281.1398	1	97079	8.691	49.91
3-Hydroxydodecanedioic acid	-4.66	247.1551	1	22242	8.7	44.57
2-ethyl-3E-hexenoic acid	2	143.1064	1	43210	8.705	49.49
3-Hydroxydodecanedioic acid	-1.29	247.1543	1	17825	8.722	99.12
(-)-Carvone	-0.37	151.1118	1	13460	8.739	99.96
2Z,6E-decadienoic acid	-0.8	169.1224	1	30800	8.741	49.9
N-methyl-Gabapentin	-1.37	186.1491	1	39582	8.742	49.65
2-ethyl-3E-hexenoic acid	4.3	143.106	1	75866	8.743	47.67
DL-2-Aminooctanoic acid	1.4	160.133	1	20694	8.745	99.41
N-methyl-Gabapentin	-1.31	186.1491	1	43057	8.812	49.68
2Z,6E-decadienoic acid	0.83	169.1222	1	35784	8.816	49.89

(-)-Carvone	3.04	151.1113	1	16102	8.818	97.46
N-methyl-Gabapentin	-0.11	186.1489	1	17548	8.821	50
2Z,6E-decadienoic acid	1.64	169.122	1	14164	8.823	49.56
Lactone of PGF-MUM	0	297.1697	1	12139	8.886	100
3-Hydroxydodecanedioic acid	-4.32	247.1551	1	33583	8.898	45.29
2-Methoxyestradiol	4.56	303.1941	1	14007	8.988	43.5
2-Methoxyestradiol	2.82	303.1946	1	21678	8.997	47.4
2-Methoxyestradiol	4.7	303.1941	1	9406	9.017	86.27
N-methyl-Gabapentin	-2.71	186.1494	1	28856	9.073	48.65
2-ethyl-3E-hexenoic acid	3.11	143.1062	1	71371	9.083	48.76
DL-2-Aminooctanoic acid	0.75	160.1331	1	21680	9.084	49.91
Idebenone Metabolite (Benzenehexanoic acid, 2,5-dihydroxy-3,4-dimethoxy-6-methyl-)	-2.63	299.1497	1	11748	9.099	47.77
12-amino-dodecanoic acid	-4.47	216.1968	1	40017	9.101	45.69
Idebenone Metabolite (Benzenehexanoic acid, 2,5-dihydroxy-3,4-dimethoxy-6-methyl-)	-4.25	299.1502	1	13788	9.105	44.37
Arg Gly Gly	1.5	289.1614	1	5480	9.119	49.29
Idebenone Metabolite (Benzenehexanoic acid, 2,5-dihydroxy-3,4-dimethoxy-6-methyl-)	1.81	299.1484	1	24559	9.125	48.93
N1,N4-Diacetylsulfanilamide	-2.97	257.0598	1	40549	9.405	47.61
N1,N4-Diacetylsulfanilamide	-2.51	257.0597	1	32578	9.412	48.28
N1,N4-Diacetylsulfanilamide	-4.9	257.0603	1	26213	9.418	43.75
N1,N4-Diacetylsulfanilamide	2.8	257.0583	1	23425	9.422	47.87
sebacic acid	-2.55	203.1283	1	9701	9.422	97.33
N1,N4-Diacetylsulfanilamide	1.3	257.0587	1	37938	9.426	49.53

N1,N4-Diacetylsulfanilamide	-2.39	257.0597	1	31246	9.442	48.43
N1,N4-Diacetylsulfanilamide	0.09	257.059	1	34844	9.443	50
N1,N4-Diacetylsulfanilamide	-1.92	257.0595	1	31832	9.469	48.98
Cys Cys Lys	1.75	353.1306	1	7602	9.499	97.62
Cilastatin	4.77	359.1618	1	12153	9.503	83.39
N1,N4-Diacetylsulfanilamide	0.43	257.0589	1	36944	9.508	49.95
N1,N4-Diacetylsulfanilamide	3.14	257.0583	1	31396	9.535	47.33
Oxprenolol	-4.01	266.1761	1	11702	9.578	91.1
Oxprenolol	-1.8	266.1755	1	14135	9.597	98.13
Oxprenolol	2.07	266.1745	1	8761	9.612	97.56
Oxprenolol	-0.71	266.1753	1	18734	9.622	99.71
Oxprenolol	4.9	266.1738	1	11803	9.624	87.02
4-Ethylbenzoic acid	-3.69	151.0759	1	16374	9.647	48.14
methyl 8-[2-(2-formyl-vinyl)-3-hydroxy-5-oxo-cyclopentyl]-octanoate	-1.64	311.1858	1	14911	9.701	98.17
methyl 8-[2-(2-formyl-vinyl)-3-hydroxy-5-oxo-cyclopentyl]-octanoate	-4.24	311.1866	1	13698	9.726	88.37
methyl 8-[2-(2-formyl-vinyl)-3-hydroxy-5-oxo-cyclopentyl]-octanoate	-0.73	311.1855	1	15927	9.731	99.63
methyl 8-[2-(2-formyl-vinyl)-3-hydroxy-5-oxo-cyclopentyl]-octanoate	1.51	311.1848	1	15644	9.733	98.45
methyl 8-[2-(2-formyl-vinyl)-3-hydroxy-5-oxo-cyclopentyl]-octanoate	0.06	311.1853	1	12994	9.736	100
methyl 8-[2-(2-formyl-vinyl)-3-hydroxy-5-oxo-cyclopentyl]-octanoate	3.84	311.1841	1	14871	9.76	90.35
methyl 8-[2-(2-formyl-vinyl)-3-hydroxy-5-oxo-cyclopentyl]-octanoate	1.52	311.1848	1	12784	9.762	49.21
Arg Ala	3.79	246.1551	1	9217	9.808	92.69
ISOSAFROLE	-0.19	163.07	1	13907	9.91	49.9

		54			9	9
ISOSAFROLE	-1.33	163.0756	1	16362	9.938	99.45
ISOSAFROLE	-0.28	163.0754	1	17292	9.946	49.99
ISOSAFROLE	-2.09	163.0757	1	17999	9.952	49.33
PEUCENIN	0.61	261.112	1	31149	9.968	49.89
PEUCENIN	-0.66	261.1123	1	30783	9.972	49.88
PEUCENIN	-1.47	261.1125	1	27510	9.976	49.39
PEUCENIN	3.5	261.1112	1	23302	9.978	46.65
ISOSAFROLE	1.79	163.0751	1	18725	9.987	49.5
PEUCENIN	-0.57	261.1123	1	21918	9.989	49.91
PEUCENIN	1.4	261.1118	1	19297	9.996	49.45
PEUCENIN	2.1	261.1116	1	29571	10.016	48.77
PEUCENIN	3.73	261.1112	1	26191	10.016	46.22
PEUCENIN	3.37	261.1113	1	25302	10.04	46.88
PEUCENIN	4.66	261.1109	1	32391	10.046	44.22
Flupenthixol sulfoxide	-4.54	466.1792	1	15856	10.324	40.52
(22S)-22-hydroxy-24,25,26,27-tetranorvitamin D3 / (22S)-22-hydroxy-23,24,25,26,27-pentanorcholecalci	3.56	345.2776	1	11624	10.407	45.37
12-oxo-14,18-dihydroxy-9Z,13E,15Z-octadecatrienoic acid	0.36	325.2008	1	16534	10.484	99.9
12-oxo-14,18-dihydroxy-9Z,13E,15Z-octadecatrienoic acid	2.71	325.2001	1	17327	10.488	47.42
12-oxo-14,18-dihydroxy-9Z,13E,15Z-octadecatrienoic acid	-2.57	325.2018	1	22453	10.495	47.67
12-oxo-14,18-dihydroxy-9Z,13E,15Z-octadecatrienoic acid	0.58	325.2008	1	15789	10.499	99.75
emedastine	-3.15	303.2189	1	15016	10.499	93.58

emedastine	-0.23	303.218	1	11906	10.499	99.97
12-oxo-14,18-dihydroxy-9Z,13E,15Z-octadecatrienoic acid	-2.5	325.2018	1	22859	10.5	47.8
emedastine	0.76	303.2177	1	13068	10.501	99.61
12-oxo-14,18-dihydroxy-9Z,13E,15Z-octadecatrienoic acid	1.72	325.2004	1	13898	10.502	48.95
emedastine	0.41	303.2178	1	15371	10.507	49.94
12-oxo-14,18-dihydroxy-9Z,13E,15Z-octadecatrienoic acid	1.23	325.2006	1	18295	10.507	49.46
emedastine	1.03	303.2176	1	14048	10.51	99.29
Met Asn Arg	-4.31	420.2042	1	15623	10.517	84.11
12-oxo-14,18-dihydroxy-9Z,13E,15Z-octadecatrienoic acid	-0.4	325.2011	1	20262	10.52	49.94
emedastine	-2.42	303.2187	1	14172	10.523	96.16
12-oxo-14,18-dihydroxy-9Z,13E,15Z-octadecatrienoic acid	-2.37	325.2017	1	17529	10.524	48.02
Ramipril glucuronide	4.41	593.2679	1	12517	10.525	78.56
emedastine	-3.31	303.2189	1	15251	10.527	92.94
Ramipril glucuronide	1.51	593.2696	1	14550	10.538	97.22
Flupenthixol sulfoxide	-1.89	466.1779	1	9559	10.557	96.42
Ramipril glucuronide	2.98	593.2687	1	17065	10.571	89.57
Acitretin Ro 23-4750	-1.77	343.191	1	8914	10.571	97.64
Flupenthixol sulfoxide	-4.04	466.1789	1	7114	10.595	84.67
Pinacidil	-2.77	246.172	1	21572	10.622	48.02
Pinacidil	-3.44	246.1722	1	96721	10.625	46.97
Pinacidil	-1.12	246.1716	1	50446	10.631	49.67
EUPATORIOCHROMENE	-4.56	219.1026	1	17321	10.634	45.46
N,O-Didesmethylvenlafaxine	1.15	250.17	1	15240	10.6	99.2

		99			88	9
N,O-Didesmethylvenlafaxine	3.98	250.1792	1	15082	10.695	91.82
Pinacidil	1.32	246.171	1	42620	10.703	49.54
N,O-Didesmethylvenlafaxine	-0.9	250.1804	1	12312	10.719	99.56
Metoprolol	-4.49	268.1919	1	5685	10.734	88.89
N,O-Didesmethylvenlafaxine	2.12	250.1796	1	12575	10.748	97.6
9S-hydroxy-2E-decenoic acid	-4.7	187.1337	1	17811	10.802	92.08
9S-hydroxy-2E-decenoic acid	-3.53	187.1335	1	26849	10.812	47.72
Propranolol glucuronide	0.48	436.1964	1	7616	10.877	99.78
Propranolol glucuronide	3.33	436.1951	1	12703	10.88	89.87
3,5-hexadienoic acid	3.38	113.0593	1	16229	10.993	97.94
Phenylmethyl methyl ketone	-1.74	135.0807	1	36983	10.996	49.64
RHODOMYRTOXIN	-2.2	429.1917	1	8530	10.998	95.53
Phenylmethyl methyl ketone	0.67	135.0804	1	51522	11	49.95
Phenylmethyl methyl ketone	3.47	135.08	1	35506	11.003	48.59
3,5-hexadienoic acid	4.82	113.0592	1	27543	11.006	95.87
Phenylmethyl methyl ketone	3.36	135.08	1	33275	11.011	97.35
3,5-hexadienoic acid	-2.8	113.06	1	30187	11.012	98.59
Methyl jasmonate	-4.62	225.1496	1	43337	11.012	45.18
Methyl jasmonate	-4.84	225.1496	1	23057	11.015	44.74
3,5-hexadienoic acid	-0.67	113.0598	1	18400	11.029	99.92
Methyl jasmonate	-4.97	225.1496	1	24615	11.032	88.94
Phenylmethyl methyl ketone	2.24	135.0801	1	60172	11.032	49.41
Phenylmethyl methyl ketone	-3.41	135.0809	1	107225	11.035	48.64
Methyl jasmonate	-3.27	225.1493	1	32955	11.04	47.53

Phenylmethyl methyl ketone	0.78	135.0803	1	78721	11.047	49.93
3,5-hexadienoic acid	1.93	113.0595	1	39063	11.056	49.66
3,5-hexadienoic acid	-2.28	113.06	1	15238	11.057	99.06
Phenylmethyl methyl ketone	1.95	135.0802	1	28926	11.064	49.55
Phenylmethyl methyl ketone	3.61	135.08	1	36334	11.074	48.48
Lys Cys His	-4.81	387.1828	1	100750	11.18	40.96
Lys Cys His	-3.69	387.1823	1	109438	11.182	44.46
Lys Cys His	-2.04	387.1817	1	72958	11.209	48.25
Idebenone	2.31	339.2158	1	23170	11.227	96.05
Idebenone	3.17	339.2155	1	20436	11.242	46.36
Lisuride	-0.75	339.2182	1	27349	11.248	99.57
Lisuride	-0.36	339.2181	1	23706	11.255	99.9
Lisuride	0.57	339.2177	1	22417	11.259	99.75
PGF2alpha-11-acetate methyl ester	1.31	411.2736	1	18746	11.261	98.45
8E-Heptadecenedioic acid	0.45	299.2216	1	7371	11.266	99.87
8E-Heptadecenedioic acid	-1.49	299.2221	1	11410	11.268	98.54
PGF2alpha-11-acetate methyl ester	4.68	411.2722	1	13904	11.275	81.89
Lisuride	0.76	339.2177	1	25968	11.277	99.57
8E-Heptadecenedioic acid	-2.52	299.2224	1	9170	11.281	95.9
Idebenone	2.23	339.2158	1	12923	11.283	96.32
PGF2alpha-11-acetate methyl ester	-0.77	411.2744	1	18784	11.284	99.46
Idebenone	-0.44	339.2167	1	10808	11.287	99.85
Idebenone	2.03	339.2159	1	16789	11.288	96.95
PGF2alpha-11-acetate methyl ester	3.07	411.2729	1	16458	11.291	91.75
8E-Heptadecenedioic acid	-4.93	299.2232	1	13156	11.293	85.18

PGF2alpha-11-acetate methyl ester	-2.61	411.2752	1	16303	11.295	93.99
PGF2alpha-11-acetate methyl ester	-2.2	411.275	1	21000	11.303	95.68
PGF2alpha-11-acetate methyl ester	4.26	411.2724	1	11618	11.306	84.78
PGF2alpha-11-acetate methyl ester	1.51	411.2735	1	14754	11.307	97.95
8E-Heptadecenedioic acid	-3.16	299.2226	1	8592	11.308	93.63
PGF2alpha-11-acetate methyl ester	-1.6	411.2748	1	21434	11.311	97.69
N-(2-hydroxyethyl)icosanamide	-4.5	356.3539	1	28133	11.334	42.59
PGF2alpha-11-acetate methyl ester	0.58	411.2739	1	13126	11.336	99.7
O-Desmethylvenlafaxine	3.11	264.195	1	7819	11.353	94.6
O-Desmethylvenlafaxine	1.08	264.1955	1	8708	11.409	99.33
3,3,45-Tetrahydroxystilbene	2.22	245.0803	1	25646	11.423	97.44
10-hydroxy-8E-Decene-2,4,6-triynoic acid	-2.41	177.055	1	199808	11.423	49
3,3,45-Tetrahydroxystilbene	4.79	245.0797	1	27940	11.425	88.63
10-hydroxy-8E-Decene-2,4,6-triynoic acid	-2.78	177.0551	1	155341	11.426	48.68
3,3,45-Tetrahydroxystilbene	-1.52	245.0812	1	30066	11.429	98.8
10-hydroxy-8E-Decene-2,4,6-triynoic acid	-3.22	177.0552	1	311843	11.429	48.23
3,3,45-Tetrahydroxystilbene	3.91	245.0799	1	33974	11.436	92.29
3,3,45-Tetrahydroxystilbene	-0.14	245.0809	1	13824	11.446	99.99
10-hydroxy-8E-Decene-2,4,6-triynoic acid	-1.83	177.0549	1	180993	11.448	49.42
10-hydroxy-8E-Decene-2,4,6-triynoic acid	-2.61	177.0551	1	176640	11.449	48.83
3,3,45-Tetrahydroxystilbene	-1.66	245.0812	1	19699	11.453	98.56
10-hydroxy-8E-Decene-2,4,6-triynoic acid	-3.97	177.0553	1	236324	11.457	47.34
3,3,45-Tetrahydroxystilbene	1.28	245.0805	1	25421	11.466	99.14
10-hydroxy-8E-Decene-2,4,6-triynoic acid	-0.96	177.0548	1	101081	11.492	49.84
methyl 8-[3,5-epidioxy-2-(3-hydroperoxy-1-pentenyl)-	-3.97	397.26	1	15817	11.556	87

cyclopentyl]-octanoate						
Met Arg Met	1.93	437.1991	1	17371	11.567	96.49
methyl 8-[3,5-epidioxy-2-(3-hydroperoxy-1-pentenyl)-cyclopentyl]-octanoate	-3.4	397.2598	1	14229	11.568	90.28
methyl 8-[3,5-epidioxy-2-(3-hydroperoxy-1-pentenyl)-cyclopentyl]-octanoate	-3.97	397.26	1	11806	11.578	43.51
Met His Lys	-4.58	415.2141	1	167764	11.588	41.22
Met His Lys	-5	415.2143	1	203623	11.591	39.75
Met Arg Met	4.2	437.1981	1	14184	11.602	84.33
methyl 8-[3,5-epidioxy-2-(3-hydroperoxy-1-pentenyl)-cyclopentyl]-octanoate	-3.62	397.2599	1	15328	11.602	89.09
Met Arg Met	3.12	437.1986	1	11326	11.609	91.06
Met Arg Met	1.09	437.1994	1	15582	11.62	98.87
Rifabutin	-2.31	847.4507	1	32216	11.624	91.91
C17 Sphinganine	-4.69	288.2911	1	17371	11.769	87.01
C17 Sphinganine	1.91	288.2892	1	13169	11.815	97.72
Beclomethasone	-2.2	409.1785	1	15794	11.85	95.72
Beclomethasone	-1.17	409.1781	1	16486	11.858	98.77
Arg Gln Thr	4.35	404.2235	1	605041	11.862	42.19
Beclomethasone	-1.07	409.1781	1	16853	11.869	98.97
Beclomethasone	-1.97	409.1784	1	19211	11.872	96.53
Beclomethasone	-1.17	409.1781	1	16829	11.875	98.77
Arg Gln Thr	4.18	404.2235	1	419768	11.877	42.76
Arg Gln Thr	3.53	404.2238	1	537361	11.881	44.7
C17 Sphinganine	-3.66	288.2908	1	9680	11.882	91.86
Arg Gln Thr	3.28	404.2239	1	639689	11.882	45.4
Allocortol	-4.72	369.2653	1	8925	11.887	83.28

Arg Gln Thr	1.09	404.2248	1	666542	11.891	49.47
Arg Gln Thr	3.22	404.2239	1	479006	11.892	45.56
Pro Arg Asp	4.23	387.1971	1	618032	11.898	42.87
Allocortol	-4.45	369.2652	1	7689	11.898	84.97
Arg Gln Thr	0.02	404.2252	1	712297	11.899	50
Beclomethasone	-3.2	409.1789	1	15994	11.901	91.13
Arg Gln Thr	-1.16	404.2257	1	848057	11.904	49.4
Pro Arg Asp	3.41	387.1974	1	647407	11.905	45.23
Allocortol	-3.74	369.2649	1	9753	11.906	89.14
Arg Gln Thr	2.22	404.2243	1	655499	11.911	47.84
Beclomethasone	-3.67	409.1791	1	18302	11.913	88.52
Pro Arg Asp	1.79	387.198	1	883980	11.913	48.64
Arg Gln Thr	1.33	404.2247	1	707546	11.923	49.21
10-keto tridecanoic acid	-1.79	229.1802	1	12699	11.924	98.45
Arg Gln Thr	-1.31	404.2257	1	677252	11.927	49.24
Pro Arg Asp	2.22	387.1979	1	621089	11.931	47.92
10-keto tridecanoic acid	-3.39	229.1806	1	15047	11.946	94.59
2-amino-tetradecanoic acid	-4.12	244.2281	1	16455	12.015	91.49
2-amino-tetradecanoic acid	-4.97	244.2283	1	20576	12.02	87.88
5,8-tetradecadienal	-2.06	209.1904	1	13781	12.025	98.19
5,8-tetradecadienal	-2.01	209.1904	1	19951	12.026	98.26
5,8-tetradecadienal	-3.43	209.1907	1	16255	12.03	95.04
5,8-tetradecadienal	-2.39	209.1905	1	14967	12.042	97.56
Met Trp Glu	-3.29	465.1818	1	11869	12.045	89.55
Met Trp Glu	-3.24	465.1817	1	20977	12.046	89.85

Met Trp Glu	-2.63	465.1815	1	18523	12.05	93.18
2-amino-tetradecanoic acid	-3.19	244.2279	1	39522	12.057	47.41
Tetradecylamine	-4.08	214.2538	1	52097	12.069	46.42
5,8-tetradecadienal	-3.11	209.1906	1	14687	12.07	95.91
Tetradecylamine	-3.55	214.2537	1	46011	12.072	94.55
Tetradecylamine	-1.97	214.2533	1	11758	12.081	98.28
Met Trp Glu	-4.27	465.1822	1	17281	12.086	83.07
Tetradecylamine	-1.73	214.2533	1	32442	12.099	49.33
Pregnenolone sulfate	2.35	397.2034	1	8572	12.129	95.24
N-HISTIDYL-2-AMINONAPHTHALENE (betaNA)	-1.91	281.1402	1	17378	12.131	97.77
N-HISTIDYL-2-AMINONAPHTHALENE (betaNA)	-0.84	281.1399	1	23630	12.133	99.56
Met His Lys	-2.91	415.2134	1	228006	12.137	46.26
Pregnenolone sulfate	2.42	397.2034	1	15076	12.14	94.95
N-HISTIDYL-2-AMINONAPHTHALENE (betaNA)	-1.47	281.1401	1	23611	12.143	98.67
N-HISTIDYL-2-AMINONAPHTHALENE (betaNA)	-1.28	281.14	1	18612	12.144	99
N-HISTIDYL-2-AMINONAPHTHALENE (betaNA)	-1.64	281.1401	1	17582	12.147	98.36
Pregnenolone sulfate	-0.93	397.2047	1	11810	12.156	99.25
N-HISTIDYL-2-AMINONAPHTHALENE (betaNA)	-4.63	281.141	1	23888	12.16	87.64
Pregnenolone sulfate	1.38	397.2038	1	10450	12.17	98.33
Pregnenolone sulfate	-4.5	397.2061	1	19756	12.175	83.64
Pregnenolone sulfate	0.67	397.2041	1	17048	12.18	99.6
Pregnenolone sulfate	-0.19	397.2044	1	12700	12.187	99.97

N-HISTIDYL-2-AMINONAPHTHALENE (betaNA)	-2.66	281.1404	1	20612	12.187	95.73
N-HISTIDYL-2-AMINONAPHTHALENE (betaNA)	-3.55	281.1407	1	27065	12.208	92.51
4-hydroxy lauric acid	-4.05	217.1807	1	20991	12.249	92.83
9-Hydroxyfluorene	-2.83	183.081	1	43556	12.261	97.13
9-Hydroxyfluorene	-3.18	183.081	1	34790	12.264	96.4
4-hydroxy lauric acid	-3.59	217.1806	1	26714	12.271	94.31
9-Hydroxyfluorene	-0.22	183.0805	1	19772	12.272	99.98
Met Arg Met	2.53	437.1988	1	23364	12.294	94.03
9-Hydroxyfluorene	-4.38	183.0812	1	31850	12.298	93.27
1-Hexadecylamine	-4.89	242.2854	1	67331	12.299	88.34
1-Hexadecylamine	-4.5	242.2853	1	38293	12.3	90.03
1-Hexadecylamine	-2.44	242.2848	1	41140	12.302	96.95
1-Hexadecylamine	-2.56	242.2848	1	31770	12.305	48.33
1-Hexadecylamine	-3.03	242.285	1	39992	12.306	95.36
9-Hydroxyfluorene	-4.39	183.0812	1	61720	12.317	93.24
n-Pentadecylamine	-3.36	228.2693	1	22436	12.317	94.72
n-Pentadecylamine	-4.28	228.2695	1	12922	12.339	91.55
13R-hydroxy-9E,11Z-octadecadienoic acid	-4.58	297.2438	1	20017	12.361	87.15
PGC1	1.58	337.2368	1	19751	12.367	98.15
CARYOPHYLLENE [t(-)]	-2.47	191.1799	1	65989	12.372	48.84
PGC1	1.84	337.2367	1	24952	12.375	97.49
13R-hydroxy-9E,11Z-octadecadienoic acid	-4.22	297.2437	1	27542	12.378	89
CARYOPHYLLENE [t(-)]	-2.38	191.1799	1	110411	12.381	48.92
CARYOPHYLLENE [t(-)]	-0.69	191.1796	1	62153	12.383	49.91

CARYOPHYLLENE [t(-)]	-0.34	191.1795	1	44582	12.384	49.98
PGC1	1.32	337.2369	1	13953	12.385	98.7
CARYOPHYLLENE [t(-)]	-0.76	191.1796	1	52368	12.386	49.89
3Z,9Z-hexadecadienoic acid	-4.75	253.2174	1	36177	12.387	88.4
13R-hydroxy-9E,11Z-octadecadienoic acid	-3.25	297.2434	1	11368	12.389	93.31
5,8-tetradecadienal	-0.03	209.19	1	5815	12.389	100
5,8-tetradecadienal	-4.03	209.1908	1	11610	12.394	93.21
CARYOPHYLLENE [t(-)]	-3.45	191.1801	1	63080	12.395	47.76
PGC1	0.61	337.2371	1	17927	12.397	99.72
3Z,9Z-hexadecadienoic acid	-2.41	253.2168	1	38041	12.397	96.88
3Z,9Z-hexadecadienoic acid	-3.56	253.2171	1	21878	12.397	93.33
p-Cymene	2.16	135.1165	1	10611	12.399	98.9
8-hydroxy-9,11-octadecadiynoic acid	1.02	293.2108	1	8644	12.402	99.32
3Z,9Z-hexadecadienoic acid	-3.72	253.2171	1	34645	12.404	92.72
PGC1	2.8	337.2364	1	13852	12.405	94.3
PGC1	1.08	337.237	1	19405	12.411	99.12
PGC1	-1.83	337.238	1	18916	12.412	97.51
3Z,9Z-hexadecadienoic acid	-1.66	253.2166	1	24215	12.413	49.26
PGC1	1.86	337.2367	1	11262	12.414	97.45
PGC1	0.23	337.2373	1	17840	12.416	99.96
CARYOPHYLLENE [t(-)]	-3.98	191.1802	1	51532	12.419	94.09
PGC1	-3.1	337.2384	1	16088	12.42	93.06
PGC1	-4.86	337.239	1	12834	12.426	83.76
PGC1	3.37	337.2362	1	21979	12.435	45.91
AVOCADENE ACETATE	-4.72	329.2702	1	15951	12.47	84.95

Rutin	0.63	611.1603	1	38670	12.476	99.49
Rutin	4.54	611.1579	1	21695	12.485	76.95
4-hydroxy lauric acid	-4.12	217.1807	1	28249	12.489	92.61
Rutin	2.58	611.1591	1	29953	12.489	91.88
AVOCADENE ACETATE	-3.59	329.2698	1	22507	12.493	90.99
Rutin	0.5	611.1604	1	66541	12.497	99.68
Rutin	1.16	611.16	1	49311	12.497	49.15
Rutin	-2.17	611.162	1	51315	12.506	94.18
Rutin	-2.12	611.162	1	48478	12.508	94.47
AVOCADENE ACETATE	-4.81	329.2702	1	26746	12.517	84.44
Rutin	0.17	611.1606	1	50904	12.532	49.98
Rutin	-2.99	611.1625	1	63624	12.539	89.26
Rutin	-0.6	611.161	1	51520	12.544	99.54
4-hydroxy lauric acid	-4.09	217.1807	1	28062	12.55	92.7
7-lauroleic acid	-4.59	199.1702	1	17168	12.567	91.82
4-hydroxy lauric acid	-2.62	217.1804	1	20118	12.571	96.94
4-hydroxy lauric acid	-2.05	217.1803	1	28315	12.571	98.1
4-hydroxy lauric acid	-3.6	217.1806	1	23386	12.582	94.29
AVOCADENE ACETATE	-4.56	329.2701	1	29016	12.591	85.9
4'-HYDROXYCHALCONE	-3.91	225.0919	1	33765	12.608	46.5
2-amino-tetradecanoic acid	-3.16	244.2279	1	11070	12.61	94.91
2-amino-tetradecanoic acid	-2.74	244.2278	1	10517	12.618	96.13
4'-HYDROXYCHALCONE	-4.23	225.092	1	19588	12.62	91.87
Fexofenadine	-4.87	502.2976	1	22074	12.667	77.25
decoquinate	-2.6	418.2599	1	6098	12.739	93.95

Arachidonyl lysolecithin	-2.55	544.3412	1	6167	12.743	92.73
decoquinate	-3.08	418.2601	1	7526	12.753	91.62
decoquinate	-4.51	418.2607	1	6351	12.755	82.84
AMBELLINE	3.17	332.1482	1	16435	12.852	92.86
DEOXYSAPPANONE B 7,3'-DIMETHYL ETHER	0.75	315.1225	1	10075	12.853	99.61
Thr Pro Asp	0.37	332.1451	1	7153	12.867	99.9
Dihydropteroic acid	-4	315.1213	1	8820	12.877	89.43
Thr Pro Asp	-0.17	332.1453	1	10979	12.882	99.98
Thr Pro Asp	0.83	332.145	1	10153	12.887	99.5
Ciprofloxacin	-3.83	332.1418	1	12884	12.904	89.74
DEOXYSAPPANONE B 7,3'-DIMETHYL ETHER	1.2	315.1223	1	15157	12.907	98.99
AMBELLINE	2.87	332.1483	1	14851	12.909	94.1
Thr Pro Asp	-4.75	332.1468	1	28287	12.913	84.64
AMBELLINE	4.43	332.1478	1	17338	12.919	86.52
DEOXYSAPPANONE B 7,3'-DIMETHYL ETHER	1.98	315.1221	1	10222	12.924	97.31
8-methoxy-13-hydroxy-9,11-octadecadienoic acid	-3.8	327.2542	1	18437	12.94	45.02
sn-1,2-Dioctanoylglycerol	-4.92	345.2652	1	43342	12.948	41.5
8-methoxy-13-hydroxy-9,11-octadecadienoic acid	-3.7	327.2542	1	22067	12.949	45.26
sn-1,2-Dioctanoylglycerol	-4.82	345.2652	1	51193	12.955	41.84
Allocortolone	2.71	367.2469	1	25868	12.956	47.09
Allocortolone	1.68	367.2473	1	23816	12.964	48.86
8-methoxy-13-hydroxy-9,11-octadecadienoic acid	-4.65	327.2545	1	20153	12.977	85.46
Allocortolone	-0.06	367.2479	1	31439	12.98	50
Allocortolone	-1.34	367.2484	1	30789	12.982	98.53
Allocortolone	0.78	367.2476	1	29994	12.982	99.51

8-methoxy-13-hydroxy-9,11-octadecadienoic acid	-4.84	327.2546	1	39740	12.983	42.17
Allocortolone	1.73	367.2473	1	24698	12.992	48.79
Allocortolone	-2.41	367.2488	1	39204	12.996	47.68
Allocortolone	0.7	367.2476	1	25784	13.018	99.6
Allocortolone	-3.46	367.2492	1	35994	13.028	90.66
Allocortolone	-0.91	367.2482	1	35756	13.034	49.67
Allocortolone	-4.62	367.2496	1	30484	13.037	84.02
1-Hexadecylamine	-4.85	242.2854	1	17077	13.139	88.52
1-Hexadecylamine	-4.3	242.2853	1	14365	13.182	90.87
GPEtnNMe(16:0/18:1(9Z))[U]	2.49	732.552	1	15119	13.228	91.44
Val His Asn	3.9	369.1867	1	44808	13.298	88.27
Arg Pro Asn	1.85	386.2139	1	140014	13.306	48.55
Val His Asn	4.47	369.1864	1	32480	13.308	84.87
Arg Pro Asn	2.86	386.2135	1	108819	13.308	46.6
Arg Pro Asn	4.87	386.2128	1	100555	13.321	40.77
Trp Trp Val	0.3	490.2447	1	5943	13.588	99.91
Trp Trp Val	-0.33	490.245	1	7049	13.604	99.88
Trp Trp Val	-3.9	490.2468	1	9682	13.607	85.05
Trp Trp Val	-3.36	490.2465	1	10097	13.618	88.65
Dihydrolevobunolol	-3.87	294.2075	1	32636	13.618	45.37
Trp Trp Val	-4.72	490.2472	1	6716	13.621	78.86
Dihydrolevobunolol	-4.98	294.2078	1	19740	13.63	42.56
Trp Trp Val	-2.5	490.2461	1	6941	13.632	93.57
Dihydrolevobunolol	-3.81	294.2075	1	16069	13.639	45.52
Trp Trp Val	-3.95	490.2468	1	8723	13.651	84.68

Trp Trp Val	-3.67	490.2467	1	10997	13.661	86.62
Docosanamide	-2.59	340.3583	1	13617	13.696	47.52
Natamycin	1.49	666.311	1	16422	13.71	97.05
Gualenate (Sodium Gualenate)	0.27	279.1049	1	29268	13.714	99.96
Gualenate (Sodium Gualenate)	2.32	279.1043	1	30157	13.717	96.77
Gualenate (Sodium Gualenate)	4.87	279.1036	1	34255	13.718	43.24
2,15-dihydroxy-pentadecylic acid	-3.63	275.2227	1	9479	13.729	92.39
Gualenate (Sodium Gualenate)	3.14	279.1041	1	18828	13.739	94.17
Gualenate (Sodium Gualenate)	-0.82	279.1052	1	26641	13.74	99.59
Natamycin	-0.2	666.3122	1	16991	13.74	99.95
Gualenate (Sodium Gualenate)	-0.71	279.1051	1	63273	13.741	49.84
2,15-dihydroxy-pentadecylic acid	-4.72	275.223	1	24312	13.742	43.73
2,15-dihydroxy-pentadecylic acid	-3.12	275.2225	1	7275	13.747	94.31
Gualenate (Sodium Gualenate)	2.82	279.1042	1	28908	13.756	47.63
Trp Pro Pro	2.75	399.2016	1	10342	13.821	93.52
Trp Pro Pro	0.59	399.2024	1	9700	13.83	99.69
Trp Pro Pro	-4.55	399.2045	1	10630	13.833	83.22
Docosanamide	-3.66	340.3586	1	11825	13.841	90.38
1-Octadecanamine	-4.25	270.3167	1	15820	13.847	89.9
GPGro(14:0/0:0)[U]	4.19	457.2542	1	5304	13.878	83.84
GPGro(14:0/0:0)[U]	-1.13	457.2566	1	5700	13.89	98.72
PGF2alpha isopropyl ester	0.87	397.2945	1	5931	13.909	49.67
1-(11E-octadecenoyl)-rac-glycerol	-3.87	357.3013	1	33507	13.999	44.39
1-(11E-octadecenoyl)-rac-glycerol	-4.24	357.3014	1	31551	14.011	43.34
PGF2alpha isopropyl ester	1.5	397.2943	1	10214	14.016	98.03

1-(11E-octadecenoyl)-rac-glycerol	-4.82	357.3017	1	17346	14.023	41.56
PGF2alpha isopropyl ester	-0.88	397.2952	1	9409	14.066	99.32
PGF2alpha isopropyl ester	-2.37	397.2958	1	6621	14.069	95.15
PGF2alpha isopropyl ester	-2.69	397.2959	1	11090	14.111	93.81
Dihydrolevobunolol	-3.89	294.2075	1	14508	14.175	90.66
2-ISOPROPYL-3-METHOXYCINNAMIC ACID	-3.13	221.1179	1	92508	14.327	47.78
2-ISOPROPYL-3-METHOXYCINNAMIC ACID	-2.43	221.1178	1	51940	14.333	48.65
cyclandelate	-2.34	277.1805	1	68188	14.34	48.37
2-ISOPROPYL-3-METHOXYCINNAMIC ACID	-1.29	221.1175	1	39703	14.341	49.61
cyclandelate	-4.23	277.181	1	102743	14.343	44.86
GPEtn(16:0/18:2(9Z,12Z))	2.31	716.5208	1	5951	14.346	92.68
2-ISOPROPYL-3-METHOXYCINNAMIC ACID	-4.75	221.1183	1	77376	14.347	45.04
2-ISOPROPYL-3-METHOXYCINNAMIC ACID	-4.79	221.1183	1	85145	14.369	44.96
Gemeprost	-1.9	395.2799	1	15781	14.408	96.88
Gemeprost	-1.82	395.2799	1	24489	14.421	97.12
Arg Pro Asn	2.09	386.2138	1	7550	14.451	96.34
Gemeprost	-0.22	395.2793	1	13229	14.454	99.96
Gemeprost	0.33	395.2791	1	14026	14.467	99.9
Gemeprost	1.54	395.2786	1	5264	14.506	97.95
Gemeprost	-0.47	395.2794	1	7759	14.555	99.81
Gemeprost	1.77	395.2785	1	10154	14.595	48.64
Zopiclone	-4.87	389.1142	1	14383	14.636	81.45
Zopiclone	-0.61	389.1126	1	7943	14.64	99.68
Pregnenolone sulfate	1.5	397.2037	1	9920	14.912	98.04
Pregnenolone sulfate	1.44	397.2038	1	48999	14.925	98.19

Pregnenolone sulfate	2.3	397.2034	1	34216	14.925	95.44
Pregnenolone sulfate	1.92	397.2036	1	17316	14.929	96.8
Pregnenolone sulfate	-0.99	397.2047	1	51241	14.93	99.15
Pregnenolone sulfate	2.33	397.2034	1	38790	14.931	95.34
GPA(18:0/22:6(4Z,7Z,10Z,13Z,16Z,19Z))	2.81	749.5095	1	7617	14.951	89.11
GPA(18:0/22:6(4Z,7Z,10Z,13Z,16Z,19Z))	4.87	749.5079	1	11552	14.952	70.66
Pregnenolone sulfate	-2.65	397.2054	1	135221	14.954	94.01
GPA(18:0/22:6(4Z,7Z,10Z,13Z,16Z,19Z))	-0.32	749.5118	1	8164	14.959	99.85
Pregnenolone sulfate	-2.76	397.2054	1	64425	14.966	93.51
Pregnenolone sulfate	2.15	397.2035	1	54342	14.972	95.99
GPA(18:0/22:6(4Z,7Z,10Z,13Z,16Z,19Z))	-0.3	749.5118	1	35311	14.976	99.87
Pregnenolone sulfate	0.96	397.2039	1	58418	14.977	99.2
GPA(18:0/22:6(4Z,7Z,10Z,13Z,16Z,19Z))	-0.32	749.5118	1	16754	14.98	99.85
GPA(18:0/22:6(4Z,7Z,10Z,13Z,16Z,19Z))	4.98	749.5079	1	12132	14.986	69.55
GPA(18:0/22:6(4Z,7Z,10Z,13Z,16Z,19Z))	3.18	749.5092	1	15004	14.99	86.26
Nanoxynol	-3.27	617.4279	1	11325	15.11	87.22
Nanoxynol	-3.49	617.4281	1	16676	15.119	85.6
Nanoxynol	-3.59	617.4281	1	6623	15.127	84.82
Nanoxynol	-4.46	617.4287	1	29021	15.129	77.52
50oxo-ETE-d7	-4	326.272	1	9257	15.478	89.06
Simvastatin	-3.39	419.2806	1	8322	15.521	89.9
Simvastatin	-4.28	419.281	1	6749	15.535	84.38
Simvastatin	-2.56	419.2803	1	10341	15.557	94.09
GPEtnNMe(16:0/18:1(9Z))[U]	-1.49	732.5549	1	11269	15.625	96.85
GPEtnNMe(16:0/18:1(9Z))[U]	1	732.5531	1	25275	15.628	49.29

GPEtnNMe(16:0/18:1(9Z))[U]	2.81	732.5517	1	6546	15.647	89.23
Val Val Trp	1.24	403.2335	1	12832	15.818	49.32
Val Val Trp	-0.96	403.2344	1	9461	15.825	49.59
Val Val Trp	-0.83	403.2343	1	9051	15.832	49.69
Val Val Trp	-3.01	403.2352	1	9323	15.835	46.11
Val Val Trp	-3.74	403.2355	1	10743	15.857	88.25
Hexadecanedioic acid	-3.93	287.2228	1	9444	15.88	90.71
54:3 SLBPA	-1.03	520.401	2	8212	16.553	98.16
methyl 9,10-epoxy-12,15-octadecadienoate	-1.2	309.2428	1	6743	16.601	49.51
7,11-hexadecadien-1-ol	-3.94	239.2379	1	29052	17.624	46.18
1-O-(1Z-tetradecenyl)-2-(9Z-octadecenoyl)-sn-glycerol	-1.81	551.5044	1	10434	17.657	96.21
Oleamide	-4	282.2804	1	29457	18.936	45.29
1-heptadecanoyl-rac-glycerol	-4.32	345.3014	1	80440	18.99	43.33
7,11-hexadecadien-1-ol	0.94	239.2367	1	9268	19.148	99.55
3-methyl-pentadecanoic acid	-1	257.2478	1	11089	19.156	99.45
11-deoxy-16,16-dimethyl-PGE2	2.11	365.2679	1	5224	19.182	96.43
Eicosanedioic acid	-4.02	343.2857	1	10743	19.183	88.4
20-oxo-heneicosanoic acid	-2.55	341.3059	1	50959	19.795	47.59
1a,1b-dihomo-15-deoxy-delta-12,14-PGD2	-4.46	363.2546	1	15551	20.013	85.13
1-octadecanoyl-rac-glycerol	-4.71	359.3173	1	7943	20.596	41.89
1-octadecanoyl-rac-glycerol	-1.72	359.3162	1	6076	20.615	48.82
24-Nor-5beta-cholane-3alpha,7alpha,12alpha,23-tetrol	2.66	381.2989	1	9412	20.622	47.08
24-Nor-5beta-cholane-3alpha,7alpha,12alpha,23-tetrol	3.14	381.2987	1	12831	20.626	45.99
24-Nor-5beta-cholane-3alpha,7alpha,12alpha,23-tetrol	-2.38	381.3008	1	11096	20.634	95.3
24-Nor-5beta-cholane-3alpha,7alpha,12alpha,23-tetrol	-1.32	381.3004	1	15056	20.635	49.27

20-oxo-heneicosanoic acid	-2.92	341.306	1	131491	20.64	46.86
24-Nor-5beta-cholane-3alpha,7alpha,12alpha,23-tetrol	-1.55	381.3005	1	13439	20.644	48.99
24-Nor-5beta-cholane-3alpha,7alpha,12alpha,23-tetrol	-1.82	381.3006	1	12280	20.645	97.23
3E,13Z-octadecadien-1-ol	-2.41	267.2689	1	15486	20.655	48.33
24-Nor-5beta-cholane-3alpha,7alpha,12alpha,23-tetrol	1.53	381.2994	1	13020	20.655	49.02
24-Nor-5beta-cholane-3alpha,7alpha,12alpha,23-tetrol	0.34	381.2998	1	7553	20.657	49.95
24-Nor-5beta-cholane-3alpha,7alpha,12alpha,23-tetrol	2.01	381.2992	1	18841	20.681	48.31
24-Nor-5beta-cholane-3alpha,7alpha,12alpha,23-tetrol	1.9	381.2992	1	148529	20.684	48.5
24-Nor-5beta-cholane-3alpha,7alpha,12alpha,23-tetrol	-0.92	381.3003	1	11118	20.717	99.28
24-Nor-5beta-cholane-3alpha,7alpha,12alpha,23-tetrol	0.67	381.2997	1	14180	20.717	49.81
1-octadecanoyl-rac-glycerol	-4.95	359.3174	1	20865	20.72	41.12
Stearamide	-3.96	284.2959	1	21448	21.952	45.35
TG(20:3(8Z,11Z,14Z)/20:4(5Z,8Z,11Z,14Z)/22:5(7Z,10Z,13Z,16Z,19Z))[iso6]	1.78	490.3902	2	7948	21.996	94.74
GPA(18:0/18:0)[U]	-0.14	705.543	1	5632	23.334	99.97

Table S4. Putative metabolite identifications by accurate mass with METLIN search.

	Retention Time	Retention Time	Mass	Mass	Abundance	Abundance	
Feature ID	Value	Standard Deviation	Value	Standard Deviation	Value	Relative Standard Deviation	Number of replicates detected
1	5.173	0.072	2299.421	0.0082	10712300	1.76	11
2	4.966	0.089	1950.26	0.0033	3383959	0.95	11
3	9.525	0.01	5105.319	0.0111	1985346	1.2	7
4	5.074	0.089	2044.262	0.0071	1814915	1.66	10
5	5.369	0.053	4616.801	0.0093	1403083	1.25	9
6	6.725	0.049	2990.891	0.0061	1063425	1.02	8
7	7.187	0.038	2718.765	0.0109	783807.2	1.62	8
8	6.323	0.064	2027.31	0.0034	759346.6	1.52	9
9	7.07	0.052	4000.529	0.0088	645555.9	1.78	7
10	6.466	0.077	2311.426	0.0049	508573.8	1.09	9
11	5.064	0.083	1713.164	0.0025	431022.8	1.54	9
12	4.894	0.106	1216.723	0.0042	302935.8	0.95	11
13	4.194	0.083	1223.802	0.0026	202507.2	1.3	8
14	6.675	0.047	3380.156	0.0091	181467.8	1.02	8
15	4.864	0.069	1328.849	0.0026	167090.9	2.19	7
16	8.03	0.007	388.2251	0.001	135835.5	0.85	9
17	7.437	0.02	334.1449	0.0006	91489.84	1.05	8
18	9.496	0.006	516.2809	0.0011	83118.66	0.86	8

19	9.495	0.006	534.2933	0.0009	81963.34	0.92	8
20	7.794	0.008	292.131	0.0008	75743.84	0.79	9
21	7.332	0.009	298.1868	0.0006	68577.66	0.95	7
22	9.439	0.009	490.2644	0.0014	56360.92	0.88	8

Table S5a. Quantitation by features in peptide detection SCX runs. Averages across all runs.

			Abundance	Abundance	
Feature ID	Retention Time	Mass	Value	Relative Standard Deviation	Number of replicates detected
1	5.143	2299.4211	19743080	1.22	5
2	4.925	1950.26	3872292	0.92	5
3	9.525	5105.3222	256379.7	2.45	1
4	5.044	2044.2621	3147434	1.23	6
5	5.344	4616.804	771782.2	1.52	3
6	6.707	2990.8882	674499.7	1.66	2
7	7.178	2718.766	403623.8	2.29	2
8	6.322	2027.312	307694.8	1.14	3
9	6.997	4000.5272	63567.5	2.45	1
10	6.42	2311.4268	236574.2	1.35	3
11	5	1713.1632	485356.3	1.67	3
12	4.859	1216.7226	380874.3	1	6
13	4.198	1223.8012	152642.7	1.88	2
14	6.655	3380.1521	142568.8	1.56	2
15	4.869	1328.8475	22501.33	2.45	1
16	8.029	388.2248	84382	1.56	3
17	7.444	334.1451	61107	1.61	2
18	9.492	516.2816	41529.33	1.69	2
19	9.492	534.2935	26942.67	1.64	2
20	7.797	292.131	58045.17	1.36	3
21	7.339	298.1874	28566.67	2.45	1

22	9.429	490.2657	22861.67	1.57	2

Table S5b. Quantitation by features in peptide detection SCX runs. Experimental (infected) samples.

			Abundance	Abundance	
ID	Retention Time	Mass	Value	Relative Standard Deviation	Number of replicates detected
1	5.199	2299.4207	1681507	1.29	6
2	4.999	1950.2598	2895625	1.06	6
3	9.525	5105.3184	3714313	0.59	6
4	5.12	2044.2617	482395.7	1.75	4
5	5.381	4616.7999	2034384	1.04	6
6	6.731	2990.8912	1452350	0.68	6
7	7.189	2718.7644	1163991	1.31	6
8	6.324	2027.3094	1210998	1.25	6
9	7.082	4000.5294	1227544	1.18	6
10	6.489	2311.425	780573.5	0.81	6
11	5.097	1713.1648	376689.3	1.48	6
12	4.937	1216.7227	224997.3	0.67	5
13	4.193	1223.8021	252371.7	1.01	6
14	6.681	3380.1575	220366.8	0.67	6
15	4.863	1328.8494	311680.5	1.58	6
16	8.031	388.2253	187289	0.41	6
17	7.434	334.1448	121872.7	0.76	6
18	9.498	516.2807	124708	0.37	6
19	9.496	534.2932	136984	0.43	6
20	7.793	292.1311	93442.5	0.31	6
21	7.33	298.1867	108588.7	0.21	6
22	9.442	490.2639	89860.16	0.42	6

Table S5c. Quantitation by features in peptide detection SCX runs. Uninfected samples.

	Difference	Difference			
ID	Retention Time	Mass	log2 of fold change	Directionality	Difference Score (Mass Profiler)
1	0.055	-0.0004	3.55	up	90.201
2	0.074	-0.0002	0.42	up	37.7258
3	0	-0.0038	-3.86	down	99.5874
4	0.076	-0.0004	2.71	up	86.9826
5	0.037	-0.0041	-1.4	down	77.0709
6	0.024	0.003	-1.11	down	76.8964
7	0.011	-0.0016	-1.53	down	67.8575

8	0.001	-0.0026	-1.98	down	81.4423
9	0.085	0.0022	-4.27	down	92.2189
10	0.069	-0.0018	-1.72	down	91.0606
11	0.096	0.0016	0.37	up	20.8016
12	0.078	0.0001	0.76	up	62.5016
13	-0.005	0.0009	-0.73	down	46.1446
14	0.026	0.0055	-0.63	down	50.8959
15	-0.006	0.0019	-3.79	down	81.6749
16	0.002	0.0005	-1.15	down	87.0767
17	-0.011	-0.0002	-1	down	70.448
18	0.006	-0.0009	-1.59	down	96.4052
19	0.004	-0.0002	-2.35	down	99.5737
20	-0.004	0.0001	-0.69	down	67.3768
21	-0.009	-0.0008	-1.93	down	97.6409
22	0.013	-0.0017	-1.97	down	99.009

Table S5d. Quantitation by features in peptide detection SCX runs. Control vs infected comparison.

Table S5. Peptide features extracted for high salt runs. Nanoflow-SCX high salt elution runs were profiled for endogenous peptide features, and retention time and peak areas were quantified by MassHunter.

Supplemental Methods.

Animal Infection Protocol

Six juvenile pigtailed macaques (*Macaca nemestrina*) were infected with SIV by intravenous inoculation with both an immunosuppressive swarm (SIV/DeltaB670) at a dose of 10,000 times 50% animal infectious dose and a neurovirulent clone (SIV/17E-Fr) at a dose of 50 times 50% animal infectious dose, as described previously.(Clements et al., 2008) Sacrifice and necropsy were at 7 days post-infection. Negative controls were six juvenile pigtailed macaques, mock inoculated with PBS and then sacrificed. Spleen tissue samples were collected from all 12 macaques and fresh frozen. Animal protocols were approved by the Johns Hopkins University Institutional Animal Care and Use

Committee in accordance with Animal Welfare Act regulations and the USPHS Policy on Humane Care and Use of Laboratory Animals.

Animal Studies Ethics Statement

"Animal studies were approved by the Johns Hopkins Animal Care and Use Committee (IACUC protocol #PR12M310); animals were humanely treated in accordance with federal guidelines and institutional policies. Pigtailed macaques (Macaca nemestrina) used in this study were obtained from nonhuman primate breeding facilities within the United States, and were housed in Johns Hopkins University facilities that are fully accredited by the association for the Assessment and Accreditation of Laboratory Animal Care, International (AALAC). All housing met or exceeded guidelines of the National Institutes of Health "Guide for the Care and Use of Laboratory Animals" and the United States Department of Agriculture Animal Welfare Act. Macaques were fed a balanced, commercial macaque chow (Purina Mills, Gray Summit, MO, USA) once a day supplemented with a variety of food enrichment."

Tissue Sample Collection and Preparation

Miltex 3 mm biopsy punches of fresh-frozen spleens were resuspended in 500 µL 0.1% ascorbic acid in a 1 mL Kontes Duall Tissue Grinder, and homogenized by hand for 10 minutes. Metabolites were extracted by a modified(Sana & Fischer, 2007) Bligh-Dyer protocol: 150 µL homogenate was added to 600 µL methanol at -20°C. 450 µL room-temperature chloroform was then added, and the solution vortexed and returned to an ice bath. The solution was then vortexed every 5 minutes for 30 minutes, returning to the ice bath each time. At the penultimate step, 150 µL ice cold MilliQ water was added, and samples were maintained at -20°C for 2 hours to create phase separation. The upper (aqueous) phase was then collected.

Next, in order to maximize metabolite yield, the above extraction procedure was repeated with 2% ammonium hydroxide at pH 9, and with 1% formic acid at pH 2. Specifically, the organic phase from the first extraction was dried and then resuspended in water. The methanol and chloroform steps were repeated as above, and then the pH 9 buffer was added to create the phase. The aqueous phase following this step was collected, and the procedure was repeated with a buffer at pH 2. All three extractions were filtered with a 50,000 MWCO to remove large particulates, and flowthroughs were combined, dried, and resuspended in 2% ACN/0.1% FA for HPLC-MS analysis.

Protein Normalization for Quantitative Profiling

For quantitative metabolite profiling, protein amounts in each homogenate were estimated by a modified Lowry method after a deoxycholate precipitation (2D Quant Kit, GE Healthcare). Protein estimations were confirmed by 1D gel electrophoresis and SYPRO Ruby (Life Technologies) staining. For gels, 2 µg sample was combined with 2.5 µL SDS sample buffer, and 1 µL 100mM DTT, and the final solution diluted up to 10 µL with MilliQ water. Running buffer was prepared by diluting MES SDS running buffer (Life Technologies) 1:20 in MilliQ water with 20% methanol. Samples were denatured for 10 minutes at 70°C, and run for ~40 minutes at 200 V constant voltage.

Chapter 3. Micropeptidomics by RNAseq and proteomics.

Introduction

In the previous chapter, we have developed a high-sensitivity peptidomics method to detect low-abundance novel micropeptides in various genomes. We now apply this method to biological samples in order to discover micropeptides being translated. First, in this chapter, we apply the method to the HepG2 cell line, which is a widely used line(Mersch-Sundermann, Knasmuller, Wu, Darroudi, & Kassie, 2004). Such studies will inform both cases in which this cell line is used as a model for hepatocellular carcinoma(Samarakoon, Thabrew, Galhena, & Tennekoon, 2012) as well as cases in which HepG2 is used in other model systems, such as in malaria infection(Chattopadhyay et al., 2011). In order to discover novel genes by proteomics, it is necessary to include candidates of novel genes in the database used to search the mass spectrometry data. In this study, we have developed a strategy for generation of databases which include both known genes and novel micropeptides, in order to facilitate novel micropeptide discovery by RNA sequencing by searching an *in silico* translation of the transcriptome. Thus, the combination of our novel LC-MS/MS method and the novel bioinformatics method developed here allows the discovery of micropeptides encoded by the human genome. In a second experiment, we searched in a human pathogen genome, the HIV-1 genome, for novel micropeptides, using a similar strategy of high-sensitivity mass spectrometry for acquisition of spectra from micropeptides and then our bioinformatics technique to detect translation of novel micropeptides.

Methods

HepG2 experiment.

HepG2 dataset. The HepG2 cell line proteomics dataset was downloaded from the ProteomeXchange Consortium(Deutsch et al., 2017) by the dataset identifier PXD000682. In that study(Deutsch et al., 2017), HepG2 cells were treated or untreated with HGF (50 ng/ml, for 24 hours), then subcellular enrichment was performed upon cellular lysis to enrich for membrane or cytosolic proteins. Soluble proteins were extracted by 4 cycle freeze thaw in the presence of protease inhibitors. The cell remainder was pelleted, and membrane proteins were extracted by lysis in SDST buffer. Finally, both sets of lysates were fractionated by the 2D strong cation exchange system described in Chapter 2 of this thesis, fractionating each sample run into 0, 15, 30, 45, 60, 120, 160, and 300 mM NaCl fractions which were analyzed online. All fractions were re-combined for peak-picking to produce a single Mascot Generic Format (MGF) file, in a Multidimensional Protein Identification Technology (MuDPIT) strategy(Kislinger, Gramolini, MacLennan, & Emili, 2005). The datasets from that publication which were re-analyzed for this publication are detailed in Table 1. Briefly, datasets from three biological replicates of the HGF experiment were re-analyzed. For the first replicate, 2 replicate injections of the membrane extraction and 3 replicate injections of the cytosolic extraction for the HGF treated cells were used, and 2 replicate injections of the membrane extraction and 4 replicate injections of the cytosolic extraction of the HGF-untreated cells were used. For the second replicate, 2 replicate injections of the membrane extraction and 4 replicate injections of the cytosolic extraction of the HGF treated cells were used, and 2 replicate injections of the membrane extraction and 4 replicate injections of the cytosolic extraction of the untreated cells were used. For the third replicate, 1 injection of the membrane fraction, and 2 replicate injections of the cytosolic extractions of the HGF-treated cells were used, and 1 replicate injection of the membrane extraction and 2 replicate injections of the cytosolic extraction of the

untreated cells were used. Not all replicate datasets of the original publication were used, in order to minimize the computational resources necessary.

HepG2 Analysis transcriptome assembly and database generation. Assembled transcriptome for HepG2 cells was obtained from the ENCODE project data(Djebali et al., 2012). A database of all possible transcribed open reading frames was generated using the EMBOSS tools through Galaxy version 5.0.0: the getorf(Blankenberg et al., 2007; Rice, Longden, & Bleasby, 2000) tool was used with standard codon table with alternative start codons (NUG) recoding Met for alternative start, a minimum open reading frame size of 15 nucleotides, corresponding to 5 amino acids(Koskinen, Emery, Creasy, & Cottrell, 2011), and a max of 300 nucleotides, corresponding to 100 amino acids, encompassing the ORF size range from 5-100 codons. Open reading frames were considered as translated regions from start to stop codons, rather than from stop to stop codons, and the translated sequences were output rather than the nucleic acids. All start codons were forced to code for methionine including alternative start codons(Peabody, 1989). Circular sequences were not allowed, ORFs were not searched in the reverse complement sequences (as this is transcript, not genomic, data), no flanking nucleotides were output, and output format was NCBI FASTA. The database thus generated was concatenated with Swissprot(The UniProt, 2017) delimited for taxonomy to human, and the final database contains 1,313,498 protein sequences.

HIV-1 experiment.

HIV-1 isolation and purification. Three lab isolates of HIV-1 were used for this study: first, virus produced from the NCI's HIV-1(MN)/H9 CL.4 cell line, which is a cell line containing a single active provirus cloned by limiting dilution(Ott, Nigida, Henderson, & Arthur, 1995); second, virus produced from the NCI's HIV-1(MN)CL.4/CEMx174(T1) cell line(Salter, Howell, & Cresswell, 1985), which is a B cell/T cell hybridoma cell line,

infected with the cloned virus above; third, virus produced from the NCI's HIV-1 ADA/SUPT1-CCR5 CL.30 cell line(Del Prete et al., 2009), which is infected by a swarm of viruses produced by infecting human primary peripheral blood mononuclear cells with the HIV-1 ADA strain. These three viruses were used as three biological replicates in which to search for novel virus-encoded micropeptides. Viral purification was done by continuous flow ultracentrifugation in a sucrose density gradient, followed by direct pelleting to remove sucrose. All preparations were then treated with aldrithiol-2 to render virions intact but uninfectious(Rossio et al., 1998) before further biochemical processing.

Deep sequencing of HIV-1 genomes. Random hexamers were used to prime first-strand cDNA synthesis of viral RNA in a genome-wide, unbiased fashion(Hughes et al., 2012). Libraries were then prepared from vRNA by a Nextera tagmentation kit and sequenced by MiSeq by standard protocols.

Protein extraction from purified HIV-1 virions. Virions were secondarily destroyed and inactivated by the addition of 3 volumes of methanol, and the protein allowed to precipitate and pelleted. The pellet was dried and lysed in a standard Urea-based proteomics lysis buffer (8M Urea, 2M Thiourea, 2% CHAPS, 2% ASB-14, 1% Triton X-100, 1% Triton X-114, 10 mM DTT, 150 mM NaCl, 50 mM Tris) for an approximate concentration of 1 mg/ml. Reduction and alkylation was performed, then all detergents were removed by methanol/chloroform precipitation. The remaining pellet was then resuspended in a standard Urea-based proteomics buffer without detergent (8M Urea, 2M Thiourea, 25 mM DTT, 100 mM NaCl). Trypsin digestion was then performed by diluting protein solution to 2M by addition of ammonium bicarbonate to a final concentration of 50 mM, and trypsin was then added at 1:80 trypsin:protein ratio. Digestion was performed at 37ºC for 24 hours with agitation. Samples were resuspended in 3% buffer B for HPLC desalting (90% acetonitrile, 9.9% water, 0.1%

formic acid), and desalted using a C18 column on an Agilent 1200 HPLC system with an 11 minute HPLC protocol: 4 min, 3% B, 4 min 99% B, 3 min 3% B with a flow rate of 500 uL/minute, with UV detection at 214nm for peak collection. Sample was collected and desalted twice.

Mass spectrometry proteomics analysis. Mass spectrometry of HIV-1 derived purified tryptic peptides was performed by an ABSciex 5600 TripleTOF mass spectrometer running in data-dependent acquisition (DDA) mode using an online Eksigent NanoLC 400 HPLC system. Peptides were resuspended in buffer B (0.1% (v/v) formic acid, 90% (v/v) acetonitrile) and run on a 105 minute HPLC gradient of 10-98% buffer A (0.1% (v/v) formic acid, 2% (v/v) acetonitrile) at a flow rate of 750nL/min. MS/MS spectra were collected in the range of 100-1500m/z. All three samples were run in triplicate, and replicates were analyzed together.

HIV-1 genome assembly and database generation. Assembly of genomes was performed with Trinity de novo assembler(Grabherr et al., 2011) (Trinity Galaxy version 0.0.1). The group pairs distance was set for 500 nucleotides, the path reinforcement distance was set at 75 nucleotides, the minimum kmer coverage for contig construction was set to 1, the max transcript reads per graph was set to 2,000,000, and the minimum contig length was set to 200 nucleotides. Since the transcripts (RNA genomes) thus assembled were only considered to produce candidates for the proteomics search, the assembler settings were not optimized. Databases were produced from all three HIV-1 strains described above, in a manner identical to that for the HepG2 study, and as above, each database was concatenated to the human Swissprot database, since HIV virions are well known to contain human host proteins, and viral purifications can also contain host cell exosomes of the same density as virions, which may also contain both human and viral proteins. For the HIV-1(MN)/H9 CL.4 virus, this analysis produced

34,834 candidate novel protein sequences, which after concatenation expanded to 55,485 sequences. For the HIV-1(MN)CL.4/CEMx174(T1) virus, this analysis produced 41,366 candidate novel protein sequences, which after concatenation expanded to 62,017 sequences. For the HIV-1 ADA/SUPT1-CCR5 CL.30 virus, this analysis produced 48,641 candidate novel protein sequences, which after concatenation expanded to 69,292 sequences.

Bioinformatics analysis for both experiments.

The datasets detailed above were searched with Mascot version 2.5.1.2 (Matrix Science, London, UK)(Perkins, Pappin, Creasy, & Cottrell, 1999), and the protein identification results from these Mascot searches were further analyzed in Scaffold 4.4.5(Proteome Software, Portland, OR, USA) in a subset database search approach(Tharakan, Edwards, & Graham, 2010) with X!Tandem CYCLONE(Fenyo & Beavis, 2003), version 2010.12.01.1. Both Mascot and X!Tandem searches were run with a parent ion mass tolerance and fragment ion mass tolerance of 50 ppm and 0.60 Da, respectively. Two missed cleavages were allowed. Variable modifications were set in Mascot as deamidation of asparagine and glutamine, oxidation of methionine, carbamylation of lysine and carbamidomethylation of cysteine. In the X!Tandem subset database search, the variable modifications list was allowed to expand to take advantage of the smaller search space (cite), allowing conversion of glutamate or glutamine to pyroglutamate at the N-terminus, ammonia-loss of the N-terminus, deamidation of asparagine and glutamine, oxidation of methionine, carbamylation of lysine and carbamidomethylation of cysteine. Both peptide and protein identifications were accepted if they could be established at greater than 95% probability by the PeptideProphet algorithm(Keller, Nesvizhskii, Kolker, & Aebersold, 2002) with Scaffold delta-mass correction and by the ProteinProphet algorithm(Nesvizhskii, Keller, Kolker, & Aebersold, 2003), respectively.

Results and Discussion

In order to discover novel micropeptides in the human genome, we took a proteogenomics approach to the HepG2 cell line. We used RNA sequencing data from the ENCODE project to assemble a database of all possible short open reading frames which are transcribed in that cell line. This database was then concatenated with a database of known, well-annotated human proteins, Swissprot. This large database thus contains known human proteins as well as potential proteins which could be transcribed from short open reading frames. Concatenation is necessary in order to prevent many spurious proteomic matches by known human proteins to the short open reading frame (sORF) database, which, since they will overlap with many sORFs in the transcriptome, such as alternate start site sORFs, are not unambiguously identified from proteomics data(Vanderperre et al., 2013). For this reason, the database is first concatenated with a generic known protein database, and so any alternate frame sORF will be mapped twice, both to the sORF database entry and to the known protein database entry. For these hits, we consider them not to be unambiguously identified as micropeptides, since any alternate start internal sORF will be matched if its corresponding canonical protein is matched. Furthermore, since the SwissProt database is well-annotated, but does not contain all known human proteins, we cannot assume that all possible ambiguous coding frames mapping to a known human gene can be eliminated by this process(The UniProt, 2017). Therefore, we use a second step of filtering to eliminate alternate coding open reading frames which are not represented in the SwissProt database, by using BLAST searches(Altschul, Gish, Miller, Myers, & Lipman, 1990) against all protein sequences represented in NCBI nr, which is a comprehensive and highly redundant

protein database. The protein BLAST matches were then evaluated for whether the transcripts they mapped to could be considered to be novel or not.

The complete list of proteins identified in the HepG2 proteomics analysis is shown in Table 2. Allowing a threshold of 95% confidence (see Methods), produces a dataset of 2864 proteins, with .3% peptide FDR and 1% protein FDR. These proteins can be clustered by shared peptides, assuming that proteins that share peptides cannot be unambiguously identified, and that proteins that share peptides are similar enough in sequence to be similar in function or isoforms of each other(Ubaida Mohien et al., 2010). Clustering the proteins in this manner reduces the protein list to 2629 clusters of similar, undifferentiable proteins. Thus, the analysis identifies a large component of the proteome successfully, a proof of principle that the analysis can be used to discover novel peptides as well. A second validation is that proteins which would be expected to be enriched in their respective fractions are indeed enriched. Table 3 shows proteomic identifications separated into HepG2 HGF treated and untreated, and into membrane and cytosolic fractions. Estimates can be derived in a general manner by spectral counts(Choi, Fermin, & Nesvizhskii, 2008). The table shows that several proteins which are expected to be enriched in cytosolic fractions were indeed enriched. For example, the chaperone proteins heat shock protein 90a and 90b are both enriched in the soluble fraction, which is to be expected since they are primarily cytosolic(Wandinger, Richter, & Buchner, 2008). Similarly, UQCRC2(Hosokawa, Suzuki, Toda, Nishikimi, & Ozawa, 1989), which is a component of Complex III of the respiratory chain, is found only in fractions processed for membrane enrichment, as is ATP Synthase 5B(Neckelmann et al., 1989). However, many of the membrane-enriched proteins are soluble proteins found in membrane-enclosed fractions, such as lamins(Gruenbaum, Wilson, Harel, Goldberg, & Cohen, 2000) and histones(Marino-Ramirez, Kann, Shoemaker, &

Landsman, 2005) in the nucleus, suggesting that the membrane fraction may better be considered a non-cytosolic fraction. Finally, the analysis is also validated by the probability distributions generated by the PeptideProphet(Ma, Vitek, & Nesvizhskii, 2012) algorithm. As the algorithm is described, two distributions are generated from the protein scores of all proteins, both of which follow a Gaussian distribution. If the Gaussian model fits well to the distributions of scores, the lower distribution can be considered a distribution of 'incorrect' matches, while the higher distribution can be considered correct matches. If the dataset is too sparse, the distributions cannot be modeled and the probabilities are not accurate. Figure 1 shows the distributions modeled by the PeptideProphet algorithm for this analysis, for charge state +2, showing that the probabilities thus calculated can be considered accurate.

After filtering by probability as described, the list of 2629 clustered proteins contains 27 proteins which map to sORFs from the HepG2 ENCODE transcriptome without any shared peptides with known proteins. Of these, only 2 survived the BLAST homology filtering step described above, with the remainder found to be homologous with known proteins. These latter two can be considered to be novel micropeptides discovered by our proteogenomics approach. The first peptide, shown in Figure 2, is represented by a single spectrum, which has fairly good coverage but several unidentified peaks. The peptide is produced from the gene SLC35A3(Ishida, Yoshioka, Chiba, Takeuchi, & Kawakita, 1999), which is a UDP-GlcNAc transporter in the Golgi apparatus. The transcript is 5708 nt long, with a ~1100 nucleotide CDS and a long (~4500 nucleotide) 3'UTR. The 12-codon ORF is in the 3'UTR of the transcript at positions 5410-5448, and has an alternative start leucine codon which is recoded as NUG to Methionine, for a final translation of MSVCCFICNYKII. The peptide is detected only in the membrane fractions. The second peptide, shown in Figure 3, is represented

by 4 spectra, which are shown in 4b. The spectra appear to have a clear B and Y series, but do also contain prominent unidentified peaks. The peptide hit is contained in gene WASHC4(Ropers et al., 2011), which has a transcript 5812 nucleotides long, with a ~3500 nucleotide CDS and a long (~2300 nucleotide) 3'UTR. The 3'UTR contains a 34-codon ORF at positions 4154-4255 with an in-frame stop. The translation initiation site is a leucine codon recoded to methionine, in a second case of alternative initiation. The peptide, like WASHC4 itself, is detected only in soluble proteome fractions. The translation product sequence is MMILLSLLISCDSQELLMSLMRHFITSLHCFENI, of which a tryptic portion is detected, ILLSLLISCDSQELLMSLMR. In both these cases, long 3'UTRs produce cryptic micropeptides in transcripts which have that structure. This is similar to a case described in another SLC transporter-class protein, in which SLC35A4 was found to produce a cryptic micropeptide from a long 5'UTR(Andreev et al., 2015). Thus, this proteogenomics analysis can be shown to be robust for describing the proteome in a normal fashion, and also finds translation of at least one (from the WASHC4 transcript) and possibly two novel micropeptide genes.

In a second approach to discovering novel micropeptides in genome, we targeted an important human pathogen, HIV-1. We produced proteomic and genomic data from three HIV-1 lab isolates: first, a virus grown from HIV-1(MN)/H9 CL.4, a cloned cell line infected with a single HIV-1 clone; second, a virus grown from HIV-1(MN)CL.4/CEMx174(T1), an uncloned cell line infected with many different HIV-1 clone, and producing them all; and third, HIV-1 ADA/SUPT1-CCR5 CL.30, which is an uncloned cell line infected by a swarm of HIV-1 viruses produced from human primary PBMC (J. Bess, Personal Communication, and see Methods). The viral isolates could thus be considered to have increasing levels of genomic heterogeneity. The three viral isolates were analyzed by proteomics; in this case, a higher-sensitivity mass

spectrometer was used (see Methods) obviating the need to use 2D fractionation for high sensitivity. In parallel, viral RNA was extracted from each isolate and their genomes sequenced. These sequences were assembled *de novo* into sets of putative HIV-1 genome sequences, and a database was generated from them using methods similar to that used for the HepG2 experiment above. Finally, these proteomics datasets was searched against the databases thus generated in a proteogenomics approach to novel micropeptide discovery.

De novo assembly generated several thousand genomic sequences for each isolate (see Methods). We emphasize that these sequences should not be taken to demonstrate that each viral isolate has many thousands of completely divergent genomic sequences. Indeed, *de novo* assembly is difficult and all known *de novo* assemblers are adapted for cellular transcriptomes, rather than the viral ssRNA genomes. However, we nevertheless argue that we can use the genomic sequences thus assembled as candidate sequences of the HIV genomes present in the actual samples. Importantly, the sequences thus generated are used as candidates for the proteomic analysis, and thus if the proteomics and the genomic sequences match we may say that we have a putatively translated novel sequence. Finally, we show in Figure 4 that our pipeline identifies a novel isoform of the Env protein, which is known to by hypermutated to evade the immune response. Thus, our pipeline does indeed match proteins which are expected to highly mutated, and expected to exist in the sample, thus validating the proteogenomics approach. Finally, a single novel micropeptide was also found, as shown in Figure 5.

As in the HepG2 experiment above, the proteogenomics pipeline captures a substantial number of proteins, showing that the proteogenomics pipeline successfully recapitulates the standard proteome along with the novel sORF proteome: at the filtering

thresholds described in Methods, for the HIV-1(MN)/H9 CL.4 virus, 1606 proteins were found, reduced to 1319 after clustering, of which 1 mapped to a novel sORF; for the HIV-1(MN)CL.4/CEMx174(T1), 1775 proteins were found, reduced to 1457 after clustering, of which 4 mapped to novel sORFs; for the HIV-1 ADA/SUPT1-CCR5 CL.30, 1420 proteins were found, reduced to 1105 after clustering, of which 7 mapped to novel sORFs. All but one of these were eliminated by the BLAST search filtering. The complete results are shown in Table 4.

Thus, in this chapter we have shown that, by our 2D LC-MS/MS platform, along with a bioinformatic approach to generating databases which include micropeptides generated by short open reading frames, by directly translating *in silico* all open reading frames shorter 100 codons and longer than 5 codons in assembled transcriptomes. We utilize this system to find evidence of translation of two novel micropeptides expressed in the HepG2 cell line, and one novel micropeptide in a purified HIV-1 strain.

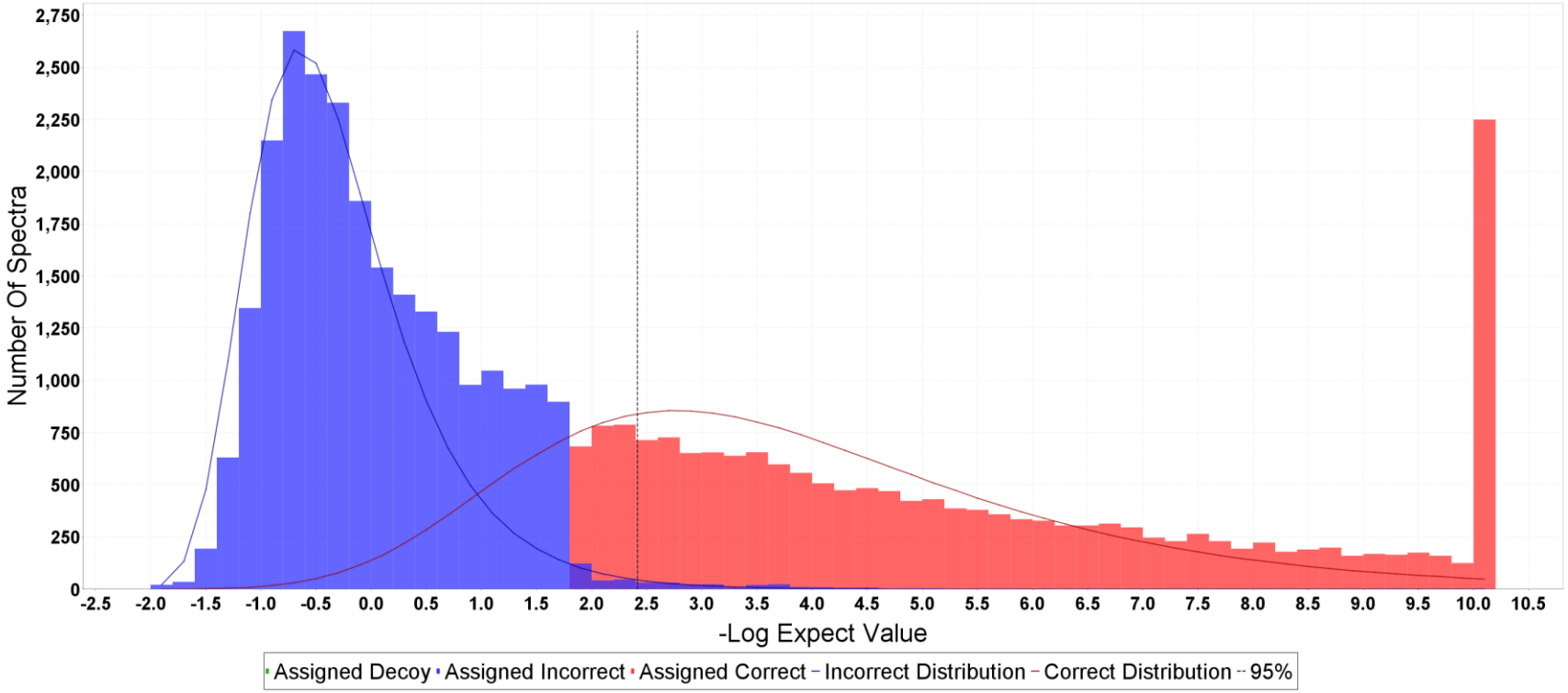

Figure 1a. Gaussian fit and raw distribution for PeptideProphet for X!Tandem results, for hits with charge state +2

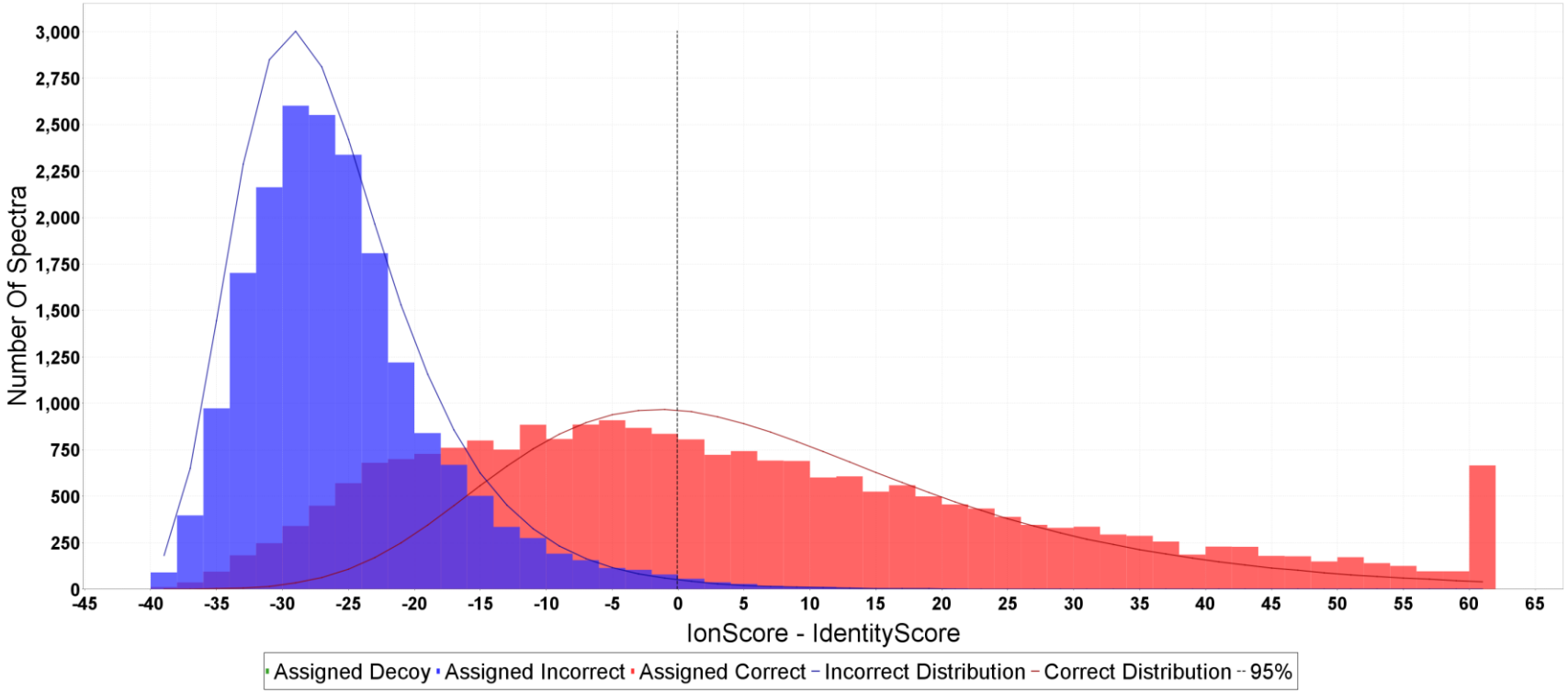

Figure 1b. Gaussian fit and raw distribution for PeptideProphet for Mascot results, for hits with charge state +2

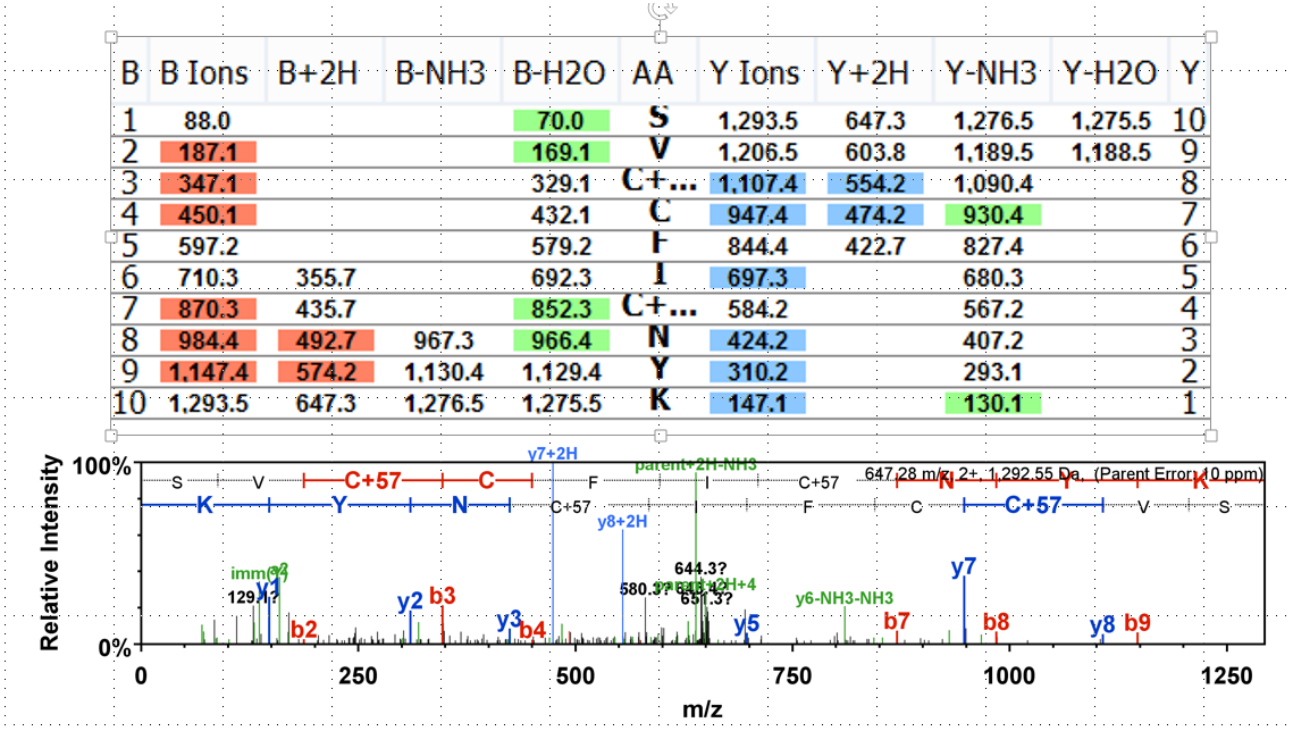

B	B Ions	B+2H	B-NH3	B-H2O	AA	Y Ions	Y+2H	Y-NH3	Y-H2O	Y
1	88.0			70.0	S	1,293.5	647.3	1,276.5	1,275.5	10
2	187.1			169.1	V	1,206.5	603.8	1,189.5	1,188.5	9
3	347.1			329.1	C+...	1,107.4	554.2	1,090.4		8
4	450.1			432.1	C	947.4	474.2	930.4		7
5	597.2			579.2	F	844.4	422.7	827.4		6
6	710.3	355.7		692.3	I	697.3		680.3		5
7	870.3	435.7		852.3	C+...	584.2		567.2		4
8	984.4	492.7	967.3	966.4	N	424.2		407.2		3
9	1,147.4	574.2	1,130.4	1,129.4	Y	310.2		293.1		2
10	1,293.5	647.3	1,276.5	1,275.5	K	147.1		130.1		1

Figure 2a. Micropeptide hit in gene SLC35A3. Fragmentation table shows good coverage of both B and Y ions. Mass spectrum shows one set of unidentified peaks which are likely due to incomplete fragmentation of doubly charged precursor.

Figure 2b. Micropeptide sequence maps to the gene Solute carrier family 35 member A3 (ENST00000370153.6), whose function is a UDP-GlcNAc transporter in the Golgi apparatus. The transcript is 5708 nt long, with a ~1100 nucleotide CDS and a long (~4500 nucleotide) 3'UTR. The 12-codon ORF is in the 3'UTR at positions 5410-5448 with an in-frame stop, and alternative start leucine codon which is recoded as NUG to Methionine, for a final translation of MSVCCFICNYKII. The peptide is detected only in the membrane fractions.

B	B Ions	B+2H	B-NH3	B-H2O	AA	Y Ions	Y+2H	Y-NH3	Y-H2O	Y
1	114.1				I	2,294.2	1,147.6	2,277.2	2,276.2	20
2	227.2				L	2,181.1	1,091.1	2,164.1	2,163.1	19
3	340.3				L	2,068.0	1,034.5	2,051.0	2,050.0	18
4	427.3			409.3	S	1,955.0	978.0	1,937.9	1,937.0	17
5	540.4			522.4	L	1,867.9	934.5	1,850.9	1,849.9	16
6	653.5	327.2		635.4	L	1,754.8	877.9	1,737.8	1,736.8	15
7	766.5	383.8		748.5	I	1,641.8	821.4	1,624.7	1,623.8	14
8	853.6	427.3		835.6	S	1,528.7	764.8	1,511.7	1,510.7	13
9	956.6	478.8		938.6	C	1,441.6	721.3	1,424.6	1,423.6	12
10	1,071.6	536.3		1,053.6	D	1,338.6	669.8	1,321.6	1,320.6	11
11	1,158.6	579.8		1,140.6	S	1,223.6	612.3	1,206.6	1,205.6	10
12	1,286.7	643.9	1,269.7	1,268.7	Q	1,136.6	568.8	1,119.6	1,118.6	9
13	1,415.7	708.4	1,398.7	1,397.7	E	1,008.5	504.8	991.5	990.5	8
14	1,528.8	764.9	1,511.8	1,510.8	L	879.5	440.2	862.5	861.5	7
15	1,641.9	821.5	1,624.9	1,623.9	L	766.4	383.7	749.4	748.4	6
16	1,773.0	887.0	1,755.9	1,754.9	M	653.3		636.3	635.3	5
17	1,860.0	930.5	1,843.0	1,842.0	S	522.3		505.2	504.3	4
18	1,973.1	987.0	1,956.0	1,955.1	L	435.2		418.2		3
19	2,120.1	1,060.6	2,103.1	2,102.1	M...	322.2		305.1		2
20	2,294.2	1,147.6	2,277.2	2,276.2	R	175.1		158.1		1

Figure 3a. A Micropeptide Hit in Gene WASHC4 (WASH complex subunit 4) (ENST00000332180.9). Transcript is 5812 nt long, with a ~3500 nucleotide CDS and a long (~2300 nucleotide) 3'UTR. Left, top, the 3'UTR contains 34-codon ORF in the 3'UTR at positions 4154-4255 with an in-frame stop. Translation initiation site is a leucine codon recoded as NUG to Methionine (alternative initiation). The peptide, like WASHC4 itself, is detected only in soluble proteome fractions. The translation product sequence is MMILLSLLISCDSQELLMSLMRHFITSLHCFENI, of which a tryptic portion is detected. Right, example fragmentation table of a spectrum identifying this peptide.

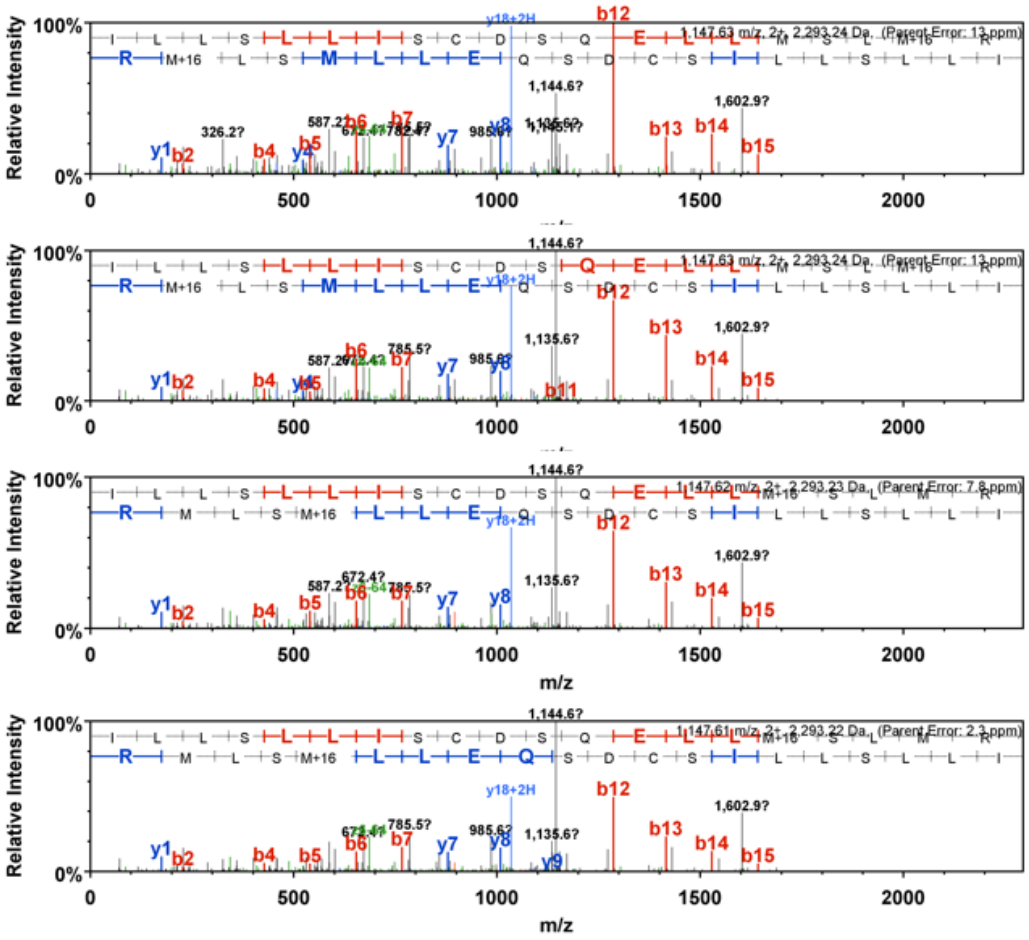

Figure 3b. Four spectra detecting the novel peptide.

gnl|unk|TRINITY_DN764_c26_g1_i1_5 (100%), 7,306.7 Da
[16 - 207] len=207 path=[473:0-149 474:150-154 475:155-173 476:174-178 477:179-206] [-1, 473, 474, 475, 476, 477, -2]
1 exclusive unique peptides, 2 exclusive unique spectra, 59 total spectra, 23/64 amino acids (36% coverage)

MWQEVGR**AMY** **APPISGQIR**C SSNITGLLLT RDGGKDNSTK **EIFRPIGGNM**
RDNWRSELYK YKVV

```
413 MWQKVGKAIYAPPIAGSINCSSNITGMILTRDGG-NNTHNETFRPGGGDM    461
    |||:||:|:|||||:|.|.|||||||::|||||| :|:..|.|||.||:|
  1 MWQEVGRAMYAPPISGQIRCSSNITGLLLTRDGGKDNSTKEIFRPIGGNM     50

462 RDNWRSELYK    471
    ||||||||||
 51 RDNWRSELYK     60
```

Figure 4. Novel gp120 isoform in Strain HIV-1_{ADA-M}. The ORF discovered maps to within the normal Env gene. The protein is hypermutated and so does not map normally when searched with a standard database of proteins. Discovery of novel Env isoforms is to be expected due to HIV biology, and thus shows that the proteogenomics method used here is Shows that de novo assembly finds viral sequence variants. Alignment of novel sequence with canonical HIV Env isoform done by Jaligner with standard settings.

B	B Ions	B+2H	B-NH3	B-H2O	AA	Y Ions	Y+2H	Y-NH3	Y-H2O	Y
1	132.0				M	1,435.7		1,418.7	1,417.7	12
2	245.1				L	1,304.6		1,287.6	1,286.6	11
3	360.2			342.1	D	1,191.6		1,174.5	1,173.5	10
4	488.2		471.2	470.2	Q	1,076.5		1,059.5	1,058.5	9
5	589.3		572.2	571.3	I	948.5		931.4	930.5	8
6	702.3	351.7	685.3	684.3	L	847.4		830.4	829.4	7
7	815.4	408.2	798.4	797.4	L	734.3		717.3	716.3	6
8	930.5	465.7	913.4	912.4	D	621.3		604.2	603.2	5
9	1,043.5	522.3	1,026.5	1,025.5	L	506.2		489.2	488.2	4
10	1,157.6	579.3	1,140.6	1,139.6	N	393.1		376.1	375.1	3
11	1,286.6	643.8	1,269.6	1,268.6	E	279.1			261.1	2
12	1,435.7	718.3	1,418.7	1,417.7	M	150.1				1

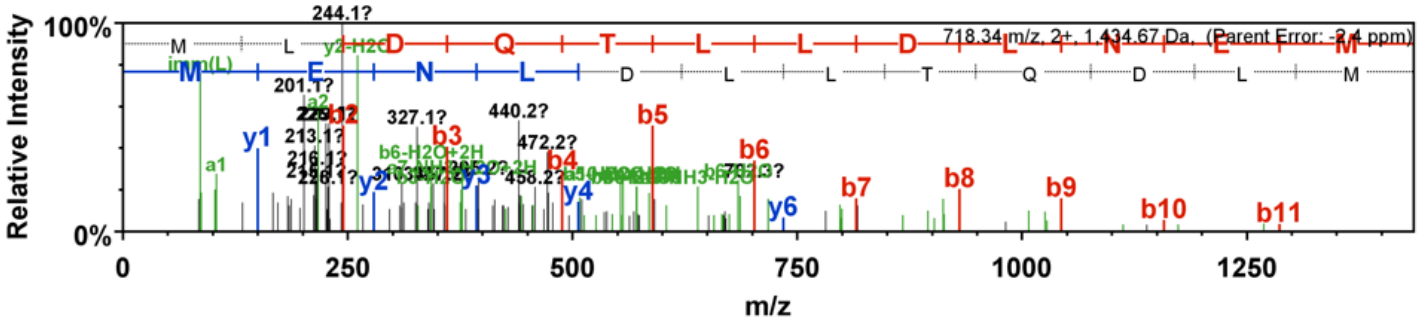

Figure 5a. Micropeptide Hit in Strain HIV-1_{MN} from HIV-1(MN)CL.4/CEMx174(T1). Spectrum was acquired a total of 9 times across replicate injections, at an average elute time of 6786 seconds, with 6.8 standard deviation. The peptide acquired covers the complete open reading frame. Shown here is an example spectrum with corresponding mass table.

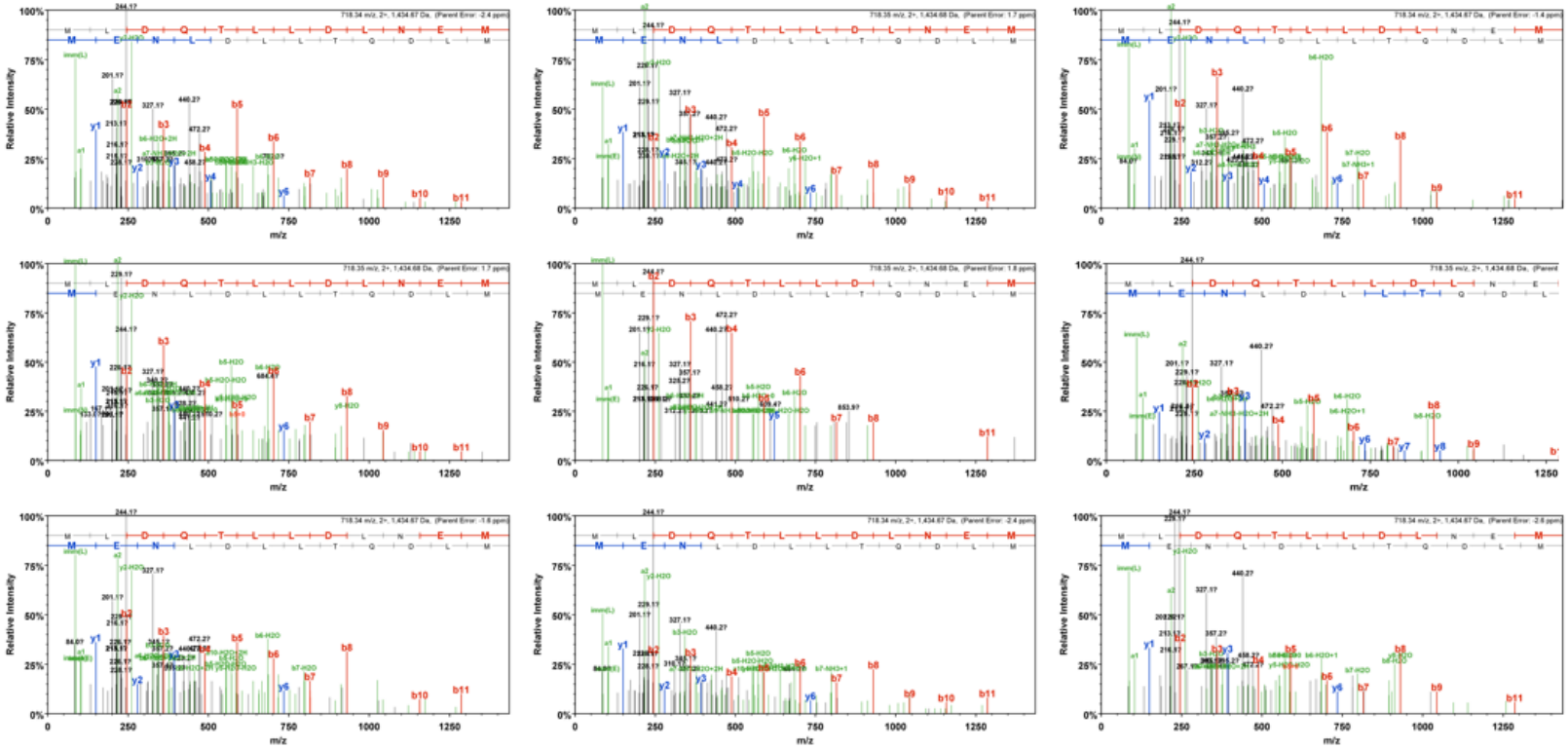

Figure 5b. All spectra acquired from novel HIV-1 micropeptide.

HGF			
Replicate 1		Replicate 1	
Membrane		Membrane	
1	HepG2HGFFASPB01T02a (HepG2HGFFASPB01T01a).mzid _HepG2HGFFASPB01T02a_ (HepG2HGFFASPB01T01a).MGF	1	HepG2naiveFASPB01T01a.mzid_ HepG2naiveFASPB01T01a.MGF
2	HepG2HGFFASPB01T02b (HepG2HGFFASPB01T01b).mzid _HepG2HGFFASPB01T02b_ (HepG2HGFFASPB01T01b).MGF	2	HepG2naiveFASPB01T01b.mzid_ HepG2naiveFASPB01T01b.MGF
Cytosol		Cytosol	
1	HepG2HGFsolB01T01a.mzid_ HepG2HGFsolB01T01a.MGF	1	HepG2naiveGFsolB01T01a (HepG2naivesolB01T01a).mzid _HepG2naiveGFsolB01T01a_ (HepG2naivesolB01T01a).MGF
2	HepG2HGFsolB01T01b.mzid_ HepG2HGFsolB01T01b.MGF	2	HepG2naiveGFsolB01T01b (HepG2naivesolB01T01b).mzid _HepG2naiveGFsolB01T01b_ (HepG2naivesolB01T01b).MGF
3	HepG2HGFsolB01T01c.mzid_ HepG2HGFsolB01T01c.MGF	3	HepG2naiveGFsolB01T01c (HepG2naivesolB01T01c).mzid _HepG2naiveGFsolB01T01c_ (HepG2naivesolB01T01c).MGF
		4	HepG2naiveGFsolB01T01d (HepG2naivesolB01T01d).mzid _HepG2naiveGFsolB01T01d_ (HepG2naivesolB01T01d).MGF
Replicate 2		Replicate 2	

Membrane		Membrane	
1	HepG2HGFFASPB02T01a.mzid_ HepG2HGFFASPB02T01a.MGF	1	HepG2naiveFASPB01T02a.mzid_ HepG2naiveFASPB01T02a.MGF
2	HepG2HGFFASPB02T01b.mzid_ HepG2HGFFASPB02T01b.MGF	2	HepG2naiveFASPB01T02b.mzid_ HepG2naiveFASPB01T02b.MGF
Cytosol		Cytosol	
1	HepG2HGFsolB02T01a.mzid_ HepG2HGFsolB02T01a.MGF	1	HepG2naiveGFsolB01T02a (HepG2naivesolB01T02a).mzid _HepG2naiveGFsolB01T02a_ (HepG2naivesolB01T02a).MGF
2	HepG2HGFsolB02T01b.mzid_ HepG2HGFsolB02T01b.MGF	2	HepG2naiveGFsolB01T02b (HepG2naivesolB01T02b).mzid _HepG2naiveGFsolB01T02b_ (HepG2naivesolB01T02b).MGF
3	HepG2HGFsolB02T01c.mzid_ HepG2HGFsolB02T01c.MGF	3	HepG2naiveGFsolB01T02c (HepG2naivesolB01T02c).mzid _HepG2naiveGFsolB01T02c_ (HepG2naivesolB01T02c).MGF
4	HepG2HGFsolB02T01d.mzid_ HepG2HGFsolB02T01d.MGF	4	HepG2naiveGFsolB01T02d (HepG2naivesolB01T02d).mzid _HepG2naiveGFsolB01T02d_ (HepG2naivesolB01T02d).MGF
Replicate 3		Replicate 3	
Membrane		Membrane	
1	HepG2HGFFASPB02T02a.mzid_ HepG2HGFFASPB02T02a.MGF	1	HepG2naiveFASPB02T01a.mzid_ HepG2naiveFASPB02T01a.MGF
Cytosol		Cytosol	
1	HepG2HGFsolB02T02a.mzid_ HepG2HGFsolB02T02a.MGF	1	HepG2naiveGFsolB02T01a (HepG2naivesolB02T01a).mzid _HepG2naiveGFsolB02T01a_

			(HepG2naivesolB02T01a).MGF
2	HepG2HGFsolB02T02b.mzid_ HepG2HGFsolB02T02b.MGF	2	HepG2naiveGFsolB02T01b (HepG2naivesolB02T01b).mzid _HepG2naiveGFsolB02T01b_

Table 1. All datasets used in the HepG2 analysis.

Protein accession numbers	Identification probability	Total Spectrum count
SC61G_HUMAN,gnl|unk|ENST00000352861_4,gnl|unk|ENST00000395535_4,gnl|unk|ENST00000415949_8,gnl|unk|ENST00000450622_4	100.00%	29
gnl|unk|ENST00000557933_37	96.10%	5
HKDC1_HUMAN	100.00%	6
TBL3_HUMAN	96.10%	6
MGAT2_HUMAN	96.10%	1
ALG11_HUMAN	100.00%	4
IF5A1_HUMAN	100.00%	8
HS71A_HUMAN,HS71B_HUMAN	100.00%	41
GNAI3_HUMAN	100.00%	21
S39AE_HUMAN	100.00%	44
SPS2L_HUMAN	100.00%	5
LICH_HUMAN	96.10%	3
SAR1B_HUMAN	60.60%	3
HNRPC_HUMAN	100.00%	33
CTDS1_HUMAN	94.80%	4
SRSF2_HUMAN	100.00%	4
gnl|unk|ENST00000487233_4	97.40%	1
CCHL_HUMAN	100.00%	9
NOP56_HUMAN	100.00%	49
RAB1B_HUMAN	100.00%	57

MGST2_HUMAN,gnl|unk|ENST00000506797_5,gnl|unk|ENST00000515067_3	56.50%	1
VATE1_HUMAN	100.00%	15
AHSA1_HUMAN	96.10%	5
ATM_HUMAN	96.10%	6
CY24A_HUMAN	100.00%	2
DDRGK_HUMAN	100.00%	13
ECHP_HUMAN	96.10%	3
VAPA_HUMAN	100.00%	53
PRS8_HUMAN	96.10%	1
VTA1_HUMAN	68.00%	1
DIDO1_HUMAN	96.10%	6
TRAM1_HUMAN	99.10%	1
NDUV1_HUMAN	100.00%	59
SEPT9_HUMAN	100.00%	7
IDHC_HUMAN	99.90%	3
EF1A1_HUMAN	100.00%	695
CXAR_HUMAN	100.00%	15
NT5D2_HUMAN	100.00%	1
VATL_HUMAN	96.10%	9
NONO_HUMAN	100.00%	43
DX39A_HUMAN	52.70%	14
TIM14_HUMAN	100.00%	1
ACTB_HUMAN	100.00%	2091
PROX1_HUMAN	96.90%	1
SAC1_HUMAN	100.00%	11
FAF2_HUMAN	100.00%	37

CND3_HUMAN	100.00%	11
TCPD_HUMAN	100.00%	4
QCR1_HUMAN	100.00%	140
LITAF_HUMAN	96.10%	4
SLU7_HUMAN	96.10%	4
WDR75_HUMAN	100.00%	8
RS2_HUMAN	100.00%	44
SRPRB_HUMAN	100.00%	33
RINT1_HUMAN	96.10%	1
TM41B_HUMAN	96.10%	10
SNAA_HUMAN	100.00%	45
STF1_HUMAN	96.10%	1
CR3L2_HUMAN	96.10%	1
ALG2_HUMAN	100.00%	23
K2013_HUMAN	100.00%	5
LETM1_HUMAN	100.00%	28
ELOV1_HUMAN	96.10%	8
TMX3_HUMAN	100.00%	4
NU5M_HUMAN	100.00%	10
DHCR7_HUMAN	100.00%	15
ESF1_HUMAN	96.10%	4
NDUF3_HUMAN	96.10%	8
BEND3_HUMAN	96.10%	3
SFXN1_HUMAN	100.00%	35
RL31_HUMAN	100.00%	18
ARFG1_HUMAN	100.00%	4

P121C_HUMAN	100.00%	4
BAZ2A_HUMAN	99.90%	1
AUP1_HUMAN	100.00%	6
HEAT1_HUMAN	100.00%	7
VATF_HUMAN	96.10%	6
HCD2_HUMAN	100.00%	11
RNPS1_HUMAN	100.00%	11
CDC20_HUMAN	99.80%	2
EXOS3_HUMAN	96.10%	4
SC11C_HUMAN,gnl|unk|ENST00000299714_4	96.10%	1
TGM2_HUMAN	100.00%	6
NC2B_HUMAN	96.10%	4
NUP53_HUMAN	8.50%	0
NDUAA_HUMAN	100.00%	19
ERG28_HUMAN	100.00%	3
PHB2_HUMAN	100.00%	143
TRRAP_HUMAN	100.00%	4
SCAM1_HUMAN	96.10%	6
3MG_HUMAN	96.10%	5
TMED9_HUMAN	100.00%	55
NKD1_HUMAN	100.00%	2
MTFP1_HUMAN	95.20%	1
GL8D1_HUMAN	78.10%	3
SF3A1_HUMAN	96.10%	2
PNKD_HUMAN	100.00%	19
TCOF_HUMAN	99.80%	1

HMGA1_HUMAN	100.00%	35
SRSF3_HUMAN	99.90%	14
SMD1_HUMAN	100.00%	18
H2AV_HUMAN,H2AZ_HUMAN	100.00%	84
TP53B_HUMAN	96.10%	1
RL13A_HUMAN	100.00%	16
RAP2B_HUMAN	96.10%	6
RFA1_HUMAN	100.00%	8
NU188_HUMAN	100.00%	7
TEBP_HUMAN	99.80%	9
UBP7_HUMAN	100.00%	9
IPO9_HUMAN	96.10%	1
MTCH1_HUMAN	96.10%	2
VAMP3_HUMAN,gnl|unk|ENST00000054666_6	100.00%	11
CBX3_HUMAN	99.90%	3
IFM3_HUMAN	26.60%	0
SPCS1_HUMAN	100.00%	24
SYFA_HUMAN	88.70%	3
VRK3_HUMAN	94.70%	1
SC61B_HUMAN,gnl|unk|ENST00000223641_2	100.00%	10
OS9_HUMAN	100.00%	11
PLCA_HUMAN	96.10%	4
RPF2_HUMAN	96.10%	1
HNRPU_HUMAN	100.00%	157
RS4Y1_HUMAN	100.00%	26
SATT_HUMAN	96.10%	2

TM209_HUMAN	96.10%	6
ANO6_HUMAN	96.10%	6
ITIH2_HUMAN	100.00%	9
ANXA6_HUMAN	100.00%	12
P5CR2_HUMAN	5.50%	0
FARP1_HUMAN	100.00%	2
VAS1_HUMAN	99.90%	4
YIF1B_HUMAN	96.10%	6
PTN1_HUMAN	100.00%	22
gnl|unk|ENST00000352511_93	72.80%	1
TM9S2_HUMAN	100.00%	15
TMCO1_HUMAN	100.00%	7
RBM39_HUMAN	100.00%	3
RL3_HUMAN	100.00%	59
GCN1_HUMAN	100.00%	10
DNJC9_HUMAN	100.00%	8
NUP98_HUMAN	100.00%	5
CTNB1_HUMAN	100.00%	65
MCU_HUMAN	100.00%	5
HCFC1_HUMAN	100.00%	11
ITB1_HUMAN	100.00%	86
SMC3_HUMAN	100.00%	9
XPO5_HUMAN	65.70%	1
GLYR1_HUMAN	100.00%	3
ABD12_HUMAN	96.10%	1
ENOA_HUMAN	100.00%	38

CO3_HUMAN	100.00%	39
AURKB_HUMAN	99.80%	2
EZRI_HUMAN	6.20%	1
LTOR2_HUMAN	96.10%	6
SSBP_HUMAN	100.00%	19
WFS1_HUMAN	100.00%	16
CN166_HUMAN	96.10%	2
RL36_HUMAN	100.00%	11
SYK_HUMAN	96.10%	3
FA83H_HUMAN	64.60%	1
ILF3_HUMAN	100.00%	39
ZGPAT_HUMAN	98.90%	1
SND1_HUMAN	100.00%	32
F210B_HUMAN	100.00%	10
DHC24_HUMAN	100.00%	53
gnl|unk|ENST00000493646_6	96.10%	4
RL23A_HUMAN	100.00%	9
RRP1B_HUMAN	100.00%	4
H32_HUMAN	99.90%	40
B4GA1_HUMAN	100.00%	4
PP1G_HUMAN	89.60%	52
NDUAB_HUMAN	100.00%	22
SCAM2_HUMAN	100.00%	14
TPM4_HUMAN	100.00%	10
SNR40_HUMAN	100.00%	5
NUP37_HUMAN	96.10%	2

GAR1_HUMAN	96.10%	2
gnl|unk|ENST00000502784_11	74.40%	1
RL7A_HUMAN	100.00%	45
DPM1_HUMAN	100.00%	19
SAS10_HUMAN	96.10%	3
LTOR1_HUMAN	99.80%	4
PSIP1_HUMAN	99.00%	5
68MP_HUMAN,gnl|unk|ENST00000286953_5,gnl|unk|ENST00000557040_6	99.90%	3
PON3_HUMAN	96.10%	1
STX5_HUMAN	100.00%	6
SEC62_HUMAN,gnl|unk|ENST00000460513_4,gnl|unk|ENST00000487736_9	96.10%	1
RAB5B_HUMAN	99.90%	16
RFA2_HUMAN	96.10%	5
PRDX5_HUMAN	96.10%	11
SC22B_HUMAN	100.00%	27
H2A2B_HUMAN	97.40%	210
MRP1_HUMAN	100.00%	8
FER_HUMAN	96.10%	1
VATA_HUMAN	100.00%	2
TBB4B_HUMAN	100.00%	279
UD2B7_HUMAN	100.00%	5
SPCS2_HUMAN	100.00%	33
PIGS_HUMAN	100.00%	18
RBBP5_HUMAN	96.10%	1
RTN4_HUMAN	100.00%	45
RL28_HUMAN,gnl|unk|ENST00000428193_4,gnl|unk|ENST00000431533_4,gnl|unk|ENST0	100.00%	11

0000558131_4,gnl|unk|ENST00000560881_4		
RLA0_HUMAN	100.00%	33
CCD47_HUMAN	100.00%	37
ARF1_HUMAN,ARF3_HUMAN	100.00%	8
ACTN1_HUMAN	96.30%	13
NEP1_HUMAN	58.90%	1
BAG2_HUMAN	100.00%	25
RAD50_HUMAN	98.50%	1
TMED4_HUMAN	100.00%	19
FACE1_HUMAN	100.00%	16
RBM15_HUMAN	100.00%	6
NIPA1_HUMAN	96.10%	1
TOIP2_HUMAN	100.00%	2
CSTF3_HUMAN	10.40%	0
PALM_HUMAN	96.10%	4
UBXN6_HUMAN	96.10%	1
F169A_HUMAN	100.00%	6
TCP4_HUMAN	100.00%	19
UTRO_HUMAN	99.80%	1
RUXF_HUMAN	57.80%	1
DEST_HUMAN	96.10%	4
APOA1_HUMAN	100.00%	22
EMC3_HUMAN	96.10%	3
THEM6_HUMAN	100.00%	35
DHRS7_HUMAN	100.00%	18
CSN3_HUMAN	55.40%	1

PRS6B_HUMAN	32.50%	0
DEGS1_HUMAN	96.10%	5
IPO4_HUMAN	82.70%	3
TM45B_HUMAN	96.10%	1
CHDH_HUMAN	100.00%	3
COASY_HUMAN	100.00%	4
SAMC_HUMAN	96.10%	4
SSRA_HUMAN	100.00%	114
EFTS_HUMAN	96.10%	5
ACTBL_HUMAN	100.00%	67
LBR_HUMAN	100.00%	14
K2C8_HUMAN	100.00%	428
CHD1_HUMAN	96.10%	2
BRI3B_HUMAN	100.00%	6
TRI25_HUMAN	100.00%	5
H33_HUMAN	99.90%	42
TI23B_HUMAN,TIM23_HUMAN	100.00%	3
RAB18_HUMAN	100.00%	12
UB2G2_HUMAN	96.10%	5
GTR1_HUMAN	100.00%	87
WDR55_HUMAN	96.10%	3
UGGG1_HUMAN	98.20%	0
CWC22_HUMAN	96.10%	2
RSMB_HUMAN,RSMN_HUMAN	13.90%	0
NUP93_HUMAN	100.00%	34
gnl|unk|ENST00000377524_2	97.50%	1

DHB11_HUMAN	100.00%	11
UGDH_HUMAN	100.00%	2
DDX24_HUMAN	99.30%	6
MESD_HUMAN	96.10%	4
RM45_HUMAN	100.00%	9
VATB2_HUMAN	100.00%	10
BAF_HUMAN,gnl|unk|ENST00000312175_10,gnl|unk|ENST00000445560_7	100.00%	43
UDB10_HUMAN	99.20%	2
SEC63_HUMAN	100.00%	27
PSA3_HUMAN	96.10%	1
RPB9_HUMAN	96.10%	5
UD2A3_HUMAN	100.00%	13
VPS45_HUMAN	96.10%	3
VWA8_HUMAN	96.10%	1
DIC_HUMAN	100.00%	62
NSF_HUMAN	100.00%	21
THOC2_HUMAN	93.90%	1
DEFM_HUMAN	100.00%	4
ABCF2_HUMAN	96.10%	6
OPA1_HUMAN	100.00%	27
PP1B_HUMAN	100.00%	54
FADS1_HUMAN	100.00%	4
TOM34_HUMAN	100.00%	2
T126A_HUMAN	100.00%	11
TIM16_HUMAN	96.10%	4
ZNT7_HUMAN	99.90%	3

TM55B_HUMAN	96.10%	1
RSF1_HUMAN	96.10%	1
PKP2_HUMAN	100.00%	24
CNBP_HUMAN	100.00%	5
MSH3_HUMAN	96.10%	1
NUP85_HUMAN	100.00%	28
TKT_HUMAN	100.00%	8
ACADV_HUMAN	100.00%	25
RUXG_HUMAN,gnl|unk|ENST00000272348_6	96.10%	7
GALT1_HUMAN	98.60%	1
EMC4_HUMAN	100.00%	10
AT1B3_HUMAN	100.00%	13
HM13_HUMAN	100.00%	22
ERG7_HUMAN	100.00%	52
NPM3_HUMAN	100.00%	9
RL18A_HUMAN	100.00%	7
LRC8D_HUMAN	73.90%	0
MYO1B_HUMAN	100.00%	30
ASGR2_HUMAN	100.00%	31
RU1C_HUMAN	96.10%	7
RM37_HUMAN	15.90%	0
COX6C_HUMAN,gnl|unk|ENST00000297564_4,gnl|unk|ENST00000517682_4,gnl|unk|ENST00000522940_7,gnl|unk|ENST00000524245_5	100.00%	18
CISD1_HUMAN,gnl|unk|ENST00000489785_8	100.00%	3
THOC4_HUMAN	100.00%	153
IMDH2_HUMAN	100.00%	2

REEP6_HUMAN	100.00%	4
LSM5_HUMAN,gnl|unk|ENST00000450169_6	96.10%	5
PPIH_HUMAN	96.10%	4
HINT3_HUMAN	96.10%	1
CAZA2_HUMAN	100.00%	11
MOT1_HUMAN	100.00%	15
NOC3L_HUMAN	100.00%	3
1433E_HUMAN	99.60%	1
RL23_HUMAN	100.00%	10
DDX5_HUMAN	100.00%	50
NDUA7_HUMAN	100.00%	6
HDAC1_HUMAN	100.00%	7
NP1L4_HUMAN	13.60%	0
PLIN2_HUMAN	100.00%	63
HNRPQ_HUMAN	70.80%	1
AT2C1_HUMAN	96.10%	2
ZNT1_HUMAN	100.00%	11
CEAM1_HUMAN	100.00%	29
RAB21_HUMAN	100.00%	12
ENPL_HUMAN	100.00%	72
MFF_HUMAN	100.00%	6
RS18_HUMAN	100.00%	2
TXD15_HUMAN	96.10%	2
SYIC_HUMAN	100.00%	24
UBXN1_HUMAN	96.10%	1
CP51A_HUMAN	100.00%	30

TFAM_HUMAN	100.00%	36
CALU_HUMAN	100.00%	11
CSK2B_HUMAN	72.00%	1
COMT_HUMAN	100.00%	88
DNJC5_HUMAN	100.00%	10
DHRS2_HUMAN	100.00%	112
RTCB_HUMAN	100.00%	6
CDC27_HUMAN	99.90%	2
CO4A_HUMAN,CO4B_HUMAN	100.00%	10
UHRF1_HUMAN	100.00%	26
SPTC1_HUMAN	100.00%	21
PRP6_HUMAN	100.00%	13
CD63_HUMAN	100.00%	4
PRAF3_HUMAN	100.00%	10
ST1A3_HUMAN,ST1A4_HUMAN	96.10%	4
ATD3A_HUMAN	100.00%	52
DX39B_HUMAN	99.60%	14
GTF2I_HUMAN	100.00%	18
MRE11_HUMAN	77.70%	1
KIF22_HUMAN	96.10%	1
COBL_HUMAN	96.10%	1
SFXN2_HUMAN	96.10%	7
HNRPK_HUMAN	100.00%	4
QCR8_HUMAN,gnl|unk|ENST00000378667_5	96.10%	5
AT5F1_HUMAN	100.00%	41
PVR_HUMAN	100.00%	9

CTBL1_HUMAN	99.90%	5
COX11_HUMAN	100.00%	4
CETN2_HUMAN	43.00%	0
SSRP1_HUMAN	100.00%	66
APOH_HUMAN	100.00%	6
SYRC_HUMAN	100.00%	12
SMRD2_HUMAN	99.90%	3
NDUB6_HUMAN	100.00%	18
IF2G_HUMAN	100.00%	16
RL15_HUMAN	100.00%	11
RCC1_HUMAN	100.00%	104
SRS10_HUMAN	96.10%	2
H2A1D_HUMAN,H2A1H_HUMAN,H2A1J_HUMAN,H2A1_HUMAN,H2AJ_HUMAN	100.00%	221
RS27_HUMAN,gnl|unk|ENST00000368567_2,gnl|unk|ENST00000457554_4,gnl|unk|ENST00000495392_4	100.00%	8
CNIH4_HUMAN,gnl|unk|ENST00000468318_8	96.10%	12
ROMO1_HUMAN,gnl|unk|ENST00000374078_3,gnl|unk|ENST00000397416_1	96.10%	7
SP3_HUMAN	96.10%	1
ICT1_HUMAN,gnl|unk|ENST00000580800_9	6.90%	0
TF3C5_HUMAN	96.10%	6
PWP2_HUMAN	96.10%	2
GABT_HUMAN	92.40%	2
IF2P_HUMAN	96.10%	8
TF3C4_HUMAN	96.10%	5
TBA1C_HUMAN	100.00%	144
FMNL2_HUMAN	99.70%	1

PDIA3_HUMAN	100.00%	163
ADT2_HUMAN	100.00%	103
SGT1_HUMAN	15.00%	0
DYLT1_HUMAN,gnl|unk|ENST00000367085_4	100.00%	10
ERLN1_HUMAN	100.00%	18
ZW10_HUMAN	100.00%	10
MIC26_HUMAN	96.10%	6
RT35_HUMAN	95.60%	1
TM189_HUMAN	100.00%	7
ESAM_HUMAN	96.10%	4
COX1_HUMAN	99.40%	36
ROA0_HUMAN	100.00%	13
PGK1_HUMAN	83.80%	0
CALM_HUMAN	100.00%	52
RS21_HUMAN,gnl|unk|ENST00000343986_2,gnl|unk|ENST00000450116_2,gnl|unk|ENST00000492356_2	96.10%	8
SF3A3_HUMAN	97.90%	0
P4HA1_HUMAN	96.10%	2
NDUA8_HUMAN	100.00%	25
HDAC2_HUMAN	28.10%	4
PLIN3_HUMAN	100.00%	3
K22E_HUMAN	99.40%	3
SOAT1_HUMAN	100.00%	5
STEA3_HUMAN	100.00%	1
AL1A1_HUMAN	100.00%	7
K1C19_HUMAN	100.00%	400

NSUN5_HUMAN	96.10%	1
E41L5_HUMAN	6.40%	0
RS19_HUMAN	100.00%	9
DNJB1_HUMAN	99.90%	4
SMCA1_HUMAN	100.00%	7
TIM50_HUMAN	100.00%	22
NDUS6_HUMAN	100.00%	9
ARAP1_HUMAN	96.10%	6
APMAP_HUMAN	100.00%	93
SNF5_HUMAN	98.20%	4
PRP19_HUMAN	100.00%	47
ITPR2_HUMAN	100.00%	16
THIK_HUMAN	96.10%	3
SMC1A_HUMAN	100.00%	6
ATD3B_HUMAN	100.00%	34
SAHH_HUMAN	99.30%	6
RBBP4_HUMAN	100.00%	11
S61A1_HUMAN	100.00%	41
IL6RB_HUMAN	100.00%	2
HMOX2_HUMAN	100.00%	20
RPOM_HUMAN	96.10%	5
GOLP3_HUMAN	96.10%	2
JAK1_HUMAN	96.10%	4
TAF5_HUMAN	99.10%	1
VIGLN_HUMAN	96.10%	1
TMEDA_HUMAN	100.00%	61

IF5_HUMAN	96.10%	3
PHB_HUMAN	100.00%	118
TOP1_HUMAN	100.00%	40
ACSL5_HUMAN	100.00%	90
ALBU_HUMAN	100.00%	24
NDUA2_HUMAN	100.00%	1
ZN326_HUMAN	99.10%	1
HNRPL_HUMAN	100.00%	26
2AAA_HUMAN	100.00%	4
TKFC_HUMAN	5.60%	0
DDB1_HUMAN	100.00%	4
DDX50_HUMAN	41.00%	2
RN149_HUMAN	96.10%	6
CAF1A_HUMAN	100.00%	2
PUR2_HUMAN	21.20%	0
AT2B4_HUMAN	99.90%	10
COX15_HUMAN	96.10%	4
UBQL2_HUMAN	96.10%	1
H12_HUMAN	100.00%	120
gnl|unk|ENST00000424846_20,gnl|unk|ENST00000492121_18	100.00%	12
RRBP1_HUMAN	100.00%	64
ATP5H_HUMAN	100.00%	117
RAD21_HUMAN	100.00%	8
DNJA3_HUMAN	100.00%	5
KIF4A_HUMAN	96.10%	4
LMAN1_HUMAN	100.00%	114

RALB_HUMAN	93.10%	0
OCAD1_HUMAN	100.00%	4
FA83D_HUMAN	96.10%	2
TOP2B_HUMAN	100.00%	35
MLF2_HUMAN	96.10%	2
NBAS_HUMAN	99.40%	0
PGAM1_HUMAN	99.90%	4
SUN1_HUMAN	100.00%	8
AMPN_HUMAN	100.00%	122
S26A6_HUMAN	96.10%	1
ADT3_HUMAN	100.00%	128
GDIB_HUMAN	100.00%	6
ERLN2_HUMAN	100.00%	22
FLNB_HUMAN	100.00%	12
CDC5L_HUMAN	100.00%	14
MPC2_HUMAN	99.90%	1
ERBB2_HUMAN	77.10%	0
B2CL1_HUMAN	96.10%	1
PO210_HUMAN	100.00%	56
MIC27_HUMAN	100.00%	2
HNRPF_HUMAN	100.00%	16
DPP4_HUMAN	100.00%	77
SKP1_HUMAN	96.10%	1
CP2W1_HUMAN	100.00%	8
ATAD1_HUMAN	100.00%	2
VATG1_HUMAN	100.00%	10

PEG3_HUMAN	99.80%	5
ELOV5_HUMAN	96.10%	6
COPB2_HUMAN	96.10%	1
NFIP1_HUMAN,gnl|unk|ENST00000509436_2	96.10%	2
NUP43_HUMAN	100.00%	7
NSDHL_HUMAN	100.00%	12
NDUB1_HUMAN,gnl|unk|ENST00000553514_8,gnl|unk|ENST00000555441_6	99.00%	3
OSBL2_HUMAN	96.10%	1
DAG1_HUMAN	99.80%	7
IF2B_HUMAN	99.90%	4
RL10_HUMAN	100.00%	54
SP16H_HUMAN	100.00%	38
TOM6_HUMAN,gnl|unk|ENST00000335515_36,gnl|unk|ENST00000398881_6,gnl|unk|ENST00000398884_6,gnl|unk|ENST00000456057_41,gnl|unk|ENST00000487182_39	100.00%	29
ROA1_HUMAN	100.00%	41
ATP5L_HUMAN	100.00%	12
TBB2B_HUMAN	99.90%	239
ML12A_HUMAN,ML12B_HUMAN	100.00%	105
CALX_HUMAN	100.00%	414
NPM_HUMAN	100.00%	90
VDAC1_HUMAN	100.00%	484
RAN_HUMAN	100.00%	29
BASI_HUMAN	100.00%	110
SYMC_HUMAN	100.00%	39
PININ_HUMAN	100.00%	8
NDUS7_HUMAN	96.10%	10

TPP1_HUMAN	100.00%	4
HSP72_HUMAN	27.70%	44
ZFPL1_HUMAN	96.10%	6
LAT1_HUMAN	100.00%	21
RT30_HUMAN	12.50%	0
ABCD1_HUMAN	99.90%	1
MPCP_HUMAN	100.00%	62
SF3B2_HUMAN	99.90%	1
RL5_HUMAN	100.00%	6
SUZ12_HUMAN	96.10%	1
TCPG_HUMAN	100.00%	14
GSLG1_HUMAN	100.00%	129
RM16_HUMAN	35.90%	0
MET7A_HUMAN	100.00%	12
HMGB2_HUMAN	99.20%	5
TFR1_HUMAN	100.00%	104
SPTN1_HUMAN	100.00%	470
LAMP2_HUMAN	100.00%	12
MIC19_HUMAN	100.00%	17
RS5_HUMAN	100.00%	74
DYL2_HUMAN	6.30%	11
SAHH2_HUMAN	85.20%	2
RPN2_HUMAN	100.00%	532
HNRH1_HUMAN	100.00%	39
COPE_HUMAN	96.10%	5
ALG5_HUMAN	99.90%	8

STT3A_HUMAN	100.00%	29
ACY1_HUMAN	96.10%	1
IMPA3_HUMAN	35.70%	0
K1C14_HUMAN	99.80%	13
MD1L1_HUMAN	100.00%	4
RS14_HUMAN,gnl|unk|ENST00000519690_58	100.00%	29
DMD_HUMAN	100.00%	2
RASH_HUMAN	99.30%	10
TOM22_HUMAN	100.00%	70
GRWD1_HUMAN	96.10%	3
NH2L1_HUMAN	100.00%	26
GPI8_HUMAN	100.00%	10
NDUS1_HUMAN	100.00%	101
AT131_HUMAN	100.00%	15
PDLI1_HUMAN	100.00%	12
EXOS6_HUMAN	96.10%	1
DNJA4_HUMAN	96.10%	1
GPC5C_HUMAN	96.10%	1
UFL1_HUMAN	100.00%	25
TOP2A_HUMAN	100.00%	125
LAMC1_HUMAN	100.00%	6
SUN2_HUMAN	100.00%	44
UTP20_HUMAN	96.10%	2
T2FA_HUMAN	96.10%	4
SCAM4_HUMAN	100.00%	11
TIM9_HUMAN,gnl|unk|ENST00000395159_12,gnl|unk|ENST00000555061_8,gnl|unk|ENST	100.00%	8

00000555404_9,gnl|unk|ENST00000555593_8		
KCY_HUMAN	77.10%	1
HG2A_HUMAN	100.00%	10
BCS1_HUMAN	99.90%	3
RT05_HUMAN	19.20%	0
MDC1_HUMAN	100.00%	2
PR40A_HUMAN	100.00%	10
COIA1_HUMAN	96.10%	5
gnl|unk|ENST00000354895_3	96.10%	4
AKAP1_HUMAN	100.00%	12
ATAD2_HUMAN	100.00%	14
SEPT2_HUMAN	18.30%	0
RAB7A_HUMAN	100.00%	34
GLYM_HUMAN	99.80%	1
SQRD_HUMAN	100.00%	41
UXS1_HUMAN	100.00%	4
BAZ1B_HUMAN	100.00%	23
PAIRB_HUMAN	100.00%	20
TMTC3_HUMAN	96.10%	2
SFPQ_HUMAN	100.00%	122
RMD3_HUMAN	99.90%	1
CPT2_HUMAN	100.00%	8
K1C23_HUMAN	96.10%	3
TOM7_HUMAN,gnl|unk|ENST00000358435_4	99.90%	4
NCEH1_HUMAN	100.00%	5
TMOD3_HUMAN	100.00%	7

CLCC1_HUMAN	100.00%	6
AN32B_HUMAN	7.40%	4
ICAM1_HUMAN	100.00%	9
PRDX2_HUMAN	99.80%	5
YIPF5_HUMAN	96.10%	3
PYC_HUMAN	96.10%	1
HEMH_HUMAN	96.10%	2
SMHD1_HUMAN	100.00%	10
NUP50_HUMAN	96.10%	1
RS4X_HUMAN	100.00%	38
DC1I2_HUMAN	100.00%	12
CAZA1_HUMAN	100.00%	10
S12A7_HUMAN	99.10%	1
PLXB2_HUMAN	99.90%	5
SC5A6_HUMAN	100.00%	3
SMRC1_HUMAN	100.00%	9
KAD4_HUMAN	99.90%	14
TM115_HUMAN	90.70%	1
SCPDL_HUMAN	100.00%	10
MIA3_HUMAN	100.00%	17
HSPB1_HUMAN	100.00%	25
SF3B3_HUMAN	100.00%	2
RL6_HUMAN	100.00%	37
CTND1_HUMAN	100.00%	114
EMD_HUMAN	100.00%	22
SNX5_HUMAN	96.10%	4

U5S1_HUMAN	100.00%	30
GBB2_HUMAN	100.00%	29
NGDN_HUMAN	96.10%	4
SMC6_HUMAN	96.10%	4
RAB6C_HUMAN	96.10%	1
MP2K3_HUMAN	96.10%	4
TPIS_HUMAN	100.00%	3
RING1_HUMAN,RING2_HUMAN	96.10%	6
FXR1_HUMAN	96.10%	3
ALDOC_HUMAN	99.20%	9
ESYT1_HUMAN	100.00%	64
GBG5_HUMAN	100.00%	26
NDUB5_HUMAN	100.00%	29
IF4G2_HUMAN	99.40%	1
K1C15_HUMAN	45.90%	11
IR3IP_HUMAN,gnl|unk|ENST00000256433_3,gnl|unk|ENST00000588705_3	98.60%	6
CDS2_HUMAN	100.00%	22
AOFB_HUMAN	100.00%	20
GPX1_HUMAN	37.80%	0
CXB1_HUMAN	99.20%	6
ARC1B_HUMAN	96.10%	4
NDUS2_HUMAN	100.00%	34
SPNS1_HUMAN	100.00%	18
TM41A_HUMAN	100.00%	4
NOP10_HUMAN,gnl|unk|ENST00000328848_6	96.10%	1
KHDR1_HUMAN	100.00%	24

MOT4_HUMAN	100.00%	15
UBIA1_HUMAN	96.10%	5
NNTM_HUMAN	100.00%	11
ADNP_HUMAN	92.50%	2
CND1_HUMAN	99.80%	1
TCPB_HUMAN	100.00%	4
TIM13_HUMAN,gnl|unk|ENST00000215570_5	99.90%	3
LAMA5_HUMAN	100.00%	6
G45IP_HUMAN	96.10%	5
WDR18_HUMAN	96.10%	2
ZYX_HUMAN	100.00%	7
LC7L2_HUMAN	98.10%	5
IMB1_HUMAN	100.00%	19
SCRIB_HUMAN	100.00%	6
NECT2_HUMAN	100.00%	7
ITAV_HUMAN	100.00%	8
EPT1_HUMAN	100.00%	6
RADI_HUMAN	98.80%	2
SRSF7_HUMAN	99.90%	11
DAD1_HUMAN	100.00%	16
TMX1_HUMAN	100.00%	12
IF4A1_HUMAN	100.00%	26
DHE3_HUMAN	100.00%	11
RMND1_HUMAN	100.00%	4
ACSL3_HUMAN	100.00%	146
PGRC2_HUMAN	100.00%	14

AR6P1_HUMAN	98.20%	2
VATD_HUMAN	96.10%	1
RSSA_HUMAN	100.00%	7
ACINU_HUMAN	99.90%	2
TOM70_HUMAN	100.00%	71
STAT3_HUMAN	100.00%	3
CND2_HUMAN	96.10%	6
SYJ2B_HUMAN,gnl|unk|ENST00000618385_4	96.10%	6
AGRIN_HUMAN	100.00%	3
YBOX1_HUMAN	100.00%	14
RBP56_HUMAN	99.20%	9
DDX27_HUMAN	100.00%	5
CYB5B_HUMAN	100.00%	500
ATPG_HUMAN	100.00%	55
TBL2_HUMAN	100.00%	15
ARF6_HUMAN	96.10%	2
ACTN4_HUMAN	100.00%	25
WDR12_HUMAN	96.10%	3
CLH1_HUMAN	100.00%	141
MK03_HUMAN	96.10%	2
TMED7_HUMAN	100.00%	34
DSRAD_HUMAN	100.00%	10
COX2_HUMAN	100.00%	58
EMC2_HUMAN	100.00%	25
FCGRN_HUMAN	99.90%	6
EPN4_HUMAN	96.00%	1

GOGB1_HUMAN	100.00%	3
NU133_HUMAN	100.00%	22
SRSF1_HUMAN	100.00%	6
SNW1_HUMAN	96.10%	4
H2AX_HUMAN	100.00%	216
ABI1_HUMAN	96.10%	6
ADRM1_HUMAN	14.50%	0
B4GT1_HUMAN	96.10%	1
ACPM_HUMAN	100.00%	25
ASPH_HUMAN	100.00%	12
P2RX4_HUMAN	96.10%	1
RS26_HUMAN	99.90%	2
ITB5_HUMAN	100.00%	4
SRC_HUMAN	100.00%	6
DGLB_HUMAN	100.00%	1
RM39_HUMAN	42.50%	0
LYSC_HUMAN	96.10%	6
ETFB_HUMAN	96.10%	4
HACD3_HUMAN	100.00%	58
RM44_HUMAN	100.00%	11
GANAB_HUMAN	100.00%	7
MLEC_HUMAN	100.00%	38
gnl|unk|ENST00000509601_5	100.00%	5
SSRD_HUMAN	100.00%	59
PUF60_HUMAN	96.10%	2
INT3_HUMAN	99.80%	1

DDX21_HUMAN	100.00%	76
SYVN1_HUMAN	99.90%	1
VRK1_HUMAN	100.00%	9
TRIPC_HUMAN	100.00%	8
CHD4_HUMAN	100.00%	61
SEH1_HUMAN	100.00%	9
SGPL1_HUMAN	100.00%	20
ANXA4_HUMAN	100.00%	8
RAB23_HUMAN	100.00%	2
H1X_HUMAN	100.00%	30
ERO1A_HUMAN	16.20%	0
S12A2_HUMAN	96.10%	1
TCPZ_HUMAN	96.10%	6
CERS2_HUMAN	100.00%	11
MAP4_HUMAN	100.00%	10
SELS_HUMAN	96.10%	1
CLCN7_HUMAN	99.40%	3
MCM3_HUMAN	91.20%	1
TM2D2_HUMAN	96.10%	6
RUVB1_HUMAN	100.00%	13
ACATN_HUMAN	96.10%	6
RALY_HUMAN	100.00%	6
MAVS_HUMAN	100.00%	2
CALR_HUMAN	100.00%	50
AGK_HUMAN	100.00%	21
M2OM_HUMAN	100.00%	19

PMM2_HUMAN	96.10%	8
PESC_HUMAN	7.70%	0
SRPRA_HUMAN	100.00%	23
LC7L3_HUMAN	96.10%	4
KAP2_HUMAN	100.00%	12
MDHM_HUMAN	96.10%	7
RB11B_HUMAN	100.00%	7
PDIP3_HUMAN	100.00%	5
TFCP2_HUMAN	77.00%	0
ALG1_HUMAN	100.00%	23
gnl|unk|ENST00000514511_3	96.10%	3
PRDX4_HUMAN	100.00%	11
HNRPR_HUMAN	100.00%	11
HYEP_HUMAN	100.00%	188
MARC1_HUMAN	99.80%	6
HS2ST_HUMAN	99.20%	1
K1C10_HUMAN	100.00%	16
DERL1_HUMAN	97.80%	0
S27A2_HUMAN	100.00%	7
AP2A2_HUMAN	42.80%	5
NIP7_HUMAN	99.20%	6
ASAH1_HUMAN	100.00%	12
TBB5_HUMAN	100.00%	318
PBIP1_HUMAN	100.00%	6
NDUB8_HUMAN	83.30%	1
U520_HUMAN	100.00%	36

DREB_HUMAN	100.00%	6
SRRM1_HUMAN	100.00%	1
DIM1_HUMAN	98.90%	1
RAB32_HUMAN	100.00%	17
gnl|unk|ENST00000347364_6,gnl|unk|ENST00000399054_11,gnl|unk|ENST00000609375_11	96.10%	1
CHP1_HUMAN	100.00%	4
MTX2_HUMAN	100.00%	10
EMAL4_HUMAN	96.10%	2
MPPA_HUMAN	96.10%	5
CLIC1_HUMAN	100.00%	7
BYST_HUMAN	96.10%	6
PEBP1_HUMAN	96.10%	8
METK2_HUMAN	96.10%	2
ERP29_HUMAN	100.00%	8
CTNA1_HUMAN	100.00%	16
DJC10_HUMAN	100.00%	2
H2AY_HUMAN	100.00%	97
STAU1_HUMAN	100.00%	18
CP27A_HUMAN	100.00%	11
FIBG_HUMAN	100.00%	104
ARK72_HUMAN	9.90%	0
3BHS7_HUMAN	100.00%	7
IMA4_HUMAN	96.10%	2
AOFA_HUMAN	100.00%	20
MATR3_HUMAN	100.00%	13

ERG1_HUMAN	100.00%	32
TAP2_HUMAN	96.10%	1
VTNC_HUMAN	96.10%	2
NIPBL_HUMAN	96.10%	1
AP2B1_HUMAN	100.00%	13
FSCN1_HUMAN	96.10%	2
ERLEC_HUMAN	100.00%	29
ATPO_HUMAN	100.00%	54
GNA11_HUMAN	100.00%	10
MARE2_HUMAN	96.10%	5
ATPB_HUMAN	100.00%	1252
RL26_HUMAN	100.00%	6
gnl|unk|ENST00000576925_5	99.00%	11
SYDC_HUMAN	100.00%	11
SCFD2_HUMAN	96.10%	6
LAD1_HUMAN	100.00%	13
MBOA5_HUMAN	100.00%	3
GRN_HUMAN	100.00%	7
NDRG1_HUMAN	98.30%	6
ANXA5_HUMAN	100.00%	9
LMO7_HUMAN	100.00%	13
NSMA3_HUMAN	100.00%	31
TMED2_HUMAN	100.00%	18
KPYM_HUMAN	100.00%	61
DNMT1_HUMAN	100.00%	7
FLOT1_HUMAN	100.00%	20

SNP23_HUMAN	100.00%	25
SELT_HUMAN,gnl|unk|ENST00000466234_3	96.10%	3
UBXN4_HUMAN	100.00%	9
PRR11_HUMAN	100.00%	5
EMC1_HUMAN	100.00%	68
FIBA_HUMAN	100.00%	35
MK67I_HUMAN	100.00%	7
MFAP1_HUMAN	99.60%	1
FND3A_HUMAN	100.00%	10
MYH10_HUMAN	100.00%	293
EHD1_HUMAN	96.10%	5
RPB2_HUMAN	100.00%	6
ITM2C_HUMAN	96.10%	6
OSTB_HUMAN	68.00%	1
ECE1_HUMAN	100.00%	5
LASP1_HUMAN	100.00%	17
M4K4_HUMAN	100.00%	7
C560_HUMAN	100.00%	9
EF1G_HUMAN	100.00%	9
HERP1_HUMAN	100.00%	10
GPAA1_HUMAN	99.30%	2
RL3L_HUMAN	99.90%	19
STML2_HUMAN	100.00%	86
H2A1B_HUMAN,H2A1C_HUMAN,H2A3_HUMAN	100.00%	216
ACTS_HUMAN	99.30%	187
RBMX_HUMAN	100.00%	30

APC1_HUMAN	96.10%	3
NCLN_HUMAN	100.00%	39
JAG1_HUMAN	96.10%	1
YES_HUMAN	100.00%	14
MA1B1_HUMAN	100.00%	8
COX5B_HUMAN	100.00%	21
ETFA_HUMAN	100.00%	8
RL35_HUMAN	100.00%	28
NDUB9_HUMAN	100.00%	39
LPP_HUMAN	96.10%	1
RL18_HUMAN	100.00%	27
ILF2_HUMAN	100.00%	13
PLPP6_HUMAN	96.10%	2
NDUS4_HUMAN	100.00%	10
H31_HUMAN	99.90%	95
FDFT_HUMAN	100.00%	136
CH60_HUMAN	100.00%	247
SYNE3_HUMAN	100.00%	3
H14_HUMAN	100.00%	110
IGSF1_HUMAN	100.00%	12
UCRIL_HUMAN	99.90%	17
ABCE1_HUMAN	100.00%	3
SRBD1_HUMAN	100.00%	5
RT29_HUMAN	96.10%	3
UB2L3_HUMAN	96.10%	1
PNO1_HUMAN	96.10%	10

RER1_HUMAN	100.00%	9
UCRI_HUMAN	100.00%	50
TPM3_HUMAN	100.00%	12
ST1A1_HUMAN	96.10%	2
ACSF2_HUMAN	96.10%	1
HS90B_HUMAN	100.00%	95
PON2_HUMAN	100.00%	26
H2B1C_HUMAN,H2B1D_HUMAN,H2B1H_HUMAN,H2B1K_HUMAN,H2B1L_HUMAN,H2B1N_HUMAN,H2B2F_HUMAN	100.00%	952
NPTN_HUMAN	99.80%	11
IKIP_HUMAN	100.00%	6
ITA2_HUMAN	100.00%	13
XPC_HUMAN	99.80%	6
IF2B1_HUMAN	100.00%	10
FUBP3_HUMAN	100.00%	5
JAGN1_HUMAN	100.00%	4
MPZL1_HUMAN	96.10%	1
ADT1_HUMAN	100.00%	115
TIF1B_HUMAN	100.00%	37
MBOA7_HUMAN	96.10%	6
BST2_HUMAN,gnl|unk|ENST00000533098_5	96.10%	7
UBAC2_HUMAN	35.50%	0
NDUB3_HUMAN	99.90%	2
APT_HUMAN	91.60%	1
RD23B_HUMAN	96.10%	3
TBB4A_HUMAN	99.90%	159

RRS1_HUMAN	100.00%	17
gnl|unk|ENST00000394186_3,gnl|unk|ENST00000485011_2,gnl|unk|ENST00000488775_2	57.00%	24
RAB10_HUMAN	100.00%	37
FBRL_HUMAN	100.00%	57
XRCC6_HUMAN	100.00%	16
RTN3_HUMAN	25.80%	0
FABP5_HUMAN	17.80%	0
RL27_HUMAN	100.00%	40
AIMP2_HUMAN	96.10%	1
S19A1_HUMAN	99.40%	6
TSN6_HUMAN	99.90%	5
VDAC3_HUMAN	100.00%	115
VMP1_HUMAN	100.00%	15
NOG1_HUMAN	100.00%	3
RHDF2_HUMAN	96.10%	1
PCYOX_HUMAN	100.00%	94
RBM14_HUMAN	96.10%	3
C1QBP_HUMAN	96.10%	6
TOIP1_HUMAN	100.00%	21
SURF1_HUMAN	96.10%	2
SMCA4_HUMAN	100.00%	5
RUXE_HUMAN,gnl|unk|ENST00000414487_4	100.00%	11
LDHA_HUMAN	100.00%	6
FIBB_HUMAN	100.00%	49
AT1B1_HUMAN	100.00%	24
AP1M1_HUMAN	95.50%	1

FND3B_HUMAN	100.00%	16
INT1_HUMAN	96.10%	1
UBB_HUMAN,UBC_HUMAN	100.00%	85
SAR1A_HUMAN	94.40%	3
HIG1A_HUMAN,gnl|unk|ENST00000418900_4,gnl|unk|ENST00000625589_4	98.10%	9
PINX1_HUMAN	96.10%	1
SUCB1_HUMAN	96.10%	2
RBBP7_HUMAN	100.00%	8
JAM1_HUMAN	100.00%	17
LCLT1_HUMAN	99.90%	8
OSTC_HUMAN	96.10%	10
EF2_HUMAN	100.00%	110
RPAC1_HUMAN	89.30%	1
DHB4_HUMAN	100.00%	37
NDUC2_HUMAN,gnl|unk|ENST00000525085_5	99.00%	3
RHOG_HUMAN	90.50%	0
RL21_HUMAN	100.00%	26
SMU1_HUMAN	99.80%	2

Table 2. All proteins identified in HepG2 by this analysis. Database searching was performed on the datasets described in Table 1. In column 1, protein identifications are shown along with their cluster partners. In column 2, identification probabilities are shown. In column 3, spectral counts are shown for each protein idenfication. Probabilities here were calculated by the PeptideProphet algorithm and by the ProteinProphet algorithm, and the protein probabilities are displayed.

Accession Number	Treated Membrane	Untreated Membrane	Treated Cytosolic	Untreated Cytosolic
ACTB_HUMAN	2091	2018	765	745
ACTG_HUMAN	2088	2023	757	742
ACTBL_HUMAN	67	72	53	48
POTEE_HUMAN	1293	1121	363	343
ACTBM_HUMAN	110	113	114	112
ACTS_HUMAN	187	200	188	185
ACTC_HUMAN	187	200	188	185
CH60_HUMAN	247	237	1486	1647
HS90B_HUMAN	95	73	808	717
HS90A_HUMAN	37	32	748	695
HS905_HUMAN	0	0	139	113
H90B2_HUMAN	0	0	133	121
HS904_HUMAN	0	0	0	46
H90B4_HUMAN	0	0	44	0
ATPB_HUMAN	1252	1161	87	88
gnl|unk|ENST00000548474_4	0	34	0	0
FAS_HUMAN	101	114	987	896
H2B1C_HUMAN	952	961	68	40
H2B1D_HUMAN	952	961	68	40
H2B1H_HUMAN	952	961	68	40
H2B1K_HUMAN	952	961	68	40
H2B1L_HUMAN	952	961	68	40
H2B1N_HUMAN	952	961	68	40
H2B2F_HUMAN	952	961	68	40
H2B3B_HUMAN	933	939	68	37
H2B1A_HUMAN	0	0	0	0

EF1A1_HUMAN	695	424	388	342
EF1A2_HUMAN	0	0	0	0
TBB5_HUMAN	318	338	539	537
TBB3_HUMAN	180	218	336	327
TBB2B_HUMAN	239	269	396	401
TBB4B_HUMAN	279	300	488	483
TBB4A_HUMAN	159	160	304	312
TBB1_HUMAN	0	0	0	0
H4_HUMAN	622	583	3	7
SPTB2_HUMAN	621	545	74	52
SPTN2_HUMAN	0	0	0	0
SPTN4_HUMAN	0	0	0	0
SPTB1_HUMAN	0	0	0	0
ATPA_HUMAN	690	713	28	29
MYH9_HUMAN	526	489	0	0
MYH10_HUMAN	293	273	2	0
MYH14_HUMAN	31	33	0	0
MYH11_HUMAN	0	0	0	0
G3P_HUMAN	22	17	651	597
G3PT_HUMAN	0	0	0	0
PDIA1_HUMAN	76	68	546	531
GRP78_HUMAN	166	134	475	470
K2C8_HUMAN	428	428	64	65
K2C1_HUMAN	17	20	11	0
K22E_HUMAN	3	2	0	0
K2C80_HUMAN	0	0	0	0
gnl|unk|ENST00000547031_7	26	0	0	0
K2C5_HUMAN	0	0	0	0
K2C7_HUMAN	0	0	0	0

PDIA3_HUMAN	163	156	443	410
ENPL_HUMAN	72	54	589	528
ENPLL_HUMAN	0	0	0	0
ACTN4_HUMAN	25	23	413	397
ACTN1_HUMAN	13	13	286	240
ACTN2_HUMAN	0	0	0	0
ACTN3_HUMAN	0	0	0	0
SPTN1_HUMAN	470	410	25	25
EF2_HUMAN	110	98	405	381
RPN2_HUMAN	532	482	5	6
CYB5B_HUMAN	500	471	6	5
CALR_HUMAN	50	37	415	399
CALX_HUMAN	414	412	7	6
VDAC1_HUMAN	484	472	1	0
CLH1_HUMAN	141	115	271	262
ENOA_HUMAN	38	35	396	350
ENOG_HUMAN	0	0	60	74
TBA1B_HUMAN	171	149	231	227
TBA1C_HUMAN	144	138	195	203
TBA8_HUMAN	0	0	0	0
K1C18_HUMAN	354	325	27	32
AL1A1_HUMAN	7	6	166	145
AL1B1_HUMAN	2	1	138	142
ALDH2_HUMAN	1	1	91	98
AL1A2_HUMAN	0	0	0	0
AL1A3_HUMAN	0	0	0	0
HSP7C_HUMAN	101	106	315	290
HSP72_HUMAN	44	46	99	96
NPM_HUMAN	90	83	346	338

NUCL_HUMAN	68	43	339	311
LPPRC_HUMAN	1	2	294	317
HNRPU_HUMAN	157	154	179	170
ECHA_HUMAN	139	156	147	166
RPN1_HUMAN	323	278	1	0
TERA_HUMAN	56	55	271	256
PEX1_HUMAN	0	0	0	0
K1C19_HUMAN	400	336	30	30
K1C16_HUMAN	9	8	0	0
gnl|unk|ENST00000405746_3	0	1	0	0
K1C15_HUMAN	11	11	0	1
K1C14_HUMAN	13	0	0	0
K1C17_HUMAN	0	9	0	0
KPYM_HUMAN	61	66	280	253
HNRPK_HUMAN	4	10	273	291
LMNA_HUMAN	273	238	0	0
DHRS2_HUMAN	112	97	177	193
SERPH_HUMAN	144	172	81	79
ROA1_HUMAN	41	57	365	295
XRCC5_HUMAN	51	32	240	230
PDIA6_HUMAN	30	39	270	255
PRKDC_HUMAN	185	216	38	31
DESP_HUMAN	258	230	0	0
DHE3_HUMAN	11	7	231	246
CKAP4_HUMAN	247	227	0	0
XRCC6_HUMAN	16	16	224	237
RS7_HUMAN	176	111	128	121
ALDOA_HUMAN	13	5	228	249
HNRPM_HUMAN	114	100	88	89

RL4_HUMAN	92	77	89	94
H2A1D_HUMAN	221	256	14	20
H2A1H_HUMAN	221	256	14	20
H2A1J_HUMAN	221	256	14	20
H2A1_HUMAN	221	256	14	20
H2AJ_HUMAN	221	256	14	20
H2A1B_HUMAN	216	251	0	0
H2A1C_HUMAN	216	251	0	0
H2A3_HUMAN	216	251	0	0
H2A2B_HUMAN	210	250	0	0
H2AX_HUMAN	216	256	0	0
LDHA_HUMAN	6	6	223	195
LDHC_HUMAN	0	1	0	0
LDH6A_HUMAN	0	0	0	0
gnl|unk|ENST00000394996_12	0	0	0	0
ALBU_HUMAN	24	20	189	191
gnl|unk|ENST00000504043_6	0	0	0	0
RACK1_HUMAN	121	127	120	88
gnl|unk|ENST00000504726_4	0	0	7	8
NCPR_HUMAN	225	230	0	4
H31_HUMAN	95	97	11	0
H32_HUMAN	40	31	1	0
H33_HUMAN	42	27	0	0
H31T_HUMAN	23	21	0	0
H3C_HUMAN	0	0	0	0
EFTU_HUMAN	75	85	106	124
ADT2_HUMAN	103	114	0	0
ADT3_HUMAN	128	92	0	0

ADT1_HUMAN	115	79	0	0
PCBP1_HUMAN	27	27	141	123
PCBP2_HUMAN	0	4	67	68
PCBP4_HUMAN	0	0	0	0
PCBP3_HUMAN	0	0	0	0
gnl|unk|ENST00000550910_3	0	0	0	0
OST48_HUMAN	149	79	0	0
SFPQ_HUMAN	122	85	80	75
UGDH_HUMAN	2	0	226	225
gnl|unk|ENST00000503779_5	0	0	0	0
HYEP_HUMAN	188	174	2	3
DYHC1_HUMAN	162	162	14	11
P5CS_HUMAN	103	108	62	52
CH10_HUMAN	9	8	166	155
GRP75_HUMAN	47	42	148	172
MIC60_HUMAN	149	122	0	0
ROA2_HUMAN	34	27	296	202
RS4X_HUMAN	38	40	81	84
RS4Y1_HUMAN	26	21	50	48
U520_HUMAN	36	50	154	129
ROA3_HUMAN	42	35	131	123
gnl|unk|ENST00000424736_5	0	0	65	60
EST1_HUMAN	15	10	165	174
HYOU1_HUMAN	40	27	184	151
RAB10_HUMAN	37	53	4	7
RAB14_HUMAN	38	35	7	8
RAB1B_HUMAN	57	50	8	15
RAB1A_HUMAN	49	55	8	15
RAB8A_HUMAN	21	27	0	0

RAB35_HUMAN	15	23	0	7
RAB4A_HUMAN	11	15	0	0
RAB3A_HUMAN	0	0	0	0
TRFE_HUMAN	80	76	83	93
LMNB1_HUMAN	180	159	0	0
DDX5_HUMAN	50	43	70	68
DDX17_HUMAN	19	29	50	42
DDX49_HUMAN	0	0	0	0
gnl|unk|ENST00000601772_1	0	0	0	0
NB5R3_HUMAN	192	144	0	0
FLNB_HUMAN	12	22	149	193
RCC1_HUMAN	104	94	0	0
PDIA4_HUMAN	13	19	150	181
TPIS_HUMAN	3	0	192	180
FIBG_HUMAN	104	106	62	56
RRBP1_HUMAN	64	61	87	106
PTBP1_HUMAN	16	12	166	153
NDKB_HUMAN	6	0	159	136
NDKA_HUMAN	2	2	46	46
NDK8_HUMAN	0	0	0	0
COF1_HUMAN	7	4	137	142
COF2_HUMAN	6	3	44	47
ILF3_HUMAN	39	22	112	114
STRBP_HUMAN	0	0	0	14
PRDX6_HUMAN	0	0	151	165
FLNA_HUMAN	84	118	78	72
THOC4_HUMAN	153	149	13	11
GANAB_HUMAN	7	6	152	136
PRDX1_HUMAN	14	13	130	132

H12_HUMAN	120	128	1	0
H14_HUMAN	110	102	1	0
H11_HUMAN	0	0	0	0
H13_HUMAN	0	0	0	0
H1T_HUMAN	0	0	0	0
PHB2_HUMAN	143	118	0	0
PPIB_HUMAN	43	33	79	62
AMPN_HUMAN	122	89	44	37
PLEC_HUMAN	130	122	8	11
RL3_HUMAN	59	52	57	51
RL3L_HUMAN	19	12	9	8
RS3A_HUMAN	85	82	59	49
gnl|unk|ENST00000461022_14	0	0	0	0
QCR1_HUMAN	140	143	20	17
FETA_HUMAN	18	16	130	112
UBB_HUMAN	85	82	44	38
UBC_HUMAN	85	82	44	38
4F2_HUMAN	141	129	4	1
LRC59_HUMAN	138	145	0	0
CATD_HUMAN	10	12	139	149
TOP2A_HUMAN	125	115	0	0
TOP2B_HUMAN	35	51	0	0
ACLY_HUMAN	1	0	134	142
PHB_HUMAN	118	134	0	0
PARP1_HUMAN	101	92	9	10
AT2A2_HUMAN	113	119	0	0
AT2A3_HUMAN	0	0	0	0
AT2A1_HUMAN	0	0	0	0

HNRPC_HUMAN	33	40	87	85
HNRC1_HUMAN	0	0	0	0
HNRC2_HUMAN	0	0	0	0
HNRC3_HUMAN	0	0	0	0
HNRC4_HUMAN	0	0	0	0
HS71A_HUMAN	41	40	108	120
HS71B_HUMAN	41	40	108	120
HS71L_HUMAN	22	22	69	62
RL1D1_HUMAN	57	63	65	76
gnl|unk|ENST00000572090_5	0	0	0	0
RL12_HUMAN	68	71	76	72
RL7_HUMAN	52	53	80	74
LMAN1_HUMAN	114	132	0	0
THIC_HUMAN	9	6	144	147
ATP5H_HUMAN	117	127	0	0
PPIA_HUMAN	10	12	116	91
TCPG_HUMAN	14	9	119	114
TPM4_HUMAN	10	9	34	53
TPM3_HUMAN	12	11	27	40
gnl|unk|ENST00000509601_5	5	4	30	38
TPM1_HUMAN	6	4	13	15
MDHM_HUMAN	7	4	134	145
FINC_HUMAN	150	120	0	0
VDAC2_HUMAN	118	121	0	0
TCPE_HUMAN	4	2	120	135
TCPB_HUMAN	4	1	130	118
NIPS1_HUMAN	94	76	53	43
PEBP1_HUMAN	8	3	129	108
GSLG1_HUMAN	129	113	0	0

RSSA_HUMAN	7	3	115	108
HNRPL_HUMAN	26	25	96	90
MATR3_HUMAN	13	24	104	106
ML12A_HUMAN	105	108	0	0
ML12B_HUMAN	105	108	0	0
gnl|unk|ENST00000577510_4	0	0	0	0
IDHC_HUMAN	3	9	132	125
DHX9_HUMAN	19	17	81	88
RL10A_HUMAN	51	50	34	32
QCR2_HUMAN	101	89	7	5
gnl|unk|ENST00000567597_5	0	0	0	0
ACSL3_HUMAN	146	117	3	7
FDFT_HUMAN	136	131	0	0
gnl|unk|ENST00000446331_6	0	0	0	0
RL7A_HUMAN	45	56	55	46
GDIB_HUMAN	6	5	116	124
PUR9_HUMAN	5	3	127	118
RLA2_HUMAN	67	64	92	80
SODC_HUMAN	0	0	142	146
PGK1_HUMAN	0	0	119	105
PGK2_HUMAN	0	0	0	0
PP1B_HUMAN	54	43	64	53
PP1G_HUMAN	52	39	69	57
PP1A_HUMAN	52	39	64	54
ACSL4_HUMAN	97	91	24	42
DDX21_HUMAN	76	65	48	49
LMNB2_HUMAN	112	112	0	0
SURF4_HUMAN	134	105	0	0
TCPD_HUMAN	4	7	126	136

PEG10_HUMAN	23	24	73	75
PCKGM_HUMAN	8	15	79	101
PLIN3_HUMAN	3	5	118	116
CISY_HUMAN	0	0	108	104
RL6_HUMAN	37	35	62	66
TXND5_HUMAN	22	16	104	97
CALM_HUMAN	52	46	33	50
gnl|unk|ENST00000553422_3	0	0	17	20
gnl|unk|ENST00000486500_1 1	0	0	0	0
CTND1_HUMAN	114	81	0	0
GLYM_HUMAN	1	0	111	106
HNRH1_HUMAN	39	29	101	97
HNRH2_HUMAN	0	0	61	60
RS3_HUMAN	41	46	44	36
RS2_HUMAN	44	54	62	56
NDUS1_HUMAN	101	105	5	3
TIF1B_HUMAN	37	29	92	77
RS5_HUMAN	74	80	49	47
C1QBP_HUMAN	6	4	115	88
ANXA6_HUMAN	12	6	79	76
SAHH_HUMAN	6	5	100	111
TKT_HUMAN	8	12	96	80
TCPZ_HUMAN	6	4	87	93
TCPW_HUMAN	0	0	0	0
PDLI1_HUMAN	12	6	89	85
UBA1_HUMAN	3	0	107	115
KTN1_HUMAN	71	89	0	0
RS13_HUMAN	32	27	42	45

MTCH2_HUMAN	104	93	0	0
PGAM1_HUMAN	4	3	99	86
DX39B_HUMAN	14	13	87	88
DX39A_HUMAN	14	13	65	58
SF3B1_HUMAN	10	16	83	90
BASI_HUMAN	110	95	0	0
gnl|unk|ENST00000576925_5	11	10	0	0
TFR1_HUMAN	104	84	0	1
MYL6_HUMAN	93	77	14	13
MYL6B_HUMAN	0	0	0	0
RS9_HUMAN	25	19	25	22
ECHB_HUMAN	34	43	45	51
PCYOX_HUMAN	94	62	0	0
TCPH_HUMAN	9	5	81	92
ETFA_HUMAN	8	5	98	101
SND1_HUMAN	32	24	59	57
CY1_HUMAN	112	86	0	0
RAN_HUMAN	29	22	70	62
APMAP_HUMAN	93	86	0	0
ANXA4_HUMAN	8	6	79	75
DPP4_HUMAN	77	66	0	0
MOGS_HUMAN	93	72	0	0
RS12_HUMAN	33	31	60	63
LA_HUMAN	0	0	100	92
gnl|unk|ENST00000494051_10	0	0	0	0
ANXA5_HUMAN	9	4	69	75
RL8_HUMAN	75	54	34	35
AATM_HUMAN	0	0	102	105

RL10_HUMAN	54	61	38	31
FBRL_HUMAN	57	55	24	31
IMB1_HUMAN	19	21	64	81
NOP56_HUMAN	49	68	15	29
KAD4_HUMAN	14	11	72	56
TCPQ_HUMAN	0	0	71	86
CMC2_HUMAN	64	70	0	0
CMC1_HUMAN	9	13	0	0
PLIN2_HUMAN	63	43	37	28
TKFC_HUMAN	0	0	104	98
gnl|unk|ENST00000530329_5	0	0	0	0
RL27_HUMAN	40	39	35	28
VILI_HUMAN	21	17	58	75
SSRA_HUMAN	114	47	0	0
PROF1_HUMAN	7	8	80	86
IF5A1_HUMAN	8	4	92	82
IF5A2_HUMAN	0	0	0	0
ABCD3_HUMAN	90	79	0	0
SYAC_HUMAN	0	0	71	72
YBOX1_HUMAN	14	17	82	74
YBOX3_HUMAN	0	0	23	21
IF4A1_HUMAN	26	24	81	89
IF4A2_HUMAN	19	19	44	52
PABP1_HUMAN	0	0	81	80
PABP4_HUMAN	0	0	42	45
PAP1M_HUMAN	0	0	0	0
GCSP_HUMAN	0	0	89	93
TCPA_HUMAN	7	6	84	79
VDAC3_HUMAN	115	106	3	0

COPA_HUMAN	5	9	75	83
COX2_HUMAN	58	77	0	0
MPRI_HUMAN	95	73	0	0
IF2B1_HUMAN	10	13	77	80
COMT_HUMAN	88	72	28	21
TMEDA_HUMAN	61	72	0	0
UGGG1_HUMAN	0	1	82	80
UGGG2_HUMAN	0	0	0	0
RLA0_HUMAN	33	42	43	44
RLA0L_HUMAN	23	26	22	25
PSME2_HUMAN	0	0	97	92
AT1A1_HUMAN	86	78	0	0
AT1A4_HUMAN	12	0	0	0
AT1A2_HUMAN	0	0	0	0
ATP4A_HUMAN	0	0	0	0
H2AY_HUMAN	97	138	0	0
QCR6_HUMAN	88	84	0	0
gnl|unk|ENST00000311672_9	88	84	0	0
APOB_HUMAN	49	49	7	7
U5S1_HUMAN	30	21	49	38
CALU_HUMAN	11	8	56	40
PRP19_HUMAN	47	33	38	37
SSRP1_HUMAN	66	67	7	7
1433E_HUMAN	1	2	85	92
ARF4_HUMAN	20	24	27	41
ARF1_HUMAN	8	12	35	47
ARF3_HUMAN	8	12	35	47
ARF5_HUMAN	0	6	0	0
GTR1_HUMAN	87	68	0	0

VIGLN_HUMAN	1	0	83	88
G6PI_HUMAN	0	0	79	75
gnl|unk|ENST00000586425_14	0	0	0	0
ACSL5_HUMAN	90	61	0	0
PRDX4_HUMAN	11	10	72	61
FIBB_HUMAN	49	52	19	15
HNRPF_HUMAN	16	20	84	90
PRP8_HUMAN	24	23	41	46
EF1G_HUMAN	9	12	41	40
AL4A1_HUMAN	26	23	48	42
TOM40_HUMAN	68	76	0	0
STML2_HUMAN	86	64	11	29
RL17_HUMAN	35	17	36	28
TLN1_HUMAN	0	0	78	87
TLN2_HUMAN	0	0	0	0
ATPG_HUMAN	55	65	0	0
CO3_HUMAN	39	35	38	34
ATD3A_HUMAN	52	50	0	0
ATD3B_HUMAN	34	28	0	0
ADRO_HUMAN	0	0	64	69
HMCS1_HUMAN	0	0	66	79
NP1L1_HUMAN	0	0	100	93
CHD4_HUMAN	61	44	8	7
CHD3_HUMAN	0	0	0	0
CHD5_HUMAN	0	0	0	0
RL30_HUMAN	28	34	44	40
EMAL4_HUMAN	2	2	65	55
MPCP_HUMAN	62	43	0	0

RS8_HUMAN	37	38	30	34
TOP1_HUMAN	40	56	0	0
TOP1M_HUMAN	4	7	0	0
RS17_HUMAN	29	18	46	44
ASGR1_HUMAN	43	36	0	0
DDX3X_HUMAN	38	32	30	28
DDX3Y_HUMAN	30	20	27	27
DDX4_HUMAN	0	0	0	0
DDX1_HUMAN	13	4	57	61
ECHM_HUMAN	0	1	76	73
ITB1_HUMAN	86	59	0	0
RS10_HUMAN	46	53	20	21
VAPA_HUMAN	53	50	0	1
1A02_HUMAN	31	26	0	0
1A23_HUMAN	26	19	0	0
1A24_HUMAN	26	19	0	0
1A80_HUMAN	7	7	0	0
1B37_HUMAN	0	0	0	0
CTNB1_HUMAN	65	53	25	26
IDHP_HUMAN	0	0	84	80
RTN4_HUMAN	45	55	18	16
ITPR3_HUMAN	50	21	0	0
ITPR2_HUMAN	16	19	0	0
ITPR1_HUMAN	0	0	0	0
COPB_HUMAN	12	5	74	54
DHB4_HUMAN	37	31	19	28
PRDX3_HUMAN	32	32	35	25
ACOT2_HUMAN	0	0	70	77
ACOT1_HUMAN	0	0	61	68

AL3A2_HUMAN	79	75	0	0
AL3B1_HUMAN	0	0	0	0
KHDR1_HUMAN	24	13	56	46
NDUA9_HUMAN	60	50	0	0
THIL_HUMAN	21	23	55	48
ERP29_HUMAN	8	2	66	61
CLIC1_HUMAN	7	6	66	69
ESYT1_HUMAN	64	64	0	3
PA2G4_HUMAN	14	8	60	56
RS19_HUMAN	9	14	16	19
SET_HUMAN	0	0	56	72
UBP7_HUMAN	9	5	58	49
P5CR1_HUMAN	20	36	39	45
RL18_HUMAN	27	30	28	33
gnl|unk|ENST00000552705_19	0	0	0	0
RS11_HUMAN	21	20	33	25
DIC_HUMAN	62	60	0	0
HACD3_HUMAN	58	73	0	0
ILF2_HUMAN	13	4	60	60
SYEP_HUMAN	21	20	39	40
TOM70_HUMAN	71	56	0	0
GABT_HUMAN	2	0	68	73
EMC1_HUMAN	68	53	0	0
ERG7_HUMAN	52	65	0	0
HNRPR_HUMAN	11	13	69	57
NDUV1_HUMAN	59	54	0	0
DHC24_HUMAN	53	36	0	0
RLA1_HUMAN	45	42	42	38

NOMO2_HUMAN	66	51	0	0
NOMO3_HUMAN	66	51	0	0
gnl|unk|ENST00000569051_14	0	0	0	0
gnl|unk|ENST00000570346_4	0	0	0	0
DHB12_HUMAN	63	52	0	0
LAP2B_HUMAN	51	55	0	0
LAP2A_HUMAN	20	45	0	1
PRDX5_HUMAN	11	6	49	54
ADHX_HUMAN	0	0	75	69
APOE_HUMAN	49	46	4	17
SCFD1_HUMAN	27	25	42	43
gnl|unk|ENST00000554776_5	0	0	0	0
WDR1_HUMAN	4	0	47	40
DDB1_HUMAN	4	13	57	62
GBB1_HUMAN	47	44	0	0
GBB2_HUMAN	29	29	0	0
ATPO_HUMAN	54	63	0	0
NU205_HUMAN	65	43	0	0
TM214_HUMAN	48	52	0	0
SP16H_HUMAN	38	33	8	11
ACOX1_HUMAN	19	14	36	47
PRDX2_HUMAN	5	6	48	53
U2AF2_HUMAN	21	10	33	43
NONO_HUMAN	43	36	7	11
SAP_HUMAN	6	4	52	49
UCRI_HUMAN	50	58	0	0
UCRIL_HUMAN	17	16	0	0
GLSK_HUMAN	14	10	37	36

NU155_HUMAN	70	51	0	0
CX6B1_HUMAN	69	64	0	0
RL5_HUMAN	6	8	37	41
XPO2_HUMAN	7	7	34	40
RL15_HUMAN	11	6	30	30
gnl|unk|ENST00000465786_15	0	0	0	0
LONM_HUMAN	0	0	53	52
UB2L3_HUMAN	1	0	64	56
RL35_HUMAN	28	32	14	14
AT5F1_HUMAN	41	50	0	0
TPR_HUMAN	19	29	5	4
CATA_HUMAN	0	2	46	55
RS14_HUMAN	29	32	24	26
gnl|unk|ENST00000519690_58	29	32	24	26
SDHA_HUMAN	57	30	8	7
NOP58_HUMAN	39	34	18	5
gnl|unk|ENST00000478941_7	0	0	0	1
PCNA_HUMAN	5	9	44	45
SERA_HUMAN	0	2	42	44
THIM_HUMAN	0	0	54	54
H2AV_HUMAN	84	96	1	1
H2AZ_HUMAN	84	96	1	1
SYQ_HUMAN	17	13	27	25
TOM22_HUMAN	70	67	0	0
AK1C3_HUMAN	0	0	47	40
AK1C2_HUMAN	0	0	8	7
AK1C1_HUMAN	0	0	0	0

FIBA_HUMAN	35	35	18	18
TADBP_HUMAN	0	0	63	65
PO210_HUMAN	56	61	0	0
ERG1_HUMAN	32	37	0	0
PLAK_HUMAN	82	68	12	8
HCD2_HUMAN	11	9	46	58
1433Z_HUMAN	0	2	57	64
DHB2_HUMAN	57	53	0	0
RBP2_HUMAN	33	36	24	10
RGPD1_HUMAN	0	0	0	0
RGPD2_HUMAN	0	0	0	0
RGPD8_HUMAN	0	0	0	0
RGPD4_HUMAN	0	0	0	0
RS20_HUMAN	13	13	28	24
SF3B3_HUMAN	2	2	44	44
TRAP1_HUMAN	0	0	78	85
CNPY2_HUMAN	0	0	59	53
DSG2_HUMAN	35	44	7	9
QOR_HUMAN	0	0	62	57
SYMC_HUMAN	39	24	13	21
CDC42_HUMAN	16	19	6	19
RAC1_HUMAN	11	11	4	6
RAC2_HUMAN	6	6	0	0
RHOG_HUMAN	0	3	0	0
RHOQ_HUMAN	0	0	0	0
HSP74_HUMAN	0	0	50	51
SAM50_HUMAN	50	48	0	0
SERC_HUMAN	0	0	42	40
ETFB_HUMAN	4	3	34	52

SYIC_HUMAN	24	17	23	23
TECR_HUMAN	34	30	0	0
AL7A1_HUMAN	0	0	44	57
MDHC_HUMAN	0	0	49	46
PSA7_HUMAN	0	0	60	49
PUR6_HUMAN	12	7	50	33
ACPM_HUMAN	25	27	20	22
GLU2B_HUMAN	5	0	51	42
BAF_HUMAN	43	15	0	0
gnl|unk|ENST00000312175_10	43	15	0	0
gnl|unk|ENST00000445560_7	43	15	0	0
IMDH2_HUMAN	2	2	51	36
RAB5C_HUMAN	46	39	0	2
RAB5B_HUMAN	16	6	0	0
SSRD_HUMAN	59	49	0	0
XRN2_HUMAN	0	0	40	24
CAPZB_HUMAN	32	29	28	17
PGRC1_HUMAN	61	37	7	4
RL22_HUMAN	17	13	44	32
RL38_HUMAN	14	15	6	7
gnl|unk|ENST00000311111_5	14	15	6	7
gnl|unk|ENST00000439590_6	14	15	6	7
gnl|unk|ENST00000533498_7	14	15	6	7
GTR3_HUMAN	46	42	0	0
PSMD3_HUMAN	4	0	48	36
RS16_HUMAN	13	15	16	16
SC23A_HUMAN	32	19	15	18
SC23B_HUMAN	7	6	0	0

ACDSB_HUMAN	0	0	36	43
PSMD2_HUMAN	4	5	47	42
PTK7_HUMAN	46	39	3	0
AHNK_HUMAN	0	0	55	38
PSD11_HUMAN	0	0	31	24
RBBP4_HUMAN	11	14	31	29
MYO1B_HUMAN	30	30	1	3
MYO1A_HUMAN	0	0	0	0
6PGD_HUMAN	0	0	48	57
CNDP2_HUMAN	0	0	35	47
NDUS3_HUMAN	46	52	0	0
SYRC_HUMAN	12	22	15	21
PSB3_HUMAN	0	0	51	50
LGUL_HUMAN	0	0	50	50
PSA2_HUMAN	0	0	52	59
RAB7A_HUMAN	34	35	5	7
EIF3A_HUMAN	0	0	38	48
FUMH_HUMAN	0	0	47	56
KAD2_HUMAN	0	0	44	36
OAT_HUMAN	0	0	40	60
PYC_HUMAN	1	0	52	51
SE1L1_HUMAN	55	25	0	0
AMPL_HUMAN	0	3	40	45
CCD47_HUMAN	37	40	0	0
HSPB1_HUMAN	25	18	30	22
NASP_HUMAN	0	0	42	49
CO4A_HUMAN	10	8	33	40
CO4B_HUMAN	10	8	33	40
DKC1_HUMAN	12	6	25	24

DNJA1_HUMAN	15	16	27	25
G3BP1_HUMAN	0	2	20	19
HNRPQ_HUMAN	1	4	51	51
RL23_HUMAN	10	22	28	22
RL9_HUMAN	25	28	17	18
STT3A_HUMAN	29	29	0	0
HS105_HUMAN	2	0	50	51
RS25_HUMAN	25	28	13	15
gnl|unk|ENST00000524864_18	25	28	13	15
IF6_HUMAN	7	9	47	41
gnl|unk|ENST00000444717_7	0	0	0	0
PSMD7_HUMAN	0	0	44	42
RL21_HUMAN	26	24	14	14
TCP4_HUMAN	19	17	27	30
FABPL_HUMAN	0	0	48	57
RS15A_HUMAN	12	10	26	21
gnl|unk|ENST00000569083_3	12	10	26	21
gnl|unk|ENST00000574723_4	0	0	0	0
SFXN1_HUMAN	35	30	0	0
SFXN3_HUMAN	0	0	0	0
gnl|unk|ENST00000508290_7	0	0	0	0
S61A1_HUMAN	41	29	0	0
MAP4_HUMAN	10	8	26	30
TEBP_HUMAN	9	11	32	24
2AAA_HUMAN	4	7	26	34
ANM5_HUMAN	0	0	31	28
IPYR_HUMAN	0	0	41	35
PSB1_HUMAN	0	0	41	40

COX41_HUMAN	34	34	0	0
KAD3_HUMAN	0	0	42	30
EIF3C_HUMAN	0	0	48	44
HNRPD_HUMAN	0	4	58	46
PARK7_HUMAN	0	0	31	31
SEC13_HUMAN	13	12	24	26
STIP1_HUMAN	0	0	29	49
COX5A_HUMAN	22	16	22	17
DPYL2_HUMAN	0	0	36	54
DPYL1_HUMAN	0	0	0	0
NUP62_HUMAN	45	35	2	4
PSMD1_HUMAN	0	0	38	40
FPPS_HUMAN	0	0	34	48
G6PD_HUMAN	0	0	28	26
NDUS5_HUMAN	33	28	0	0
NQO1_HUMAN	0	2	29	29
RS6_HUMAN	15	16	13	14
RTCB_HUMAN	6	7	15	14
GSHR_HUMAN	0	0	38	44
IMA1_HUMAN	6	10	36	30
NDUAD_HUMAN	22	18	0	0
PSME1_HUMAN	0	0	42	37
SYSC_HUMAN	0	0	45	46
DHX15_HUMAN	12	14	20	15
ERP44_HUMAN	12	9	29	19
RL13A_HUMAN	16	21	6	10
RL13_HUMAN	12	11	16	12
A2MG_HUMAN	0	0	31	38
C1TC_HUMAN	0	1	34	36

SF3B2_HUMAN	1	1	23	35
SNAA_HUMAN	45	45	0	0
TMED9_HUMAN	55	44	3	0
ASGR2_HUMAN	31	22	0	0
CP51A_HUMAN	30	29	0	0
ERO1A_HUMAN	0	0	37	28
RANG_HUMAN	0	0	51	42
SQRD_HUMAN	41	34	0	0
SLIRP_HUMAN	0	0	27	30
gnl|unk|ENST00000556831_5	0	0	27	30
gnl|unk|ENST00000557623_5	0	0	27	30
gnl|unk|ENST00000613856_5	0	0	27	30
gnl|unk|ENST00000553981_4	0	0	0	15
ECH1_HUMAN	0	0	22	43
NDUS2_HUMAN	34	19	0	1
DDX18_HUMAN	8	11	39	28
FSCN1_HUMAN	2	4	31	32
LYAG_HUMAN	0	0	32	34
PSA1_HUMAN	0	0	32	32
RM12_HUMAN	20	19	21	20
S39AE_HUMAN	44	37	0	0
TM9S4_HUMAN	35	41	0	0
ANGT_HUMAN	0	0	45	41
CAP1_HUMAN	0	0	39	39
CBX3_HUMAN	3	3	34	33
GDIR1_HUMAN	0	0	36	38
RALY_HUMAN	6	10	17	22
RS24_HUMAN	7	6	31	25
SUN2_HUMAN	44	22	0	0

TPD54_HUMAN	15	10	30	31
CYB5_HUMAN	30	29	0	1
gnl|unk|ENST00000494131_5	30	29	0	1
F162A_HUMAN	40	35	0	0
NCLN_HUMAN	39	32	0	0
RL27A_HUMAN	3	8	24	26
SYK_HUMAN	3	1	26	30
TSN_HUMAN	0	0	46	40
GFPT1_HUMAN	30	19	1	1
GFPT2_HUMAN	0	0	0	0
ACON_HUMAN	0	0	24	38
GCN1_HUMAN	10	14	24	19
SYDC_HUMAN	11	11	9	14
ARL8B_HUMAN	38	21	0	2
KS6A3_HUMAN	15	13	18	13
CUTA_HUMAN	0	0	48	44
SAFB1_HUMAN	17	18	22	20
SAFB2_HUMAN	11	11	22	17
TMED7_HUMAN	34	31	0	0
IF2G_HUMAN	16	15	15	18
PAIRB_HUMAN	20	11	23	17
PPGB_HUMAN	0	0	36	32
PRS8_HUMAN	1	0	29	33
GNAI2_HUMAN	32	19	0	0
GNAI3_HUMAN	21	11	0	0
GNAL_HUMAN	2	2	0	0
GNAT3_HUMAN	0	0	0	0
GNAI1_HUMAN	0	0	0	0
EIF3L_HUMAN	0	0	20	20

FUBP2_HUMAN	0	0	35	45
VAT1_HUMAN	33	36	1	7
1433B_HUMAN	3	2	53	54
gnl|unk|ENST00000633979_13	0	0	0	0
ANM1_HUMAN	0	0	39	33
H15_HUMAN	33	33	0	0
IF4A3_HUMAN	27	31	36	35
RBMX_HUMAN	30	28	9	10
RL23A_HUMAN	9	16	8	6
RL7L_HUMAN	5	7	20	14
ECI2_HUMAN	23	18	21	17
HMOX1_HUMAN	30	24	0	1
LETM1_HUMAN	28	29	0	0
RUVB1_HUMAN	13	14	21	30
SEC63_HUMAN	27	20	0	0
FAF2_HUMAN	37	30	0	0
NDUB9_HUMAN	39	35	0	0
NUP93_HUMAN	34	35	1	0
PON2_HUMAN	26	22	0	0
SMD2_HUMAN	11	16	18	21
NDUAC_HUMAN	18	18	0	0
NH2L1_HUMAN	26	19	4	9
RPR1B_HUMAN	14	13	24	20
RPR1A_HUMAN	0	0	0	0
UFL1_HUMAN	25	24	0	0
CD59_HUMAN	25	27	0	0
ACOD_HUMAN	42	20	0	0
AIFM1_HUMAN	0	2	34	34

BAG2_HUMAN	25	19	17	10
CAZA1_HUMAN	10	10	23	22
MLEC_HUMAN	38	25	0	0
NDUBA_HUMAN	34	26	0	0
SC31A_HUMAN	0	0	19	16
PTMA_HUMAN	5	4	40	28
gnl|unk|ENST00000481928_5	5	4	40	28
ALDOC_HUMAN	9	2	56	64
ALDR_HUMAN	0	0	25	28
LASP1_HUMAN	17	15	12	14
RETST_HUMAN	33	25	0	0
RINI_HUMAN	0	0	36	43
RL24_HUMAN	5	9	14	17
TFAM_HUMAN	36	40	0	0
SMD3_HUMAN	19	8	19	11
COPG1_HUMAN	0	1	43	39
FKB10_HUMAN	0	0	17	22
NHRF1_HUMAN	6	5	32	31
RL32_HUMAN	19	19	11	6
MCFD2_HUMAN	0	0	18	23
ATPK_HUMAN	34	27	0	0
gnl|unk|ENST00000359832_3	34	27	0	0
gnl|unk|ENST00000394186_3	24	21	0	0
gnl|unk|ENST00000485011_2	24	21	0	0
gnl|unk|ENST00000488775_2	24	21	0	0
CPVL_HUMAN	0	0	37	27
IPO5_HUMAN	9	4	19	23
PTH2_HUMAN	36	37	0	0
SPCS2_HUMAN	33	33	0	0

SPEB_HUMAN	0	0	34	37
1433T_HUMAN	0	0	48	42
HMGA1_HUMAN	35	42	0	0
PRS4_HUMAN	0	0	33	18
SYFA_HUMAN	3	4	21	15
TM9S3_HUMAN	26	24	0	0
TXTP_HUMAN	16	19	0	0
RL14_HUMAN	25	15	12	10
gnl|unk|ENST00000461368_5	0	0	0	0
AFG32_HUMAN	24	25	0	0
ANK2_HUMAN	0	0	0	0
AATC_HUMAN	0	0	37	37
ATP5J_HUMAN	29	33	0	0
BAZ1B_HUMAN	23	29	0	0
SIAS_HUMAN	0	0	24	22
ACBP_HUMAN	0	0	31	33
CPPED_HUMAN	0	0	27	23
CYBP_HUMAN	0	0	41	24
ES1_HUMAN	0	0	38	35
SMD1_HUMAN	18	18	17	14
SYIM_HUMAN	0	0	26	21
CYC_HUMAN	0	0	31	23
EZRI_HUMAN	1	0	22	16
RADI_HUMAN	2	0	8	8
MOES_HUMAN	0	0	0	0
AIMP1_HUMAN	5	5	20	12
FUS_HUMAN	39	35	15	11
BOLA2_HUMAN	0	0	24	22
RL31_HUMAN	18	13	7	7

gnl|unk|ENST00000441435_6	0	0	0	0
A1AT_HUMAN	3	0	8	11
ACY1_HUMAN	1	0	19	18
ERLEC_HUMAN	29	24	0	0
MBB1A_HUMAN	5	11	24	16
MPPA_HUMAN	5	2	33	19
PREB_HUMAN	37	25	0	0
RL11_HUMAN	23	19	8	14
SYVC_HUMAN	0	0	22	48
U2AF1_HUMAN	16	18	8	8
U2AF5_HUMAN	16	18	8	8
gnl|unk|ENST00000492222_7	13	19	22	15
gnl|unk|ENST00000591758_7	13	19	22	15
RSMB_HUMAN	0	4	6	9
RSMN_HUMAN	0	4	6	9
gnl|unk|ENST00000461548_10	0	0	3	6
COPB2_HUMAN	1	1	30	25
EIF3B_HUMAN	0	0	26	25
KCRB_HUMAN	0	0	34	25
PUF60_HUMAN	2	3	35	26
RS18_HUMAN	2	4	4	13
TMM97_HUMAN	21	23	0	0
RP1BL_HUMAN	29	16	0	0
RAP1A_HUMAN	19	11	0	0
RASH_HUMAN	10	6	0	0
NDUA8_HUMAN	25	25	0	0
NUMA1_HUMAN	6	12	26	18
QCR7_HUMAN	24	23	0	0

STIM1_HUMAN	21	18	0	0
THEM6_HUMAN	35	29	0	0
RS29_HUMAN	15	8	6	13
gnl|unk|ENST00000245458_3	15	8	6	13
gnl|unk|ENST00000401543_3	15	8	6	13
gnl|unk|ENST00000611563_5	15	8	6	13
COPE_HUMAN	5	5	26	18
EPIPL_HUMAN	6	0	33	40
F10A1_HUMAN	0	0	25	25
PFKAL_HUMAN	0	0	27	27
ERF3A_HUMAN	0	0	24	24
ERF3B_HUMAN	0	0	8	9
FLOT1_HUMAN	20	18	0	0
M2OM_HUMAN	19	23	0	0
NACAM_HUMAN	0	0	24	23
NU133_HUMAN	22	24	0	0
PTN1_HUMAN	22	18	0	0
SRPRB_HUMAN	33	20	0	0
BTF3_HUMAN	0	0	34	26
PGAM5_HUMAN	18	20	0	0
RBBP7_HUMAN	8	6	20	13
VAPB_HUMAN	22	22	0	0
VATA_HUMAN	2	3	22	25
ODPA_HUMAN	0	0	37	33
ODPAT_HUMAN	0	0	0	0
PA1B2_HUMAN	0	0	30	30
PSB5_HUMAN	0	0	27	29
SODM_HUMAN	0	0	29	30
SUCB2_HUMAN	0	0	26	22

UGPA_HUMAN	0	0	31	23
RS26_HUMAN	2	5	24	25
COX1_HUMAN	36	31	0	0
CATB_HUMAN	0	0	20	16
gnl|unk|ENST00000526481_2	0	0	0	0
ACSS3_HUMAN	0	0	24	25
RS21_HUMAN	8	6	22	28
gnl|unk|ENST00000343986_2	8	6	22	28
gnl|unk|ENST00000450116_2	8	6	22	28
gnl|unk|ENST00000492356_2	8	6	22	28
RT29_HUMAN	3	1	15	11
SC22B_HUMAN	27	30	0	0
SPEE_HUMAN	0	0	32	29
TOM6_HUMAN	29	30	0	0
gnl|unk|ENST00000335515_36	29	30	0	0
gnl|unk|ENST00000398881_6	29	30	0	0
gnl|unk|ENST00000398884_6	29	30	0	0
gnl|unk|ENST00000456057_41	29	30	0	0
gnl|unk|ENST00000487182_39	29	30	0	0
TRA2B_HUMAN	19	11	12	6
BRX1_HUMAN	11	6	17	8
AOFA_HUMAN	20	19	0	0
BAP31_HUMAN	21	23	0	0
GPX1_HUMAN	0	0	19	25
NDUAA_HUMAN	19	15	7	9
RM39_HUMAN	0	0	1	8
LAMP1_HUMAN	23	19	5	6

NDUB5_HUMAN	29	27	0	0
HINT1_HUMAN	0	0	17	19
gnl|unk|ENST00000508495_9	0	0	0	0
ASPH_HUMAN	12	11	0	0
CN37_HUMAN	17	14	7	7
HP1B3_HUMAN	9	23	1	0
MARE1_HUMAN	6	5	21	19
MIC19_HUMAN	17	21	0	0
NSF_HUMAN	21	19	0	0
NU1M_HUMAN	25	28	0	0
RAGP1_HUMAN	0	0	29	23
UBP5_HUMAN	0	0	21	26
DECR_HUMAN	17	10	16	13
NOP2_HUMAN	8	8	20	15
OTUB1_HUMAN	0	0	28	24
PSA_HUMAN	0	0	26	29
TMM33_HUMAN	26	15	0	0
COX6C_HUMAN	18	23	0	0
gnl|unk|ENST00000297564_4	18	23	0	0
gnl|unk|ENST00000517682_4	18	23	0	0
gnl|unk|ENST00000522940_7	18	23	0	0
gnl|unk|ENST00000524245_5	18	23	0	0
COPZ1_HUMAN	5	9	15	11
HNRL2_HUMAN	0	0	21	26
MA1A1_HUMAN	21	17	1	0
MTDC_HUMAN	2	1	20	19
NUP85_HUMAN	28	30	0	0
PH4H_HUMAN	0	2	23	20
PLOD1_HUMAN	0	0	18	23

PRS7_HUMAN	0	0	21	22
SMCA5_HUMAN	20	25	0	0
SRSF3_HUMAN	14	15	25	24
ABHEB_HUMAN	0	0	27	25
ACADV_HUMAN	25	22	7	6
AT131_HUMAN	15	15	0	0
COX5B_HUMAN	21	27	0	0
GTF2I_HUMAN	18	17	7	10
SDHB_HUMAN	14	12	0	0
SSBP_HUMAN	19	23	6	4
ST1A3_HUMAN	4	5	26	40
ST1A4_HUMAN	4	5	26	40
STOM_HUMAN	23	26	0	0
XPO1_HUMAN	0	0	33	25
TMED2_HUMAN	18	16	0	0
CDC5L_HUMAN	14	17	14	8
CSK21_HUMAN	6	1	33	21
EIF3G_HUMAN	1	0	31	28
FADS2_HUMAN	13	12	0	0
HSDL2_HUMAN	0	0	27	24
IPO7_HUMAN	1	0	35	26
MPP10_HUMAN	7	1	16	7
OPA1_HUMAN	27	19	0	0
RL26_HUMAN	6	6	4	4
ROA0_HUMAN	13	13	14	13
CN166_HUMAN	2	1	22	26
GLPK_HUMAN	30	20	0	0
ILVBL_HUMAN	19	19	0	0
NSMA3_HUMAN	31	25	0	0

PKP2_HUMAN	24	30	0	0
SF01_HUMAN	1	0	16	17
SPCS1_HUMAN	24	26	0	0
AOFB_HUMAN	20	16	0	0
CYTB_HUMAN	3	1	18	19
EF1B_HUMAN	2	2	23	31
ETHE1_HUMAN	0	0	21	21
GRHPR_HUMAN	0	0	17	19
MTX1_HUMAN	16	13	0	0
NPC2_HUMAN	0	0	24	39
PESC_HUMAN	0	1	19	15
PRS6B_HUMAN	0	0	19	19
RBM39_HUMAN	3	5	20	26
SF3A3_HUMAN	0	0	12	11
ST1A1_HUMAN	2	4	24	40
SC61G_HUMAN	29	26	0	0
gnl|unk|ENST00000352861_4	29	26	0	0
gnl|unk|ENST00000395535_4	29	26	0	0
gnl|unk|ENST00000415949_8	29	26	0	0
gnl|unk|ENST00000450622_4	29	26	0	0
AT2B1_HUMAN	21	18	0	0
AT2B4_HUMAN	10	11	0	0
AT1B1_HUMAN	24	23	0	0
CCAR2_HUMAN	0	0	29	23
ECI1_HUMAN	0	0	22	26
ELAV1_HUMAN	0	0	24	25
H1X_HUMAN	30	31	0	0
ITIH2_HUMAN	9	6	11	10
MGST1_HUMAN	30	26	0	0

RUXE_HUMAN	11	13	13	8
gnl|unk|ENST00000414487_4	11	13	13	8
GBG5_HUMAN	26	29	0	0
AK1A1_HUMAN	1	0	26	27
CEAM1_HUMAN	29	24	0	0
HMOX2_HUMAN	20	12	0	0
MCCB_HUMAN	0	0	23	19
PABP2_HUMAN	1	2	33	23
SRPRA_HUMAN	23	21	0	0
SRSF1_HUMAN	6	11	15	14
VATG1_HUMAN	10	11	9	10
ERMP1_HUMAN	13	12	0	0
GUAA_HUMAN	0	0	18	30
IQGA1_HUMAN	0	0	27	28
PYGB_HUMAN	0	0	24	25
RU17_HUMAN	6	6	15	15
MMSA_HUMAN	8	11	0	5
EMD_HUMAN	22	23	0	0
FIS1_HUMAN	27	25	0	0
HM13_HUMAN	22	16	0	0
IPO4_HUMAN	3	3	22	22
LMAN2_HUMAN	17	13	0	0
RM13_HUMAN	12	8	11	8
DHRS7_HUMAN	18	17	0	0
HPPD_HUMAN	0	0	28	24
IMA4_HUMAN	2	2	23	21
PSMD6_HUMAN	0	1	16	13
STT3B_HUMAN	21	23	0	0
STX18_HUMAN	33	16	0	0

SMRC1_HUMAN	9	4	2	0
SMRC2_HUMAN	3	5	0	0
ACSL1_HUMAN	16	11	0	0
BIEA_HUMAN	0	0	14	13
GT251_HUMAN	1	2	13	16
PRS10_HUMAN	0	1	27	28
PSA6_HUMAN	0	0	24	32
SOX_HUMAN	0	0	10	20
SYG_HUMAN	0	0	22	17
UBE2N_HUMAN	0	0	22	23
VINC_HUMAN	0	0	18	25
LBR_HUMAN	14	13	0	0
MESD_HUMAN	4	0	22	21
AHSA1_HUMAN	5	6	18	21
ALG1_HUMAN	23	15	0	0
ALG2_HUMAN	23	13	0	0
BUB3_HUMAN	0	0	19	14
CDC37_HUMAN	0	0	24	21
NU160_HUMAN	17	9	0	2
SF3A1_HUMAN	2	0	20	18
DNJC8_HUMAN	0	0	25	23
UHRF1_HUMAN	26	17	0	0
UHRF2_HUMAN	0	0	0	0
3HIDH_HUMAN	0	0	23	26
AGK_HUMAN	21	10	0	0
FKBP4_HUMAN	0	0	30	18
H2AW_HUMAN	56	75	0	0
KCY_HUMAN	1	0	19	17
LKHA4_HUMAN	0	0	17	18

OLA1_HUMAN	0	0	11	17
PCY2_HUMAN	0	0	18	26
PDXD1_HUMAN	4	1	12	19
RL36_HUMAN	11	5	1	4
RRS1_HUMAN	17	14	6	4
SAE1_HUMAN	0	0	15	23
STAU1_HUMAN	18	9	0	3
RS27_HUMAN	8	11	3	5
gnl|unk|ENST00000368567_2	8	11	3	5
gnl|unk|ENST00000457554_4	8	11	3	5
gnl|unk|ENST00000495392_4	8	11	3	5
RS27L_HUMAN	0	0	0	0
IF4B_HUMAN	0	0	11	12
gnl|unk|ENST00000549592_1 1	0	0	0	0
ATAD2_HUMAN	14	11	0	0
NDUB6_HUMAN	18	20	0	0
NUP98_HUMAN	5	13	0	0
RL19_HUMAN	15	17	2	3
SMHD1_HUMAN	10	6	0	0
SRP72_HUMAN	14	14	10	8
TM9S2_HUMAN	15	15	0	0
WFS1_HUMAN	16	14	0	0
ACINU_HUMAN	2	5	4	5
ADH4_HUMAN	0	0	24	22
CISD2_HUMAN	16	13	0	0
DPP3_HUMAN	0	0	21	23
ESTD_HUMAN	0	0	16	17
FLOT2_HUMAN	18	23	0	0

FTCD_HUMAN	0	0	24	23
GLOD4_HUMAN	0	0	23	19
LYRIC_HUMAN	16	18	0	0
NSUN2_HUMAN	0	0	28	18
ODP2_HUMAN	0	0	21	22
PNPO_HUMAN	0	0	14	26
PSA5_HUMAN	0	0	23	17
RHOA_HUMAN	16	16	2	3
SNP23_HUMAN	25	22	0	0
SNTB1_HUMAN	16	15	1	1
MGN2_HUMAN	5	2	10	6
MGN_HUMAN	0	0	10	6
APOA1_HUMAN	22	22	0	0
APT_HUMAN	1	0	17	20
BAG6_HUMAN	0	0	21	24
CATC_HUMAN	0	0	11	10
CAZA2_HUMAN	11	10	12	7
CDS2_HUMAN	22	15	0	0
DCTN2_HUMAN	0	0	23	19
DPM1_HUMAN	19	14	0	0
EIF3F_HUMAN	0	0	23	27
GRSF1_HUMAN	0	0	15	23
HMGA2_HUMAN	25	19	0	0
NU153_HUMAN	15	10	1	0
NU214_HUMAN	11	16	0	1
OFUT1_HUMAN	0	0	20	21
RL18A_HUMAN	7	9	8	11
SON_HUMAN	15	18	0	0
NTF2_HUMAN	0	0	21	19

gnl|unk|ENST00000424846_20	12	6	7	9
gnl|unk|ENST00000492121_18	12	6	7	9
OS9_HUMAN	11	7	0	0
gnl|unk|ENST00000550848_8	1	2	0	0
gnl|unk|ENST00000551285_7	1	2	0	0
CSK22_HUMAN	0	0	15	14
F213A_HUMAN	16	23	0	0
MIF_HUMAN	1	0	12	13
P4HA1_HUMAN	2	0	19	18
PEG3_HUMAN	5	4	17	14
PGES2_HUMAN	20	11	5	5
PSD13_HUMAN	0	0	23	14
PUR2_HUMAN	0	3	15	12
RT23_HUMAN	0	0	16	16
UBF1_HUMAN	15	6	0	0
NOG1_HUMAN	3	7	10	7
VATB2_HUMAN	10	10	6	8
VATB1_HUMAN	0	0	0	0
LYPA2_HUMAN	0	0	22	21
gnl|unk|ENST00000374502_10	0	0	0	0
COR1C_HUMAN	7	10	11	13
DEK_HUMAN	12	9	0	0
ERLN2_HUMAN	22	30	0	0
FARP1_HUMAN	2	4	12	15
KAP0_HUMAN	4	3	15	20
LG3BP_HUMAN	0	0	17	23
SGTA_HUMAN	0	0	20	24

SPTC1_HUMAN	21	19	0	0
USMG5_HUMAN	17	17	0	0
gnl|unk|ENST00000309579_4	17	17	0	0
gnl|unk|ENST00000337003_10	17	17	0	0
gnl|unk|ENST00000369815_11	17	17	0	0
gnl|unk|ENST00000369825_14	17	17	0	0
gnl|unk|ENST00000425964_4	17	17	0	0
RL28_HUMAN	11	7	5	2
gnl|unk|ENST00000428193_4	11	7	5	2
gnl|unk|ENST00000431533_4	11	7	5	2
gnl|unk|ENST00000558131_4	11	7	5	2
gnl|unk|ENST00000560881_4	11	7	5	2
AP2B1_HUMAN	13	17	0	4
AP1B1_HUMAN	0	0	1	3
NMT1_HUMAN	8	5	9	8
NMT2_HUMAN	0	0	0	0
ARPC2_HUMAN	1	0	18	16
C1TM_HUMAN	3	2	14	12
EBP2_HUMAN	5	5	10	6
EST2_HUMAN	0	0	13	19
KI67_HUMAN	14	15	0	0
ODO1_HUMAN	0	0	13	17
RM03_HUMAN	0	1	16	15
SEPT9_HUMAN	7	10	9	5
SRSF7_HUMAN	11	13	11	15
TALDO_HUMAN	0	0	10	15
TMX1_HUMAN	12	4	0	0

DAD1_HUMAN	16	13	0	0
SMU1_HUMAN	2	5	6	7
CAPR1_HUMAN	0	0	10	13
A16A1_HUMAN	0	0	22	25
ACS2L_HUMAN	0	0	19	22
NDUA5_HUMAN	14	11	6	6
PRP6_HUMAN	13	17	0	2
SART3_HUMAN	0	0	19	17
TFB1M_HUMAN	0	0	13	10
HCFC1_HUMAN	11	12	11	10
AP2A1_HUMAN	5	7	7	14
AP2A2_HUMAN	5	6	1	1
KAP2_HUMAN	12	7	12	10
KAP3_HUMAN	0	0	0	0
SSRG_HUMAN	22	15	0	0
R39L5_HUMAN	5	6	0	0
RL39_HUMAN	5	6	0	0
gnl|unk|ENST00000361575_1	5	6	0	0
gnl|unk|ENST00000424573_3	5	6	0	0
gnl|unk|ENST00000446011_4	5	6	0	0
gnl|unk|ENST00000468844_34	5	6	0	0
RALA_HUMAN	3	7	0	0
RALB_HUMAN	0	2	0	0
gnl|unk|ENST00000470417_6	0	0	0	0
AT1B3_HUMAN	13	15	0	0
FUBP1_HUMAN	0	0	9	15
ISOC2_HUMAN	0	0	20	15
LAMB1_HUMAN	7	8	5	6

MOT4_HUMAN	15	13	0	0
NOLC1_HUMAN	0	0	21	8
ODPB_HUMAN	0	0	12	15
RM04_HUMAN	0	0	16	19
TMM43_HUMAN	16	11	0	0
SYYC_HUMAN	0	0	18	27
gnl|unk|ENST00000490826_10	0	0	0	0
CXAR_HUMAN	15	15	0	0
FACE1_HUMAN	16	8	0	0
H10_HUMAN	17	15	0	0
MANF_HUMAN	0	0	13	10
MIA3_HUMAN	17	17	0	0
NAT10_HUMAN	19	10	3	2
PSA4_HUMAN	0	0	21	12
PSME3_HUMAN	0	0	14	22
RDH11_HUMAN	16	13	0	0
TOIP1_HUMAN	21	11	0	0
UD2A3_HUMAN	13	18	0	0
CCAR1_HUMAN	0	0	11	10
GSTO1_HUMAN	0	0	16	15
NPM3_HUMAN	9	12	12	12
gnl|unk|ENST00000420712_6	13	11	5	8
ARC1B_HUMAN	4	6	16	12
CERS2_HUMAN	11	11	0	0
CSK2B_HUMAN	1	0	20	16
GLRX1_HUMAN	0	0	16	20
HEM6_HUMAN	0	0	19	17
IF2A_HUMAN	0	4	12	8

MAVS_HUMAN	2	7	10	12
NOP9_HUMAN	0	0	20	20
NUCB1_HUMAN	8	2	13	11
NUDC_HUMAN	0	0	17	17
OXA1L_HUMAN	9	4	0	0
PTRD1_HUMAN	0	0	20	17
RM44_HUMAN	11	10	6	7
SGPL1_HUMAN	20	12	0	0
SYLC_HUMAN	0	0	12	21
TBL2_HUMAN	15	20	0	0
TBL3_HUMAN	6	3	11	14
TIM50_HUMAN	22	16	0	0
TM9S1_HUMAN	11	21	0	0
SC11A_HUMAN	11	14	0	0
THIO_HUMAN	0	0	7	7
TPP1_HUMAN	4	5	9	5
NDUAB_HUMAN	22	19	0	0
RBM3_HUMAN	4	1	11	16
SNR40_HUMAN	5	2	7	5
DHRS1_HUMAN	14	15	0	0
gnl|unk|ENST00000559483_7	7	0	0	0
RAB32_HUMAN	17	14	0	0
RAB7L_HUMAN	0	0	0	0
ADH6_HUMAN	0	0	18	14
AIFM2_HUMAN	23	10	0	0
ARK72_HUMAN	0	0	13	12
DAZP1_HUMAN	0	0	13	8
DDX42_HUMAN	0	1	15	13
DOHH_HUMAN	0	0	21	18

EPCAM_HUMAN	27	16	0	0
JAM1_HUMAN	17	16	0	0
LAT1_HUMAN	21	19	0	0
M4K4_HUMAN	7	9	6	6
MCM2_HUMAN	0	0	17	17
PA1B3_HUMAN	0	0	11	15
PR40A_HUMAN	10	7	2	0
PSB4_HUMAN	0	0	18	16
PUR4_HUMAN	0	0	19	9
RB11B_HUMAN	7	4	0	2
ROAA_HUMAN	0	0	21	22
STAT3_HUMAN	3	5	13	8
SYWC_HUMAN	0	0	28	12
TR150_HUMAN	0	0	16	13
ZO2_HUMAN	12	6	8	4
AN32A_HUMAN	4	0	25	25
IF4G1_HUMAN	0	0	17	17
IF4G3_HUMAN	0	0	0	0
AAAT_HUMAN	15	13	0	0
ACSF2_HUMAN	1	0	20	15
CPNE1_HUMAN	0	0	8	13
ELYS_HUMAN	10	17	0	0
EMC2_HUMAN	25	14	0	0
GRN_HUMAN	7	3	10	7
HCDH_HUMAN	0	0	13	21
NSDHL_HUMAN	12	17	0	0
PUR8_HUMAN	0	0	8	18
ACSA_HUMAN	0	0	9	8
ARP3_HUMAN	2	2	12	11

CK5P3_HUMAN	19	9	0	0
DCXR_HUMAN	0	0	15	16
DHCR7_HUMAN	15	13	0	0
FND3B_HUMAN	16	14	0	0
GLRX3_HUMAN	0	0	13	19
HUWE1_HUMAN	0	0	18	12
MARCS_HUMAN	16	8	7	9
NDUB4_HUMAN	8	9	0	0
NNTM_HUMAN	11	14	0	0
PSDE_HUMAN	0	0	12	12
RD23B_HUMAN	3	3	19	12
RPB2_HUMAN	6	9	0	0
SCAM2_HUMAN	14	9	0	0
THTM_HUMAN	0	0	14	18
DJB11_HUMAN	16	10	5	6
DNJB1_HUMAN	4	3	1	3
RRP5_HUMAN	0	2	8	5
ECHP_HUMAN	3	0	7	14
HNRDL_HUMAN	0	0	33	24
MYO1C_HUMAN	16	12	0	2
NP1L4_HUMAN	0	1	29	27
PIGS_HUMAN	18	12	0	0
PNKD_HUMAN	19	17	0	0
RENT1_HUMAN	0	0	11	13
RNT2_HUMAN	0	0	11	11
SYYM_HUMAN	1	7	10	7
SPNS1_HUMAN	18	13	0	0
HMGB1_HUMAN	5	3	4	8
SRRM1_HUMAN	1	2	12	12

MCA3_HUMAN	12	12	4	4
ABCF1_HUMAN	6	9	6	6
CATH_HUMAN	0	0	18	18
COPD_HUMAN	0	0	15	18
DHB11_HUMAN	11	10	0	0
DNPEP_HUMAN	0	0	15	10
EIF3H_HUMAN	0	0	9	11
GNL3_HUMAN	7	9	1	0
LMO7_HUMAN	13	11	3	4
MCM6_HUMAN	0	0	13	8
MSMO1_HUMAN	19	19	0	0
NEP1_HUMAN	1	2	9	12
NU188_HUMAN	7	13	0	0
P5CR2_HUMAN	0	4	24	16
PGM1_HUMAN	0	0	17	20
PSA3_HUMAN	1	0	15	14
RAB2A_HUMAN	16	13	0	0
RS23_HUMAN	13	11	0	4
SEPT2_HUMAN	0	0	10	8
SRRM2_HUMAN	0	0	13	12
SGMR1_HUMAN	14	15	0	0
CTBL1_HUMAN	5	5	3	5
NEDD8_HUMAN	0	0	15	17
gnl|unk|ENST00000250495_5	0	0	15	17
gnl|unk|ENST00000527046_11	0	0	15	17
gnl|unk|ENST00000531430_6	0	0	15	17
gnl|unk|ENST00000560427_14	0	0	15	17

1433F_HUMAN	0	0	30	27
1433G_HUMAN	0	0	31	28
1433S_HUMAN	0	0	31	28
ALAT2_HUMAN	0	0	12	18
ATP5L_HUMAN	12	11	0	0
MRP_HUMAN	18	6	5	4
NUP58_HUMAN	12	13	0	0
PNPH_HUMAN	0	0	15	14
RAVR1_HUMAN	0	0	12	10
SCAM4_HUMAN	11	12	0	0
CCD86_HUMAN	16	15	0	0
ELMD2_HUMAN	10	8	0	0
SRP14_HUMAN	4	3	12	13
gnl|unk|ENST00000517881_4	0	0	16	10
AGM1_HUMAN	0	0	16	11
CAND1_HUMAN	0	0	15	11
CHDH_HUMAN	3	5	0	0
EF1D_HUMAN	0	2	16	18
MK67I_HUMAN	7	8	9	4
PYM1_HUMAN	0	0	16	18
SMC1A_HUMAN	6	10	0	0
SPRE_HUMAN	0	0	13	20
TTL12_HUMAN	0	0	14	20
AAAS_HUMAN	9	10	0	0
PSB6_HUMAN	0	0	13	14
GRPE1_HUMAN	0	0	9	9
HSDL1_HUMAN	10	11	0	0
AP1M1_HUMAN	1	1	5	4
RFA3_HUMAN	5	6	6	5

68MP_HUMAN	3	5	0	0
gnl|unk|ENST00000286953_5	3	5	0	0
gnl|unk|ENST00000557040_6	3	5	0	0
COX20_HUMAN	15	9	0	0
DDX47_HUMAN	11	12	6	2
EDC4_HUMAN	2	0	11	11
FABP5_HUMAN	0	0	6	15
FAKD2_HUMAN	0	0	16	11
GALT2_HUMAN	7	15	0	0
GLGB_HUMAN	0	0	16	16
HDGF_HUMAN	0	0	17	12
PGRC2_HUMAN	14	11	0	0
PRS6A_HUMAN	0	0	14	11
TRXR1_HUMAN	0	0	14	14
SRSF2_HUMAN	4	2	15	8
THOC2_HUMAN	1	2	7	5
NDUF3_HUMAN	8	7	0	0
DHPR_HUMAN	0	0	10	17
DNJC5_HUMAN	10	3	0	0
IGSF1_HUMAN	12	17	0	0
LSM2_HUMAN	0	0	14	17
gnl|unk|ENST00000375661_7	0	0	14	17
MTX2_HUMAN	10	11	0	0
SNW1_HUMAN	4	4	14	13
SPB1_HUMAN	2	4	16	12
USO1_HUMAN	0	0	18	15
EIF3M_HUMAN	0	2	18	11
DC1I2_HUMAN	12	13	0	0
RM50_HUMAN	0	0	18	11

VTA1_HUMAN	1	1	0	2
G3BP2_HUMAN	4	4	11	6
LAD1_HUMAN	13	13	3	3
LAMA5_HUMAN	6	9	1	0
NDUS6_HUMAN	9	16	0	0
RT27_HUMAN	0	0	12	14
ST2A1_HUMAN	0	0	5	10
TRIPC_HUMAN	8	10	0	0
MINP1_HUMAN	0	0	18	14
SRS11_HUMAN	0	1	19	10
NPTN_HUMAN	11	5	0	0
SNUT2_HUMAN	9	8	5	3
ACL6A_HUMAN	11	13	3	2
ARL1_HUMAN	10	14	0	0
BOP1_HUMAN	1	3	12	16
DD19A_HUMAN	0	0	9	12
DSRAD_HUMAN	10	4	4	6
E41L2_HUMAN	1	0	10	9
ENPP1_HUMAN	10	13	0	0
IF5_HUMAN	3	1	11	6
YMEL1_HUMAN	17	13	0	0
ATX2L_HUMAN	0	0	11	11
TRI25_HUMAN	5	2	2	4
S29A1_HUMAN	14	10	0	0
CX7A2_HUMAN	9	10	0	0
NOL6_HUMAN	6	1	11	12
MOT1_HUMAN	15	8	0	0
LSM5_HUMAN	5	2	10	10
gnl|unk|ENST00000450169_6	5	2	10	10

KINH_HUMAN	0	1	8	6
KIF5A_HUMAN	0	0	0	0
AP3D1_HUMAN	2	2	8	5
BGAL_HUMAN	0	0	8	10
CHERP_HUMAN	3	0	11	12
PIGT_HUMAN	14	14	0	0
RM46_HUMAN	0	1	11	10
TIM44_HUMAN	2	4	9	13
TM205_HUMAN	17	15	0	0
CHSP1_HUMAN	0	0	14	10
MIMIT_HUMAN	13	16	0	0
LSM8_HUMAN	0	0	13	11
MIC25_HUMAN	14	7	0	0
UB2D2_HUMAN	0	0	15	13
UB2D3_HUMAN	0	0	15	13
LC7L2_HUMAN	5	2	0	0
LUC7L_HUMAN	0	0	0	0
LTOR2_HUMAN	6	9	8	5
PDS5B_HUMAN	8	5	0	0
PDS5A_HUMAN	1	1	1	0
AMRP_HUMAN	0	0	7	8
CLIC4_HUMAN	0	0	12	14
CSTF3_HUMAN	0	0	16	13
DGAT1_HUMAN	19	11	0	0
DLDH_HUMAN	0	0	11	15
DNJC9_HUMAN	8	11	0	0
HEAT1_HUMAN	7	7	2	2
MA2A1_HUMAN	9	8	0	0
MVD1_HUMAN	0	0	14	12

NCEH1_HUMAN	5	11	0	0
NDUS8_HUMAN	14	11	0	0
PPM1G_HUMAN	0	0	6	5
RFA1_HUMAN	8	7	6	6
VPS35_HUMAN	0	0	8	11
WDR75_HUMAN	8	1	8	5
ZNT1_HUMAN	11	5	0	0
NADC_HUMAN	0	0	9	13
AN32B_HUMAN	4	3	20	19
MYDGF_HUMAN	0	0	12	12
ARP2_HUMAN	2	4	6	5
SAMH1_HUMAN	0	0	13	8
FEN1_HUMAN	0	0	12	12
NDUA4_HUMAN	15	13	0	0
gnl|unk|ENST00000339600_9	15	13	0	0
NUCB2_HUMAN	7	3	6	7
DNJC3_HUMAN	0	0	14	11
ASNA_HUMAN	11	2	1	2
C560_HUMAN	9	13	0	0
DEST_HUMAN	4	3	11	10
SIAT1_HUMAN	10	12	0	0
HNF4A_HUMAN	7	6	1	4
6PGL_HUMAN	0	0	14	11
CSN1_HUMAN	0	0	9	10
FUBP3_HUMAN	5	5	7	10
GSTK1_HUMAN	1	2	10	9
IDE_HUMAN	0	0	7	4
ITAV_HUMAN	8	3	0	0
ITPA_HUMAN	0	0	16	15

MCM3_HUMAN	1	4	10	5
MET7A_HUMAN	12	13	0	0
PP2AA_HUMAN	0	0	13	13
RT22_HUMAN	0	0	13	13
STAT1_HUMAN	10	7	0	1
SYNC_HUMAN	0	0	7	14
WDR12_HUMAN	3	3	8	6
IF2P_HUMAN	8	2	9	7
BMS1_HUMAN	0	0	11	5
PICAL_HUMAN	2	1	10	14
FBX2_HUMAN	0	0	7	6
YES_HUMAN	14	14	0	0
HCK_HUMAN	0	0	0	0
CCD58_HUMAN	0	0	10	11
gnl|unk|ENST00000590792_3	0	0	0	3
ASNS_HUMAN	0	0	7	19
CTNA1_HUMAN	16	14	0	0
EIF3E_HUMAN	0	0	12	8
EMC7_HUMAN	10	8	0	0
IKIP_HUMAN	6	4	0	0
PBIP1_HUMAN	6	8	0	0
RPB1_HUMAN	10	8	3	3
TXNL1_HUMAN	0	0	14	12
PSD12_HUMAN	0	0	11	7
BCLF1_HUMAN	1	0	8	9
PGM2_HUMAN	0	0	16	11
CNN2_HUMAN	0	0	15	12
PRAF3_HUMAN	10	9	0	0
EIF3I_HUMAN	0	0	13	12

SOAT1_HUMAN	5	2	0	0
ODO2_HUMAN	0	0	12	16
CNBP_HUMAN	5	4	7	7
SKP1_HUMAN	1	3	15	11
CAB45_HUMAN	1	0	3	6
LCLT1_HUMAN	8	8	0	0
TOM20_HUMAN	10	10	0	0
gnl|unk|ENST00000467767_4	10	10	0	0
METK2_HUMAN	2	5	4	5
METK1_HUMAN	0	0	4	7
SYJ2B_HUMAN	6	6	0	0
gnl|unk|ENST00000618385_4	6	6	0	0
CD166_HUMAN	12	11	0	0
FND3A_HUMAN	10	13	0	0
LYPA1_HUMAN	0	0	12	12
MAGT1_HUMAN	14	14	0	0
MIRO2_HUMAN	8	9	0	0
RS15_HUMAN	5	4	2	3
RT18B_HUMAN	0	0	5	10
SGT1_HUMAN	0	0	8	11
PDIP2_HUMAN	0	0	12	11
TXD12_HUMAN	0	0	9	11
NOL10_HUMAN	2	2	9	7
VPS29_HUMAN	0	0	9	14
SAR1A_HUMAN	3	9	1	0
SAR1B_HUMAN	3	4	0	2
ARI3A_HUMAN	0	0	7	12
ARI3C_HUMAN	0	0	0	0
GNS_HUMAN	0	0	11	10

GPI8_HUMAN	10	8	0	0
HN1_HUMAN	0	0	11	12
IQGA2_HUMAN	5	6	3	4
NAMPT_HUMAN	0	0	15	10
RAB21_HUMAN	12	13	1	1
SCRB2_HUMAN	12	3	0	0
RUVB2_HUMAN	5	5	2	6
TMED4_HUMAN	19	21	0	0
DJC11_HUMAN	12	10	0	0
ERH_HUMAN	0	2	6	7
NOC3L_HUMAN	3	8	1	6
UCHL3_HUMAN	0	0	8	9
VMP1_HUMAN	15	8	0	0
VATE1_HUMAN	15	8	0	0
GNPI1_HUMAN	0	0	13	11
HDAC1_HUMAN	7	1	2	4
HDAC2_HUMAN	4	0	4	3
PMM2_HUMAN	8	5	7	7
MGST3_HUMAN	5	2	0	0
A1CF_HUMAN	0	0	9	16
CENPV_HUMAN	11	11	0	0
EMC4_HUMAN	10	3	0	0
MAAI_HUMAN	0	0	12	11
MEP50_HUMAN	0	0	12	10
MK01_HUMAN	0	0	21	14
NDUV2_HUMAN	4	9	0	0
OSBL8_HUMAN	7	9	0	0
RAD21_HUMAN	8	8	0	0
SAC1_HUMAN	11	5	0	0

SAE2_HUMAN	0	0	9	7
TMED5_HUMAN	9	11	0	0
TCOF_HUMAN	1	1	4	6
GAMT_HUMAN	0	0	9	7
MARH5_HUMAN	11	4	0	0
MUTA_HUMAN	0	0	3	0
MARC1_HUMAN	6	8	0	0
PFD5_HUMAN	0	0	10	12
PNO1_HUMAN	10	8	0	0
UBP10_HUMAN	0	0	9	7
NDUA6_HUMAN	3	3	0	0
EBP_HUMAN	13	12	0	0
TYB10_HUMAN	0	0	13	12
gnl|unk|ENST00000233143_3	0	0	13	12
ASPC1_HUMAN	0	0	9	7
IPO9_HUMAN	1	1	7	10
LC7L3_HUMAN	4	6	9	4
MCU_HUMAN	5	2	0	0
MTAP_HUMAN	0	0	11	15
NU107_HUMAN	10	3	0	0
PLOD3_HUMAN	0	0	3	8
RBM15_HUMAN	6	3	5	2
RM45_HUMAN	9	4	1	0
SC61B_HUMAN	10	9	0	0
gnl|unk|ENST00000223641_2	10	9	0	0
TMEM2_HUMAN	8	7	0	0
TMOD3_HUMAN	7	8	0	0
ABCE1_HUMAN	3	1	5	5
RRP1B_HUMAN	4	7	0	1

PEPD_HUMAN	0	0	10	10
SUCA_HUMAN	0	1	4	13
PIMT_HUMAN	0	0	8	7
TBRG4_HUMAN	0	0	10	6
HNRL1_HUMAN	0	0	14	7
NU5M_HUMAN	10	11	0	0
NOP16_HUMAN	9	6	6	2
BCCIP_HUMAN	4	2	7	6
DDX24_HUMAN	6	4	7	3
HNRH3_HUMAN	1	1	0	5
MAL2_HUMAN	15	10	0	0
RT05_HUMAN	0	1	5	5
GOSR2_HUMAN	10	4	0	0
EHD1_HUMAN	5	2	3	3
TI17B_HUMAN	11	11	0	0
GNA11_HUMAN	10	10	0	2
GNAQ_HUMAN	1	0	0	0
ACPH_HUMAN	0	0	6	10
ESYT2_HUMAN	11	7	0	0
GORS2_HUMAN	0	2	11	9
PLST_HUMAN	0	0	6	8
PYGL_HUMAN	0	0	9	6
RAB18_HUMAN	12	12	0	0
SARDH_HUMAN	0	0	9	10
SCMC1_HUMAN	12	5	0	0
STRAP_HUMAN	0	0	9	13
TDIF2_HUMAN	10	6	0	2
THIK_HUMAN	3	3	7	6
TIM9_HUMAN	8	7	0	0

gnl|unk|ENST00000395159_12	8	7	0	0
gnl|unk|ENST00000555061_8	8	7	0	0
gnl|unk|ENST00000555404_9	8	7	0	0
gnl|unk|ENST00000555593_8	8	7	0	0
TMX2_HUMAN	4	5	0	0
UTRO_HUMAN	1	1	7	11
IVD_HUMAN	4	0	4	8
MYO1D_HUMAN	10	11	0	0
NDUBB_HUMAN	8	9	0	0
CP27A_HUMAN	11	5	0	0
ZYX_HUMAN	7	4	5	6
ADPGK_HUMAN	10	3	0	0
SRS10_HUMAN	2	0	8	6
PERQ2_HUMAN	6	2	9	7
PHS_HUMAN	1	1	4	2
COA3_HUMAN	6	4	0	0
ZN326_HUMAN	1	2	7	6
ACTZ_HUMAN	0	0	6	7
ACTY_HUMAN	0	0	3	0
AKAP1_HUMAN	12	4	0	0
DDRGK_HUMAN	13	7	0	0
EXOSX_HUMAN	0	0	7	2
MRP2_HUMAN	12	6	0	0
NUDT5_HUMAN	0	0	12	9
PSMD4_HUMAN	0	0	14	4
S38A3_HUMAN	13	8	0	0
SRRT_HUMAN	0	0	3	11
TF3C1_HUMAN	0	2	7	9

TSR1_HUMAN	12	8	0	0
ADK_HUMAN	0	0	12	11
CND3_HUMAN	11	9	0	0
CSN3_HUMAN	1	0	9	3
MRRP1_HUMAN	3	6	5	1
SRP68_HUMAN	2	3	6	6
THTR_HUMAN	0	0	9	9
PIGU_HUMAN	13	9	0	0
ERG28_HUMAN	3	2	0	0
MAT2B_HUMAN	0	0	6	6
SPS2L_HUMAN	5	7	0	0
GMFB_HUMAN	0	0	11	11
MIC27_HUMAN	2	4	0	0
GMDS_HUMAN	0	0	12	7
MACF1_HUMAN	0	0	1	2
LTOR1_HUMAN	4	3	3	1
TPX2_HUMAN	5	5	0	0
ASAH1_HUMAN	12	6	0	2
BT3L4_HUMAN	0	0	12	12
FERM2_HUMAN	0	0	4	10
KPRA_HUMAN	0	0	12	11
RM37_HUMAN	0	6	6	5
RRP12_HUMAN	5	3	10	0
THRB_HUMAN	3	3	0	0
AUP1_HUMAN	6	5	0	0
OCAD1_HUMAN	4	4	0	0
DDX46_HUMAN	1	0	4	5
LAMP2_HUMAN	12	6	0	0
CPSF6_HUMAN	6	3	6	4

STMN1_HUMAN	0	0	9	6
VATL_HUMAN	9	6	0	0
GPC6_HUMAN	11	8	0	0
ICAM1_HUMAN	9	9	0	0
MAOM_HUMAN	0	0	7	9
SEH1_HUMAN	9	10	0	0
SMCA1_HUMAN	7	2	0	0
RMND1_HUMAN	4	4	0	0
SCPDL_HUMAN	10	10	0	0
PRKRA_HUMAN	0	0	8	7
TIA1_HUMAN	0	0	24	19
CREL1_HUMAN	8	10	0	0
CSTF1_HUMAN	0	0	8	13
PCM1_HUMAN	3	5	0	0
PFD3_HUMAN	0	0	11	11
PVR_HUMAN	9	7	0	0
LTOR3_HUMAN	6	4	3	6
MPC2_HUMAN	1	0	0	0
DYL1_HUMAN	13	14	24	20
gnl|unk|ENST00000242577_8	13	14	24	20
gnl|unk|ENST00000392508_8	13	14	24	20
gnl|unk|ENST00000392509_8	13	14	24	20
gnl|unk|ENST00000548342_9	13	14	24	20
gnl|unk|ENST00000549989_9	13	14	24	20
RU1C_HUMAN	7	6	6	4
ZFPL1_HUMAN	6	5	0	0
SMRD2_HUMAN	3	2	0	0
SMRD1_HUMAN	1	1	0	0
APEX1_HUMAN	11	6	0	0

DUS9_HUMAN	0	3	6	7
ERLN1_HUMAN	18	19	0	0
HG2A_HUMAN	10	10	0	0
IF2B2_HUMAN	0	0	15	30
PININ_HUMAN	8	9	0	0
RIF1_HUMAN	10	7	0	0
RMD3_HUMAN	1	10	0	0
UBE2K_HUMAN	0	0	13	2
gnl|unk|ENST00000510719_9	0	0	13	2
COASY_HUMAN	4	5	3	4
PAK2_HUMAN	0	0	5	6
S10A1_HUMAN	0	0	3	7
MCM4_HUMAN	0	0	10	9
SRC_HUMAN	6	4	0	0
NAKD2_HUMAN	0	0	10	10
RER1_HUMAN	9	5	0	0
TTC38_HUMAN	0	0	10	10
AP2M1_HUMAN	5	5	6	6
CB047_HUMAN	8	5	0	0
HMGN3_HUMAN	4	13	0	0
PREP_HUMAN	0	0	12	10
RM15_HUMAN	0	0	5	12
RS28_HUMAN	0	3	6	10
gnl|unk|ENST00000441378_1	0	3	6	10
gnl|unk|ENST00000442562_1	0	3	6	10
gnl|unk|ENST00000473748_1	0	3	6	10
gnl|unk|ENST00000600659_1	0	3	6	10
S38A2_HUMAN	16	6	0	0
MOV10_HUMAN	0	0	4	3

TMCO1_HUMAN	7	4	0	0
HBA_HUMAN	6	7	0	0
RL29_HUMAN	4	5	4	5
TOM7_HUMAN	4	3	0	0
gnl|unk|ENST00000358435_4	4	3	0	0
TM41B_HUMAN	10	5	0	0
RM47_HUMAN	0	0	8	12
TCTP_HUMAN	0	0	9	9
RAB6A_HUMAN	11	14	0	0
gnl|unk|ENST00000536566_12	0	0	0	0
CPNS1_HUMAN	0	0	10	4
CPT2_HUMAN	8	7	0	0
EEA1_HUMAN	0	0	3	6
ITA2_HUMAN	13	4	0	0
MSH6_HUMAN	3	7	0	0
PDIP3_HUMAN	5	6	0	0
PTCD3_HUMAN	0	0	5	5
SMCA4_HUMAN	5	5	0	0
VAMP3_HUMAN	11	7	0	0
gnl|unk|ENST00000054666_6	11	7	0	0
ZW10_HUMAN	10	8	0	0
ELOB_HUMAN	0	0	12	9
NDUA7_HUMAN	6	6	0	0
RNZ2_HUMAN	0	0	10	7
AK1BA_HUMAN	0	0	8	8
CHRD1_HUMAN	0	0	9	6
MDR1_HUMAN	6	3	0	0
CP20A_HUMAN	4	6	0	0

PCY1A_HUMAN	6	5	0	0
VKGC_HUMAN	7	7	0	0
HKDC1_HUMAN	6	6	0	0
SPB6_HUMAN	0	0	6	3
RAE1L_HUMAN	7	4	0	0
CLU_HUMAN	0	0	3	4
3BHS7_HUMAN	7	4	0	0
AP1G1_HUMAN	0	1	7	8
ARMT1_HUMAN	0	0	6	8
F210B_HUMAN	10	9	0	0
HERP1_HUMAN	10	10	0	0
HSBP1_HUMAN	0	0	11	10
gnl|unk|ENST00000433866_6	0	0	11	10
gnl|unk|ENST00000570259_5	0	0	11	10
NDUS4_HUMAN	10	5	0	0
PLLP_HUMAN	7	7	0	0
SCRB1_HUMAN	9	9	0	0
TMEM9_HUMAN	13	6	0	0
CD99_HUMAN	11	6	0	0
AIMP2_HUMAN	1	1	10	4
CY24A_HUMAN	2	3	0	0
GALM_HUMAN	0	0	7	7
BLVRB_HUMAN	0	0	8	9
QCR8_HUMAN	5	4	0	0
gnl|unk|ENST00000378667_5	5	4	0	0
RM41_HUMAN	0	0	9	8
BST2_HUMAN	7	6	0	0
gnl|unk|ENST00000533098_5	7	6	0	0
ARAP1_HUMAN	6	5	5	5

COX7R_HUMAN	12	9	0	0
OSTC_HUMAN	10	9	0	0
ADDA_HUMAN	4	4	2	1
CPT1A_HUMAN	12	8	0	0
CSN6_HUMAN	0	0	6	7
EFTS_HUMAN	5	6	4	4
PECR_HUMAN	0	0	10	8
RT31_HUMAN	0	0	10	10
FKBP3_HUMAN	0	0	8	8
CAN1_HUMAN	0	0	7	10
CADH2_HUMAN	2	1	0	0
KPYR_HUMAN	0	0	18	18
DREB_HUMAN	6	4	4	1
STX5_HUMAN	6	8	0	0
QSOX2_HUMAN	6	5	0	0
SUCB1_HUMAN	2	0	2	5
TMED1_HUMAN	6	4	0	0
GPDA_HUMAN	0	0	7	7
MFF_HUMAN	6	4	0	0
CPNE3_HUMAN	0	0	4	8
NFS1_HUMAN	0	0	10	10
TXD17_HUMAN	0	0	6	7
IMP3_HUMAN	0	1	7	4
DNMT1_HUMAN	7	3	0	0
RUXG_HUMAN	7	8	0	0
gnl|unk|ENST00000272348_6	7	8	0	0
ATAD1_HUMAN	2	0	0	0
SPG7_HUMAN	7	3	0	0
RPOM_HUMAN	5	1	3	1

DAG1_HUMAN	7	3	0	0
PELP1_HUMAN	6	6	4	2
HIG1A_HUMAN	9	9	0	0
gnl|unk|ENST00000418900_4	9	9	0	0
gnl|unk|ENST00000625589_4	9	9	0	0
GAR1_HUMAN	2	4	5	6
MLXPL_HUMAN	6	4	4	6
MPRD_HUMAN	4	8	0	0
NDUS7_HUMAN	10	7	0	0
AN32E_HUMAN	0	0	5	4
RM17_HUMAN	0	0	10	7
IF2B3_HUMAN	0	0	17	29
K1C10_HUMAN	16	1	0	0
RM01_HUMAN	0	0	3	6
TGM2_HUMAN	6	10	0	0
EFGM_HUMAN	0	0	5	9
PDXK_HUMAN	0	0	7	6
SRP09_HUMAN	0	1	8	8
gnl|unk|ENST00000304786_8	0	1	8	8
gnl|unk|ENST00000445874_6	0	1	8	8
A1AG1_HUMAN	0	0	9	7
DUS3_HUMAN	0	0	5	10
DYLT1_HUMAN	10	9	0	0
gnl|unk|ENST00000367085_4	10	9	0	0
OGFR_HUMAN	0	0	9	7
QKI_HUMAN	0	0	5	8
RCN2_HUMAN	2	5	6	5
RFC3_HUMAN	9	6	0	0
RHOB_HUMAN	5	6	0	0

RNPS1_HUMAN	11	3	2	3
TMA16_HUMAN	13	6	0	0
IF2B_HUMAN	4	5	0	0
PACN3_HUMAN	3	2	0	1
DCAKD_HUMAN	3	2	0	0
NDUA2_HUMAN	1	1	0	0
F134C_HUMAN	5	1	0	0
SC5A6_HUMAN	3	1	0	0
PDCD5_HUMAN	0	0	1	3
gnl|unk|ENST00000221784_4	0	0	1	3
gnl|unk|ENST00000586035_6	0	0	1	3
LRP1_HUMAN	6	1	0	0
ROMO1_HUMAN	7	6	0	0
gnl|unk|ENST00000374078_3	7	6	0	0
gnl|unk|ENST00000397416_1	7	6	0	0
PYR1_HUMAN	1	2	2	1
IFM3_HUMAN	0	2	4	6
ATP6_HUMAN	7	8	0	0
CNIH4_HUMAN	12	6	0	0
gnl|unk|ENST00000468318_8	12	6	0	0
GRWD1_HUMAN	3	1	0	0
ACOC_HUMAN	0	0	5	9
CNN3_HUMAN	0	0	8	1
IDI1_HUMAN	0	0	6	10
LAMC1_HUMAN	6	3	3	1
ODR4_HUMAN	9	3	0	0
UB2G2_HUMAN	5	8	0	0
UMPS_HUMAN	0	0	7	9
ZCCHV_HUMAN	8	5	0	0

NCBP1_HUMAN	0	0	5	5
EIF3K_HUMAN	0	0	7	8
LYAR_HUMAN	4	3	0	1
UCHL5_HUMAN	0	0	6	5
TACO1_HUMAN	0	0	6	6
VA0D1_HUMAN	3	1	0	0
PAPS1_HUMAN	0	0	5	7
MFN2_HUMAN	4	3	0	0
EWS_HUMAN	3	2	4	5
MFAP1_HUMAN	1	3	5	5
MRE11_HUMAN	1	1	2	3
PRP4_HUMAN	6	7	4	0
REEP6_HUMAN	4	5	0	3
GSHB_HUMAN	0	0	6	2
BYST_HUMAN	6	6	1	2
SUMO1_HUMAN	0	0	3	3
RPAC1_HUMAN	1	1	1	1
TF3C5_HUMAN	6	4	6	2
NDUA3_HUMAN	4	4	0	0
gnl|unk|ENST00000391763_4	4	4	0	0
gnl|unk|ENST00000419113_4	4	4	0	0
UT14A_HUMAN	3	2	0	4
UT14C_HUMAN	0	0	0	0
CCHL_HUMAN	9	7	0	0
CP2W1_HUMAN	8	8	0	0
ECE1_HUMAN	5	5	0	0
GNA1_HUMAN	0	0	8	9
HS2ST_HUMAN	1	3	0	0
NDUB7_HUMAN	4	4	0	0

TNPO1_HUMAN	0	0	23	29
ATP5I_HUMAN	0	10	0	0
gnl|unk|ENST00000304312_4	0	10	0	0
MPPB_HUMAN	0	0	4	6
SSDH_HUMAN	0	0	6	8
FN3K_HUMAN	1	0	7	7
SNRPA_HUMAN	0	0	7	7
NT5D2_HUMAN	1	3	3	4
TOM34_HUMAN	2	3	4	4
EXOS5_HUMAN	0	0	10	6
SRC8_HUMAN	0	0	7	6
ARSB_HUMAN	0	0	8	6
FADS1_HUMAN	4	6	0	0
HAT1_HUMAN	0	0	10	7
MA1B1_HUMAN	8	5	0	0
MTPN_HUMAN	0	0	0	5
RM16_HUMAN	0	5	0	3
SBP1_HUMAN	0	0	9	7
TSN6_HUMAN	5	4	0	0
WDR18_HUMAN	2	0	6	6
SK2L2_HUMAN	2	1	4	2
LONP2_HUMAN	3	3	0	0
ALG5_HUMAN	8	1	0	0
DEFM_HUMAN	4	4	0	0
CPSF2_HUMAN	0	0	6	4
SH3G1_HUMAN	0	0	7	5
VISL1_HUMAN	2	1	5	2
RBM25_HUMAN	0	0	6	6
LSM4_HUMAN	0	0	4	5

GGH_HUMAN	0	0	2	4
IR3IP_HUMAN	6	6	0	0
gnl|unk|ENST00000256433_3	6	6	0	0
gnl|unk|ENST00000588705_3	6	6	0	0
ILK_HUMAN	3	0	0	0
TIM13_HUMAN	3	0	0	1
gnl|unk|ENST00000215570_5	3	0	0	1
HEM3_HUMAN	0	0	9	6
RO60_HUMAN	0	0	5	4
gnl|unk|ENST00000487233_4	1	4	5	2
gnl|unk|ENST00000412502_4	0	0	0	0
EXOS3_HUMAN	4	4	5	3
LYSC_HUMAN	6	2	5	4
gnl|unk|ENST00000352511_93	1	2	2	2
BCAT1_HUMAN	0	0	8	7
P121C_HUMAN	4	1	0	0
P121A_HUMAN	0	0	0	0
ACADM_HUMAN	0	0	3	8
CBX1_HUMAN	0	0	7	8
CSN2_HUMAN	0	0	5	4
DHSO_HUMAN	0	0	4	6
GLRX5_HUMAN	0	0	6	9
I2BP2_HUMAN	0	0	11	3
ORNT1_HUMAN	3	5	0	0
PCAT1_HUMAN	10	6	0	0
UD2B7_HUMAN	5	5	0	0
VRK1_HUMAN	9	5	0	0
CBR1_HUMAN	0	0	7	2

AMPB_HUMAN	0	0	7	6
TIAR_HUMAN	0	0	23	15
SRSF5_HUMAN	0	0	8	6
CARM1_HUMAN	0	0	8	7
FA98A_HUMAN	2	1	3	2
PSPC1_HUMAN	1	0	5	8
SUN1_HUMAN	8	0	0	0
CNPY3_HUMAN	0	0	4	9
PCP_HUMAN	0	0	4	7
PPID_HUMAN	0	0	6	7
PYRG1_HUMAN	0	0	10	6
RM49_HUMAN	1	1	6	8
SMC3_HUMAN	9	3	0	0
TAM41_HUMAN	9	7	0	0
UBXN4_HUMAN	9	7	0	0
XPC_HUMAN	6	7	0	0
NDC1_HUMAN	1	2	0	0
MCM7_HUMAN	0	0	8	6
RT34_HUMAN	0	0	7	9
DCTP1_HUMAN	0	0	0	2
SPCS3_HUMAN	1	1	0	0
TM189_HUMAN	7	0	0	0
ANXA7_HUMAN	0	0	5	1
PUM3_HUMAN	0	1	5	6
RENR_HUMAN	6	0	0	0
TIF1A_HUMAN	0	0	6	6
VAS1_HUMAN	4	4	0	0
ATP8_HUMAN	3	0	0	0
MMS19_HUMAN	0	0	6	5

VAMP8_HUMAN	5	4	0	0
gnl|unk|ENST00000263864_8	5	4	0	0
CNOT1_HUMAN	0	0	2	2
SNF5_HUMAN	4	4	0	0
CXB1_HUMAN	6	9	0	0
NIP7_HUMAN	6	4	0	0
NDUC2_HUMAN	3	4	0	0
gnl|unk|ENST00000525085_5	3	4	0	0
ABCF2_HUMAN	6	1	1	2
LICH_HUMAN	3	2	4	2
RFA2_HUMAN	5	3	1	0
RFC5_HUMAN	8	2	0	0
RPF2_HUMAN	1	4	1	0
SORT_HUMAN	7	4	0	0
SDF2L_HUMAN	0	2	5	8
CRK_HUMAN	0	0	8	6
DBLOH_HUMAN	0	0	0	4
DRG2_HUMAN	0	0	7	8
GILT_HUMAN	0	0	8	8
PCCB_HUMAN	0	0	6	6
RM53_HUMAN	0	0	8	6
ATPD_HUMAN	5	6	0	0
ICAL_HUMAN	0	0	8	4
ISOC1_HUMAN	0	0	2	9
LEG1_HUMAN	0	0	4	4
LMF2_HUMAN	8	3	0	0
NUP54_HUMAN	3	4	0	0
RHG01_HUMAN	0	0	8	6
K2013_HUMAN	5	2	0	0

DTD1_HUMAN	0	0	5	4
SERB_HUMAN	0	0	6	8
BACH_HUMAN	0	0	2	3
UXS1_HUMAN	4	2	0	0
SCRIB_HUMAN	6	1	0	0
SYLM_HUMAN	0	0	4	6
S27A2_HUMAN	7	6	0	0
HINT2_HUMAN	0	0	6	7
CS052_HUMAN	3	6	0	0
DCUP_HUMAN	0	0	3	0
EIF1_HUMAN	0	0	9	6
GMPPA_HUMAN	0	0	6	8
LSM3_HUMAN	0	0	7	8
RM21_HUMAN	0	0	6	6
SYEM_HUMAN	0	0	6	4
TRM1_HUMAN	0	0	8	7
GCSH_HUMAN	0	0	6	8
gnl|unk|ENST00000564386_9	0	0	6	8
NAF1_HUMAN	0	0	6	7
REEP5_HUMAN	5	6	0	0
NDUB1_HUMAN	3	5	0	0
gnl|unk|ENST00000553514_8	3	5	0	0
gnl|unk|ENST00000555441_6	3	5	0	0
TM256_HUMAN	6	3	0	0
MTA2_HUMAN	0	2	0	0
PTN11_HUMAN	0	0	2	2
CDK1_HUMAN	3	0	0	0
DCTN1_HUMAN	0	0	2	5
NGDN_HUMAN	4	4	3	2

NEUL_HUMAN	0	0	1	1
ZGPAT_HUMAN	1	1	0	0
MIC13_HUMAN	0	5	0	0
UTP4_HUMAN	0	0	7	6
DIM1_HUMAN	1	0	0	0
CASC4_HUMAN	8	6	0	0
ELOV1_HUMAN	8	6	0	0
YKT6_HUMAN	3	0	4	3
SDC1_HUMAN	0	2	6	5
5NTC_HUMAN	0	0	7	7
CE051_HUMAN	0	0	2	6
EI2BG_HUMAN	0	0	5	9
ENOPH_HUMAN	0	0	6	6
GPX4_HUMAN	0	0	1	1
NIF3L_HUMAN	0	0	1	1
PSD10_HUMAN	0	0	9	6
SRSF6_HUMAN	0	0	2	6
gnl|unk|ENST00000605204_29	0	0	0	0
ARSE_HUMAN	6	7	0	0
MAN1_HUMAN	8	6	0	0
PSB7_HUMAN	0	0	6	7
RBP56_HUMAN	9	8	14	12
SRP54_HUMAN	0	6	3	2
KDM1A_HUMAN	3	4	0	0
ERF1_HUMAN	0	0	9	5
NUP43_HUMAN	7	6	0	0
ACACA_HUMAN	0	0	3	1
RT09_HUMAN	0	0	8	2

PHIP_HUMAN	7	4	0	0
FAH2B_HUMAN	0	0	7	6
FKB1A_HUMAN	0	0	6	5
GMPR2_HUMAN	0	0	8	4
MBOA7_HUMAN	6	8	0	0
PPIG_HUMAN	7	7	0	0
PRP31_HUMAN	0	0	6	7
SF3B6_HUMAN	0	0	8	4
SYTC_HUMAN	0	0	7	5
TOM1_HUMAN	0	0	8	6
TM127_HUMAN	5	5	0	0
PPT1_HUMAN	0	0	5	7
FUCO_HUMAN	0	0	5	7
PTPA_HUMAN	0	0	6	6
PSMD8_HUMAN	2	2	2	1
APLP2_HUMAN	2	3	0	0
PYRD_HUMAN	0	2	0	0
IDH3A_HUMAN	0	0	6	5
PSMF1_HUMAN	2	1	3	2
HPRT_HUMAN	0	0	4	6
GSTT1_HUMAN	0	0	1	2
PP14B_HUMAN	0	0	0	5
PSIP1_HUMAN	5	4	0	0
TGON2_HUMAN	3	5	3	1
DDX56_HUMAN	0	1	6	6
CUL2_HUMAN	0	0	0	1
COA1_HUMAN	2	1	0	0
KAPCA_HUMAN	2	1	3	0
MASU1_HUMAN	2	0	4	6

MIC26_HUMAN	6	7	0	0
P4K2A_HUMAN	7	6	0	0
RBM8A_HUMAN	1	4	5	4
gnl|unk|ENST00000484825_9	1	4	5	4
gnl|unk|ENST00000465744_14	4	4	1	1
gnl|unk|ENST00000471855_4	4	4	1	1
gnl|unk|ENST00000502784_11	1	4	3	0
PHOCN_HUMAN	0	1	7	1
ICT1_HUMAN	0	0	4	3
gnl|unk|ENST00000580800_9	0	0	4	3
IWS1_HUMAN	0	0	11	3
MPI_HUMAN	0	0	6	8
RM19_HUMAN	0	0	6	5
SHPK_HUMAN	0	0	6	5
STK4_HUMAN	0	0	2	5
UAP1_HUMAN	0	0	5	5
WDR43_HUMAN	0	0	6	4
TIDC1_HUMAN	6	4	0	0
gnl|unk|ENST00000463927_5	0	0	0	0
gnl|unk|ENST00000486418_5	0	0	0	0
gnl|unk|ENST00000492164_5	0	0	0	0
CADH1_HUMAN	5	4	0	0
DDX27_HUMAN	5	3	3	2
GALK1_HUMAN	0	0	3	8
MRP1_HUMAN	8	3	0	0
RBM14_HUMAN	3	7	0	0
PTPM1_HUMAN	2	4	0	0

HXK2_HUMAN	0	0	2	8
NDUF4_HUMAN	8	3	0	0
AATF_HUMAN	1	0	1	3
ESF1_HUMAN	4	1	3	0
JAGN1_HUMAN	4	5	0	0
MAK16_HUMAN	7	4	0	0
T126A_HUMAN	11	2	0	0
WDR5_HUMAN	0	3	2	2
RT07_HUMAN	0	0	2	4
TOLIP_HUMAN	4	3	3	1
MP2K2_HUMAN	0	0	8	3
OCLN_HUMAN	7	2	0	0
ACO13_HUMAN	0	0	3	4
TMX3_HUMAN	4	7	0	0
RM11_HUMAN	0	2	2	3
ACAD9_HUMAN	5	2	0	0
P3H1_HUMAN	0	0	3	2
SR140_HUMAN	0	0	6	6
SC11C_HUMAN	1	1	0	0
gnl|unk|ENST00000299714_4	1	1	0	0
CLCN7_HUMAN	3	0	0	0
S19A1_HUMAN	6	5	0	0
HMGB2_HUMAN	5	2	0	0
ABHD6_HUMAN	4	4	0	0
KAD1_HUMAN	0	0	4	2
FAHD1_HUMAN	0	0	5	7
CPSF5_HUMAN	0	0	3	4
RET4_HUMAN	0	0	4	5
SNX5_HUMAN	4	3	4	2

APOA2_HUMAN	6	3	0	0
gnl|unk|ENST00000367990_7	6	3	0	0
gnl|unk|ENST00000463273_10	6	3	0	0
gnl|unk|ENST00000463812_5	6	3	0	0
gnl|unk|ENST00000469730_5	6	3	0	0
gnl|unk|ENST00000470459_5	6	3	0	0
gnl|unk|ENST00000481413_12	6	3	0	0
gnl|unk|ENST00000481511_8	6	3	0	0
ELOV5_HUMAN	6	5	0	0
G45IP_HUMAN	5	4	0	0
REEP4_HUMAN	6	4	0	0
SFXN2_HUMAN	7	6	0	0
TF3C3_HUMAN	6	5	2	0
VATF_HUMAN	6	4	0	0
VWA8_HUMAN	1	3	6	2
CATIN_HUMAN	0	1	5	5
RT17_HUMAN	0	1	6	6
ADNP_HUMAN	2	3	2	2
BRCC3_HUMAN	0	0	2	2
GID8_HUMAN	0	0	7	6
SDHF2_HUMAN	0	0	6	6
DSC2_HUMAN	1	4	0	0
DSC3_HUMAN	0	0	0	0
ARF6_HUMAN	2	5	0	0
NLTP_HUMAN	0	0	0	5
ATX10_HUMAN	0	0	3	7
GOGB1_HUMAN	3	2	0	0

DNJA3_HUMAN	5	0	0	1
ADA10_HUMAN	2	1	0	0
SYVM_HUMAN	0	0	5	3
TM41A_HUMAN	4	0	0	0
MYADM_HUMAN	4	2	0	0
AG10A_HUMAN	7	3	0	0
AG10B_HUMAN	7	3	0	0
APOH_HUMAN	6	4	0	0
MAP2_HUMAN	0	0	4	8
NECT2_HUMAN	7	2	0	0
DHRS4_HUMAN	0	0	2	6
ARFG1_HUMAN	4	1	1	3
NEUR1_HUMAN	0	0	4	7
ZCCHL_HUMAN	4	2	0	0
SYNE3_HUMAN	3	1	0	0
SPT6H_HUMAN	0	0	2	3
S23A2_HUMAN	2	2	0	0
TSNAX_HUMAN	0	0	4	1
DERL1_HUMAN	0	4	0	0
KYNU_HUMAN	0	0	0	1
HDGR2_HUMAN	0	0	3	2
DNJC7_HUMAN	0	0	3	2
RT14_HUMAN	0	0	5	5
PWP1_HUMAN	0	0	1	1
ARPC4_HUMAN	0	0	1	1
UB2V1_HUMAN	0	0	3	2
ATM_HUMAN	6	5	0	0
APC1_HUMAN	3	3	1	0
KIF4A_HUMAN	4	2	0	0

MARE2_HUMAN	5	2	0	0
MPU1_HUMAN	6	6	0	0
RAP2B_HUMAN	6	6	0	0
RN149_HUMAN	6	5	0	0
TM135_HUMAN	3	3	0	0
UBIA1_HUMAN	5	5	0	0
YIF1B_HUMAN	6	6	0	0
gnl|unk|ENST00000514511_3	3	0	4	5
gnl|unk|ENST00000557933_37	5	3	0	0
RTN3_HUMAN	0	2	0	0
FAD1_HUMAN	0	0	6	6
HTRA2_HUMAN	0	0	5	4
IPYR2_HUMAN	0	0	3	3
NOL9_HUMAN	0	0	6	6
PFD2_HUMAN	0	0	6	6
PRPS3_HUMAN	0	0	4	4
SCOC_HUMAN	0	0	4	4
gnl|unk|ENST00000512749_5	0	0	4	4
TRM1L_HUMAN	0	0	6	6
XPO7_HUMAN	0	0	6	6
CG050_HUMAN	3	4	0	0
IF4H_HUMAN	0	0	3	8
PSME4_HUMAN	0	0	2	6
3MG_HUMAN	5	6	0	0
ENAH_HUMAN	0	0	3	1
COX11_HUMAN	4	4	0	0
B4GA1_HUMAN	4	1	0	0
F169A_HUMAN	6	3	0	0

AP3B1_HUMAN	0	0	3	6
DPOD1_HUMAN	0	0	4	4
ARMC1_HUMAN	0	0	4	6
DDX50_HUMAN	2	0	5	5
DHB7_HUMAN	6	5	0	0
GEPH_HUMAN	0	0	5	5
S100P_HUMAN	0	0	3	8
SC24C_HUMAN	4	6	0	0
CLPX_HUMAN	1	2	2	1
DOPD_HUMAN	0	0	5	2
DHX30_HUMAN	3	0	0	0
CD63_HUMAN	4	2	0	0
STEA3_HUMAN	1	0	0	0
TIM14_HUMAN	1	0	0	0
FCGRN_HUMAN	6	2	0	0
SRPK1_HUMAN	0	0	3	3
SLK_HUMAN	0	0	3	1
MCAT_HUMAN	2	1	0	0
SSFA2_HUMAN	5	4	0	0
PPAC_HUMAN	0	0	0	1
EIF3J_HUMAN	0	0	3	3
IF4G2_HUMAN	1	0	1	2
SPRY7_HUMAN	0	1	0	0
IMA3_HUMAN	0	0	5	2
RIR2_HUMAN	0	0	3	4
CYTC_HUMAN	0	0	4	5
MAP11_HUMAN	0	0	2	0
RN126_HUMAN	1	1	0	0
ANO6_HUMAN	6	5	0	0

ATF2_HUMAN	7	4	0	0
MGAT2_HUMAN	1	5	0	0
PLK1_HUMAN	5	0	0	0
PTTG_HUMAN	2	3	1	3
RING1_HUMAN	6	5	0	0
RING2_HUMAN	6	5	0	0
SCAM1_HUMAN	6	5	0	0
C2AIL_HUMAN	0	2	4	5
CCD12_HUMAN	0	0	6	4
COA7_HUMAN	0	0	5	6
CUL4A_HUMAN	0	0	6	5
NIT2_HUMAN	0	0	5	6
PCTL_HUMAN	0	0	5	6
PPIF_HUMAN	0	0	6	5
RBM10_HUMAN	0	0	5	6
SUOX_HUMAN	0	0	5	4
TIGAR_HUMAN	0	0	5	5
TRUA_HUMAN	0	0	4	4
WASL_HUMAN	3	2	0	2
XPOT_HUMAN	0	0	4	4
YLPM1_HUMAN	0	0	6	3
SEP14_HUMAN	0	0	0	0
SEPT7_HUMAN	0	0	1	1
gnl|unk|ENST00000338231_11	0	0	0	0
gnl|unk|ENST00000428414_16	0	0	0	0
BCAM_HUMAN	3	5	0	0
UBR4_HUMAN	1	0	5	1

MD1L1_HUMAN	4	6	0	0
MBOA5_HUMAN	3	2	0	0
GBF1_HUMAN	0	0	4	4
BCS1_HUMAN	3	2	0	0
EPT1_HUMAN	6	4	0	0
MTND_HUMAN	0	0	0	3
PEX14_HUMAN	5	2	0	0
RIR1_HUMAN	0	0	0	3
UFSP2_HUMAN	0	3	0	0
PISD_HUMAN	3	2	0	0
DNLI1_HUMAN	0	0	4	4
PPCE_HUMAN	0	0	3	4
DDB2_HUMAN	1	0	0	0
NDUB3_HUMAN	2	0	0	0
GLYC_HUMAN	0	0	4	5
TFG_HUMAN	0	0	1	4
PLXB2_HUMAN	5	1	0	0
PSB2_HUMAN	0	0	2	0
XPO5_HUMAN	1	0	4	0
MDN1_HUMAN	0	0	2	1
FMNL2_HUMAN	1	0	0	0
PRC2A_HUMAN	5	0	0	0
LRC8D_HUMAN	0	1	0	0
DRG1_HUMAN	1	1	0	1
LRC8E_HUMAN	5	0	0	0
NDRG1_HUMAN	6	1	0	0
CF089_HUMAN	6	4	0	0
CHD7_HUMAN	6	2	0	0
DIDO1_HUMAN	6	3	0	0

ESAM_HUMAN	4	3	0	0
FRAS1_HUMAN	5	3	0	0
MK03_HUMAN	2	4	7	5
RLP24_HUMAN	6	4	0	0
SELT_HUMAN	3	4	0	0
gnl|unk|ENST00000466234_3	3	4	0	0
SLTM_HUMAN	6	4	0	0
TF3C4_HUMAN	5	4	0	0
TI17A_HUMAN	6	2	0	0
gnl|unk|ENST00000478378_16	6	2	0	0
TM209_HUMAN	6	3	0	0
TM2D2_HUMAN	6	4	0	0
UBP30_HUMAN	6	2	0	0
gnl|unk|ENST00000480219_5	4	2	0	0
NU2M_HUMAN	1	2	0	0
gnl|unk|ENST00000361453_7	1	2	0	0
gnl|unk|ENST00000457540_8	1	2	0	0
ASF1A_HUMAN	0	0	6	4
ATG5_HUMAN	0	0	2	1
CSN5_HUMAN	0	0	6	2
DPH2_HUMAN	0	0	4	6
GCDH_HUMAN	0	0	4	3
GELS_HUMAN	0	0	4	6
GGA2_HUMAN	0	0	4	6
MISSL_HUMAN	0	0	4	6
PAPOB_HUMAN	0	0	4	5
PGP_HUMAN	0	0	5	5
PRC2C_HUMAN	0	0	2	1

RM10_HUMAN	0	0	3	7
RPC5_HUMAN	0	0	6	4
SF3A2_HUMAN	0	0	3	0
SYHC_HUMAN	0	0	3	6
TRI33_HUMAN	0	0	2	2
DC1L1_HUMAN	1	0	0	0
DC1L2_HUMAN	1	0	0	0
CLPT1_HUMAN	1	6	0	0
CRKL_HUMAN	0	0	0	3
TI23B_HUMAN	3	6	0	0
TIM23_HUMAN	3	6	0	0
LRC47_HUMAN	0	0	4	3
GLYR1_HUMAN	3	2	0	0
THOP1_HUMAN	0	0	3	4
TNPO2_HUMAN	0	0	19	24
DJC13_HUMAN	5	0	0	0
ARPC3_HUMAN	0	0	4	4
gnl|unk|ENST00000426440_5	0	0	4	4
gnl|unk|ENST00000547365_3	0	0	4	4
CLCC1_HUMAN	6	1	0	0
HEXA_HUMAN	0	0	4	4
PLCA_HUMAN	4	5	0	0
MRS2_HUMAN	5	4	0	0
LSM7_HUMAN	0	0	1	5
DDX6_HUMAN	4	1	1	0
SNG2_HUMAN	4	3	0	0
CND1_HUMAN	1	1	0	0
BAZ2A_HUMAN	1	2	0	0
TRAM1_HUMAN	1	3	0	0

SPF27_HUMAN	3	3	1	0
NBAS_HUMAN	0	2	0	0
S39A4_HUMAN	0	2	0	0
HACD2_HUMAN	1	3	0	0
RU2A_HUMAN	0	1	1	3
CS025_HUMAN	6	2	0	0
gnl|unk|ENST00000578324_21	0	0	2	2
gnl|unk|ENST00000582050_8	0	0	2	2
gnl|unk|ENST00000582746_14	0	0	2	2
YLAT2_HUMAN	6	2	0	0
DPM3_HUMAN	3	3	0	0
gnl|unk|ENST00000368400_3	3	3	0	0
gnl|unk|ENST00000377524_2	1	0	0	0
ABI1_HUMAN	6	2	0	0
CD151_HUMAN	3	0	0	0
CHSTD_HUMAN	7	1	0	0
COIA1_HUMAN	5	0	0	2
DNLI3_HUMAN	4	1	0	0
ITM2C_HUMAN	6	3	0	0
MTCH1_HUMAN	2	2	0	0
NUP50_HUMAN	1	0	3	5
PPIH_HUMAN	4	1	0	0
PWP2_HUMAN	2	0	5	2
gnl|unk|ENST00000433009_10	4	3	0	0
GL8D1_HUMAN	3	4	0	0
SAHH2_HUMAN	2	2	0	0
DDX20_HUMAN	0	0	3	3

EDF1_HUMAN	0	0	5	4
HDAC6_HUMAN	0	0	5	2
HDHD3_HUMAN	0	0	5	4
HELLS_HUMAN	0	0	2	5
RL22L_HUMAN	0	0	1	1
RWDD1_HUMAN	0	0	3	4
gnl|unk|ENST00000518117_1 1	0	0	3	4
gnl|unk|ENST00000332180_7 0	0	0	4	4
gnl|unk|ENST00000550053_7 1	0	0	4	4
gnl|unk|ENST00000620430_7 1	0	0	4	4
AGRIN_HUMAN	3	4	0	0
TOIP2_HUMAN	2	1	0	0
NKD1_HUMAN	2	4	0	0
TAGL2_HUMAN	0	0	4	1
ACS2B_HUMAN	0	0	3	3
UBP14_HUMAN	0	0	3	1
ALG11_HUMAN	4	3	0	0
BRI3B_HUMAN	6	2	0	0
DLRB1_HUMAN	1	3	0	2
gnl|unk|ENST00000357156_3	1	3	0	2
H1BP3_HUMAN	0	0	3	5
ITB5_HUMAN	4	0	0	0
LSR_HUMAN	1	5	0	0
PRR11_HUMAN	5	2	0	0
RUS1_HUMAN	4	4	0	0
SRBD1_HUMAN	5	2	0	0

CSN4_HUMAN	0	0	5	2
CHP1_HUMAN	4	2	0	0
CISD1_HUMAN	3	3	0	0
gnl|unk|ENST00000489785_8	3	3	0	0
SYFB_HUMAN	0	0	1	4
RBBP9_HUMAN	0	0	4	1
BEND3_HUMAN	3	4	0	0
BZW1_HUMAN	0	1	0	0
SPF45_HUMAN	3	3	0	0
FA8A1_HUMAN	5	1	0	0
ZNT7_HUMAN	3	3	0	0
PCNP_HUMAN	0	0	3	4
ADRM1_HUMAN	0	0	0	1
PTPRK_HUMAN	2	1	0	0
SEC62_HUMAN	1	3	0	0
gnl|unk|ENST00000460513_4	1	3	0	0
gnl|unk|ENST00000487736_9	1	3	0	0
DRS7B_HUMAN	3	4	0	0
SMYD5_HUMAN	0	0	4	0
COPG2_HUMAN	0	0	6	9
MY18A_HUMAN	3	1	0	0
AR6P1_HUMAN	2	0	0	0
ACATN_HUMAN	6	2	0	0
AT2C1_HUMAN	2	4	0	0
CND2_HUMAN	6	2	0	0
GCP2_HUMAN	1	0	0	0
JAK1_HUMAN	4	2	0	0
LAP4A_HUMAN	6	2	0	0
gnl|unk|ENST00000483117_1	6	2	0	0

0				
MP2K3_HUMAN	4	1	0	0
RPB9_HUMAN	5	3	0	0
SLU7_HUMAN	4	4	0	0
TIM16_HUMAN	4	4	0	0
TIM8B_HUMAN	4	4	0	0
UBXN1_HUMAN	1	0	4	3
VPS45_HUMAN	3	4	0	0
WDR55_HUMAN	3	0	0	0
gnl|unk|ENST00000347364_6	1	2	0	0
gnl|unk|ENST00000399054_11	1	2	0	0
gnl|unk|ENST00000609375_11	1	2	0	0
gnl|unk|ENST00000354895_3	4	4	0	0
gnl|unk|ENST00000493646_6	4	1	0	0
PRPF3_HUMAN	1	2	1	0
gnl|unk|ENST00000493553_7	1	2	1	0
RUXF_HUMAN	1	1	0	2
CTDS1_HUMAN	4	4	0	0
CUL1_HUMAN	0	0	2	1
MP2K4_HUMAN	0	0	2	4
NDUF5_HUMAN	0	0	4	4
PAIP1_HUMAN	0	0	0	3
PTMS_HUMAN	0	0	3	1
RRP44_HUMAN	0	0	4	4
GHC1_HUMAN	1	5	0	0
NUP53_HUMAN	0	6	0	0
MCM5_HUMAN	0	2	1	2

ACADS_HUMAN	0	0	1	4
CNNM3_HUMAN	4	2	0	0
MCMBP_HUMAN	0	0	2	3
NRBP_HUMAN	0	0	3	0
SDF2_HUMAN	4	2	0	0
gnl|unk|ENST00000591903_1 1	4	2	0	0
SYMPK_HUMAN	0	0	3	4
SYSM_HUMAN	0	0	0	3
TRRAP_HUMAN	4	1	0	0
CHD1_HUMAN	2	3	0	0
DIAP1_HUMAN	0	0	1	2
ABHDA_HUMAN	0	0	0	1
RPAB1_HUMAN	0	3	0	1
TAF4_HUMAN	0	0	0	2
NXF1_HUMAN	1	3	0	0
COR1B_HUMAN	0	0	1	1
DGLB_HUMAN	1	1	0	0
ABD12_HUMAN	1	1	0	0
EIF3D_HUMAN	0	0	1	1
FTO_HUMAN	0	0	3	0
IMPA3_HUMAN	0	2	0	0
RT30_HUMAN	0	1	1	0
CBPD_HUMAN	2	1	0	0
SP9_HUMAN	0	0	4	0
RSU1_HUMAN	0	1	0	0
S12A2_HUMAN	1	4	0	0
E41L5_HUMAN	0	2	0	0
LIMS1_HUMAN	0	2	0	0

TCRG1_HUMAN	0	0	2	2
EPHB4_HUMAN	6	1	0	0
RRAS2_HUMAN	0	1	0	0
COX15_HUMAN	4	3	0	0
DEGS1_HUMAN	5	1	0	0
EMC3_HUMAN	3	4	0	0
KIF23_HUMAN	4	0	0	0
LACTB_HUMAN	2	0	0	0
NC2B_HUMAN	4	3	0	0
NOC2L_HUMAN	1	0	0	1
P4HA2_HUMAN	2	0	0	0
RBX1_HUMAN	4	2	1	0
gnl|unk|ENST00000476110_6	4	2	1	0
RNF5_HUMAN	3	3	0	0
SAS10_HUMAN	3	0	0	0
SCFD2_HUMAN	6	1	0	0
TAF8_HUMAN	2	3	0	0
TBG1_HUMAN	5	0	0	0
TBG2_HUMAN	5	0	0	0
TTYH3_HUMAN	2	0	0	0
TXD15_HUMAN	2	0	0	0
ZCHC3_HUMAN	2	1	0	0
gnl|unk|ENST00000599243_8	5	0	0	0
AGRG1_HUMAN	0	1	0	0
ERGI1_HUMAN	0	1	0	0
gnl|unk|ENST00000521392_10	0	1	0	0
gnl|unk|ENST00000523650_6	0	1	0	0
GTR8_HUMAN	1	2	0	0

RS30_HUMAN	0	1	0	1
gnl|unk|ENST00000279259_5	0	1	0	1
STX16_HUMAN	0	2	0	0
gnl|unk|ENST00000493301_7	0	2	0	0
TM115_HUMAN	1	4	0	0
AIP_HUMAN	0	0	2	5
CMBL_HUMAN	0	0	1	0
ES8L2_HUMAN	0	0	4	3
NELFB_HUMAN	0	0	3	4
RPB4_HUMAN	0	0	4	3
SYNM_HUMAN	0	0	1	4
WDR3_HUMAN	0	0	2	3
XPP1_HUMAN	0	0	2	4
HN1L_HUMAN	0	0	0	4
gnl|unk|ENST00000568376_3	0	0	0	0
ABCB6_HUMAN	0	4	0	0
MDC1_HUMAN	2	0	0	0
ULA1_HUMAN	0	0	3	1
ADDG_HUMAN	0	4	0	0
AQR_HUMAN	0	0	1	5
CDV3_HUMAN	0	0	1	3
GOLP3_HUMAN	2	4	0	0
PKP4_HUMAN	3	1	0	0
SPS1_HUMAN	0	0	3	2
TAP1_HUMAN	3	0	0	0
VATH_HUMAN	0	1	0	4
ZFR_HUMAN	0	0	5	0
CD032_HUMAN	2	2	0	0
NR3L1_HUMAN	3	2	0	0

GEMI5_HUMAN	0	0	1	1
DMD_HUMAN	2	0	0	0
LIS1_HUMAN	0	0	3	1
PRIO_HUMAN	5	1	0	0
PX11B_HUMAN	1	2	0	0
PPME1_HUMAN	0	0	0	1
SUGP2_HUMAN	0	0	0	1
SYVN1_HUMAN	1	0	0	0
NUBP2_HUMAN	0	0	0	2
RM38_HUMAN	0	0	0	1
ILEU_HUMAN	0	0	3	2
NDUB8_HUMAN	1	2	0	0
CDC27_HUMAN	2	1	0	0
EXOS7_HUMAN	0	0	2	3
DDAH1_HUMAN	0	0	1	2
GPAA1_HUMAN	2	3	0	0
INF2_HUMAN	0	0	2	2
ARC1A_HUMAN	0	0	5	3
ELP1_HUMAN	0	0	1	2
CETN2_HUMAN	0	3	0	0
EMC8_HUMAN	2	3	0	0
gnl|unk|ENST00000435200_9	2	3	0	0
gnl|unk|ENST00000595980_6	2	3	0	0
ENY2_HUMAN	4	2	0	0
gnl|unk|ENST00000518584_5	4	2	0	0
MSH3_HUMAN	1	0	0	0
NOL7_HUMAN	1	5	0	0
SNUT1_HUMAN	1	0	2	2
STX7_HUMAN	4	1	0	0

WBP11_HUMAN	1	1	2	0
YIPF5_HUMAN	3	2	0	0
ERBB2_HUMAN	0	1	0	0
FIP1_HUMAN	3	2	0	0
IDH3B_HUMAN	0	2	0	0
MGST2_HUMAN	1	2	0	0
gnl|unk|ENST00000506797_5	1	2	0	0
gnl|unk|ENST00000515067_3	1	2	0	0
SFXN4_HUMAN	3	2	0	0
SYDM_HUMAN	0	0	0	1
CEBPZ_HUMAN	0	0	0	3
CNOT3_HUMAN	0	0	1	1
F192A_HUMAN	0	0	1	2
FCL_HUMAN	0	0	0	3
GTPB3_HUMAN	0	0	3	3
IDH3G_HUMAN	0	0	2	1
IF1AY_HUMAN	0	0	5	1
KGUA_HUMAN	0	0	1	1
MCTS1_HUMAN	0	0	1	0
NTM1A_HUMAN	0	0	3	2
PDPR_HUMAN	0	0	1	5
PPIL1_HUMAN	0	0	1	2
gnl|unk|ENST00000483552_4	0	0	1	2
RBM4_HUMAN	0	0	5	1
RBPMS_HUMAN	0	0	2	4
RPAC2_HUMAN	0	0	4	0
SMAP_HUMAN	0	0	4	1
SPB8_HUMAN	0	0	1	3
TGT_HUMAN	0	0	4	2

gnl|unk|ENST00000445547_4	0	0	3	1
DNJA2_HUMAN	5	0	0	0
DJC10_HUMAN	2	0	0	0
PEX3_HUMAN	1	3	0	0
KIME_HUMAN	0	0	1	4
TEX10_HUMAN	0	0	3	2
TSN14_HUMAN	3	0	0	0
UBQL2_HUMAN	1	0	2	2
VP26A_HUMAN	0	0	1	4
PLCE_HUMAN	1	4	0	0
ARPC5_HUMAN	0	0	0	4
CTBP1_HUMAN	0	0	1	3
NSF1C_HUMAN	0	0	1	2
NUCKS_HUMAN	0	0	1	2
ABCD1_HUMAN	1	1	0	0
TIM8A_HUMAN	0	0	1	1
NFXL1_HUMAN	1	1	0	0
AURKB_HUMAN	2	0	0	0
GGT2_HUMAN	0	1	0	0
GGT3_HUMAN	0	1	0	0
NT5D1_HUMAN	0	0	2	1
MGME1_HUMAN	0	0	1	1
F120A_HUMAN	0	0	1	2
TMM70_HUMAN	0	2	0	0
RAD50_HUMAN	1	0	0	0
TFCP2_HUMAN	0	1	0	0
SC16A_HUMAN	0	0	0	2
DDX23_HUMAN	0	0	2	0
CDIPT_HUMAN	1	1	0	0

EXOS6_HUMAN	1	0	1	2
GDAP1_HUMAN	1	0	0	0
HM20A_HUMAN	4	1	0	0
K1C23_HUMAN	3	0	0	0
KTAP2_HUMAN	2	2	0	0
gnl|unk|ENST00000463527_6	2	2	0	0
LAT4_HUMAN	3	0	0	0
NIPBL_HUMAN	1	2	0	0
S20A1_HUMAN	3	0	0	0
S35F6_HUMAN	2	3	0	0
SGPP1_HUMAN	3	1	0	0
SMC6_HUMAN	4	1	0	0
T2FA_HUMAN	4	1	0	0
VTNC_HUMAN	2	3	0	0
COR2A_HUMAN	0	2	0	0
gnl|unk|ENST00000370153_118	1	1	0	0
gnl|unk|ENST00000465289_111	1	1	0	0
ADX_HUMAN	0	0	3	2
AFAD_HUMAN	0	0	0	1
CPSM_HUMAN	0	0	1	4
D2HDH_HUMAN	0	0	2	3
EHBP1_HUMAN	0	0	1	2
F1142_HUMAN	0	0	5	0
FETUA_HUMAN	0	0	0	3
FL2D_HUMAN	0	0	2	2
HEAT3_HUMAN	0	0	1	2
KIF2C_HUMAN	0	0	1	4

MT2_HUMAN	0	0	2	3
gnl|unk|ENST00000245185_6	0	0	2	3
gnl|unk|ENST00000561491_4	0	0	2	3
NQO2_HUMAN	0	0	2	0
PGTA_HUMAN	0	0	1	0
PRUNE_HUMAN	0	0	3	2
QTRD1_HUMAN	0	0	2	3
RDH13_HUMAN	0	0	1	4
TWF2_HUMAN	0	0	1	2
UFM1_HUMAN	0	0	0	2
gnl|unk|ENST00000239878_5	0	0	0	2
MIPEP_HUMAN	0	0	0	2
NICA_HUMAN	0	2	0	0
VPP2_HUMAN	2	1	0	0
SPS2_HUMAN	0	0	1	2
MA2B1_HUMAN	0	0	2	1
EI2BD_HUMAN	0	0	3	1
KNOP1_HUMAN	0	3	0	0
EHMT2_HUMAN	1	2	1	0
SMCE1_HUMAN	0	2	0	0
IL6RB_HUMAN	2	0	0	0
RM43_HUMAN	0	0	1	0
F136A_HUMAN	1	0	1	0
S35E1_HUMAN	1	1	0	0
RN213_HUMAN	0	0	1	0
SARNP_HUMAN	0	0	0	1
XYLB_HUMAN	0	0	0	2
DDX54_HUMAN	1	1	0	0
SPTC2_HUMAN	1	0	0	0

TM165_HUMAN	1	1	0	0
GSTA3_HUMAN	0	0	0	2
ANKH1_HUMAN	0	0	1	0
STX4_HUMAN	0	1	0	0
GHITM_HUMAN	0	2	0	0
STRN3_HUMAN	0	0	0	1
RPE_HUMAN	0	0	0	2
GALT1_HUMAN	1	0	0	0
NLRX1_HUMAN	2	1	0	0
SF3B5_HUMAN	0	0	0	1
gnl|unk|ENST00000367569_6	0	0	0	1
B2MG_HUMAN	0	2	0	0
PROX1_HUMAN	1	1	0	0
XPP3_HUMAN	0	0	2	2
CDCA3_HUMAN	1	3	0	0
CNIH1_HUMAN	3	1	0	0
CSMT1_HUMAN	3	1	0	0
DDX52_HUMAN	3	0	1	0
FXR1_HUMAN	3	0	0	0
HEMH_HUMAN	2	1	0	0
HNRLL_HUMAN	2	0	0	0
LITAF_HUMAN	4	0	0	0
MA1A2_HUMAN	1	0	0	0
MLF2_HUMAN	2	2	0	0
NFIP1_HUMAN	2	2	0	0
gnl|unk|ENST00000509436_2	2	2	0	0
NID1_HUMAN	3	1	0	0
PALM_HUMAN	4	0	0	0
PLPP6_HUMAN	2	2	0	0

RM54_HUMAN	2	0	1	1
SAMC_HUMAN	4	0	0	0
SURF1_HUMAN	2	2	0	0
T10B_HUMAN	2	0	0	0
gnl|unk|ENST00000530751_2	2	0	0	0
TCF20_HUMAN	2	0	0	0
TR112_HUMAN	1	1	0	0
UQCC2_HUMAN	2	2	0	0
gnl|unk|ENST00000374231_3	2	2	0	0
VATD_HUMAN	1	0	0	0
ZO1_HUMAN	1	0	0	0
CLUS_HUMAN	0	2	1	1
gnl|unk|ENST00000622242_5	0	1	1	1
OSTB_HUMAN	1	3	0	0
CBPE_HUMAN	0	0	0	1
DIP2B_HUMAN	0	0	2	2
DUT_HUMAN	0	0	2	0
EIF2A_HUMAN	0	0	2	2
GPX2_HUMAN	0	0	0	4
GYS1_HUMAN	0	0	2	0
HEXI1_HUMAN	0	0	1	2
KPCA_HUMAN	0	0	3	0
MISP_HUMAN	0	0	0	2
MRT4_HUMAN	0	0	0	2
NOL11_HUMAN	0	0	2	1
OGFD1_HUMAN	0	0	3	0
P3H3_HUMAN	0	0	1	3
RFC4_HUMAN	0	0	0	1
SZRD1_HUMAN	0	0	1	2

UBC9_HUMAN	0	0	1	0
UFD1_HUMAN	0	0	2	1
gnl|unk|ENST00000495554_46	0	0	0	1
gnl|unk|ENST00000612404_5	0	0	0	2
VASP_HUMAN	0	0	1	0
PDCD6_HUMAN	0	0	0	2
EPHA2_HUMAN	3	0	0	0
PURA2_HUMAN	0	0	1	2
RM23_HUMAN	0	1	0	2
SVIL_HUMAN	3	0	0	0
CAF1A_HUMAN	2	0	0	0
RAB23_HUMAN	2	0	0	0
UBAC2_HUMAN	0	2	0	0
PKP3_HUMAN	0	1	0	0
HD_HUMAN	0	0	1	1
ATLA2_HUMAN	1	1	0	0
BLMH_HUMAN	0	0	1	0
MIA2_HUMAN	0	2	0	0
HPBP1_HUMAN	0	0	1	0
RBM12_HUMAN	0	0	0	1
OSTF1_HUMAN	0	0	2	0
ZN638_HUMAN	0	2	0	0
CDC20_HUMAN	2	0	0	0
RHG18_HUMAN	0	0	0	2
UDB10_HUMAN	2	1	0	0
MPRIP_HUMAN	0	1	0	0
SYCC_HUMAN	0	0	1	0
TBCD_HUMAN	0	0	0	1

S12A7_HUMAN	1	0	0	0
PB1_HUMAN	0	2	0	0
PHF5A_HUMAN	0	0	1	0
DDX41_HUMAN	1	0	0	0
LGMN_HUMAN	0	0	1	1
NPC1_HUMAN	0	1	0	0
ACOX3_HUMAN	3	0	0	0
COBL_HUMAN	1	0	0	0
CR3L2_HUMAN	1	2	0	0
CWC22_HUMAN	2	0	0	0
FA83D_HUMAN	2	1	0	0
KIF22_HUMAN	1	0	0	0
MBD1_HUMAN	2	1	0	0
MTA1_HUMAN	1	2	0	0
NSUN5_HUMAN	1	1	0	0
NUP37_HUMAN	2	1	0	0
OSBL9_HUMAN	1	0	0	0
PINX1_HUMAN	1	2	0	0
RBBP5_HUMAN	1	2	0	0
RHOF_HUMAN	1	1	0	0
RINT1_HUMAN	1	0	0	0
S26A6_HUMAN	1	2	0	0
SATT_HUMAN	2	0	0	0
TBP_HUMAN	2	1	0	0
TMTC3_HUMAN	2	0	0	0
APOC3_HUMAN	0	2	0	0
gnl|unk|ENST00000470144_2	0	2	0	0
COIL_HUMAN	0	2	0	0
CTNA2_HUMAN	0	3	0	0

CWC27_HUMAN	0	1	1	1
FA83H_HUMAN	1	1	0	0
MICB_HUMAN	0	3	0	0
ODB2_HUMAN	0	2	0	0
PEMT_HUMAN	0	1	0	0
SC24D_HUMAN	0	1	1	0
SCAF8_HUMAN	0	1	2	0
TAP26_HUMAN	1	2	0	0
UBQL4_HUMAN	0	1	0	0
AASS_HUMAN	0	0	0	2
API5_HUMAN	0	0	1	2
CAH13_HUMAN	0	0	2	1
CIP4_HUMAN	0	0	2	1
COG8_HUMAN	0	0	2	1
CS043_HUMAN	0	0	1	2
DFFA_HUMAN	0	0	1	2
GSCR2_HUMAN	0	0	1	0
HNMT_HUMAN	0	0	0	2
HYES_HUMAN	0	0	1	2
IPO11_HUMAN	0	0	1	1
JMJD6_HUMAN	0	0	1	2
LSM1_HUMAN	0	0	0	1
MCES_HUMAN	0	0	1	1
NIPA_HUMAN	0	0	1	0
PAXB1_HUMAN	0	0	0	3
PLPP_HUMAN	0	0	1	2
RT25_HUMAN	0	0	0	3
gnl|unk|ENST00000444840_5	0	0	0	3
gnl|unk|ENST00000447299_8	0	0	0	3

RUSD2_HUMAN	0	0	1	0
S10AB_HUMAN	0	0	3	0
SMC4_HUMAN	0	0	1	2
TAGL_HUMAN	0	0	0	2
TX1B3_HUMAN	0	0	1	1
ZC3H4_HUMAN	1	0	1	0
TM177_HUMAN	0	1	0	0
RT26_HUMAN	0	0	0	2
SF3B4_HUMAN	0	0	1	0
DYL2_HUMAN	11	11	0	0
UBP15_HUMAN	0	0	0	1
INT3_HUMAN	1	0	0	0
ROCK2_HUMAN	0	0	1	0
PKCB1_HUMAN	0	1	0	0
ORC2_HUMAN	1	0	0	0
PACN2_HUMAN	0	0	1	0
NFU1_HUMAN	0	0	0	1
TAF5_HUMAN	1	0	0	0
CPLX2_HUMAN	0	0	0	1
LARP1_HUMAN	1	0	0	0
LRRF1_HUMAN	0	0	0	1
B4GT1_HUMAN	1	1	0	0
CLN6_HUMAN	2	0	0	0
FER_HUMAN	1	1	0	0
FRIH_HUMAN	1	0	0	0
MPZL1_HUMAN	1	1	0	0
NIPA1_HUMAN	1	1	0	0
OSBL2_HUMAN	1	1	0	0
PLCB_HUMAN	2	0	0	0

PON3_HUMAN	1	1	0	0
RAB6C_HUMAN	1	1	0	0
REEP3_HUMAN	2	0	0	0
SFR19_HUMAN	1	1	0	0
SKT_HUMAN	1	0	0	0
SUZ12_HUMAN	1	0	0	0
TAP2_HUMAN	1	1	0	0
TP53B_HUMAN	1	0	0	0
UTP20_HUMAN	2	0	0	0
EXOC4_HUMAN	0	1	0	0
BAK_HUMAN	0	1	0	0
CASP_HUMAN	0	2	0	0
CHCH1_HUMAN	0	2	0	0
CHD1L_HUMAN	0	1	0	0
ERG24_HUMAN	0	2	0	0
FKBP8_HUMAN	0	2	0	0
GOGA5_HUMAN	0	1	0	0
HIG2A_HUMAN	0	1	0	0
HMDH_HUMAN	0	1	0	0
HSF1_HUMAN	0	1	0	0
MLX_HUMAN	0	1	0	0
NTH_HUMAN	0	2	0	0
PRAF1_HUMAN	0	1	0	0
SFT2C_HUMAN	0	1	0	0
STX12_HUMAN	1	1	0	0
TM109_HUMAN	0	2	0	0
TX264_HUMAN	0	2	0	0
RT35_HUMAN	1	0	0	0
MTFP1_HUMAN	1	0	0	0

AKA12_HUMAN	0	0	0	1
AMRA1_HUMAN	0	0	1	0
ATG4B_HUMAN	0	0	1	0
gnl|unk|ENST00000400772_3	0	0	1	0
gnl|unk|ENST00000415107_1	0	0	1	0
gnl|unk|ENST00000468018_5	0	0	1	0
gnl|unk|ENST00000479554_2	0	0	1	0
gnl|unk|ENST00000482507_3	0	0	1	0
gnl|unk|ENST00000494465_4	0	0	1	0
gnl|unk|ENST00000625810_5	0	0	1	0
CHCH2_HUMAN	0	0	0	2
CHCH9_HUMAN	0	0	0	2
COA6_HUMAN	0	0	0	1
CRYL1_HUMAN	0	0	0	1
CSTF2_HUMAN	0	0	2	0
DAXX_HUMAN	0	0	0	1
DDX10_HUMAN	0	0	2	0
DEOC_HUMAN	0	0	1	1
DYR_HUMAN	0	0	0	1
EXOS2_HUMAN	0	0	0	1
EXOS9_HUMAN	0	0	1	1
FBX22_HUMAN	0	0	1	1
FNTB_HUMAN	0	0	2	0
GET4_HUMAN	0	0	1	1
GSH0_HUMAN	0	0	1	1
GSH1_HUMAN	0	0	0	1
HEBP1_HUMAN	1	0	1	0
I2BP1_HUMAN	0	0	1	1
NHP2_HUMAN	0	0	2	0

OXSR1_HUMAN	0	0	1	0
PFD6_HUMAN	0	0	1	0
PHP14_HUMAN	0	0	1	0
PPM1F_HUMAN	0	0	0	1
PYRG2_HUMAN	0	0	1	1
RBM28_HUMAN	0	0	0	1
RT63_HUMAN	0	0	0	1
RYDEN_HUMAN	0	0	2	0
gnl|unk|ENST00000590378_6	0	0	2	0
SAP3_HUMAN	0	0	1	0
SHLB1_HUMAN	0	0	0	2
SNX1_HUMAN	0	0	0	2
SSA27_HUMAN	0	0	1	0
TRMB_HUMAN	0	0	1	1
U3IP2_HUMAN	0	0	1	1
WDR61_HUMAN	0	0	1	1
gnl|unk|ENST00000428512_3	0	0	0	2
gnl|unk|ENST00000492223_1	0	0	2	0
VRK3_HUMAN	1	0	0	0
K1C13_HUMAN	163	128	0	0
K1C9_HUMAN	1	0	0	0
B2CL1_HUMAN	1	0	0	0
DNJA4_HUMAN	1	0	0	0
GPC5C_HUMAN	1	0	0	0
HINT3_HUMAN	1	0	0	0
INT1_HUMAN	1	0	0	0
ITM2B_HUMAN	1	0	0	0
JAG1_HUMAN	1	0	0	0
LPP_HUMAN	1	0	0	0

NOP10_HUMAN	1	0	0	0
gnl|unk|ENST00000328848_6	1	0	0	0
P2RX4_HUMAN	1	0	0	0
RHDF2_HUMAN	1	0	0	0
RSF1_HUMAN	1	0	0	0
SELS_HUMAN	1	0	0	0
SP3_HUMAN	1	0	0	0
STF1_HUMAN	1	0	0	0
TM45B_HUMAN	1	0	0	0
TM55B_HUMAN	1	0	0	0
UBXN6_HUMAN	1	0	0	0
ZNRF1_HUMAN	1	0	0	0
EPN4_HUMAN	1	0	0	0
KDIS_HUMAN	1	0	0	0
CLAP2_HUMAN	0	1	0	0
CTL1_HUMAN	0	1	0	0
gnl|unk|ENST00000607692_11	0	1	0	0
DECR2_HUMAN	0	1	0	0
ERAL1_HUMAN	0	1	0	0
MEN1_HUMAN	0	1	0	0
MPRA_HUMAN	0	1	0	0
NEUA_HUMAN	0	1	0	0
P66A_HUMAN	0	1	0	0
PEX13_HUMAN	0	1	0	0
PTSS2_HUMAN	0	1	0	0
RBM26_HUMAN	0	1	0	0
RHG17_HUMAN	0	1	0	0
S27A4_HUMAN	0	1	0	0

S4A7_HUMAN	0	1	0	0
SERC1_HUMAN	0	1	0	0
SMI20_HUMAN	0	1	0	0
gnl|unk|ENST00000506197_3	0	1	0	0
TERF2_HUMAN	0	1	0	0
TFDP1_HUMAN	0	1	0	0
TMUB1_HUMAN	0	1	0	0
TRPV2_HUMAN	0	1	0	0
TYW1B_HUMAN	0	1	0	0
ZN593_HUMAN	0	1	0	0
ZN687_HUMAN	0	1	0	0
ZN740_HUMAN	0	1	0	0
gnl|unk|ENST00000552429_8	0	1	0	0
CPSF1_HUMAN	1	0	0	0
ARL3_HUMAN	0	0	0	1
AROS_HUMAN	0	0	0	1
gnl|unk|ENST00000420879_1	0	0	0	1
BPNT1_HUMAN	0	0	0	1
BZW2_HUMAN	0	0	0	1
CCD97_HUMAN	0	0	1	0
CI114_HUMAN	0	0	0	1
CIAO1_HUMAN	0	0	1	0
gnl|unk|ENST00000272402_3 1	0	0	1	0
CLPP_HUMAN	0	0	0	1
COX17_HUMAN	0	0	0	1
DLG1_HUMAN	0	0	0	1
DPY30_HUMAN	0	0	1	0
gnl|unk|ENST00000295066_9	0	0	1	0

gnl|unk|ENST00000342166_6	0	0	1	0
GAK_HUMAN	0	0	1	0
GCP60_HUMAN	0	0	0	1
GLO2_HUMAN	0	0	0	1
HAP28_HUMAN	0	0	0	1
HDHD2_HUMAN	0	0	0	1
JIP4_HUMAN	0	0	1	0
KAP1_HUMAN	0	0	0	1
KAT3_HUMAN	0	0	1	0
KCC2D_HUMAN	0	0	1	0
KPRB_HUMAN	0	0	1	0
MT1E_HUMAN	0	0	0	1
NELFD_HUMAN	0	0	0	1
PARN_HUMAN	0	0	0	1
PDCD4_HUMAN	0	0	0	1
PDE12_HUMAN	0	0	1	0
PP1R7_HUMAN	0	0	0	1
RM28_HUMAN	0	0	0	1
RT21_HUMAN	0	0	0	1
gnl|unk|ENST00000581066_7	0	0	0	1
gnl|unk|ENST00000614145_7	0	0	0	1
SSF1_HUMAN	0	0	0	1
SURF6_HUMAN	0	0	1	0
SYAM_HUMAN	0	0	1	0
SYF2_HUMAN	0	0	0	1
SYRM_HUMAN	0	0	0	1
TIPRL_HUMAN	0	0	0	1
TTC27_HUMAN	0	0	0	1
TWF1_HUMAN	0	0	1	0

UBA3_HUMAN	0	0	1	0
UBA5_HUMAN	0	0	1	0
gnl|unk|ENST00000494112_14	0	0	1	0
UBP2L_HUMAN	0	0	0	1
UBP4_HUMAN	0	0	0	1
UFC1_HUMAN	0	0	1	0
gnl|unk|ENST00000527153_6	0	0	1	0
ENTP5_HUMAN	0	0	0	1

Table 3. All proteins identified in HepG2 experiment.

Protein accession numbers	Protein identification probability	Total spectrum count
SC61G_HUMAN	95.00%	16
ELAV1_HUMAN	100.00%	5
DPB1_HUMAN	100.00%	65
ERF1_HUMAN	100.00%	16
HS71A_HUMAN,HS71B_HUMAN	100.00%	449
GNAI3_HUMAN	100.00%	245
PRS4_HUMAN	100.00%	8
CKLF6_HUMAN	98.90%	8
HNRPC_HUMAN	100.00%	46
POL_HV1C4	100.00%	3535
POL_HV1B9	100.00%	3037
POL_HV1AN	100.00%	715
WDR26_HUMAN	99.90%	2
RB22A_HUMAN	100.00%	22
RAB1B_HUMAN	100.00%	150
RL8_HUMAN	100.00%	140
POL_HV1A2	100.00%	4156
CPNS1_HUMAN	100.00%	8
SUCA_HUMAN	100.00%	3
THTM_HUMAN	99.10%	3
DDRGK_HUMAN	95.00%	1
GBB4_HUMAN	100.00%	114
OLA1_HUMAN	99.90%	11
G6PI_HUMAN	100.00%	266
PRS8_HUMAN	100.00%	14
ABHEB_HUMAN	100.00%	2
VTA1_HUMAN	100.00%	41
POL_HV19N	99.60%	794
CCNB2_HUMAN	98.10%	2
POL_HV196	100.00%	1459
POL_HV193	100.00%	1188
POL_HV192	100.00%	685
EIF3H_HUMAN	100.00%	8
VP26A_HUMAN	100.00%	8
DDAH2_HUMAN	100.00%	4
P5CR1_HUMAN	100.00%	28
ELMO1_HUMAN	100.00%	21
KCAB2_HUMAN	100.00%	41
EFHD2_HUMAN	100.00%	3
SYYC_HUMAN	100.00%	96

TCPD_HUMAN	100.00%	236
QCR1_HUMAN	100.00%	95
UMPS_HUMAN	100.00%	10
4F2_HUMAN	100.00%	525
RS2_HUMAN	100.00%	220
SMC2_HUMAN	99.90%	1
SNAA_HUMAN	100.00%	157
MANF_HUMAN	95.00%	5
CYBP_HUMAN	100.00%	121
IGSF8_HUMAN	100.00%	3
PSA6_HUMAN	100.00%	21
LETM1_HUMAN	100.00%	21
CBR1_HUMAN	100.00%	49
ARPC4_HUMAN	100.00%	41
STK4_HUMAN	99.90%	1
RL36A_HUMAN	100.00%	16
DHCR7_HUMAN	100.00%	12
ABRAL_HUMAN	99.10%	23
DIP2B_HUMAN	100.00%	23
EIF3B_HUMAN	100.00%	24
SFXN1_HUMAN	100.00%	22
ASNS_HUMAN	100.00%	62
COMD3_HUMAN	95.00%	2
PFKAP_HUMAN	100.00%	169
HCD2_HUMAN	100.00%	183
TB10B_HUMAN	95.00%	9
PSD12_HUMAN	100.00%	13
YBOX3_HUMAN	100.00%	69
NDUAA_HUMAN	100.00%	1
ARHG6_HUMAN	95.00%	3
PHB2_HUMAN	100.00%	237
IMB1_HUMAN	100.00%	141
PE2R4_HUMAN	95.00%	4
TEBP_HUMAN	100.00%	31
TMED9_HUMAN	100.00%	11
PPAC_HUMAN	95.00%	3
SSBP_HUMAN	100.00%	25
MTFP1_HUMAN	99.80%	3
TIM14_HUMAN	100.00%	5
SYIM_HUMAN	100.00%	2
CPZIP_HUMAN	100.00%	28
CD37_HUMAN	100.00%	4
TXTP_HUMAN	100.00%	21

AIMP2_HUMAN	95.00%	14
PURA_HUMAN	95.00%	8
SMD1_HUMAN	100.00%	19
H2AV_HUMAN,H2AZ_HUMAN	99.80%	34
NAA50_HUMAN	99.90%	2
RL13A_HUMAN	100.00%	104
RAP2B_HUMAN	100.00%	17
IMA5_HUMAN	97.40%	5
MYO1F_HUMAN	100.00%	18
NIBAN_HUMAN	100.00%	64
MMAB_HUMAN	95.00%	1
PLS1_HUMAN	100.00%	22
PGM1_HUMAN	100.00%	10
SPCS1_HUMAN	95.00%	3
RS13_HUMAN	100.00%	173
PDCD4_HUMAN	100.00%	9
SYFA_HUMAN	100.00%	15
SC61B_HUMAN	95.00%	9
ANTR2_HUMAN	95.00%	2
PPIB_HUMAN	100.00%	122
ACTZ_HUMAN	100.00%	8
HNRPU_HUMAN	100.00%	11
SATT_HUMAN	100.00%	144
ANO6_HUMAN	100.00%	6
ITIH2_HUMAN	100.00%	11
ANXA6_HUMAN	100.00%	635
TXNL1_HUMAN	99.90%	5
HBS1L_HUMAN	95.00%	7
SYQ_HUMAN	100.00%	51
PPP5_HUMAN	100.00%	10
AKAP5_HUMAN	99.90%	7
MCM5_HUMAN	100.00%	13
TMCO1_HUMAN	95.00%	4
RL3_HUMAN	100.00%	257
GCN1_HUMAN	100.00%	15
ODP2_HUMAN	100.00%	13
RALA_HUMAN	100.00%	71
STXB2_HUMAN	100.00%	169
JAK1_HUMAN	100.00%	11
PRS6A_HUMAN	100.00%	11
RHG04_HUMAN	100.00%	13
DEN2D_HUMAN	95.00%	5
XPO5_HUMAN	97.10%	1

G6PD_HUMAN	100.00%	21
CGL_HUMAN	100.00%	64
CPIN1_HUMAN	95.00%	1
VAV_HUMAN	100.00%	2
ENOA_HUMAN	100.00%	1748
DYH6_HUMAN	99.70%	2
GBG2_HUMAN	100.00%	13
ARPC5_HUMAN	100.00%	34
41_HUMAN	100.00%	52
CO3_HUMAN	100.00%	17
EIF3C_HUMAN,EIFCL_HUMAN	100.00%	23
EZRI_HUMAN	100.00%	1035
IF4H_HUMAN	100.00%	21
CN166_HUMAN	99.90%	14
RL36_HUMAN	100.00%	71
SYK_HUMAN	100.00%	15
HMHA1_HUMAN	100.00%	3
SND1_HUMAN	100.00%	81
WASP_HUMAN	100.00%	61
PSD13_HUMAN	100.00%	46
GALM_HUMAN	95.00%	1
SYLC_HUMAN	100.00%	9
PIMT_HUMAN	100.00%	75
RL23A_HUMAN	100.00%	40
MOT1_HUMAN	100.00%	106
PP1G_HUMAN	100.00%	59
PLXA1_HUMAN	100.00%	4
SCAM2_HUMAN	95.00%	8
NUP37_HUMAN	95.00%	1
ACBP_HUMAN	100.00%	2
CPNE3_HUMAN	100.00%	20
RL7A_HUMAN	100.00%	240
AN32E_HUMAN	100.00%	6
PSA1_HUMAN	100.00%	42
GBB2_HUMAN	100.00%	261
C1TC_HUMAN	100.00%	223
SYNC_HUMAN	100.00%	90
ITA3_HUMAN	100.00%	2
RAB5B_HUMAN	100.00%	50
PNPH_HUMAN	100.00%	66
MYO1G_HUMAN	100.00%	956
SC22B_HUMAN	100.00%	6
DNJA1_HUMAN	100.00%	22

CAPG_HUMAN	100.00%	36
MRP1_HUMAN	100.00%	91
VATA_HUMAN	100.00%	13
TBB4B_HUMAN	100.00%	1449
SPCS2_HUMAN	95.00%	3
GIT1_HUMAN	99.20%	6
COR1A_HUMAN	100.00%	443
UBC12_HUMAN	95.00%	2
ATPD_HUMAN	100.00%	29
RL28_HUMAN	100.00%	60
RLA0_HUMAN	100.00%	160
ARHG1_HUMAN	100.00%	21
CCD47_HUMAN	95.00%	2
RS24_HUMAN	100.00%	62
ARF3_HUMAN	100.00%	256
ACTN1_HUMAN	100.00%	171
DD19A_HUMAN	100.00%	7
NDRG3_HUMAN	97.90%	10
ANXA7_HUMAN	100.00%	118
BAG2_HUMAN	100.00%	22
S38A5_HUMAN	100.00%	15
IF16_HUMAN	100.00%	5
TCP4_HUMAN	100.00%	4
UTRO_HUMAN	100.00%	16
RUXF_HUMAN	100.00%	6
DEST_HUMAN	95.00%	2
TTL12_HUMAN	95.00%	7
LDHB_HUMAN	100.00%	186
S10AA_HUMAN	100.00%	67
SAR1B_HUMAN	99.90%	9
PRS6B_HUMAN	100.00%	10
THIO_HUMAN	100.00%	47
ITB2_HUMAN	100.00%	276
SUCB2_HUMAN	100.00%	12
LIMA1_HUMAN	97.90%	10
TP4A1_HUMAN	100.00%	13
PICAL_HUMAN	100.00%	6
DDX3X_HUMAN	100.00%	58
SSRA_HUMAN	100.00%	38
ACTBL_HUMAN	100.00%	298
FLVC1_HUMAN	100.00%	6
EXOC8_HUMAN	95.00%	4
STA5B_HUMAN	95.00%	6

HBB_HUMAN	100.00%	85
DLG1_HUMAN	100.00%	8
LRC57_HUMAN	98.90%	1
DYH7_HUMAN	98.90%	1
DHSO_HUMAN	99.90%	5
UBP5_HUMAN	100.00%	6
IF5_HUMAN	100.00%	13
H31T_HUMAN,H31_HUMAN,H32_HUMAN, H33_HUMAN,gnl|unk|TRINITY_DN363_c1_ g1_i1_4	99.90%	17
GSTK1_HUMAN	100.00%	33
GTR1_HUMAN	100.00%	75
UGGG1_HUMAN	100.00%	8
IST1_HUMAN	99.50%	1
RSMN_HUMAN	99.80%	4
VINC_HUMAN	100.00%	177
TAOK3_HUMAN	100.00%	15
IDHP_HUMAN	100.00%	162
RELL1_HUMAN	95.00%	7
TERA_HUMAN	100.00%	284
HPRT_HUMAN	100.00%	95
ITA4_HUMAN	100.00%	227
BAF_HUMAN	100.00%	36
SEC63_HUMAN	100.00%	2
IF2B3_HUMAN	100.00%	153
THOC4_HUMAN	95.00%	1
H2A2C_HUMAN	100.00%	228
RL31_HUMAN	100.00%	32
PSMD9_HUMAN	95.00%	1
TCPQ_HUMAN	100.00%	424
NSF_HUMAN	100.00%	20
VPS28_HUMAN	100.00%	55
CNO10_HUMAN	95.00%	4
NEB2_HUMAN	100.00%	8
PRAF3_HUMAN	100.00%	2
OPA1_HUMAN	100.00%	34
RS26_HUMAN	100.00%	143
POL_HV1OY	100.00%	4642
TCPG_HUMAN	100.00%	371
PP1B_HUMAN	100.00%	58
ARHG2_HUMAN	99.90%	1
DAZP1_HUMAN	95.00%	1
FMNL1_HUMAN	100.00%	114

LTV1_HUMAN	99.10%	5
BLMH_HUMAN	100.00%	34
LRCH4_HUMAN	100.00%	2
1C03_HUMAN	100.00%	312
ARC1B_HUMAN	100.00%	92
RUXGL_HUMAN,RUXG_HUMAN	95.00%	8
PAK2_HUMAN	100.00%	58
TNIP2_HUMAN	100.00%	16
AT1B3_HUMAN	100.00%	134
VIME_HUMAN	100.00%	669
HM13_HUMAN	99.90%	7
AIP_HUMAN	100.00%	14
LCK_HUMAN	100.00%	138
IPO5_HUMAN	100.00%	31
COX6C_HUMAN	100.00%	2
CISD1_HUMAN	100.00%	87
IMDH2_HUMAN	100.00%	94
PPIH_HUMAN	100.00%	8
HINT3_HUMAN	95.00%	9
RANG_HUMAN	100.00%	70
CAZA2_HUMAN	100.00%	50
1433E_HUMAN	100.00%	334
RL23_HUMAN	100.00%	98
DDX5_HUMAN	100.00%	137
CD3D_HUMAN	100.00%	18
NDUA7_HUMAN	99.90%	4
HDAC1_HUMAN	95.00%	3
NP1L4_HUMAN	99.50%	52
SHIP1_HUMAN	100.00%	2
ZAP70_HUMAN	100.00%	52
HNRPQ_HUMAN	100.00%	137
RAB21_HUMAN	100.00%	28
ENPL_HUMAN	100.00%	581
RS18_HUMAN	100.00%	94
SYIC_HUMAN	100.00%	102
RS11_HUMAN	100.00%	63
ERAP1_HUMAN	100.00%	22
UBXN1_HUMAN	100.00%	4
TFAM_HUMAN	100.00%	52
NEUR3_HUMAN	95.00%	1
CKAP5_HUMAN	100.00%	9
HNRDL_HUMAN	99.90%	22
CALU_HUMAN	95.00%	8

OTUB1_HUMAN	100.00%	7
CSK2B_HUMAN	100.00%	10
COMT_HUMAN	100.00%	4
TPIS_HUMAN	100.00%	339
DNJC5_HUMAN	100.00%	5
SYWC_HUMAN	100.00%	95
ITAL_HUMAN	100.00%	331
PLEK_HUMAN	100.00%	44
TNPO1_HUMAN	100.00%	7
XPO1_HUMAN	100.00%	15
UB2L6_HUMAN	100.00%	3
NDUB8_HUMAN	95.00%	2
ATD3A_HUMAN	100.00%	58
ERBIN_HUMAN	95.00%	5
PSME2_HUMAN	100.00%	24
RHOC_HUMAN	100.00%	250
CD5_HUMAN	100.00%	311
HNRPK_HUMAN	100.00%	91
FEN1_HUMAN	100.00%	9
AT5F1_HUMAN	100.00%	55
SEPT6_HUMAN	100.00%	67
EXOC3_HUMAN	99.90%	2
SYG_HUMAN	100.00%	114
VPS29_HUMAN	100.00%	13
IF2G_HUMAN	100.00%	26
RL15_HUMAN	100.00%	106
CCD51_HUMAN	95.00%	3
SASH3_HUMAN	100.00%	27
RS27_HUMAN	100.00%	35
ADAS_HUMAN	100.00%	16
NDUV1_HUMAN	100.00%	4
S43A3_HUMAN	99.80%	2
KIRR2_HUMAN	95.00%	5
RAB8A_HUMAN	100.00%	226
TOP2A_HUMAN	96.10%	2
IF2P_HUMAN	100.00%	13
RB27A_HUMAN	100.00%	86
SEPT2_HUMAN	100.00%	67
TBA1C_HUMAN	100.00%	917
EFGM_HUMAN	98.90%	1
PDIA3_HUMAN	100.00%	253
ADT2_HUMAN	100.00%	220
SGT1_HUMAN	100.00%	6

IQGA1_HUMAN	100.00%	627
RAGP1_HUMAN	100.00%	5
FLII_HUMAN	100.00%	3
STX11_HUMAN	100.00%	79
DPP3_HUMAN	95.00%	12
PSMF1_HUMAN	95.00%	10
GELS_HUMAN	100.00%	11
CSK_HUMAN	100.00%	110
PSB6_HUMAN	100.00%	13
PGK1_HUMAN	100.00%	806
RS21_HUMAN	100.00%	43
PSB4_HUMAN	100.00%	19
PI4KA_HUMAN	100.00%	3
NDUA8_HUMAN	95.00%	2
RASK_HUMAN	99.90%	86
GRPE1_HUMAN	100.00%	12
TIAR_HUMAN	100.00%	6
E41L5_HUMAN	100.00%	8
RS19_HUMAN	100.00%	97
S38A1_HUMAN	100.00%	21
PA1B3_HUMAN	100.00%	44
DNJB1_HUMAN	98.60%	1
UB2D2_HUMAN,UB2D3_HUMAN	100.00%	16
TIM50_HUMAN	95.00%	5
GHITM_HUMAN	95.00%	2
FPPS_HUMAN	100.00%	8
APMAP_HUMAN	100.00%	4
GSTO1_HUMAN	100.00%	47
SAHH_HUMAN	100.00%	116
E2AK2_HUMAN	100.00%	2
ECI2_HUMAN	100.00%	6
RBBP4_HUMAN	95.00%	2
CD47_HUMAN	100.00%	68
F10A1_HUMAN	100.00%	104
SAMN1_HUMAN	95.00%	1
TMEDA_HUMAN	100.00%	40
PSME3_HUMAN	95.00%	2
PHB_HUMAN	100.00%	204
GFPT1_HUMAN	100.00%	19
CHSP1_HUMAN	100.00%	24
ALBU_HUMAN	100.00%	56
NDUA2_HUMAN	95.00%	1
CD6_HUMAN	100.00%	288

COPD_HUMAN	99.80%	1
HNRPL_HUMAN	100.00%	32
ARRB2_HUMAN	98.70%	2
2AAA_HUMAN	100.00%	32
SEPT7_HUMAN	100.00%	91
RS30_HUMAN	95.00%	12
BIN1_HUMAN	95.00%	1
RFTN1_HUMAN	100.00%	111
C1TM_HUMAN	100.00%	3
RN149_HUMAN	95.00%	5
NIPS2_HUMAN	94.90%	1
ECHD1_HUMAN	100.00%	2
PUR2_HUMAN	100.00%	148
FBP1L_HUMAN	99.90%	4
AT2B4_HUMAN	100.00%	54
H12_HUMAN	99.90%	80
ATP5H_HUMAN	100.00%	38
LCAP_HUMAN	100.00%	319
LMAN1_HUMAN	100.00%	39
LONM_HUMAN	100.00%	158
RS27A_HUMAN	100.00%	81
PGAM1_HUMAN	100.00%	169
CD59_HUMAN	95.00%	25
DCTP1_HUMAN	100.00%	8
GAG_HV1MN	100.00%	5802
ADT3_HUMAN	99.90%	158
GDIB_HUMAN	100.00%	242
MPC2_HUMAN	95.00%	1
HEM6_HUMAN	100.00%	62
B2CL1_HUMAN	100.00%	3
SERPH_HUMAN	100.00%	56
HNRPF_HUMAN	100.00%	82
SRP09_HUMAN	95.00%	3
DPP4_HUMAN	100.00%	10
CHCH2_HUMAN	100.00%	21
SEPT1_HUMAN	100.00%	20
ELOV5_HUMAN	95.00%	10
COPB2_HUMAN	100.00%	23
PSMD5_HUMAN	100.00%	4
KS6A1_HUMAN	99.70%	2
IF2B_HUMAN	100.00%	3
BDH_HUMAN	100.00%	30
SP16H_HUMAN	100.00%	9

EF2_HUMAN	100.00%	613
GRB2_HUMAN	100.00%	17
WASF2_HUMAN	95.00%	1
ROA1_HUMAN	100.00%	89
ATP5L_HUMAN	100.00%	38
ML12A_HUMAN,ML12B_HUMAN	100.00%	213
CALX_HUMAN	100.00%	187
PHAG1_HUMAN	100.00%	8
NPM_HUMAN	100.00%	94
VDAC1_HUMAN	100.00%	203
CTDS1_HUMAN	95.50%	1
RAN_HUMAN	100.00%	153
BASI_HUMAN	100.00%	200
EIF3K_HUMAN	100.00%	10
SMAD3_HUMAN	99.40%	1
PKN1_HUMAN	100.00%	2
SYMC_HUMAN	100.00%	35
SH3K1_HUMAN	100.00%	32
NDUS7_HUMAN	95.00%	1
PSDE_HUMAN	100.00%	7
VPS4B_HUMAN	100.00%	43
SYTC_HUMAN	100.00%	47
KAD3_HUMAN	100.00%	11
LAT1_HUMAN	100.00%	51
FA5_HUMAN	100.00%	55
ODO1_HUMAN	100.00%	14
BIN2_HUMAN	100.00%	6
UGPA_HUMAN	100.00%	226
MPCP_HUMAN	100.00%	41
RL5_HUMAN	100.00%	212
CD48_HUMAN	100.00%	151
GSLG1_HUMAN	97.40%	1
HMGB2_HUMAN	99.90%	5
PSB1_HUMAN	100.00%	13
TFR1_HUMAN	100.00%	246
SPTN1_HUMAN	100.00%	347
MIC19_HUMAN	100.00%	33
RS5_HUMAN	100.00%	73
ECHM_HUMAN	97.80%	8
RPN2_HUMAN	100.00%	37
ANX11_HUMAN	100.00%	33
HNRH1_HUMAN	100.00%	29
IF4G1_HUMAN	100.00%	52

CARL2_HUMAN	97.50%	7
GBP1_HUMAN	100.00%	27
PSB10_HUMAN	95.00%	9
RS14_HUMAN	100.00%	42
EIF3E_HUMAN	100.00%	6
TOM22_HUMAN	100.00%	22
TICN2_HUMAN	100.00%	100
NDUS1_HUMAN	100.00%	3
ASSY_HUMAN	100.00%	28
OCAD2_HUMAN	100.00%	1
MLEC_HUMAN	99.90%	1
MACD1_HUMAN	100.00%	13
SYDM_HUMAN	95.00%	10
SAR1A_HUMAN	99.90%	12
BUB3_HUMAN	100.00%	4
VP26B_HUMAN	95.00%	1
KCY_HUMAN	95.00%	7
gnl|unk|TRINITY_DN8_c0_g1_i1_4	98.80%	77
HG2A_HUMAN	100.00%	52
PSA3_HUMAN	100.00%	12
CD3G_HUMAN	95.00%	6
2B14_HUMAN	100.00%	559
RAB7A_HUMAN	100.00%	192
GLYM_HUMAN	100.00%	330
SQRD_HUMAN	100.00%	10
SERB_HUMAN	100.00%	4
PAIRB_HUMAN	100.00%	9
SFPQ_HUMAN	100.00%	23
PRPS1_HUMAN	100.00%	28
N2DL2_HUMAN	100.00%	23
LY75_HUMAN	100.00%	5
DLDH_HUMAN	100.00%	171
KINH_HUMAN	100.00%	21
UPAR_HUMAN	100.00%	46
TMOD3_HUMAN	100.00%	22
QCR6_HUMAN	95.00%	16
CSDE1_HUMAN	100.00%	6
ICAM1_HUMAN	100.00%	149
PRDX2_HUMAN	100.00%	67
PABP1_HUMAN	100.00%	352
POL_HV1ND	99.60%	1984
RS4X_HUMAN	100.00%	299
DC1I2_HUMAN	95.00%	7

CAZA1_HUMAN	100.00%	149
ACAP1_HUMAN	100.00%	36
DOCK8_HUMAN	100.00%	37
SC5A6_HUMAN	100.00%	6
K2C1_HUMAN	100.00%	25
HSPB1_HUMAN	100.00%	14
RAP2C_HUMAN	100.00%	16
RL6_HUMAN	100.00%	223
TBCA_HUMAN	100.00%	8
UB2V2_HUMAN	98.10%	4
PSB2_HUMAN	100.00%	20
CNOT1_HUMAN	100.00%	30
U5S1_HUMAN	95.00%	9
DUT_HUMAN	100.00%	25
HDDC2_HUMAN	99.80%	1
SH21A_HUMAN	100.00%	6
CSK22_HUMAN	99.20%	1
FXR1_HUMAN	100.00%	18
ALDOC_HUMAN	100.00%	187
ESYT1_HUMAN	100.00%	17
STT3B_HUMAN	95.00%	3
TPP2_HUMAN	100.00%	8
ENV_HV1MN	100.00%	534
EIF3F_HUMAN	100.00%	33
STX3_HUMAN	100.00%	21
LIMS1_HUMAN	95.00%	4
NDUS2_HUMAN	96.50%	1
RPIA_HUMAN	100.00%	3
DPA1_HUMAN	100.00%	48
NHRF1_HUMAN	100.00%	408
PYRG1_HUMAN	100.00%	20
FLNB_HUMAN	100.00%	596
NNTM_HUMAN	100.00%	11
TNR6_HUMAN	100.00%	127
TCPB_HUMAN	100.00%	302
ZYX_HUMAN	100.00%	9
STIP1_HUMAN	100.00%	162
SCRIB_HUMAN	100.00%	60
PSA4_HUMAN	100.00%	35
RADI_HUMAN	100.00%	642
SRSF7_HUMAN	100.00%	8
PELO_HUMAN	95.00%	2
TPD52_HUMAN	100.00%	6

ECH1_HUMAN	100.00%	136
TMX1_HUMAN	95.00%	6
IF4A1_HUMAN	100.00%	313
NUDC_HUMAN	100.00%	67
PLSL_HUMAN	100.00%	852
IFM2_HUMAN	100.00%	81
DHE3_HUMAN	100.00%	105
ACO13_HUMAN	95.00%	1
THY1_HUMAN	100.00%	172
AIFM1_HUMAN	100.00%	53
CXCR4_HUMAN	95.00%	10
PGRC2_HUMAN	95.00%	1
ENV_HV196	100.00%	64
RSSA_HUMAN	100.00%	274
FA49B_HUMAN	100.00%	41
USP9X_HUMAN	100.00%	7
TOM70_HUMAN	100.00%	29
STAT3_HUMAN	100.00%	11
YBOX1_HUMAN	100.00%	265
CYB5B_HUMAN	95.00%	8
ATPG_HUMAN	100.00%	78
ARF6_HUMAN	100.00%	88
ACTN4_HUMAN	100.00%	542
TRXR1_HUMAN	100.00%	15
CLH1_HUMAN	100.00%	934
MK03_HUMAN	99.80%	13
COX2_HUMAN	100.00%	40
EPN4_HUMAN	100.00%	4
MAP11_HUMAN	95.00%	2
EHD4_HUMAN	100.00%	104
SRSF1_HUMAN	100.00%	9
TAGL2_HUMAN	100.00%	180
TES_HUMAN	100.00%	73
BT3L4_HUMAN	99.40%	1
EIF3I_HUMAN	100.00%	28
ACPM_HUMAN	100.00%	2
PPIL1_HUMAN	100.00%	55
COPG1_HUMAN	100.00%	23
HACD3_HUMAN	95.00%	2
GANAB_HUMAN	100.00%	141
GLRX3_HUMAN	100.00%	2
RL35A_HUMAN	100.00%	28
PAR12_HUMAN	95.00%	1

DQA1_HUMAN	100.00%	41
BACH_HUMAN	100.00%	54
SSRD_HUMAN	95.00%	9
gnl|unk|TRINITY_DN1102_c0_g1_i1_2	100.00%	63
DDX21_HUMAN	100.00%	5
1B44_HUMAN	100.00%	452
LIS1_HUMAN	100.00%	25
SETLP_HUMAN,SET_HUMAN	100.00%	14
SRSF3_HUMAN	100.00%	24
NUDT5_HUMAN	100.00%	2
RCD1_HUMAN	100.00%	25
TSP1_HUMAN	100.00%	18
RHG17_HUMAN	100.00%	20
ANXA4_HUMAN	100.00%	34
ERO1A_HUMAN	100.00%	18
PA1B2_HUMAN	100.00%	8
TCPZ_HUMAN	100.00%	197
MAP4_HUMAN	99.20%	1
AP1B1_HUMAN	100.00%	39
MCM3_HUMAN	100.00%	15
IF5A1_HUMAN	100.00%	143
S4A7_HUMAN	100.00%	77
AGK_HUMAN	100.00%	10
M2OM_HUMAN	100.00%	77
PP16B_HUMAN	100.00%	12
UN13D_HUMAN	100.00%	26
TMM43_HUMAN	95.00%	3
LC7L3_HUMAN	95.00%	2
AATM_HUMAN	100.00%	121
KAP2_HUMAN	100.00%	70
MDHM_HUMAN	100.00%	514
NIT2_HUMAN	95.00%	2
RAP1B_HUMAN	100.00%	399
PNPT1_HUMAN	100.00%	2
ARPC3_HUMAN	100.00%	34
K1C10_HUMAN	99.90%	6
ITB1_HUMAN	100.00%	122
CC50A_HUMAN	100.00%	24
HCDH_HUMAN	100.00%	45
RGAP1_HUMAN	100.00%	26
EIF3A_HUMAN	100.00%	62
PBDC1_HUMAN	94.60%	3
TBB5_HUMAN	100.00%	1573

RL34_HUMAN	99.20%	20
GPR15_HUMAN	97.30%	3
DREB_HUMAN	100.00%	77
TB10A_HUMAN	100.00%	5
ICOSL_HUMAN	99.90%	2
PSD11_HUMAN	100.00%	45
BCAT2_HUMAN	100.00%	6
CAB39_HUMAN	100.00%	24
MARK3_HUMAN	99.80%	5
SIT1_HUMAN	100.00%	41
CYFP2_HUMAN	100.00%	13
MPPA_HUMAN	100.00%	10
CLIC1_HUMAN	100.00%	493
BYST_HUMAN	95.00%	1
PEBP1_HUMAN	100.00%	53
SDF2L_HUMAN	95.00%	4
CPNE1_HUMAN	100.00%	58
ODO2_HUMAN	100.00%	26
ERP29_HUMAN	100.00%	23
PDC10_HUMAN	100.00%	45
H2AY_HUMAN	95.00%	3
ARK72_HUMAN	95.00%	5
TAP2_HUMAN	100.00%	5
VTNC_HUMAN	95.00%	94
AP2B1_HUMAN	100.00%	43
FSCN1_HUMAN	100.00%	80
VAMP2_HUMAN,VAMP3_HUMAN	95.00%	6
DQA2_HUMAN	98.20%	118
HNRL2_HUMAN	100.00%	2
ATPO_HUMAN	100.00%	79
NF1_HUMAN	95.00%	2
ATPB_HUMAN	100.00%	528
ERF3A_HUMAN	100.00%	31
SYDC_HUMAN	100.00%	202
SH3G1_HUMAN	100.00%	15
NDRG1_HUMAN	100.00%	21
ANXA5_HUMAN	100.00%	14
TMED2_HUMAN	100.00%	1
NAMPT_HUMAN	100.00%	5
KPYM_HUMAN	100.00%	1199
DNMT1_HUMAN	99.90%	1
FLOT1_HUMAN	100.00%	13
SNP23_HUMAN	100.00%	32

SYRC_HUMAN	100.00%	33
TBA4A_HUMAN	100.00%	1076
EMC1_HUMAN	99.90%	1
GLYC_HUMAN	100.00%	38
ACPH_HUMAN	100.00%	31
SCOT1_HUMAN	100.00%	15
EHD1_HUMAN	100.00%	307
H2B1C_HUMAN,H2B1D_HUMAN,H2B1H_HUMAN,H2B1L_HUMAN,H2B1M_HUMAN,H2B1N_HUMAN,H2B2F_HUMAN	100.00%	93
RL26L_HUMAN,RL26_HUMAN	100.00%	22
ACSL3_HUMAN	98.50%	20
CHM2B_HUMAN	98.70%	5
SPAG1_HUMAN	95.00%	2
LASP1_HUMAN	100.00%	89
PSMG2_HUMAN	95.00%	6
EF1G_HUMAN	100.00%	230
LGUL_HUMAN	100.00%	6
STML2_HUMAN	100.00%	43
ARRD1_HUMAN	95.00%	4
DKC1_HUMAN	100.00%	4
ETFA_HUMAN	100.00%	80
RL35_HUMAN	100.00%	91
MB12B_HUMAN	95.00%	1
MARCS_HUMAN	100.00%	43
TRAP1_HUMAN	100.00%	115
RL18_HUMAN	100.00%	176
ILF2_HUMAN	95.00%	4
ROCK1_HUMAN	100.00%	4
FDFT_HUMAN	98.30%	3
H14_HUMAN	100.00%	85
MPPB_HUMAN	100.00%	8
ABCE1_HUMAN	100.00%	53
HABP2_HUMAN	100.00%	13
UB2L3_HUMAN	100.00%	20
TIPRL_HUMAN	100.00%	4
TPM3_HUMAN	100.00%	291
FHL1_HUMAN	95.00%	9
PDIA6_HUMAN	100.00%	145
HS90B_HUMAN	100.00%	1331
NPTN_HUMAN	100.00%	6
SODM_HUMAN	100.00%	47
IF2B1_HUMAN	100.00%	82

RAB5A_HUMAN	99.60%	43
MPZL1_HUMAN	95.00%	21
ACOT9_HUMAN	98.80%	1
FUMH_HUMAN	100.00%	16
CLCA_HUMAN	100.00%	10
AFAD_HUMAN	100.00%	4
APT_HUMAN	100.00%	41
RD23B_HUMAN	100.00%	48
TBB4A_HUMAN	100.00%	1229
SNX18_HUMAN	95.00%	7
RAB10_HUMAN	100.00%	106
FBRL_HUMAN	100.00%	7
XRCC6_HUMAN	100.00%	46
RTN3_HUMAN	95.00%	5
FABP5_HUMAN	100.00%	98
RL27_HUMAN	100.00%	143
LRC47_HUMAN	100.00%	6
IDH3G_HUMAN	100.00%	3
RASN_HUMAN	100.00%	122
1A32_HUMAN,1A74_HUMAN	100.00%	354
VDAC3_HUMAN	100.00%	46
C1QBP_HUMAN	100.00%	201
ARP5L_HUMAN	100.00%	7
BROX_HUMAN	100.00%	38
RUXE_HUMAN	95.00%	16
H2B1B_HUMAN,H2B1O_HUMAN,H2B2E_ HUMAN,H2B3B_HUMAN	100.00%	71
EMC2_HUMAN	95.00%	4
LDHA_HUMAN	100.00%	377
AT1B1_HUMAN	95.00%	4
LAT3_HUMAN	95.00%	2
NAA10_HUMAN	100.00%	7
RM14_HUMAN	95.00%	4
CH60_HUMAN	100.00%	717
JAM1_HUMAN	100.00%	57
XRP2_HUMAN	100.00%	19
CD2AP_HUMAN	100.00%	15
OSTC_HUMAN	95.00%	1
GMFG_HUMAN	100.00%	38
DHB4_HUMAN	100.00%	3
COTL1_HUMAN	100.00%	118
RHOG_HUMAN	100.00%	149
H2A1C_HUMAN	100.00%	203

VPS35_HUMAN	100.00%	42
RL21_HUMAN	100.00%	83
NDUA5_HUMAN	95.00%	1
IDH3A_HUMAN	100.00%	42
GNA13_HUMAN	100.00%	94
EXOC7_HUMAN	95.00%	3
SPEE_HUMAN	100.00%	16
HBA_HUMAN	100.00%	177
PTPRC_HUMAN	100.00%	1034
ETFB_HUMAN	100.00%	66
E41L2_HUMAN	100.00%	641
RL19_HUMAN	100.00%	37
SAM50_HUMAN	100.00%	8
CDC42_HUMAN	100.00%	270
DIAP1_HUMAN	100.00%	18
H15_HUMAN	100.00%	20
1A24_HUMAN	100.00%	502
ARP2_HUMAN	100.00%	59
AHNK_HUMAN	100.00%	589
LIN7C_HUMAN	100.00%	24
AT1A3_HUMAN	100.00%	374
LKHA4_HUMAN	99.90%	3
PPCE_HUMAN	95.00%	1
SERC3_HUMAN	95.00%	3
F136A_HUMAN	95.00%	1
EF1B_HUMAN	100.00%	43
WIPF1_HUMAN	97.50%	9
PDLI7_HUMAN	95.00%	1
EI2BA_HUMAN	100.00%	6
TRI25_HUMAN	100.00%	33
AT11C_HUMAN	100.00%	26
UBE2N_HUMAN	100.00%	30
KPRB_HUMAN	100.00%	9
CDK1_HUMAN	100.00%	41
ARBK1_HUMAN	100.00%	2
CAPR1_HUMAN	100.00%	8
IF4B_HUMAN	100.00%	5
RUVB2_HUMAN	100.00%	64
RL30_HUMAN	100.00%	193
SYEP_HUMAN	100.00%	65
GRP75_HUMAN	100.00%	225
RL13_HUMAN	100.00%	113
AIMP1_HUMAN	100.00%	24

AT2B1_HUMAN	99.90%	16
PP1A_HUMAN	100.00%	75
APOC3_HUMAN	95.00%	31
GDIR2_HUMAN	100.00%	220
SYHC_HUMAN	100.00%	2
ICAM3_HUMAN	100.00%	230
AATC_HUMAN	100.00%	26
PLEC_HUMAN	100.00%	26
F162A_HUMAN	99.90%	1
SEPT9_HUMAN	100.00%	57
KRT83_HUMAN	100.00%	7
PRKDC_HUMAN	99.90%	1
MDHC_HUMAN	100.00%	161
CNDP2_HUMAN	100.00%	62
PDIA1_HUMAN	100.00%	178
NLTP_HUMAN	100.00%	43
SAHH2_HUMAN	100.00%	28
CD70_HUMAN	100.00%	31
SYVC_HUMAN	100.00%	44
ATX10_HUMAN	95.00%	5
ABCF1_HUMAN	100.00%	26
PI42A_HUMAN	100.00%	14
PAR1_HUMAN	95.00%	11
SUV3_HUMAN	99.90%	3
ETHE1_HUMAN	100.00%	59
PSMD2_HUMAN	100.00%	35
CD3Z_HUMAN	100.00%	1
RM19_HUMAN	99.80%	4
QCR7_HUMAN	100.00%	3
ACSL4_HUMAN	100.00%	32
DYN2_HUMAN	100.00%	12
RAB8B_HUMAN	100.00%	237
RS8_HUMAN	100.00%	239
RENT1_HUMAN	100.00%	28
RL22_HUMAN	100.00%	53
IDH3B_HUMAN	100.00%	9
OST48_HUMAN	100.00%	56
CPT1A_HUMAN	100.00%	7
E41L3_HUMAN	100.00%	59
AT2A3_HUMAN	99.80%	17
RS17_HUMAN	100.00%	117
LRRF1_HUMAN	95.00%	1
PIPNB_HUMAN	100.00%	9

BTF3_HUMAN	100.00%	11
NB5R3_HUMAN	100.00%	56
PUR6_HUMAN	100.00%	96
PP2BA_HUMAN	100.00%	10
TWF2_HUMAN	100.00%	52
RS15A_HUMAN	100.00%	80
SH3L3_HUMAN	95.00%	18
ARP3_HUMAN	100.00%	114
MACF1_HUMAN	99.90%	2
TRBC1_HUMAN,TRBC2_HUMAN	100.00%	25
NPS3A_HUMAN	95.00%	4
RINI_HUMAN	100.00%	13
PGAM5_HUMAN	100.00%	8
FLNA_HUMAN	100.00%	867
PRP19_HUMAN	100.00%	1
AP2M1_HUMAN	100.00%	43
gnl|unk|TRINITY_DN8_c0_g2_i1_11	100.00%	43
RL10A_HUMAN	100.00%	104
ACOT1_HUMAN	100.00%	3
RAB2A_HUMAN	100.00%	14
PSME1_HUMAN	100.00%	24
CECR5_HUMAN	99.80%	6
SRP68_HUMAN	99.90%	1
AKAP2_HUMAN	100.00%	33
COPB_HUMAN	100.00%	30
ESTD_HUMAN	100.00%	9
MTA2_HUMAN	95.00%	1
USO1_HUMAN	95.00%	3
DYHC1_HUMAN	100.00%	85
URP2_HUMAN	100.00%	340
IF4A3_HUMAN	100.00%	47
EM55_HUMAN	100.00%	16
RL14_HUMAN	100.00%	111
CUL1_HUMAN	99.70%	1
ES1_HUMAN	100.00%	7
TBG1_HUMAN	100.00%	4
LSR_HUMAN	95.00%	4
PRDX5_HUMAN	100.00%	41
THIC_HUMAN	100.00%	106
NIPS1_HUMAN	100.00%	28
3HIDH_HUMAN	100.00%	6
PABP4_HUMAN	100.00%	134
TBA1B_HUMAN	99.90%	1231

AMPL_HUMAN	100.00%	92
EFR3A_HUMAN	100.00%	8
ANM5_HUMAN	100.00%	6
SPTB2_HUMAN	100.00%	357
HS105_HUMAN	100.00%	156
HNRPD_HUMAN	100.00%	24
ADDA_HUMAN	95.00%	5
1B18_HUMAN	99.20%	647
RL9_HUMAN	100.00%	160
YKT6_HUMAN	100.00%	10
PSMD3_HUMAN	100.00%	30
RAC1_HUMAN	100.00%	137
RS9_HUMAN	100.00%	149
IPYR_HUMAN	100.00%	169
UBA1_HUMAN	100.00%	134
RS20_HUMAN	100.00%	94
FUBP2_HUMAN	100.00%	2
MTPN_HUMAN	95.00%	4
DECR_HUMAN	100.00%	13
MOGS_HUMAN	100.00%	6
STX6_HUMAN	95.00%	2
GPX4_HUMAN	100.00%	22
1A11_HUMAN	100.00%	591
GLPC_HUMAN	100.00%	19
RL27A_HUMAN	100.00%	70
SODC_HUMAN	100.00%	105
DX39B_HUMAN	100.00%	26
AHSA1_HUMAN	100.00%	47
DBNL_HUMAN	100.00%	10
ACTC_HUMAN	100.00%	2040
GLYG_HUMAN	95.00%	1
TNR8_HUMAN	100.00%	19
PARK7_HUMAN	100.00%	124
TCPE_HUMAN	100.00%	238
DQB1_HUMAN	100.00%	47
QCR2_HUMAN	100.00%	37
RS3_HUMAN	100.00%	237
DOPD_HUMAN	100.00%	7
MBNL1_HUMAN	100.00%	16
G3P_HUMAN	100.00%	1100
CD99_HUMAN	100.00%	11
PSA7_HUMAN	100.00%	28
RBM8A_HUMAN	95.00%	2

A2MG_HUMAN	100.00%	48
PSMD7_HUMAN	100.00%	28
GGT2_HUMAN	100.00%	7
RS12_HUMAN	100.00%	104
NDUF4_HUMAN	95.00%	2
MYL6_HUMAN	100.00%	177
ADA_HUMAN	100.00%	35
PUR1_HUMAN	95.00%	4
PDCL3_HUMAN	95.00%	6
MIF_HUMAN	100.00%	132
DNJA2_HUMAN	100.00%	11
PRDX6_HUMAN	100.00%	267
RU17_HUMAN	99.20%	1
RHG30_HUMAN	100.00%	11
CORO7_HUMAN	100.00%	7
SYSC_HUMAN	100.00%	68
DHX9_HUMAN	100.00%	39
DDB1_HUMAN	95.00%	1
CD38_HUMAN	100.00%	249
ROA2_HUMAN	100.00%	84
SMD2_HUMAN	100.00%	6
3BP1_HUMAN	99.90%	1
T200A_HUMAN	100.00%	8
STAT1_HUMAN	100.00%	3
CATA_HUMAN	95.00%	1
IF2A_HUMAN	100.00%	41
PCBP1_HUMAN	100.00%	161
RL37A_HUMAN,gnl|unk|TRINITY_DN277_c0_g2_i1_5	100.00%	11
FUBP3_HUMAN	95.00%	1
MCA3_HUMAN	100.00%	15
PDCD5_HUMAN	100.00%	23
SYFB_HUMAN	100.00%	32
CD166_HUMAN	100.00%	97
U2AF2_HUMAN	95.00%	2
STX7_HUMAN	95.00%	3
RAB43_HUMAN	96.40%	30
TPM4_HUMAN	100.00%	278
VPS4A_HUMAN	100.00%	19
S39AA_HUMAN	95.00%	4
PPP6_HUMAN	100.00%	14
NDUBA_HUMAN	99.90%	1
KAD2_HUMAN	100.00%	175

TIM16_HUMAN	95.00%	9
RASL3_HUMAN	100.00%	72
SF3B1_HUMAN	99.90%	2
RL4_HUMAN	100.00%	416
LAMP1_HUMAN	99.90%	5
SMC4_HUMAN	95.00%	2
CHM4A_HUMAN	95.00%	1
RPN1_HUMAN	100.00%	148
RAB6A_HUMAN	100.00%	40
MP2K1_HUMAN	100.00%	44
ALDOA_HUMAN	100.00%	663
ENOB_HUMAN	99.70%	497
NONO_HUMAN	100.00%	7
F120A_HUMAN	100.00%	6
VP37C_HUMAN	95.00%	1
TS101_HUMAN	100.00%	101
NDUV2_HUMAN	100.00%	6
RAB35_HUMAN	100.00%	131
ATPK_HUMAN	100.00%	38
GLU2B_HUMAN	100.00%	37
NDUAC_HUMAN	95.00%	1
CLIC4_HUMAN	100.00%	186
ADHX_HUMAN	100.00%	8
AAAT_HUMAN	100.00%	323
SORCN_HUMAN	100.00%	33
RS3A_HUMAN	100.00%	293
IDI1_HUMAN	95.00%	6
PRS7_HUMAN	100.00%	11
PSA2_HUMAN	95.00%	3
OAT_HUMAN	100.00%	30
RS25_HUMAN	100.00%	74
SMD3_HUMAN	100.00%	14
PCBP2_HUMAN	100.00%	131
NTF2_HUMAN	100.00%	22
RAB5C_HUMAN	100.00%	119
FKBP4_HUMAN	100.00%	50
MYH10_HUMAN	100.00%	572
SERA_HUMAN	100.00%	181
PACN2_HUMAN	100.00%	90
SSDH_HUMAN	100.00%	5
RB33A_HUMAN	97.90%	1
PLS3_HUMAN	100.00%	10
PFKAL_HUMAN	100.00%	64

MTM1_HUMAN	100.00%	5
RL32_HUMAN	100.00%	68
SPCS3_HUMAN	98.30%	4
FA98A_HUMAN	95.00%	1
PRDX1_HUMAN	100.00%	436
CTR1_HUMAN	100.00%	46
PDCD6_HUMAN	100.00%	19
CAP1_HUMAN	100.00%	170
RLA1_HUMAN	100.00%	58
HUWE1_HUMAN	100.00%	35
ARF4_HUMAN	100.00%	172
MK01_HUMAN	100.00%	19
TPSN_HUMAN	100.00%	4
H4_HUMAN	100.00%	249
TMEM2_HUMAN	99.90%	1
CNPY2_HUMAN	100.00%	14
FLOT2_HUMAN	100.00%	65
MCM7_HUMAN	98.20%	12
MIA2_HUMAN	99.80%	3
NEF_HV1MN	100.00%	4
UB2V1_HUMAN	99.90%	6
IMA1_HUMAN	100.00%	32
S10AB_HUMAN	100.00%	21
GOGA7_HUMAN	99.90%	4
GBB1_HUMAN	100.00%	278
PRDX3_HUMAN	100.00%	4
CBPN_HUMAN	95.00%	8
CHM4B_HUMAN	100.00%	23
RRAS2_HUMAN	100.00%	51
CSK21_HUMAN	100.00%	36
SC23B_HUMAN	100.00%	4
NICA_HUMAN	100.00%	3
S10A6_HUMAN	99.90%	6
GBG4_HUMAN	95.00%	3
DDX6_HUMAN	100.00%	94
PSA_HUMAN	100.00%	63
RAC2_HUMAN	100.00%	234
HSP7C_HUMAN	100.00%	1027
IKBB_HUMAN	95.00%	4
AMPB_HUMAN	100.00%	5
NDKA_HUMAN	100.00%	300
PEX14_HUMAN	95.00%	1
RL38_HUMAN	100.00%	48

DDX17_HUMAN	100.00%	93
AL9A1_HUMAN	100.00%	10
TXND5_HUMAN	95.00%	4
CUTA_HUMAN	95.00%	2
IF6_HUMAN	100.00%	15
FNBP1_HUMAN	100.00%	141
PTH2_HUMAN	95.00%	7
TCPA_HUMAN	100.00%	346
NDUB5_HUMAN	95.00%	2
RTN4_HUMAN	100.00%	14
KAP0_HUMAN	95.00%	6
DHB12_HUMAN	100.00%	4
RS10L_HUMAN,RS10_HUMAN	100.00%	18
DPM3_HUMAN	95.00%	10
TM9S2_HUMAN	95.00%	5
RHG15_HUMAN	100.00%	20
EF1D_HUMAN	100.00%	101
ITA5_HUMAN	100.00%	4
ECHA_HUMAN	100.00%	21
IFM1_HUMAN	99.80%	77
EBP_HUMAN	99.90%	3
ABHDA_HUMAN	100.00%	3
VP37B_HUMAN	95.00%	6
PFKAM_HUMAN	100.00%	16
DRA_HUMAN	100.00%	515
SDHA_HUMAN	100.00%	18
ANXA2_HUMAN	100.00%	722
COF1_HUMAN	100.00%	430
EIF1_HUMAN	95.00%	4
RLA2_HUMAN	100.00%	143
ZCHC3_HUMAN	100.00%	8
ACADV_HUMAN	100.00%	47
PTBP1_HUMAN	100.00%	43
HPBP1_HUMAN	100.00%	2
ERP44_HUMAN	98.00%	1
MIC60_HUMAN	100.00%	90
MY18A_HUMAN	100.00%	41
TMM33_HUMAN	95.00%	2
PCH2_HUMAN	95.00%	1
CH10_HUMAN	100.00%	152
LEUK_HUMAN	100.00%	79
NFKB1_HUMAN	100.00%	2
MYO1C_HUMAN	95.00%	4

MRP_HUMAN	99.90%	42
STOM_HUMAN	100.00%	104
RL18A_HUMAN	100.00%	135
TLDC1_HUMAN	95.00%	3
TP4A3_HUMAN	95.00%	3
SNTB1_HUMAN	99.80%	1
IL16_HUMAN	100.00%	204
EIF2A_HUMAN	100.00%	12
1433F_HUMAN	100.00%	79
EFTU_HUMAN	100.00%	345
PLRG1_HUMAN	95.00%	2
RL24_HUMAN	100.00%	87
CD3E_HUMAN	100.00%	23
HNRPR_HUMAN	100.00%	77
MOES_HUMAN	100.00%	1723
STK10_HUMAN	100.00%	31
NDKB_HUMAN	100.00%	267
DOCK2_HUMAN	100.00%	47
LRC59_HUMAN	100.00%	7
TBB6_HUMAN	99.90%	422
PFD2_HUMAN	100.00%	22
RL10_HUMAN	100.00%	180
CO4A_HUMAN,CO4B_HUMAN	100.00%	19
PYR1_HUMAN	100.00%	45
GTR3_HUMAN	100.00%	42
ACAD9_HUMAN	100.00%	16
B2MG_HUMAN	100.00%	77
CD81_HUMAN	100.00%	405
HSDL2_HUMAN	99.90%	6
GNAS1_HUMAN	100.00%	93
XPO2_HUMAN	100.00%	22
ACACA_HUMAN	100.00%	16
RAP1A_HUMAN	100.00%	329
ATD3B_HUMAN	99.90%	32
ACON_HUMAN	100.00%	35
ACDSB_HUMAN	100.00%	5
TKT_HUMAN	100.00%	72
ARPC2_HUMAN	100.00%	77
PTCA_HUMAN	100.00%	58
ALDR_HUMAN	100.00%	30
KIF23_HUMAN	100.00%	25
FUS_HUMAN	99.90%	9
AP2A1_HUMAN	100.00%	41

EXOC4_HUMAN	100.00%	10
ACLY_HUMAN	100.00%	207
IF4E_HUMAN	99.90%	4
EVL_HUMAN	100.00%	24
MYH9_HUMAN	100.00%	2360
GRP78_HUMAN	100.00%	418
SDHB_HUMAN	100.00%	9
LPXN_HUMAN	100.00%	10
RCC2_HUMAN	100.00%	12
PSD10_HUMAN	95.00%	2
CISY_HUMAN	100.00%	85
RS28_HUMAN,gnl|unk|TRINITY_DN1116_c0_g1_i1_2	100.00%	30
MARK2_HUMAN	100.00%	21
RAB14_HUMAN	100.00%	64
ZDHC5_HUMAN	100.00%	21
MTX1_HUMAN	95.00%	1
PUR8_HUMAN	100.00%	60
BIEA_HUMAN	100.00%	32
ECHB_HUMAN	100.00%	9
ATG3_HUMAN	100.00%	7
PARP1_HUMAN	100.00%	38
CDC37_HUMAN	100.00%	74
PDIA4_HUMAN	100.00%	79
PDC6I_HUMAN	100.00%	357
IQGA2_HUMAN	100.00%	104
XPP1_HUMAN	100.00%	11
GLPK_HUMAN	100.00%	3
DOC10_HUMAN	100.00%	11
ZCCHV_HUMAN	100.00%	60
TAP1_HUMAN	95.00%	4
IPO7_HUMAN	100.00%	22
RTCB_HUMAN	100.00%	19
SNTB2_HUMAN	100.00%	7
1433G_HUMAN	100.00%	169
PA2G4_HUMAN	100.00%	172
NACAM_HUMAN	100.00%	64
GLRX1_HUMAN	95.00%	1
LFA3_HUMAN	100.00%	14
ATPA_HUMAN	100.00%	408
COASY_HUMAN	95.00%	2
NDUA9_HUMAN	95.00%	2
COX41_HUMAN	100.00%	36

SDCB1_HUMAN	100.00%	50
YTHD2_HUMAN	95.00%	2
GRP2_HUMAN	95.00%	2
TXD17_HUMAN	100.00%	29
S38A2_HUMAN	100.00%	14
PFD3_HUMAN	99.90%	3
AK1A1_HUMAN	100.00%	63
CSRP1_HUMAN	100.00%	50
PUR9_HUMAN	100.00%	391
RN213_HUMAN	100.00%	11
PTPRA_HUMAN	100.00%	1
DNJC7_HUMAN	100.00%	3
KDIS_HUMAN	100.00%	6
CD82_HUMAN	95.00%	3
THIL_HUMAN	100.00%	29
G3BP1_HUMAN	100.00%	22
PRP8_HUMAN	99.30%	1
AN32A_HUMAN	100.00%	11
VILI_HUMAN	95.00%	2
TRUA_HUMAN	95.70%	2
RBM3_HUMAN	95.00%	1
L1CAM_HUMAN	100.00%	515
MFGM_HUMAN	100.00%	52
LPPRC_HUMAN	100.00%	129
DDX1_HUMAN	100.00%	4
HNRPM_HUMAN	100.00%	47
CAPZB_HUMAN	100.00%	103
EXOC5_HUMAN	95.00%	4
STMN1_HUMAN	100.00%	29
ODPA_HUMAN	100.00%	10
TLN1_HUMAN	100.00%	465
MB12A_HUMAN	95.00%	5
MAOM_HUMAN	100.00%	62
RL17_HUMAN	100.00%	200
CDV3_HUMAN	100.00%	19
KCNN4_HUMAN	100.00%	5
RS29_HUMAN	95.00%	3
CN37_HUMAN	100.00%	62
LMAN2_HUMAN	95.00%	3
PPIA_HUMAN	100.00%	1309
FAS_HUMAN	100.00%	709
AT1A1_HUMAN	100.00%	596
HS90A_HUMAN	100.00%	962

BAP31_HUMAN	100.00%	29
COX5A_HUMAN	100.00%	20
CNN2_HUMAN	100.00%	159
RB11B_HUMAN	100.00%	96
NAA15_HUMAN	100.00%	24
LG3BP_HUMAN	99.90%	1
COR1C_HUMAN	100.00%	114
PSMD6_HUMAN	100.00%	17
PSB8_HUMAN	100.00%	9
VPS25_HUMAN	100.00%	3
6PGD_HUMAN	100.00%	113
RL11_HUMAN	100.00%	62
PRS10_HUMAN	100.00%	10
S29A1_HUMAN	100.00%	82
RS23_HUMAN	100.00%	29
XRCC5_HUMAN	100.00%	14
CY1_HUMAN	100.00%	10
SCO1_HUMAN	95.00%	1
ILK_HUMAN	100.00%	29
CAN1_HUMAN	100.00%	8
RACK1_HUMAN	100.00%	215
VDAC2_HUMAN	100.00%	121
EIF3L_HUMAN	100.00%	15
gnl|unk|TRINITY_DN398_c12_g13_i1_4,gnl|unk|TRINITY_DN398_c12_g3_i1_6,gnl|unk|TRINITY_DN398_c12_g7_i1_4,gnl|unk|TRINITY_DN398_c12_g8_i1_6	100.00%	216
NDUS8_HUMAN	95.00%	3
PLCG1_HUMAN	97.50%	1
SR140_HUMAN	95.00%	2
CAND1_HUMAN	100.00%	53
SYPL1_HUMAN	95.00%	14
CIB1_HUMAN	100.00%	3
SDC4_HUMAN	100.00%	19
LMNB1_HUMAN	99.50%	6
THIM_HUMAN	100.00%	58
LEG1_HUMAN	100.00%	28
TCPH_HUMAN	100.00%	188
MTCH2_HUMAN	100.00%	37
CLDN1_HUMAN	99.90%	2
PTMA_HUMAN	95.00%	7
RS6_HUMAN	100.00%	155
RT29_HUMAN	97.10%	1

1433B_HUMAN	100.00%	112
CALM_HUMAN	100.00%	9
RHOF_HUMAN	100.00%	99
NP1L1_HUMAN	100.00%	132
STXB3_HUMAN	100.00%	105
ODPB_HUMAN	100.00%	12
TOM40_HUMAN	100.00%	18
PROF1_HUMAN	100.00%	678
TXD12_HUMAN	100.00%	5
DJB11_HUMAN	100.00%	6
VASP_HUMAN	100.00%	113
HYOU1_HUMAN	100.00%	19
ATX2L_HUMAN	100.00%	4
AP2S1_HUMAN	99.90%	2
PUR4_HUMAN	100.00%	26
CALR_HUMAN	100.00%	160
CNBP_HUMAN	99.90%	1
SH3L1_HUMAN	100.00%	19
PEDF_HUMAN	100.00%	3
MLF2_HUMAN	100.00%	14
IPYR2_HUMAN	99.90%	22
TIM44_HUMAN	95.00%	3
P5CS_HUMAN	99.60%	4
COX5B_HUMAN	100.00%	9
DP13A_HUMAN	95.00%	2
UN45A_HUMAN	95.00%	2
DBLOH_HUMAN	99.80%	6
HCLS1_HUMAN	100.00%	38
RFC2_HUMAN	95.00%	1
APOE_HUMAN	100.00%	42
RUVB1_HUMAN	100.00%	108
WDR1_HUMAN	100.00%	181
SQSTM_HUMAN	95.00%	1
RL12_HUMAN	100.00%	158
1B14_HUMAN	99.90%	555
CLTR1_HUMAN	100.00%	6
ROA3_HUMAN	100.00%	21
UBA5_HUMAN	100.00%	7
TCTP_HUMAN	100.00%	47
NEK7_HUMAN	95.00%	1
CASL_HUMAN	95.00%	4
GDIR1_HUMAN	100.00%	138
EF1A1_HUMAN	100.00%	1274

PCNA_HUMAN	100.00%	33
UBP14_HUMAN	100.00%	12
PSMD4_HUMAN	95.00%	2
PP2AA_HUMAN,PP2AB_HUMAN	100.00%	6
U2AF1_HUMAN,U2AF5_HUMAN	95.00%	3
EIF3M_HUMAN	100.00%	25
EDC4_HUMAN	100.00%	8
NADE_HUMAN	95.00%	2
GNAI2_HUMAN	100.00%	469
NCKPL_HUMAN	100.00%	3
PLCG2_HUMAN	99.00%	1
MTDC_HUMAN	95.00%	8
HSP74_HUMAN	100.00%	40
ACTG_HUMAN	100.00%	2528
1433Z_HUMAN	100.00%	273
GCP2_HUMAN	95.00%	1
CYTB_HUMAN	97.60%	3
RAB1A_HUMAN	99.90%	131
RL7_HUMAN	100.00%	269
TALDO_HUMAN	100.00%	35
TBCB_HUMAN	100.00%	10
RS15_HUMAN	100.00%	62
CYC_HUMAN	100.00%	40
PSMD1_HUMAN	100.00%	13
PSB3_HUMAN	100.00%	13
SNX6_HUMAN	95.00%	2
SELB_HUMAN	95.00%	1
DNPH1_HUMAN	99.90%	2
ARL8A_HUMAN,ARL8B_HUMAN	95.00%	3
HINT1_HUMAN	99.90%	1
RS7_HUMAN	100.00%	93
sp|Q9C0C9|UBE2O_HUMAN	100.00%	8
GLOD4_HUMAN	100.00%	20
FKB1A_HUMAN	100.00%	24
MPP6_HUMAN	100.00%	38
EIF3D_HUMAN	100.00%	17
SPIT2_HUMAN	97.50%	1
ACADM_HUMAN	95.00%	4
AT2A2_HUMAN	100.00%	39
RS16_HUMAN	100.00%	244
MOV10_HUMAN	100.00%	129
PI51A_HUMAN	100.00%	3
EIF3G_HUMAN	99.90%	12

STX4_HUMAN	100.00%	47
PIPNA_HUMAN	100.00%	12
OGA_HUMAN	95.00%	1
AP2A2_HUMAN	100.00%	43
NDUS3_HUMAN	100.00%	13
LYPA1_HUMAN	100.00%	28
ARI2_HUMAN	95.00%	1
BAHC1_HUMAN	95.00%	12
STK26_HUMAN	100.00%	38
ACTA_HUMAN	100.00%	1855
1433T_HUMAN	100.00%	92
ZCCHL_HUMAN	95.00%	2
MARE1_HUMAN	100.00%	13
MPRD_HUMAN	100.00%	10
POL_HV1Z2	100.00%	2594
POL_HV1YF	100.00%	1056
POL_HV1YB	99.80%	1100
POL_HV1Y2	100.00%	5181
CD44_HUMAN	100.00%	160
RM12_HUMAN	100.00%	20
SRP14_HUMAN	100.00%	12
TM41A_HUMAN	95.00%	5
POL_HV1V9	100.00%	801
DPYL2_HUMAN	100.00%	86
RHOA_HUMAN	100.00%	285
PEF1_HUMAN	99.80%	2
CX7A2_HUMAN	100.00%	16
CD97_HUMAN	100.00%	34
RAE1L_HUMAN	95.00%	7
PCKGM_HUMAN	100.00%	9
FYN_HUMAN	100.00%	106
PSA5_HUMAN	100.00%	41
COPA_HUMAN	100.00%	121
SUMO4_HUMAN	95.00%	19
SRSF8_HUMAN	98.60%	11
POL_HV1RH	100.00%	2837
IF4A2_HUMAN	100.00%	165
SC24C_HUMAN	100.00%	3
POL_HV1N5	100.00%	3562
TADBP_HUMAN	99.90%	4
POL_HV1MP	100.00%	1326
SYAC_HUMAN	100.00%	132
POL_HV1MN	100.00%	4667

POL_HV1MA	98.90%	1356
NUCB2_HUMAN	100.00%	10
POL_HV1M2	100.00%	898
NUCL_HUMAN	100.00%	23
S10A4_HUMAN	100.00%	74
VAMP8_HUMAN	100.00%	2
PRDX4_HUMAN	100.00%	39
POL_HV1JR	100.00%	4692

Table 4a. All proteins identified for the HIV-1(MN)/H9 CL.4 virus.

Protein accession numbers	Protein identification probability	Total spectrum count
POL_HV1J3	99.90%	2295
SC61G_HUMAN	95.00%	25
DPB1_HUMAN	100.00%	216
ERF1_HUMAN	100.00%	4
HS71A_HUMAN,HS71B_HUMAN	100.00%	412
GNAI3_HUMAN	100.00%	304
S39AE_HUMAN	100.00%	9
PRS4_HUMAN	99.80%	5
CKLF6_HUMAN	95.00%	15
PLS1_HUMAN	99.90%	7
SNP29_HUMAN	95.00%	4
RM04_HUMAN	99.90%	2
HNRPC_HUMAN	100.00%	19
POL_HV1C4	100.00%	2361
PTN6_HUMAN	100.00%	12
RAB1B_HUMAN	100.00%	179
RL8_HUMAN	100.00%	58
CPNS1_HUMAN	100.00%	4
SUCA_HUMAN	100.00%	23
DNPEP_HUMAN	95.00%	7
DDRGK_HUMAN	95.00%	4
OLA1_HUMAN	100.00%	11
ECI1_HUMAN	95.00%	2
ATP5I_HUMAN	100.00%	23
PRAF2_HUMAN	95.00%	1
ABHD6_HUMAN	95.00%	3
G6PI_HUMAN	100.00%	305
SNAG_HUMAN	100.00%	13
PRS8_HUMAN	100.00%	4
SSBP_HUMAN	100.00%	50
KPCD2_HUMAN	99.80%	8

VTA1_HUMAN	100.00%	11
MYH11_HUMAN	99.80%	191
POL_HV193	100.00%	662
POL_HV192	99.90%	447
QCR7_HUMAN	100.00%	22
C42S1_HUMAN	95.00%	17
ACTY_HUMAN,ACTZ_HUMAN	100.00%	13
TRAT1_HUMAN	95.00%	2
SEP15_HUMAN	95.00%	4
NDUS4_HUMAN	99.90%	2
P5CR1_HUMAN	99.80%	14
VATL_HUMAN	95.00%	8
ELMO1_HUMAN	95.00%	7
TIM14_HUMAN	95.00%	3
GSTM2_HUMAN	99.90%	2
ACTB_HUMAN	100.00%	5221
KCAB2_HUMAN	100.00%	2
ATPO_HUMAN	100.00%	140
SYYC_HUMAN	100.00%	38
TCPD_HUMAN	100.00%	138
QCR1_HUMAN	100.00%	307
4F2_HUMAN	100.00%	441
RS2_HUMAN	100.00%	235
SRPRB_HUMAN	100.00%	35
TM109_HUMAN	95.00%	22
M4K1_HUMAN	95.00%	1
SNAA_HUMAN	100.00%	37
MANF_HUMAN	100.00%	110
CYBP_HUMAN	100.00%	19
NTAL_HUMAN	100.00%	57
PSA6_HUMAN	100.00%	26
LETM1_HUMAN	100.00%	41
ARPC4_HUMAN	100.00%	100
STK4_HUMAN	97.80%	5
RL36A_HUMAN,RL36L_HUMAN	100.00%	27
GGT1_HUMAN	100.00%	79
DHCR7_HUMAN	100.00%	56
IGKC_HUMAN	100.00%	107
ABRAL_HUMAN	100.00%	16
DIP2B_HUMAN	100.00%	67
TALDO_HUMAN	95.00%	3
TNAP3_HUMAN	100.00%	99
SFXN1_HUMAN	100.00%	53

RL31_HUMAN	100.00%	18
DGUOK_HUMAN	95.00%	1
GCDH_HUMAN	100.00%	7
PFKAP_HUMAN	100.00%	77
HCD2_HUMAN	100.00%	210
TB10B_HUMAN	95.00%	6
PSD12_HUMAN	95.00%	8
SC11C_HUMAN	100.00%	1
NDUAA_HUMAN	100.00%	23
PHB2_HUMAN	100.00%	271
CLIC2_HUMAN	100.00%	94
TMED9_HUMAN	100.00%	39
PPAC_HUMAN	100.00%	20
MTFP1_HUMAN	100.00%	9
CCR7_HUMAN	100.00%	25
TXTP_HUMAN	100.00%	60
PTBP1_HUMAN	100.00%	4
SRSF3_HUMAN	100.00%	37
SMD1_HUMAN	100.00%	15
SLAF7_HUMAN	100.00%	2
EMC8_HUMAN,gnl|unk|TRINITY_DN1475_c0_g1_i1_8	95.00%	1
RL13A_HUMAN	100.00%	83
RAP2B_HUMAN	99.90%	34
TEBP_HUMAN	100.00%	22
ITB7_HUMAN	100.00%	37
BZW1_HUMAN	100.00%	2
PGM1_HUMAN	100.00%	4
ABHDA_HUMAN	100.00%	2
SPCS1_HUMAN	95.00%	12
RS13_HUMAN	100.00%	170
PDCD4_HUMAN	99.80%	3
SYFA_HUMAN	100.00%	4
SC61B_HUMAN	95.00%	12
BCAT1_HUMAN	100.00%	44
HNRPU_HUMAN	100.00%	20
SATT_HUMAN	100.00%	138
ANO6_HUMAN	100.00%	4
ITIH2_HUMAN	100.00%	33
ANXA6_HUMAN	100.00%	751
TXNL1_HUMAN	95.00%	2
P5CR2_HUMAN	94.60%	5
PPP5_HUMAN	95.00%	3

PO210_HUMAN	95.00%	1
1C01_HUMAN	100.00%	627
RL3_HUMAN	100.00%	154
GCN1_HUMAN	100.00%	2
ODP2_HUMAN	100.00%	114
RALA_HUMAN	100.00%	87
JAK1_HUMAN	100.00%	24
RIPL2_HUMAN	99.80%	1
SNX2_HUMAN	100.00%	2
PRS6A_HUMAN	97.10%	1
ITB1_HUMAN	100.00%	4
RHG04_HUMAN	95.00%	1
PUR4_HUMAN	100.00%	3
G6PD_HUMAN	95.00%	1
SAC1_HUMAN	95.00%	4
CPIN1_HUMAN	95.00%	1
VAV_HUMAN	95.00%	1
ENOA_HUMAN	100.00%	1309
GBG2_HUMAN	100.00%	21
ARPC5_HUMAN	100.00%	62
FAAA_HUMAN	95.00%	6
H2B1B_HUMAN,H2B1O_HUMAN,H2B2E_HUMAN,H2B3B_HUMAN	100.00%	40
IL3RA_HUMAN	95.00%	8
HLAF_HUMAN	100.00%	25
41_HUMAN	100.00%	123
IF4E2_HUMAN	95.00%	2
EIF3C_HUMAN,EIFCL_HUMAN	100.00%	4
EZRI_HUMAN	100.00%	1117
RD23A_HUMAN	100.00%	3
CN166_HUMAN	99.80%	20
RL36_HUMAN	100.00%	41
SYK_HUMAN	100.00%	13
MTMRC_HUMAN	95.00%	3
CNNM3_HUMAN	100.00%	11
LYRIC_HUMAN	97.50%	2
SND1_HUMAN	100.00%	40
WASP_HUMAN	100.00%	8
PSD13_HUMAN	100.00%	16
SYLC_HUMAN	100.00%	16
PIMT_HUMAN	100.00%	8
RL23A_HUMAN	100.00%	11
MOT1_HUMAN	100.00%	110

PP1G_HUMAN	99.30%	125
PLXA1_HUMAN	100.00%	6
SCAM2_HUMAN	97.00%	12
TOR1A_HUMAN	95.00%	2
CPNE3_HUMAN	100.00%	47
RL7A_HUMAN	100.00%	188
DPM1_HUMAN	100.00%	19
CCL22_HUMAN	100.00%	32
PSA1_HUMAN	100.00%	35
GBB2_HUMAN	100.00%	282
RL22L_HUMAN	96.30%	11
LIN7A_HUMAN	100.00%	37
IDHC_HUMAN	96.40%	5
SEC62_HUMAN	100.00%	14
RAB5B_HUMAN	100.00%	48
PNPH_HUMAN	100.00%	97
MYO1G_HUMAN	100.00%	1109
SC22B_HUMAN	100.00%	25
DLDH_HUMAN	100.00%	156
SSDH_HUMAN	95.00%	1
CAPG_HUMAN	100.00%	52
MRP1_HUMAN	100.00%	70
NIBAN_HUMAN	100.00%	7
VATA_HUMAN	100.00%	19
TBB4B_HUMAN	100.00%	978
TNFL9_HUMAN	100.00%	32
SPCS2_HUMAN	100.00%	15
COR1A_HUMAN	100.00%	380
PIGS_HUMAN	96.80%	10
NEDD8_HUMAN,gnl|unk|TRINITY_DN4926_c0_g2_i1_4	95.00%	2
ATPD_HUMAN	100.00%	38
RL28_HUMAN	100.00%	55
RLA0_HUMAN	100.00%	116
BCAT2_HUMAN	100.00%	77
RS24_HUMAN	100.00%	54
ARF1_HUMAN,ARF3_HUMAN	100.00%	259
ACTN1_HUMAN	99.80%	146
NDRG3_HUMAN	100.00%	20
ANXA7_HUMAN	100.00%	83
BAG2_HUMAN	100.00%	7
TMED4_HUMAN	100.00%	22
S38A5_HUMAN	100.00%	33

EPN1_HUMAN	100.00%	13
SDF2_HUMAN	95.00%	5
RUXF_HUMAN	95.00%	1
DEST_HUMAN	100.00%	67
APOA1_HUMAN	95.00%	2
TTL12_HUMAN	95.00%	2
LDHB_HUMAN	100.00%	290
TNIP1_HUMAN	100.00%	5
THEM6_HUMAN	100.00%	6
DHRS7_HUMAN	100.00%	20
MCCA_HUMAN	100.00%	4
LRC8C_HUMAN	99.90%	1
PRS6B_HUMAN	99.80%	1
THIO_HUMAN	100.00%	84
ITB2_HUMAN	100.00%	77
SUCB2_HUMAN	100.00%	43
KAT3_HUMAN	100.00%	9
LIMA1_HUMAN	100.00%	27
SYIM_HUMAN	100.00%	1
BID_HUMAN	95.00%	5
VASP_HUMAN	100.00%	75
SSRA_HUMAN	100.00%	71
EFTS_HUMAN	100.00%	10
ACTBL_HUMAN	100.00%	530
1B41_HUMAN	100.00%	1065
FLVC1_HUMAN	100.00%	11
QOR_HUMAN	100.00%	5
LPCT4_HUMAN	100.00%	11
LTOR3_HUMAN	95.00%	1
STA5B_HUMAN	95.00%	2
HBB_HUMAN	100.00%	29
DLG1_HUMAN	95.00%	10
LRC57_HUMAN	100.00%	3
TBK1_HUMAN	95.00%	1
GSTK1_HUMAN	100.00%	29
HIBCH_HUMAN	100.00%	6
GTR1_HUMAN	100.00%	84
CY24B_HUMAN	97.90%	6
UGGG1_HUMAN	100.00%	60
IST1_HUMAN	100.00%	30
TAOK3_HUMAN	100.00%	2
IDI1_HUMAN	100.00%	3
RM45_HUMAN	95.00%	2

HPRT_HUMAN	100.00%	48
ITA4_HUMAN	100.00%	152
BAF_HUMAN	100.00%	37
IF2B3_HUMAN	97.00%	8
IL18R_HUMAN	100.00%	38
IL27B_HUMAN	100.00%	39
SLK_HUMAN	100.00%	19
H2A2A_HUMAN,H2A2C_HUMAN	100.00%	174
TCPQ_HUMAN	100.00%	237
NSF_HUMAN	99.90%	4
VPS28_HUMAN	100.00%	8
CCD50_HUMAN	98.30%	2
CNO10_HUMAN	95.00%	1
NEB2_HUMAN	99.90%	3
PRAF3_HUMAN	100.00%	29
OPA1_HUMAN	100.00%	58
FRIL_HUMAN	99.90%	13
PP1B_HUMAN	100.00%	161
SC6A6_HUMAN	95.00%	2
TOIP1_HUMAN	95.00%	5
ATAD1_HUMAN	98.20%	3
BLMH_HUMAN	99.90%	3
LRCH4_HUMAN	100.00%	2
ARC1B_HUMAN	100.00%	253
RUXG_HUMAN	95.00%	3
PAK2_HUMAN	100.00%	4
UCRI_HUMAN	100.00%	22
AT1B3_HUMAN	100.00%	196
VIME_HUMAN	100.00%	427
HM13_HUMAN	100.00%	13
ERG7_HUMAN	100.00%	18
RUVB1_HUMAN	100.00%	91
RT34_HUMAN	100.00%	11
EHD4_HUMAN	100.00%	149
IPO5_HUMAN	100.00%	37
COX6C_HUMAN	100.00%	28
CISD1_HUMAN	100.00%	27
IMDH2_HUMAN	100.00%	118
TP4A2_HUMAN	100.00%	23
RANG_HUMAN	100.00%	17
1433E_HUMAN	100.00%	261
CIP4_HUMAN	95.00%	1
RL23_HUMAN	100.00%	64

DDX5_HUMAN	100.00%	64
NDUA7_HUMAN	100.00%	34
HDAC1_HUMAN	95.00%	1
NP1L4_HUMAN	97.30%	27
SHIP1_HUMAN	100.00%	11
HNRPQ_HUMAN	100.00%	52
GNA15_HUMAN	100.00%	27
MILK1_HUMAN	99.80%	1
ZNT1_HUMAN	95.70%	1
RAB21_HUMAN	100.00%	62
ENPL_HUMAN	100.00%	971
RS18_HUMAN	100.00%	78
SYIC_HUMAN	100.00%	35
LTMD1_HUMAN	100.00%	18
ERAP1_HUMAN	100.00%	56
CP51A_HUMAN	100.00%	5
TFAM_HUMAN	100.00%	13
TAGL2_HUMAN	100.00%	190
CKAP5_HUMAN	97.60%	3
CALU_HUMAN	100.00%	14
OTUB1_HUMAN	100.00%	26
CSK2B_HUMAN	95.00%	1
COMT_HUMAN	100.00%	93
TPIS_HUMAN	100.00%	359
DNJC5_HUMAN	100.00%	38
RTCB_HUMAN	100.00%	28
CD80_HUMAN	100.00%	137
PKHF2_HUMAN	99.90%	11
SYWC_HUMAN	100.00%	24
APOE_HUMAN	100.00%	29
ITAL_HUMAN	100.00%	66
CD63_HUMAN	95.00%	5
PLEK_HUMAN	100.00%	64
XPO1_HUMAN	100.00%	8
FGR_HUMAN	100.00%	31
ATD3A_HUMAN	100.00%	72
ERBIN_HUMAN	99.90%	16
RT26_HUMAN	95.00%	1
E41L2_HUMAN	100.00%	3
PSME2_HUMAN	100.00%	46
BASP1_HUMAN	100.00%	164
HNRPK_HUMAN	100.00%	33
FEN1_HUMAN	95.00%	1

QCR8_HUMAN	100.00%	8
AT5F1_HUMAN	100.00%	123
SEPT6_HUMAN	100.00%	65
PLP2_HUMAN	95.00%	13
SYG_HUMAN	100.00%	18
FKBP2_HUMAN	100.00%	50
RRAS2_HUMAN	100.00%	77
IF2G_HUMAN	99.80%	7
CCD51_HUMAN	95.00%	1
RS27L_HUMAN,RS27_HUMAN	95.00%	5
CNIH4_HUMAN	95.00%	2
ADAS_HUMAN	100.00%	81
NDUV1_HUMAN	100.00%	30
PTSS1_HUMAN	95.00%	4
ICT1_HUMAN	95.00%	2
TRFL_HUMAN	99.90%	13
S43A3_HUMAN	100.00%	129
SYDM_HUMAN	100.00%	14
FMNL1_HUMAN	100.00%	55
CLPP_HUMAN	100.00%	2
TOP2A_HUMAN	100.00%	3
BAX_HUMAN	100.00%	8
RB27A_HUMAN	100.00%	124
SEPT2_HUMAN	100.00%	58
TBA1C_HUMAN	100.00%	646
EFGM_HUMAN	99.80%	5
PDIA3_HUMAN	100.00%	833
ADT2_HUMAN	100.00%	286
SGT1_HUMAN	95.00%	1
IQGA1_HUMAN	100.00%	356
SYEP_HUMAN	100.00%	36
NSDHL_HUMAN	100.00%	9
STX11_HUMAN	100.00%	81
MIC26_HUMAN	98.40%	4
DPP3_HUMAN	95.00%	4
GELS_HUMAN	100.00%	32
CSK_HUMAN	100.00%	67
PSB6_HUMAN	100.00%	12
DAF_HUMAN	100.00%	15
PGK1_HUMAN	100.00%	610
RS21_HUMAN	100.00%	12
PSB4_HUMAN	100.00%	14
UFM1_HUMAN	100.00%	5

RL15_HUMAN	100.00%	122
PI4KA_HUMAN	100.00%	11
P4HA1_HUMAN	100.00%	31
NDUA8_HUMAN	100.00%	29
HYAS1_HUMAN	95.00%	3
K22E_HUMAN	100.00%	14
RASK_HUMAN	100.00%	201
GRPE1_HUMAN	100.00%	27
RAB7L_HUMAN	100.00%	2
RS19_HUMAN	100.00%	24
EF1A1_HUMAN	100.00%	803
DQB1_HUMAN	100.00%	235
S38A1_HUMAN	95.00%	3
AGFG1_HUMAN	95.00%	3
UB2D2_HUMAN,UB2D3_HUMAN	95.00%	16
TIM50_HUMAN	100.00%	3
GHITM_HUMAN	95.00%	5
NDUS6_HUMAN	97.80%	2
FPPS_HUMAN	100.00%	68
APMAP_HUMAN	100.00%	50
GSTO1_HUMAN	100.00%	35
P3H1_HUMAN	95.00%	1
PLCC_HUMAN	95.00%	2
THIK_HUMAN	100.00%	16
ATD3B_HUMAN	99.90%	38
SAHH_HUMAN	100.00%	92
S61A1_HUMAN	100.00%	47
CD47_HUMAN	100.00%	51
F10A1_HUMAN	100.00%	43
RM15_HUMAN	95.00%	2
HMOX2_HUMAN	95.00%	4
SAMN1_HUMAN	100.00%	6
RT27_HUMAN	100.00%	12
TMEDA_HUMAN	100.00%	99
PHB_HUMAN	100.00%	204
TOP1_HUMAN	99.80%	3
GFPT1_HUMAN	100.00%	10
ALBU_HUMAN	100.00%	179
NDUA2_HUMAN	100.00%	2
S12A6_HUMAN	100.00%	40
HNRPL_HUMAN	100.00%	17
2AAA_HUMAN	100.00%	39
SEPT7_HUMAN	100.00%	63

TKFC_HUMAN	100.00%	14
RFTN1_HUMAN	100.00%	227
CTL2_HUMAN	100.00%	30
RN149_HUMAN	97.30%	2
NIPS2_HUMAN	100.00%	3
PUR2_HUMAN	100.00%	54
AT2B4_HUMAN	100.00%	100
MRRP3_HUMAN	95.00%	1
H12_HUMAN	97.20%	8
ATP5H_HUMAN	100.00%	125
LMAN1_HUMAN	100.00%	58
GYS1_HUMAN	95.00%	4
LONM_HUMAN	100.00%	80
OCAD1_HUMAN	95.00%	3
RS27A_HUMAN	100.00%	98
PGAM1_HUMAN	100.00%	182
DCTP1_HUMAN	100.00%	3
GAG_HV1MN	100.00%	4231
ADT3_HUMAN	100.00%	225
EIF3K_HUMAN	95.00%	1
1B47_HUMAN	100.00%	974
RT21_HUMAN	95.00%	2
SEC63_HUMAN	100.00%	7
RS28_HUMAN	100.00%	30
ERLN2_HUMAN	100.00%	10
PEX14_HUMAN	96.80%	10
MPC2_HUMAN	100.00%	8
HEM6_HUMAN	100.00%	147
MIC27_HUMAN	95.00%	2
SERPH_HUMAN	100.00%	100
SRP09_HUMAN	100.00%	39
GCSAM_HUMAN	100.00%	49
SEPT1_HUMAN	100.00%	9
LEG3_HUMAN	100.00%	13
ELOV5_HUMAN	95.00%	14
COPB2_HUMAN	100.00%	25
BDH_HUMAN	100.00%	75
EF2_HUMAN	100.00%	537
GRB2_HUMAN	100.00%	19
WASF2_HUMAN	100.00%	6
ROA1_HUMAN	100.00%	24
ATP5L_HUMAN	100.00%	86
1433Z_HUMAN	100.00%	236

ML12A_HUMAN,ML12B_HUMAN	100.00%	169
PPR18_HUMAN	100.00%	32
NAA15_HUMAN	100.00%	3
PSMG1_HUMAN	95.00%	4
NPM_HUMAN	100.00%	92
VDAC1_HUMAN	100.00%	419
GDS1_HUMAN	100.00%	3
RAN_HUMAN	100.00%	92
BASI_HUMAN	100.00%	346
DNJB2_HUMAN	95.00%	1
MZB1_HUMAN	100.00%	123
PKN1_HUMAN	95.00%	1
SYMC_HUMAN	100.00%	14
SH3K1_HUMAN	100.00%	24
NDUS7_HUMAN	100.00%	13
PSDE_HUMAN	100.00%	4
VPS4B_HUMAN	100.00%	14
SYTC_HUMAN	100.00%	9
LAT1_HUMAN	100.00%	36
FBLL1_HUMAN	98.00%	10
FA5_HUMAN	100.00%	24
UGPA_HUMAN	95.00%	3
CAB39_HUMAN	100.00%	48
MPCP_HUMAN	100.00%	155
RL5_HUMAN	100.00%	129
TCPG_HUMAN	100.00%	179
PSB1_HUMAN	100.00%	14
TFR1_HUMAN	100.00%	417
SPTN1_HUMAN	100.00%	876
BRI3B_HUMAN	95.00%	4
LAMP2_HUMAN	100.00%	37
MIC19_HUMAN	100.00%	27
RS5_HUMAN	100.00%	36
ECHM_HUMAN	100.00%	42
SAHH2_HUMAN	100.00%	39
ARF5_HUMAN	99.80%	159
RRAS_HUMAN	98.10%	22
RPN2_HUMAN	100.00%	182
ANX11_HUMAN	100.00%	34
HNRH1_HUMAN	100.00%	11
CISD2_HUMAN	100.00%	24
STT3A_HUMAN	100.00%	28
IF4G1_HUMAN	100.00%	4

GBP1_HUMAN	95.00%	12
STXB2_HUMAN	100.00%	67
PSB10_HUMAN	95.00%	10
RS14_HUMAN	100.00%	8
TOM22_HUMAN	100.00%	31
GPI8_HUMAN	95.00%	6
NDUS1_HUMAN	100.00%	80
MESD_HUMAN	99.80%	6
WDFY1_HUMAN	99.80%	3
PDLI1_HUMAN	100.00%	7
NDUB8_HUMAN	100.00%	16
C42S2_HUMAN	100.00%	15
OCAD2_HUMAN	95.00%	1
MACD1_HUMAN	100.00%	3
1C12_HUMAN	100.00%	757
USMG5_HUMAN	100.00%	14
GLIP1_HUMAN	100.00%	2
RT22_HUMAN	100.00%	10
TIM9_HUMAN	100.00%	2
KCY_HUMAN	100.00%	11
HG2A_HUMAN	100.00%	339
NECT1_HUMAN	100.00%	11
PSA3_HUMAN	97.40%	18
SRSF6_HUMAN	98.70%	1
AT5EL_HUMAN,ATP5E_HUMAN	95.00%	2
RAB7A_HUMAN	100.00%	161
RL10_HUMAN	100.00%	169
GLYM_HUMAN	100.00%	348
CATC_HUMAN	100.00%	10
PRS7_HUMAN	99.90%	9
PRPS1_HUMAN	100.00%	21
CPT2_HUMAN	100.00%	7
LY75_HUMAN	100.00%	84
KINH_HUMAN	97.10%	1
CSDE1_HUMAN	95.00%	1
AN32B_HUMAN	96.10%	5
ICAM1_HUMAN	100.00%	527
PRDX2_HUMAN	100.00%	57
MOB1A_HUMAN,MOB1B_HUMAN	100.00%	4
PABP1_HUMAN	100.00%	79
RS4X_HUMAN	100.00%	303
CAZA1_HUMAN	100.00%	172
DOCK8_HUMAN	100.00%	31

SC5A6_HUMAN	100.00%	16
ENV_HV1Z8	99.10%	28
KAD4_HUMAN	100.00%	5
OFUT1_HUMAN	100.00%	5
KPCB_HUMAN	100.00%	39
HSPB1_HUMAN	100.00%	5
RT14_HUMAN	95.00%	3
RL6_HUMAN	100.00%	151
TBCA_HUMAN	100.00%	14
OSTC_HUMAN	99.80%	24
CD37_HUMAN	100.00%	149
PSB2_HUMAN	100.00%	31
EF1A2_HUMAN	100.00%	292
NOP56_HUMAN	95.00%	1
DUT_HUMAN	100.00%	10
ALDOC_HUMAN	100.00%	222
TRPV2_HUMAN	100.00%	37
ESYT1_HUMAN	100.00%	26
PROSC_HUMAN	100.00%	2
STT3B_HUMAN	100.00%	32
GBG5_HUMAN	100.00%	29
RM24_HUMAN	95.00%	1
IF4G2_HUMAN	95.00%	1
CDS2_HUMAN	95.00%	7
ENV_HV1MN	100.00%	274
NUD10_HUMAN,NUD11_HUMAN,NUDT4_HUMAN	95.00%	1
EIF3F_HUMAN	100.00%	7
CEPT1_HUMAN	95.00%	6
ANXA2_HUMAN	100.00%	217
NDUS2_HUMAN	100.00%	45
RPIA_HUMAN	99.90%	5
ADRO_HUMAN	100.00%	6
NHRF1_HUMAN	100.00%	346
MOT4_HUMAN	100.00%	65
TNR5_HUMAN	100.00%	66
FLNB_HUMAN	100.00%	8
NNTM_HUMAN	100.00%	22
TCPB_HUMAN	100.00%	196
GP183_HUMAN	100.00%	8
VCAM1_HUMAN	100.00%	5
E41LB_HUMAN	95.00%	1
ENV_HV1B9	99.80%	33

IMB1_HUMAN	100.00%	43
SCRIB_HUMAN	100.00%	42
RT06_HUMAN	95.00%	4
ITAV_HUMAN	95.00%	3
PSA4_HUMAN	100.00%	18
SUMO3_HUMAN	95.00%	12
RADI_HUMAN	100.00%	955
SRSF7_HUMAN	100.00%	29
RM47_HUMAN	95.00%	6
DAD1_HUMAN	100.00%	12
ECH1_HUMAN	100.00%	165
TMX1_HUMAN	100.00%	61
IF4A1_HUMAN	100.00%	157
NUDC_HUMAN	100.00%	2
PLSL_HUMAN	100.00%	1376
HS74L_HUMAN	99.50%	6
DHE3_HUMAN	100.00%	216
ACO13_HUMAN	99.90%	13
OSBP2_HUMAN	94.90%	1
THY1_HUMAN	100.00%	18
AIFM1_HUMAN	100.00%	93
DDX3X_HUMAN	100.00%	30
CXCR4_HUMAN	95.00%	8
PGRC2_HUMAN	99.90%	1
AR6P1_HUMAN	95.00%	6
MRP4_HUMAN	100.00%	24
RSSA_HUMAN	100.00%	95
FA49B_HUMAN	100.00%	50
USP9X_HUMAN	99.80%	6
TOM70_HUMAN	100.00%	30
gnl|unk|TRINITY_DN1330_c0_g1_i1_4	95.00%	2
YBOX1_HUMAN	100.00%	12
ERG24_HUMAN	95.00%	1
ICOS_HUMAN	99.80%	23
ATPG_HUMAN	100.00%	164
ARF6_HUMAN	100.00%	184
ACTN4_HUMAN	100.00%	590
MRRP1_HUMAN	100.00%	4
CLH1_HUMAN	100.00%	790
TMED7_HUMAN	100.00%	4
DSRAD_HUMAN	95.00%	1
COX2_HUMAN	100.00%	66

PPOX_HUMAN	95.00%	1
TYK2_HUMAN	100.00%	22
RM03_HUMAN	95.00%	3
SRSF1_HUMAN	100.00%	16
ARPC3_HUMAN	100.00%	69
TMC8_HUMAN	100.00%	2
PKHO2_HUMAN	100.00%	7
ACPM_HUMAN	100.00%	66
C1TC_HUMAN	100.00%	104
RS26_HUMAN	100.00%	78
SRC_HUMAN	100.00%	77
RM39_HUMAN	95.00%	2
ETFB_HUMAN	100.00%	99
HACD3_HUMAN	100.00%	6
MYDGF_HUMAN	100.00%	22
GANAB_HUMAN	100.00%	571
RL35A_HUMAN	100.00%	45
SEP11_HUMAN	99.80%	52
MLEC_HUMAN	100.00%	65
DQA1_HUMAN	95.00%	70
SSRD_HUMAN	100.00%	74
INSR_HUMAN	100.00%	52
SYVN1_HUMAN	95.00%	5
RCD1_HUMAN	100.00%	6
TSP1_HUMAN	95.00%	1
DRA_HUMAN	100.00%	820
ANXA4_HUMAN	100.00%	65
ERO1A_HUMAN	100.00%	182
S12A2_HUMAN	100.00%	37
PA1B2_HUMAN	100.00%	15
TCPZ_HUMAN	100.00%	102
PLRKT_HUMAN	99.90%	1
CERS2_HUMAN	95.00%	2
AP1B1_HUMAN	100.00%	50
L2HDH_HUMAN	95.00%	5
FAF1_HUMAN	95.00%	2
S4A7_HUMAN	100.00%	104
AGK_HUMAN	100.00%	43
M2OM_HUMAN	100.00%	148
PP16B_HUMAN	100.00%	63
GTR14_HUMAN	100.00%	31
SRPRA_HUMAN	100.00%	7
AATM_HUMAN	100.00%	167

CCNY_HUMAN	97.40%	9
RALB_HUMAN	99.90%	60
MDHM_HUMAN	100.00%	609
NIT2_HUMAN	100.00%	10
SIPA1_HUMAN	100.00%	6
RAP1B_HUMAN	100.00%	390
PNPT1_HUMAN	100.00%	11
ZDH20_HUMAN	95.00%	2
RM48_HUMAN	95.00%	2
SYVM_HUMAN	95.00%	2
K1C10_HUMAN	100.00%	17
H2B1M_HUMAN	100.00%	62
DERL1_HUMAN	95.00%	2
CC50A_HUMAN	100.00%	23
HCDH_HUMAN	100.00%	29
AP2A2_HUMAN	100.00%	52
RGAP1_HUMAN	100.00%	70
EIF3A_HUMAN	100.00%	20
gnl|unk|TRINITY_DN3896_c0_g1_i1_2	95.00%	9
ASAH1_HUMAN	95.00%	1
KAD3_HUMAN	99.90%	9
TBB5_HUMAN	100.00%	1090
RL34_HUMAN	100.00%	13
PBIP1_HUMAN	95.00%	1
ASCC3_HUMAN	99.70%	1
DREB_HUMAN	100.00%	36
TB10A_HUMAN	100.00%	11
MARK3_HUMAN	97.70%	9
PYRG1_HUMAN	100.00%	21
MUC18_HUMAN	100.00%	32
SIT1_HUMAN	100.00%	37
MTX2_HUMAN	95.00%	4
TMCO1_HUMAN	100.00%	19
CYFP2_HUMAN	100.00%	44
PLOD3_HUMAN	100.00%	5
MPPA_HUMAN	100.00%	17
ARL2_HUMAN	100.00%	4
CLIC1_HUMAN	100.00%	806
PEBP1_HUMAN	100.00%	31
SDF2L_HUMAN	100.00%	18
CPNE1_HUMAN	100.00%	104
TRAF3_HUMAN	100.00%	4

ODO2_HUMAN	100.00%	72
ERP29_HUMAN	100.00%	59
SLAF6_HUMAN	100.00%	24
PDC10_HUMAN	100.00%	44
H2AY_HUMAN	97.80%	1
ARK72_HUMAN	100.00%	13
ACOT8_HUMAN	100.00%	7
HMCS1_HUMAN	100.00%	4
TAP2_HUMAN	100.00%	9
GRHPR_HUMAN	100.00%	56
VTNC_HUMAN	95.00%	87
AP2B1_HUMAN	100.00%	59
FSCN1_HUMAN	100.00%	406
DQA2_HUMAN	100.00%	227
ATPB_HUMAN	100.00%	990
ERF3A_HUMAN	100.00%	12
SYDC_HUMAN	100.00%	128
ANXA5_HUMAN	100.00%	11
TMED2_HUMAN	97.50%	8
KPYM_HUMAN	100.00%	1210
FLOT1_HUMAN	100.00%	258
1A31_HUMAN	100.00%	1112
SNP23_HUMAN	100.00%	93
SYRC_HUMAN	100.00%	15
TBA4A_HUMAN	100.00%	736
AL5AP_HUMAN	95.00%	9
CALX_HUMAN	100.00%	369
EMC1_HUMAN	100.00%	31
ACPH_HUMAN	96.70%	1
SCOT1_HUMAN	100.00%	53
EHD1_HUMAN	100.00%	912
HS105_HUMAN	100.00%	83
LACB2_HUMAN	100.00%	5
RL26L_HUMAN	100.00%	6
ACSL3_HUMAN	100.00%	65
LASP1_HUMAN	100.00%	10
EF1G_HUMAN	100.00%	116
LGUL_HUMAN	100.00%	13
STML2_HUMAN	100.00%	77
HLAE_HUMAN	100.00%	216
H2A1B_HUMAN,H2A1C_HUMAN,H2A3_HUMAN	100.00%	155
UCHL3_HUMAN	95.00%	14

DKC1_HUMAN	100.00%	4
CUL3_HUMAN	95.00%	4
ST17B_HUMAN	95.00%	2
LTOR1_HUMAN	100.00%	13
NCLN_HUMAN	100.00%	41
ETFA_HUMAN	100.00%	200
RL35_HUMAN	100.00%	45
NDUB9_HUMAN	100.00%	6
MARCS_HUMAN	100.00%	129
TRAP1_HUMAN	100.00%	209
RL18_HUMAN	100.00%	234
RL7_HUMAN	100.00%	245
RB22A_HUMAN	100.00%	16
FDFT_HUMAN	100.00%	11
MPPB_HUMAN	100.00%	25
1A23_HUMAN	98.60%	836
ST38L_HUMAN	97.80%	5
CD22_HUMAN	100.00%	29
ABCE1_HUMAN	100.00%	3
ITPA_HUMAN	99.90%	5
HABP2_HUMAN	98.30%	8
UB2L3_HUMAN	100.00%	24
TPM3_HUMAN	100.00%	237
AL1B1_HUMAN	100.00%	70
PDIA6_HUMAN	100.00%	369
HS90B_HUMAN	100.00%	653
OXA1L_HUMAN	99.80%	1
NPTN_HUMAN	100.00%	7
SODM_HUMAN	100.00%	32
PPIB_HUMAN	100.00%	349
MPZL1_HUMAN	100.00%	19
MICA1_HUMAN	95.00%	10
FUMH_HUMAN	100.00%	96
BST2_HUMAN	95.00%	20
PSMD7_HUMAN	100.00%	15
APT_HUMAN	100.00%	40
RD23B_HUMAN	100.00%	41
TBB4A_HUMAN	100.00%	817
RAB10_HUMAN	100.00%	143
XRCC6_HUMAN	100.00%	7
RTN3_HUMAN	97.50%	6
FABP5_HUMAN	100.00%	70
RL27_HUMAN	100.00%	123

IDH3G_HUMAN	100.00%	18
RASN_HUMAN	100.00%	207
TFG_HUMAN	100.00%	5
VDAC3_HUMAN	100.00%	175
TMED3_HUMAN	100.00%	16
FLOT2_HUMAN	100.00%	214
C1QBP_HUMAN	100.00%	202
ARP5L_HUMAN	100.00%	41
SLAF1_HUMAN	100.00%	93
BROX_HUMAN	100.00%	21
RUXE_HUMAN	95.00%	18
EMC2_HUMAN	100.00%	10
LDHA_HUMAN	100.00%	423
PKHF1_HUMAN	99.20%	3
AT1B1_HUMAN	100.00%	32
SAR1A_HUMAN	99.50%	9
RHG01_HUMAN	95.00%	4
ERGI3_HUMAN	95.00%	1
SUCB1_HUMAN	100.00%	36
CH60_HUMAN	100.00%	1290
PPIF_HUMAN	100.00%	20
XRP2_HUMAN	100.00%	37
GMFG_HUMAN	100.00%	26
DHB4_HUMAN	100.00%	125
NDUC2_HUMAN	95.00%	1
RHOG_HUMAN	100.00%	240
HSDL2_HUMAN	98.40%	4
RL21_HUMAN	100.00%	89
NDUA5_HUMAN	100.00%	14
IDH3A_HUMAN	100.00%	94
GNA13_HUMAN	100.00%	111
EVI2B_HUMAN	95.00%	1
SPEE_HUMAN	100.00%	4
HBA_HUMAN	100.00%	122
PTPRC_HUMAN	100.00%	838
COPG1_HUMAN	100.00%	16
ERMP1_HUMAN	95.00%	5
6PGL_HUMAN	95.00%	1
RL19_HUMAN	100.00%	25
CHID1_HUMAN	100.00%	29
SAM50_HUMAN	100.00%	48
POTEF_HUMAN	100.00%	1014
CDC42_HUMAN	100.00%	249

DNJC3_HUMAN	100.00%	9
RL27A_HUMAN	100.00%	42
DIAP1_HUMAN	100.00%	18
ARP2_HUMAN	100.00%	143
PLCH1_HUMAN	95.00%	2
PSD11_HUMAN	100.00%	11
EF1B_HUMAN	100.00%	24
THIOM_HUMAN	95.00%	1
VATB1_HUMAN	95.00%	1
CD59_HUMAN	100.00%	45
K2C1_HUMAN	100.00%	94
AT11C_HUMAN	100.00%	34
KPRB_HUMAN	100.00%	4
EXOC1_HUMAN	100.00%	3
RUVB2_HUMAN	100.00%	56
RL30_HUMAN	100.00%	184
NDUB4_HUMAN	100.00%	3
RL14_HUMAN	100.00%	142
GRP75_HUMAN	100.00%	564
RL13_HUMAN	100.00%	66
AIMP1_HUMAN	100.00%	15
DEFI6_HUMAN	100.00%	5
AT2B1_HUMAN	100.00%	103
RS25_HUMAN	100.00%	59
PP1A_HUMAN	100.00%	167
APOC3_HUMAN	95.00%	10
PLST_HUMAN	100.00%	245
GDIR2_HUMAN	100.00%	155
ICAM3_HUMAN	100.00%	247
AATC_HUMAN	100.00%	43
PLEC_HUMAN	99.90%	3
F162A_HUMAN	100.00%	17
PP2AA_HUMAN,PP2AB_HUMAN	99.90%	1
SEPT9_HUMAN	100.00%	58
PRKDC_HUMAN	100.00%	4
MDHC_HUMAN	100.00%	108
CNDP2_HUMAN	100.00%	7
PDIA1_HUMAN	100.00%	492
FKB11_HUMAN	100.00%	17
CD70_HUMAN	100.00%	479
SYVC_HUMAN	100.00%	24
RM21_HUMAN	95.00%	5
ABCF1_HUMAN	95.00%	6

PI42A_HUMAN	100.00%	24
TRAF1_HUMAN	100.00%	32
MIRO2_HUMAN	95.00%	7
AFG32_HUMAN	100.00%	21
PSMD2_HUMAN	100.00%	18
REEP5_HUMAN	95.00%	10
RM19_HUMAN	100.00%	10
DYN2_HUMAN	100.00%	4
GDIB_HUMAN	100.00%	127
RAB8B_HUMAN	100.00%	262
RS8_HUMAN	100.00%	230
RENT1_HUMAN	100.00%	12
RL22_HUMAN	100.00%	19
NDUA6_HUMAN	100.00%	40
IDH3B_HUMAN	100.00%	24
1B07_HUMAN	100.00%	887
EMC7_HUMAN	100.00%	9
BRK1_HUMAN	95.00%	1
AT2A3_HUMAN	99.80%	42
RS17_HUMAN	100.00%	22
PIPNB_HUMAN	100.00%	5
NB5R3_HUMAN	100.00%	150
TWF2_HUMAN	100.00%	34
RS15A_HUMAN	100.00%	60
MLF2_HUMAN	100.00%	6
SH3L3_HUMAN	95.00%	12
ARP3_HUMAN	100.00%	320
MACF1_HUMAN	99.90%	2
NPS3A_HUMAN	100.00%	15
PGAM5_HUMAN	100.00%	16
FLNA_HUMAN	100.00%	691
AP2M1_HUMAN	100.00%	76
GTR5_HUMAN	95.00%	17
RL10A_HUMAN	100.00%	21
RT25_HUMAN	100.00%	11
RAB2A_HUMAN	100.00%	37
PSME1_HUMAN	100.00%	41
CECR5_HUMAN	100.00%	26
AKAP2_HUMAN	100.00%	20
COPB_HUMAN	100.00%	42
SPRY4_HUMAN	100.00%	8
2B17_HUMAN	100.00%	862
DYHC1_HUMAN	100.00%	4

URP2_HUMAN	100.00%	197
IF4A3_HUMAN	100.00%	14
RGS19_HUMAN	100.00%	15
RS11_HUMAN	100.00%	85
TBRG4_HUMAN	100.00%	12
AIMP2_HUMAN	95.00%	18
ES1_HUMAN	100.00%	43
DNJA1_HUMAN	100.00%	35
PRDX5_HUMAN	100.00%	92
THIC_HUMAN	100.00%	41
NIPS1_HUMAN	100.00%	183
1A02_HUMAN	100.00%	1332
SNG2_HUMAN	99.60%	1
HINT2_HUMAN	100.00%	21
CLPB_HUMAN	100.00%	12
3HIDH_HUMAN	95.00%	4
PABP4_HUMAN	100.00%	34
ADT1_HUMAN	99.90%	127
EFR3A_HUMAN	100.00%	13
ADPGK_HUMAN	95.00%	5
SPTB2_HUMAN	100.00%	1052
IPYR_HUMAN	100.00%	76
MIC25_HUMAN	95.00%	1
HNRPD_HUMAN	100.00%	9
CD226_HUMAN	100.00%	41
PREB_HUMAN	100.00%	6
CLPT1_HUMAN	95.00%	1
RT17_HUMAN	95.00%	1
RUS1_HUMAN	100.00%	4
RL9_HUMAN	100.00%	112
PRPF3_HUMAN	95.00%	1
YKT6_HUMAN	100.00%	4
PSMD3_HUMAN	100.00%	2
ISOC2_HUMAN	100.00%	11
TMM68_HUMAN	100.00%	9
PSB5_HUMAN	94.70%	1
RAC1_HUMAN	100.00%	171
ACSL4_HUMAN	100.00%	187
RS9_HUMAN	100.00%	165
UBA1_HUMAN	100.00%	115
RS20_HUMAN	100.00%	52
NENF_HUMAN	95.00%	1
ENOG_HUMAN	100.00%	275

DECR_HUMAN	100.00%	44
MOGS_HUMAN	100.00%	50
1B51_HUMAN,1B78_HUMAN	100.00%	1099
EIF3I_HUMAN	95.00%	3
SLIRP_HUMAN	100.00%	16
NDUS5_HUMAN	100.00%	10
SC5A3_HUMAN	100.00%	10
SODC_HUMAN	100.00%	19
DX39B_HUMAN	100.00%	13
AHSA1_HUMAN	100.00%	17
DBNL_HUMAN	100.00%	34
ACTC_HUMAN	100.00%	1811
TNR8_HUMAN	100.00%	18
PARK7_HUMAN	100.00%	91
ADA10_HUMAN	100.00%	17
TCPE_HUMAN	100.00%	110
RM14_HUMAN	95.00%	1
QCR2_HUMAN	100.00%	129
RS3_HUMAN	100.00%	159
DOPD_HUMAN	100.00%	61
G3P_HUMAN	100.00%	952
ACD11_HUMAN	95.00%	1
SRC8_HUMAN	99.80%	3
RT09_HUMAN	100.00%	9
CD99_HUMAN	100.00%	18
FAK2_HUMAN	100.00%	1
PSA7_HUMAN	100.00%	35
DHSO_HUMAN	100.00%	34
A2MG_HUMAN	100.00%	21
TMX4_HUMAN	95.00%	4
KAPCA_HUMAN	100.00%	3
RS12_HUMAN	100.00%	62
QSOX2_HUMAN	95.00%	2
TCTP_HUMAN	100.00%	23
NDUF4_HUMAN	95.00%	12
MYL6_HUMAN	100.00%	180
ADA_HUMAN	100.00%	17
PLXB2_HUMAN	100.00%	40
PUR1_HUMAN	99.90%	3
LYN_HUMAN	99.30%	27
MIF_HUMAN	100.00%	120
DNJA2_HUMAN	100.00%	11
PRDX6_HUMAN	100.00%	117

CORO7_HUMAN	100.00%	29
SYSC_HUMAN	100.00%	13
LFA3_HUMAN	100.00%	28
F234A_HUMAN	95.00%	6
CD79B_HUMAN	95.00%	2
DHX9_HUMAN	100.00%	4
DDB1_HUMAN	97.60%	3
UBE2N_HUMAN	100.00%	50
PFD6_HUMAN	95.00%	1
SGMR1_HUMAN	95.00%	4
ROA2_HUMAN	100.00%	3
TERA_HUMAN	100.00%	95
KTHY_HUMAN	100.00%	1
RAP2C_HUMAN	100.00%	33
T200A_HUMAN	100.00%	12
PLMN_HUMAN	100.00%	32
CATA_HUMAN	100.00%	75
IF2A_HUMAN	100.00%	15
CD19_HUMAN	97.20%	1
PCBP1_HUMAN	100.00%	97
RL37A_HUMAN	95.00%	6
CTL1_HUMAN	95.00%	3
SSRG_HUMAN	95.00%	27
MCA3_HUMAN	100.00%	13
PDCD5_HUMAN	100.00%	8
SYFB_HUMAN	100.00%	6
LCAP_HUMAN	100.00%	22
OXYR_HUMAN	95.00%	1
ITIH3_HUMAN	99.80%	5
TPM4_HUMAN	100.00%	286
S39AA_HUMAN	99.90%	11
PPP6_HUMAN	95.00%	4
NDUBA_HUMAN	100.00%	20
KAD2_HUMAN	100.00%	59
PEA15_HUMAN	95.00%	3
TIM16_HUMAN	95.00%	1
RASL3_HUMAN	100.00%	545
SF3B1_HUMAN	100.00%	16
RT12_HUMAN	99.80%	1
PLCL2_HUMAN	100.00%	3
RL4_HUMAN	100.00%	317
EMB_HUMAN	97.60%	7
HMGB1_HUMAN	100.00%	35

GNAQ_HUMAN	99.90%	1
LAMP1_HUMAN	99.80%	16
TACO1_HUMAN	99.80%	2
RPN1_HUMAN	100.00%	491
RAB6A_HUMAN	100.00%	36
MP2K1_HUMAN	95.00%	1
SE1L1_HUMAN	95.00%	8
ALDOA_HUMAN	100.00%	611
ENOB_HUMAN	98.60%	356
CMC1_HUMAN	100.00%	52
SHKB1_HUMAN	99.90%	6
LEG1_HUMAN	100.00%	160
CO1A2_HUMAN	98.80%	1
NONO_HUMAN	95.00%	5
ENTP1_HUMAN	100.00%	196
EIF3D_HUMAN	100.00%	4
IF5_HUMAN	99.80%	1
ILVBL_HUMAN	99.80%	1
TS101_HUMAN	100.00%	40
NDUV2_HUMAN	100.00%	27
VATH_HUMAN	95.00%	5
RAB35_HUMAN	100.00%	167
SPCS3_HUMAN	100.00%	15
ATPK_HUMAN	100.00%	55
GLU2B_HUMAN	100.00%	119
NDUAC_HUMAN	100.00%	35
VAT1_HUMAN	95.00%	2
SCAM3_HUMAN	95.00%	1
CLIC4_HUMAN	100.00%	149
ADHX_HUMAN	95.00%	2
AAAT_HUMAN	100.00%	266
SORCN_HUMAN	100.00%	22
RS3A_HUMAN	100.00%	225
IDHP_HUMAN	100.00%	358
TREX1_HUMAN	95.00%	8
SUMO1_HUMAN	95.00%	6
SMD3_HUMAN	95.00%	9
CLM8_HUMAN	100.00%	3
NACAM_HUMAN	100.00%	14
NTF2_HUMAN	100.00%	13
RBP2_HUMAN	99.90%	1
RAB5C_HUMAN	100.00%	53
SERA_HUMAN	100.00%	31

PACN2_HUMAN	100.00%	102
ESTD_HUMAN	100.00%	2
PCBP2_HUMAN	100.00%	79
PLS3_HUMAN	99.90%	3
PFKAL_HUMAN	100.00%	90
VAMP5_HUMAN	97.70%	9
STAT1_HUMAN	100.00%	12
PRDX1_HUMAN	100.00%	212
CTR1_HUMAN	100.00%	19
PDCD6_HUMAN	95.00%	8
PIGT_HUMAN	100.00%	4
RL29_HUMAN	100.00%	21
CAP1_HUMAN	100.00%	80
RLA1_HUMAN	100.00%	39
COTL1_HUMAN	100.00%	44
HUWE1_HUMAN	100.00%	8
ARF4_HUMAN	100.00%	149
IF5A1_HUMAN,IF5AL_HUMAN	100.00%	67
MMAB_HUMAN	95.00%	3
TMED5_HUMAN	100.00%	3
GATM_HUMAN	100.00%	11
TPSN_HUMAN	100.00%	76
H4_HUMAN	100.00%	215
DTNA_HUMAN	94.70%	4
CNPY2_HUMAN	100.00%	43
RM01_HUMAN	95.00%	3
1C03_HUMAN	100.00%	723
CTGE5_HUMAN,MIA2_HUMAN	95.00%	15
TMC6_HUMAN	100.00%	15
UB2V1_HUMAN	100.00%	14
S10AB_HUMAN	98.30%	1
GLSK_HUMAN	100.00%	12
BTF3_HUMAN,gnl|unk|TRINITY_DN883_c0_g1_i1_4,gnl|unk|TRINITY_DN883_c0_g2_i1_5	95.00%	6
MCCB_HUMAN	100.00%	15
CD86_HUMAN	99.80%	14
GOGA7_HUMAN	100.00%	27
GBB1_HUMAN	100.00%	354
MSMO1_HUMAN	96.10%	2
PRDX3_HUMAN	100.00%	154
CHM4B_HUMAN	100.00%	56
CSK21_HUMAN,CSK23_HUMAN	100.00%	28

PTCD3_HUMAN	100.00%	11
GLRX1_HUMAN	97.40%	1
NICA_HUMAN	100.00%	64
DDX6_HUMAN	100.00%	11
PSA_HUMAN	99.80%	2
RAC2_HUMAN	100.00%	252
HSP7C_HUMAN	100.00%	1004
EH1L1_HUMAN	96.50%	3
CYB5B_HUMAN	100.00%	40
PAGE5_HUMAN	95.00%	11
TM205_HUMAN	100.00%	24
GLGB_HUMAN	100.00%	55
NDKA_HUMAN	100.00%	179
RL38_HUMAN	100.00%	19
DDX17_HUMAN	100.00%	50
AL9A1_HUMAN	100.00%	3
CAPZB_HUMAN	100.00%	155
TXND5_HUMAN	100.00%	221
NDUB1_HUMAN	100.00%	13
PDXK_HUMAN	95.00%	2
IF6_HUMAN	100.00%	9
FNBP1_HUMAN	100.00%	39
TNR4_HUMAN	95.00%	8
PTH2_HUMAN	95.00%	14
TCPA_HUMAN	100.00%	201
NDUB5_HUMAN	100.00%	9
QPCTL_HUMAN	95.00%	7
RTN4_HUMAN	100.00%	32
SUMF2_HUMAN	100.00%	4
KAP0_HUMAN	100.00%	8
DHB12_HUMAN	100.00%	101
KPCD_HUMAN	100.00%	27
DPM3_HUMAN	95.00%	12
TM9S2_HUMAN	95.00%	1
RHG15_HUMAN	97.60%	2
RM46_HUMAN	95.00%	3
LSP1_HUMAN	100.00%	269
EF1D_HUMAN	100.00%	56
ITA5_HUMAN	99.90%	2
PX11B_HUMAN	100.00%	10
EBP_HUMAN	100.00%	4
FCRLA_HUMAN	99.90%	1
MPU1_HUMAN	100.00%	4

FA98A_HUMAN	95.00%	1
PGRC1_HUMAN	100.00%	16
RL32_HUMAN	100.00%	56
ATLA3_HUMAN	100.00%	9
VP37B_HUMAN	95.00%	2
PFKAM_HUMAN	98.90%	23
TM214_HUMAN	95.00%	4
SDHA_HUMAN	100.00%	82
COPT1_HUMAN	95.00%	11
IVD_HUMAN	100.00%	3
COF1_HUMAN	100.00%	1188
gnl|unk|TRINITY_DN119_c0_g2_i1_3	95.00%	52
FADS2_HUMAN	100.00%	27
IGHG1_HUMAN	100.00%	141
RLA2_HUMAN	100.00%	101
WDR11_HUMAN	95.00%	1
ECHA_HUMAN	100.00%	97
ZCHC3_HUMAN	100.00%	7
ACADV_HUMAN	100.00%	48
TYB4_HUMAN	100.00%	19
MAGT1_HUMAN	99.90%	13
ERP44_HUMAN	100.00%	61
CNPY3_HUMAN	99.90%	2
SURF4_HUMAN	100.00%	15
MIC60_HUMAN	100.00%	120
TMM33_HUMAN	100.00%	23
DRB4_HUMAN	100.00%	208
CH10_HUMAN	100.00%	223
LEUK_HUMAN	100.00%	109
COX8A_HUMAN	95.00%	1
MYO1C_HUMAN	100.00%	361
MRP_HUMAN	99.90%	54
RM38_HUMAN	100.00%	4
STOM_HUMAN	100.00%	41
ACBP_HUMAN	99.90%	3
RL18A_HUMAN	100.00%	141
TLDC1_HUMAN	95.00%	6
TP4A3_HUMAN	100.00%	13
IL16_HUMAN	100.00%	39
OST48_HUMAN	100.00%	174
1433F_HUMAN	100.00%	70
EFTU_HUMAN	100.00%	487

DHB7_HUMAN	95.00%	1
GNPI1_HUMAN	100.00%	2
FA10_HUMAN	95.00%	2
RL24_HUMAN	100.00%	71
CD3E_HUMAN,gnl|unk|TRINITY_DN2282_c0_g1_i1_5	95.00%	8
HNRPR_HUMAN	100.00%	22
MOES_HUMAN	100.00%	2077
STK10_HUMAN	100.00%	49
NDKB_HUMAN	100.00%	138
DOCK2_HUMAN	100.00%	20
LRC59_HUMAN	95.00%	7
STIP1_HUMAN	100.00%	76
TBB6_HUMAN	99.90%	283
PFD2_HUMAN	100.00%	8
ERAP2_HUMAN	100.00%	2
NDUAD_HUMAN	100.00%	33
PYR1_HUMAN	100.00%	81
ACAD9_HUMAN	100.00%	9
B2MG_HUMAN	100.00%	149
CD81_HUMAN	100.00%	158
CD48_HUMAN	100.00%	531
GNAS1_HUMAN	100.00%	262
K1C9_HUMAN	100.00%	11
XPO2_HUMAN	100.00%	15
RAP1A_HUMAN	100.00%	411
PDIP2_HUMAN	95.00%	1
ACON_HUMAN	100.00%	118
ACDSB_HUMAN	100.00%	7
TKT_HUMAN	100.00%	67
ARPC2_HUMAN	100.00%	202
PTCA_HUMAN	100.00%	27
TMM43_HUMAN	100.00%	32
KIF23_HUMAN	100.00%	93
AP2A1_HUMAN	100.00%	79
EXOC4_HUMAN	95.00%	1
ACLY_HUMAN	100.00%	69
ACS2L_HUMAN	100.00%	7
EVL_HUMAN	100.00%	45
MYH9_HUMAN	100.00%	2243
GRP78_HUMAN	100.00%	1104
SDHB_HUMAN	100.00%	76
LPXN_HUMAN	100.00%	2

CISY_HUMAN	100.00%	198
GT251_HUMAN	95.00%	3
MARK2_HUMAN	100.00%	22
SC11A_HUMAN	100.00%	17
RAB14_HUMAN	100.00%	70
ZDHC5_HUMAN	100.00%	35
MTX1_HUMAN	100.00%	20
KDIS_HUMAN	100.00%	8
PUR8_HUMAN	100.00%	20
CD20_HUMAN	100.00%	507
ECHB_HUMAN	100.00%	58
THRB_HUMAN	95.00%	4
PARP1_HUMAN	100.00%	4
CDC37_HUMAN	100.00%	20
FMNL3_HUMAN	100.00%	22
ODO1_HUMAN	100.00%	40
PDIA4_HUMAN	100.00%	328
PDC6I_HUMAN	100.00%	161
CASP1_HUMAN	100.00%	21
DPA1_HUMAN	100.00%	50
SMD2_HUMAN	100.00%	2
RT36_HUMAN	95.00%	17
MYO1D_HUMAN	100.00%	18
ZCCHV_HUMAN	100.00%	20
PGES2_HUMAN	100.00%	12
SNTB2_HUMAN	97.70%	7
AMPL_HUMAN	100.00%	49
1433G_HUMAN	100.00%	104
SPP24_HUMAN	95.00%	3
PA2G4_HUMAN	100.00%	38
CLCA_HUMAN	100.00%	4
MARE1_HUMAN	100.00%	39
ATPA_HUMAN	100.00%	659
NDUA9_HUMAN	100.00%	38
COX41_HUMAN	100.00%	80
SDCB1_HUMAN	100.00%	162
PPIL1_HUMAN	100.00%	19
TMED1_HUMAN	95.00%	8
TXD17_HUMAN	100.00%	17
S38A2_HUMAN	95.00%	1
PFD3_HUMAN	95.00%	1
AK1A1_HUMAN	100.00%	45
HAX1_HUMAN	95.00%	4

CSRP1_HUMAN	100.00%	21
PUR9_HUMAN	100.00%	271
FAH2A_HUMAN,FAH2B_HUMAN	95.00%	3
OXLA_HUMAN	100.00%	4
DHRS4_HUMAN	100.00%	20
ACOT1_HUMAN	100.00%	6
CD82_HUMAN	100.00%	46
THIL_HUMAN	100.00%	114
ERGI1_HUMAN	100.00%	9
ESAM_HUMAN	100.00%	4
AN32A_HUMAN	100.00%	3
HVCN1_HUMAN	97.40%	16
BOLA2_HUMAN	100.00%	3
RT28_HUMAN	96.50%	11
LPPRC_HUMAN	100.00%	370
DDX1_HUMAN	99.90%	4
CL17A_HUMAN	100.00%	26
HNRPM_HUMAN	100.00%	7
EXOC5_HUMAN	100.00%	7
PTPRA_HUMAN	100.00%	26
ODPA_HUMAN	100.00%	124
TLN1_HUMAN	100.00%	215
FKBP4_HUMAN	100.00%	6
MB12A_HUMAN	95.00%	5
MAOM_HUMAN	100.00%	68
RL17_HUMAN	100.00%	97
IFM1_HUMAN	100.00%	50
FETUA_HUMAN	95.00%	6
KCNN4_HUMAN	100.00%	2
RS29_HUMAN	100.00%	9
GIMA5_HUMAN	100.00%	26
PANX1_HUMAN	95.00%	1
RCN1_HUMAN	100.00%	47
gnl|unk|TRINITY_DN2533_c0_g2_i1_7	100.00%	48
CN37_HUMAN	100.00%	22
LMAN2_HUMAN	100.00%	79
PPIA_HUMAN	100.00%	720
GSTP1_HUMAN	100.00%	345
FAS_HUMAN	100.00%	263
AT1A1_HUMAN	100.00%	935
PDIA5_HUMAN	100.00%	5
HS90A_HUMAN	100.00%	773

BAP31_HUMAN	100.00%	77
COX5A_HUMAN	100.00%	51
NDUB3_HUMAN	100.00%	4
CNN2_HUMAN	100.00%	178
RBG1L_HUMAN	100.00%	14
RB11B_HUMAN	100.00%	100
MVP_HUMAN	98.90%	1
CQ062_HUMAN	100.00%	3
S1PR4_HUMAN	100.00%	6
COR1C_HUMAN	100.00%	125
PSMD6_HUMAN	95.00%	1
6PGD_HUMAN	100.00%	64
RL11_HUMAN	100.00%	41
PRS10_HUMAN	100.00%	12
S29A1_HUMAN	100.00%	102
RS23_HUMAN	100.00%	28
CY1_HUMAN	100.00%	77
AP180_HUMAN	97.10%	5
NAV1_HUMAN	99.90%	1
PRC1_HUMAN	100.00%	3
SCO1_HUMAN	100.00%	6
ILK_HUMAN	100.00%	9
CAN1_HUMAN	100.00%	6
VDAC2_HUMAN	100.00%	250
NCPR_HUMAN	100.00%	38
SELPL_HUMAN	95.00%	1
PRAX_HUMAN	95.80%	3
GPX7_HUMAN	100.00%	5
NDUS8_HUMAN	100.00%	18
CAND1_HUMAN	100.00%	24
SYPL1_HUMAN	95.00%	10
STIM1_HUMAN	100.00%	11
CIB1_HUMAN	100.00%	53
THIM_HUMAN	100.00%	25
ERGI2_HUMAN,gnl|unk|TRINITY_DN1533_c0_g2_i1_4,gnl|unk|TRINITY_DN1533_c0_g2_i1_7	95.00%	4
TCPH_HUMAN	100.00%	64
MTCH2_HUMAN	100.00%	60
CLDN1_HUMAN	100.00%	18
UBC12_HUMAN	95.00%	1
LSM2_HUMAN	95.00%	3
RS6_HUMAN	100.00%	125

JAK3_HUMAN	100.00%	4
RT29_HUMAN	100.00%	8
1433B_HUMAN	100.00%	88
CALM_HUMAN	100.00%	22
RHOF_HUMAN	100.00%	137
GLPC_HUMAN	95.00%	4
TSN14_HUMAN	95.00%	4
TECR_HUMAN	100.00%	8
NDUA4_HUMAN	95.00%	7
NP1L1_HUMAN	100.00%	112
SCRB1_HUMAN	100.00%	100
TNIK_HUMAN	100.00%	12
STXB3_HUMAN	100.00%	87
ODPB_HUMAN	100.00%	144
RS15_HUMAN	100.00%	115
TOM40_HUMAN	100.00%	61
PROF1_HUMAN	100.00%	462
TXD12_HUMAN	100.00%	32
DJB11_HUMAN	100.00%	49
HYOU1_HUMAN	100.00%	430
AP2S1_HUMAN	100.00%	3
KDSR_HUMAN	100.00%	4
CALR_HUMAN	100.00%	523
KV101_HUMAN,KV102_HUMAN,KV108_HUMAN,KV115_HUMAN,KV116_HUMAN,KV117_HUMAN,KV125_HUMAN	95.00%	19
HINT1_HUMAN	99.90%	1
SYNC_HUMAN	100.00%	13
RCN2_HUMAN	99.80%	4
SH3L1_HUMAN	100.00%	32
NOMO1_HUMAN,NOMO3_HUMAN	100.00%	21
IPYR2_HUMAN	100.00%	38
GPR15_HUMAN	100.00%	21
TIM44_HUMAN	100.00%	11
MPI_HUMAN	95.00%	1
P5CS_HUMAN	100.00%	17
PEX16_HUMAN	99.90%	1
COX5B_HUMAN	100.00%	38
GSHR_HUMAN	100.00%	2
ATP6_HUMAN	95.00%	7
CD2_HUMAN	95.00%	4
SYQ_HUMAN	100.00%	19

NU1M_HUMAN	95.00%	8
HCLS1_HUMAN	100.00%	39
SERC_HUMAN	100.00%	56
WDR1_HUMAN	100.00%	282
RL12_HUMAN	100.00%	29
RDH11_HUMAN	100.00%	18
SUSD3_HUMAN	95.00%	18
ROA3_HUMAN	100.00%	27
CX6B1_HUMAN	100.00%	18
NUCB1_HUMAN	100.00%	7
TRUA_HUMAN	95.00%	1
GDIR1_HUMAN	100.00%	84
TPP1_HUMAN	95.00%	1
UBP14_HUMAN	100.00%	5
CS052_HUMAN	95.00%	2
U2AF1_HUMAN,U2AF5_HUMAN	100.00%	4
CKAP4_HUMAN	100.00%	14
PLCE_HUMAN	100.00%	11
EIF3M_HUMAN	100.00%	8
CAZA2_HUMAN	100.00%	52
ACOD_HUMAN	95.00%	3
DECR2_HUMAN	100.00%	2
FCER2_HUMAN	100.00%	79
S52A2_HUMAN	95.00%	4
GNAI2_HUMAN	100.00%	605
NCKPL_HUMAN	100.00%	8
PLCG2_HUMAN	100.00%	64
MTDC_HUMAN	100.00%	13
HSP74_HUMAN	100.00%	22
PUR6_HUMAN	100.00%	70
ACTG_HUMAN	100.00%	4972
CYTB_HUMAN	100.00%	8
RAB1A_HUMAN	100.00%	191
LIRB1_HUMAN	100.00%	11
TBCB_HUMAN	95.00%	4
CYC_HUMAN	100.00%	28
PSMD1_HUMAN	100.00%	3
MGST1_HUMAN	95.00%	10
DJC11_HUMAN	95.00%	9
PSB3_HUMAN	100.00%	6
ARL8B_HUMAN	100.00%	14
RAB8A_HUMAN	100.00%	337
RS7_HUMAN	100.00%	49

FKB1A_HUMAN	100.00%	37
MPP6_HUMAN	100.00%	74
CP054_HUMAN	100.00%	38
ACADM_HUMAN	100.00%	19
AT2A2_HUMAN	100.00%	112
RS16_HUMAN	100.00%	130
MOV10_HUMAN	100.00%	61
PI51A_HUMAN	95.00%	4
EIF3G_HUMAN	95.00%	4
STX4_HUMAN	100.00%	38
PIPNA_HUMAN	96.80%	2
NDUS3_HUMAN	100.00%	89
LYPA1_HUMAN	100.00%	36
BAHC1_HUMAN	95.00%	14
MYADM_HUMAN	95.00%	9
STK26_HUMAN	100.00%	35
1433T_HUMAN	100.00%	81
ZCCHL_HUMAN	99.70%	1
TNR6_HUMAN	100.00%	115
MPRD_HUMAN	100.00%	17
POL_HV1Z2	100.00%	1504
POL_HV1YF	100.00%	683
FETA_HUMAN	100.00%	13
POL_HV1Y2	100.00%	3133
CD44_HUMAN	100.00%	348
RM12_HUMAN	100.00%	29
IQGA2_HUMAN	100.00%	188
SRP14_HUMAN	100.00%	34
LACTB_HUMAN	99.90%	1
TM41A_HUMAN	100.00%	11
DPYL2_HUMAN	98.30%	9
RHOA_HUMAN	100.00%	279
PEF1_HUMAN	100.00%	10
CX7A2_HUMAN	100.00%	47
CD97_HUMAN	100.00%	129
TM9S4_HUMAN	100.00%	13
SCPDL_HUMAN	100.00%	14
RAE1L_HUMAN	99.80%	1
PCKGM_HUMAN	100.00%	41
FYN_HUMAN	100.00%	55
PSA5_HUMAN	100.00%	35
COPA_HUMAN	100.00%	138
RHG17_HUMAN	100.00%	14

PD1L1_HUMAN	100.00%	9
POL_HV1RH	100.00%	1646
GRSF1_HUMAN	95.00%	6
NLTP_HUMAN	100.00%	66
IF4A2_HUMAN	99.90%	83
RS10_HUMAN	100.00%	3
DAAM1_HUMAN	100.00%	3
POL_HV1OY	100.00%	2653
TNAP2_HUMAN	95.00%	2
TADBP_HUMAN	95.00%	5
POL_HV1MP	100.00%	836
SYAC_HUMAN	100.00%	18
POL_HV1MN	100.00%	2925
NUCB2_HUMAN	100.00%	3
NUCL_HUMAN	100.00%	53
RACK1_HUMAN	100.00%	100
S10A4_HUMAN	99.90%	5
VAMP8_HUMAN	95.00%	7
GNA1_HUMAN	95.00%	6
FA65B_HUMAN	100.00%	5
PRDX4_HUMAN	100.00%	84
POL_HV1JR	100.00%	2894

Table 4b. All proteins identified for the HIV-1(MN)CL.4/CEMx174(T1).

Protein accession numbers	Protein identification probability	Total spectrum count
GRK6_HUMAN	100.00%	15
POL_HV1J3	100.00%	4591
HS71A_HUMAN,HS71B_HUMAN	100.00%	216
GNAI3_HUMAN	100.00%	256
POL_HV1ET	100.00%	1513
POL_HV1EL	100.00%	4744
CD53_HUMAN	99.80%	31
PRS4_HUMAN	95.00%	13
1B18_HUMAN	100.00%	669
POL_HV1B9	100.00%	5932
RAB1B_HUMAN	100.00%	245
RL8_HUMAN	100.00%	25
POL_HV1A2	100.00%	6876
CPNS1_HUMAN	99.80%	2
VATE1_HUMAN	100.00%	4

OLA1_HUMAN	100.00%	20
ATP5I_HUMAN	95.00%	4
G6PI_HUMAN	100.00%	97
VAPA_HUMAN	100.00%	40
ATP5L_HUMAN	100.00%	41
PRS8_HUMAN	100.00%	3
VTA1_HUMAN	100.00%	86
POL_HV19N	100.00%	1615
POL_HV197	100.00%	2127
POL_HV196	100.00%	2675
POL_HV193	100.00%	2147
POL_HV192	100.00%	1306
ANTR1_HUMAN	100.00%	4
CD109_HUMAN	100.00%	3
ACYP1_HUMAN	99.90%	2
ITIH1_HUMAN	99.80%	5
SEP15_HUMAN	95.00%	1
CXAR_HUMAN	100.00%	19
PA1B3_HUMAN	100.00%	11
VATL_HUMAN	95.00%	6
ACTB_HUMAN	100.00%	2308
IL2RG_HUMAN	100.00%	25
SYYC_HUMAN	100.00%	43
TCPD_HUMAN	100.00%	109
QCR1_HUMAN	100.00%	27
4F2_HUMAN	100.00%	769
RS2_HUMAN	100.00%	127
TM109_HUMAN	95.00%	3
SNAA_HUMAN	100.00%	23
MANF_HUMAN	100.00%	4
CD38_HUMAN	100.00%	605
CYBP_HUMAN	100.00%	35
IGSF8_HUMAN	100.00%	205
AP1B1_HUMAN	100.00%	41
LETM1_HUMAN	100.00%	7
ARPC4_HUMAN	100.00%	84
PSN1_HUMAN	99.80%	14
DHCR7_HUMAN	100.00%	13
ABRAL_HUMAN	100.00%	2
DIP2B_HUMAN	100.00%	56
SFXN1_HUMAN	100.00%	33
ASNS_HUMAN	100.00%	12
IF2G_HUMAN	100.00%	5

STMN1_HUMAN	100.00%	21
ABI2_HUMAN	100.00%	2
PFKAP_HUMAN	100.00%	44
HCD2_HUMAN	100.00%	57
PSD12_HUMAN	95.00%	4
PAIP1_HUMAN	95.00%	1
PHB2_HUMAN	100.00%	106
VP26A_HUMAN	100.00%	15
CBPN_HUMAN	95.00%	2
TMED9_HUMAN	100.00%	15
RLA1_HUMAN	95.00%	7
TIM14_HUMAN	95.00%	1
TXTP_HUMAN	100.00%	28
1C07_HUMAN	100.00%	512
HMGA1_HUMAN	100.00%	12
SRSF3_HUMAN	100.00%	15
PURA_HUMAN	100.00%	23
SMD1_HUMAN	100.00%	11
H2AV_HUMAN,H2AZ_HUMAN	100.00%	107
RL13A_HUMAN	100.00%	40
OTUB1_HUMAN	100.00%	7
RAP2B_HUMAN	100.00%	38
MMAB_HUMAN	95.00%	1
PLS1_HUMAN	95.00%	17
PGM1_HUMAN	99.80%	6
GCSAM_HUMAN	100.00%	4
RS13_HUMAN	100.00%	35
MSI2H_HUMAN	100.00%	43
LDLR_HUMAN	100.00%	66
HNRPU_HUMAN	100.00%	11
SATT_HUMAN	100.00%	20
ANO6_HUMAN	100.00%	26
ITIH2_HUMAN	100.00%	60
ANXA6_HUMAN	100.00%	461
SYQ_HUMAN	95.00%	1
PTN1_HUMAN	99.90%	1
RL3_HUMAN	100.00%	90
ODP2_HUMAN	100.00%	17
RALA_HUMAN	100.00%	47
JAK1_HUMAN	99.70%	1
gnl|unk|TRINITY_DN764_c26_g3_i1_5	99.80%	40
SNX2_HUMAN	100.00%	7
ITB1_HUMAN	100.00%	354

G6PD_HUMAN	100.00%	10
SAC1_HUMAN	100.00%	10
BT3L4_HUMAN	99.90%	4
ENOA_HUMAN	100.00%	993
CHMP3_HUMAN	100.00%	17
CO4A5_HUMAN	98.00%	2
1B08_HUMAN	100.00%	756
CO3_HUMAN	100.00%	110
EIF3C_HUMAN,EIFCL_HUMAN	100.00%	3
EZRI_HUMAN	100.00%	1071
IF4H_HUMAN	95.00%	4
CN166_HUMAN	95.00%	1
RL36_HUMAN	100.00%	15
SYK_HUMAN	99.90%	1
ILF3_HUMAN	100.00%	5
MKRN1_HUMAN	98.00%	1
WASP_HUMAN	100.00%	134
PSD13_HUMAN	99.50%	3
SYLC_HUMAN	100.00%	6
PIMT_HUMAN	100.00%	17
RL23A_HUMAN	100.00%	8
MOT1_HUMAN	100.00%	108
PLXA1_HUMAN	100.00%	3
SCAM2_HUMAN	99.80%	18
KCAB2_HUMAN	95.00%	2
VP26B_HUMAN	100.00%	26
CPNE3_HUMAN	100.00%	29
RL7A_HUMAN	100.00%	89
IGSF3_HUMAN	100.00%	37
LTOR1_HUMAN	100.00%	18
PSA1_HUMAN	100.00%	10
PURB_HUMAN	100.00%	4
GBB2_HUMAN	100.00%	276
RAB5B_HUMAN	100.00%	59
ACTZ_HUMAN	100.00%	19
PNPH_HUMAN	100.00%	16
MYO1G_HUMAN	100.00%	159
SC22B_HUMAN	100.00%	22
CLCB_HUMAN	100.00%	53
MRP1_HUMAN	100.00%	7
VATA_HUMAN	100.00%	12
TBB4B_HUMAN	100.00%	1258
CD320_HUMAN	95.00%	6

PRAF2_HUMAN	95.00%	3
DHPR_HUMAN	95.50%	1
COR1A_HUMAN	100.00%	218
RTN4_HUMAN	100.00%	11
RL28_HUMAN	100.00%	6
RLA0_HUMAN	100.00%	46
TSP4_HUMAN	99.90%	13
ARHG1_HUMAN	100.00%	104
ACTN1_HUMAN	100.00%	67
NDRG3_HUMAN	99.80%	3
ANXA7_HUMAN	100.00%	39
BUB3_HUMAN	99.80%	1
TMED4_HUMAN	100.00%	2
ARC1A_HUMAN	100.00%	31
RUXF_HUMAN	100.00%	4
ERI3_HUMAN	97.00%	5
DEST_HUMAN	98.50%	1
LDHB_HUMAN	100.00%	264
RHEB_HUMAN	100.00%	3
THIO_HUMAN	100.00%	29
EHD3_HUMAN	98.40%	91
ITB2_HUMAN	100.00%	78
SUCB2_HUMAN	95.00%	1
PICAL_HUMAN	100.00%	3
SSRA_HUMAN	100.00%	20
HYES_HUMAN	100.00%	19
1B41_HUMAN	99.90%	685
LBR_HUMAN	99.30%	1
VPS36_HUMAN	100.00%	4
ANXA1_HUMAN	100.00%	237
HBB_HUMAN	100.00%	96
LRC57_HUMAN	100.00%	23
TWF2_HUMAN	100.00%	23
UBP5_HUMAN	100.00%	3
GSTK1_HUMAN	100.00%	6
UGGG1_HUMAN	100.00%	7
PORIM_HUMAN	95.00%	1
IST1_HUMAN	100.00%	96
MCP_HUMAN	95.00%	16
PKHG1_HUMAN	100.00%	2
VINC_HUMAN	100.00%	1
TAOK3_HUMAN	100.00%	7
IDI1_HUMAN	95.00%	3

RELL1_HUMAN	95.00%	2
HPRT_HUMAN	100.00%	5
ITA4_HUMAN	100.00%	527
H2B1J_HUMAN	100.00%	215
BAF_HUMAN	100.00%	14
IF2B3_HUMAN	100.00%	19
SLK_HUMAN	100.00%	9
HBEGF_HUMAN	100.00%	12
H2A2A_HUMAN,H2A2C_HUMAN	100.00%	295
STAM1_HUMAN	100.00%	7
RL31_HUMAN,gnl|unk|TRINITY_DN2162_c0_g2_i1_5	95.00%	6
TCPQ_HUMAN	100.00%	280
VPS28_HUMAN	100.00%	201
CNO10_HUMAN	100.00%	4
GIT2_HUMAN	95.00%	6
PRAF3_HUMAN	99.80%	1
RS26_HUMAN	100.00%	40
TCPG_HUMAN	100.00%	202
PP1B_HUMAN	100.00%	17
NCKP1_HUMAN	99.90%	1
KIRR1_HUMAN	100.00%	39
TM55B_HUMAN	95.00%	2
FMNL1_HUMAN	100.00%	16
BLMH_HUMAN	100.00%	6
ARC1B_HUMAN	100.00%	84
PAK2_HUMAN	100.00%	93
AT1B3_HUMAN	100.00%	201
VIME_HUMAN	100.00%	12
ERG7_HUMAN	100.00%	3
LCK_HUMAN	100.00%	461
IPO5_HUMAN	100.00%	9
COX6C_HUMAN	100.00%	14
IMDH2_HUMAN	100.00%	30
AT2B1_HUMAN	99.90%	25
SND1_HUMAN	100.00%	2
PPIH_HUMAN	100.00%	18
TP4A2_HUMAN	100.00%	74
RANG_HUMAN	100.00%	26
1433E_HUMAN	100.00%	220
CIP4_HUMAN	100.00%	10
LAT_HUMAN	95.00%	6
gnl|unk|TRINITY_DN3129_c0_g1_i1_18	95.00%	4
RL23_HUMAN	100.00%	7

DDX5_HUMAN	99.80%	22
SHIP1_HUMAN	100.00%	27
ZAP70_HUMAN	100.00%	11
HNRPQ_HUMAN	100.00%	78
RAB21_HUMAN	100.00%	20
ENPL_HUMAN	100.00%	293
RS18_HUMAN	100.00%	51
SYIC_HUMAN	100.00%	21
SH3G1_HUMAN	100.00%	9
CALU_HUMAN	99.90%	2
CSK2B_HUMAN	100.00%	24
COMT_HUMAN	100.00%	8
TPIS_HUMAN	100.00%	199
DNJC5_HUMAN	100.00%	27
SYWC_HUMAN	100.00%	19
ITAL_HUMAN	100.00%	42
CD63_HUMAN	95.00%	16
TNPO1_HUMAN	97.00%	1
XPO1_HUMAN	100.00%	2
ATD3A_HUMAN	100.00%	3
SERC5_HUMAN	95.00%	2
RHOC_HUMAN	100.00%	721
DNJC7_HUMAN	95.00%	1
CD5_HUMAN	100.00%	251
BGLR_HUMAN	95.00%	2
AT5F1_HUMAN	100.00%	46
SEPT6_HUMAN	100.00%	38
PLP2_HUMAN	100.00%	57
APOH_HUMAN	99.00%	4
SYG_HUMAN	100.00%	26
RRAS2_HUMAN	100.00%	22
VPS29_HUMAN	100.00%	29
RL15_HUMAN	100.00%	49
RS27L_HUMAN,RS27_HUMAN	100.00%	13
S43A3_HUMAN	100.00%	15
KIRR2_HUMAN	95.00%	1
RAB8A_HUMAN	100.00%	293
CLPP_HUMAN	100.00%	5
CD151_HUMAN	99.00%	18
PSA6_HUMAN	100.00%	11
PDIA3_HUMAN	100.00%	354
ADT2_HUMAN	100.00%	197
IQGA1_HUMAN	100.00%	173

GDIA_HUMAN	100.00%	93
HSP77_HUMAN	96.00%	149
SYEP_HUMAN	100.00%	59
RHOG_HUMAN	100.00%	169
STX11_HUMAN	95.00%	1
DPP3_HUMAN	95.00%	8
ELOC_HUMAN	99.40%	1
PSMF1_HUMAN	95.00%	4
GELS_HUMAN	100.00%	57
CSK_HUMAN	100.00%	22
TB10B_HUMAN	95.00%	1
GSHB_HUMAN	99.20%	1
DAF_HUMAN	100.00%	84
PGK1_HUMAN	100.00%	642
PSB4_HUMAN	100.00%	2
PI4KA_HUMAN	100.00%	3
GAG_HV2KR	100.00%	14
K22E_HUMAN	100.00%	45
RASK_HUMAN	100.00%	114
TIAR_HUMAN	99.80%	1
E41L5_HUMAN	100.00%	17
RS19_HUMAN	100.00%	9
PTN11_HUMAN	95.00%	2
S38A1_HUMAN	100.00%	14
UB2D2_HUMAN,UB2D3_HUMAN	100.00%	16
FPPS_HUMAN	100.00%	37
APMAP_HUMAN	100.00%	4
GSTO1_HUMAN	100.00%	30
SAHH_HUMAN	100.00%	34
ELAV1_HUMAN	95.00%	3
RBBP4_HUMAN	100.00%	2
CD47_HUMAN	100.00%	91
F10A1_HUMAN	100.00%	229
APCD1_HUMAN	100.00%	3
ATX2_HUMAN	99.90%	7
TMEDA_HUMAN	100.00%	89
PHB_HUMAN	100.00%	109
TOP1_HUMAN	100.00%	3
GFPT1_HUMAN	100.00%	21
CHSP1_HUMAN	96.30%	1
ALBU_HUMAN	100.00%	180
CD6_HUMAN	95.00%	7
HNRPL_HUMAN	99.90%	4

2AAA_HUMAN	100.00%	60
IF2B2_HUMAN	100.00%	43
SEPT7_HUMAN	100.00%	32
GAG_HV1Y2	100.00%	6847
RS30_HUMAN	95.00%	1
RFTN1_HUMAN	100.00%	6
CTL2_HUMAN	100.00%	33
GAG_HV1W2	100.00%	6157
RN149_HUMAN	95.00%	5
MCTS1_HUMAN	95.00%	8
PUR2_HUMAN	95.00%	2
FBP1L_HUMAN	100.00%	57
AT2B4_HUMAN	100.00%	32
H12_HUMAN	100.00%	283
ATP5H_HUMAN	100.00%	54
LCAP_HUMAN	100.00%	66
LMAN1_HUMAN	100.00%	15
LONM_HUMAN	100.00%	26
CYFP1_HUMAN	99.90%	42
RS27A_HUMAN	100.00%	209
PGAM1_HUMAN	100.00%	157
ARPC5_HUMAN	100.00%	26
GAG_HV1MN	100.00%	6225
ADT3_HUMAN	99.90%	144
NSMA2_HUMAN	100.00%	39
ABR_HUMAN	100.00%	18
MPC2_HUMAN	95.00%	4
PO210_HUMAN	100.00%	3
SERPH_HUMAN	100.00%	26
HNRPF_HUMAN	100.00%	11
SRP09_HUMAN	100.00%	21
UBE2K_HUMAN	95.00%	3
gnl|unk|TRINITY_DN2950_c0_g1_i1_2	100.00%	14
COPB2_HUMAN	96.60%	1
DNPH1_HUMAN	99.90%	6
KS6A1_HUMAN	95.00%	4
CO6A1_HUMAN	100.00%	8
BDH_HUMAN	100.00%	6
EF2_HUMAN	100.00%	315
GRB2_HUMAN	100.00%	29
WASF2_HUMAN	100.00%	6
ROA1_HUMAN	100.00%	55
GAG_HV1C4	100.00%	5198

ML12A_HUMAN,ML12B_HUMAN	100.00%	40
NPM_HUMAN	100.00%	48
VDAC1_HUMAN	100.00%	221
GDS1_HUMAN	100.00%	17
RAN_HUMAN	100.00%	105
BASI_HUMAN	100.00%	231
MZB1_HUMAN	100.00%	33
PKN1_HUMAN	100.00%	103
SYMC_HUMAN	100.00%	11
VPS4B_HUMAN	100.00%	97
HSP72_HUMAN	94.50%	493
SYTC_HUMAN	100.00%	18
LAT1_HUMAN	100.00%	202
FA5_HUMAN	100.00%	54
ODO1_HUMAN	99.90%	7
UGPA_HUMAN	100.00%	49
CAB39_HUMAN	100.00%	62
MPCP_HUMAN	100.00%	89
RL5_HUMAN	100.00%	70
S61A1_HUMAN,S61A2_HUMAN	95.00%	12
GSLG1_HUMAN	100.00%	21
HMGB2_HUMAN	99.90%	16
PSB1_HUMAN	99.90%	7
LSM1_HUMAN	95.00%	1
TFR1_HUMAN	100.00%	274
SPTN1_HUMAN	100.00%	11
LAMP2_HUMAN	100.00%	35
RS5_HUMAN	100.00%	21
M4K4_HUMAN	100.00%	16
RRAS_HUMAN	100.00%	17
RPN2_HUMAN	100.00%	44
ANX11_HUMAN	100.00%	89
GNA11_HUMAN	100.00%	40
CD1C_HUMAN	100.00%	45
HNRPK_HUMAN	100.00%	81
STXB2_HUMAN	100.00%	2
BDH2_HUMAN	97.70%	5
DHSO_HUMAN	100.00%	29
TOM22_HUMAN	98.10%	17
ASSY_HUMAN	98.70%	1
gnl|unk|TRINITY_DN764_c26_g1_i1_5,gnl|unk|TRINITY_DN764_c26_g2_i1_5	99.80%	53
MERL_HUMAN	100.00%	11

HNRPC_HUMAN	100.00%	9
MACD1_HUMAN	100.00%	5
SAR1A_HUMAN	99.90%	10
ACTBL_HUMAN	100.00%	282
DPYL2_HUMAN	100.00%	13
OCAD2_HUMAN	100.00%	8
PSA3_HUMAN	95.00%	6
HGS_HUMAN	100.00%	5
SEPT2_HUMAN	100.00%	28
RAB7A_HUMAN	100.00%	172
WIPF1_HUMAN	100.00%	21
GLYM_HUMAN	100.00%	207
SFPQ_HUMAN	100.00%	9
PRPS1_HUMAN	100.00%	28
PCBP3_HUMAN	98.50%	97
POL_HV1H2	100.00%	8018
N2DL2_HUMAN	100.00%	18
DLDH_HUMAN	100.00%	29
ICAM1_HUMAN	100.00%	57
PRDX2_HUMAN	100.00%	79
MOB1A_HUMAN,MOB1B_HUMAN	100.00%	23
PABP1_HUMAN	100.00%	488
POL_HV1ND	100.00%	3698
RS4X_HUMAN	100.00%	117
CAZA1_HUMAN	100.00%	101
POL_HV1OY	100.00%	7793
ACAP1_HUMAN	100.00%	21
CD1B_HUMAN	100.00%	219
RL38_HUMAN	95.00%	7
CA2D2_HUMAN	99.50%	2
SF3B3_HUMAN	95.00%	1
RL6_HUMAN	100.00%	103
TBCA_HUMAN	100.00%	16
UB2V2_HUMAN	97.50%	17
OSTC_HUMAN	95.00%	2
PSB2_HUMAN	100.00%	8
CNOT1_HUMAN	100.00%	72
U5S1_HUMAN	100.00%	16
NOP56_HUMAN	95.00%	7
DUT_HUMAN	98.00%	9
RB11B_HUMAN	100.00%	125
SH21A_HUMAN	100.00%	4
ENV_HV1S1	100.00%	435

CSK22_HUMAN	99.00%	11
ALDOC_HUMAN	100.00%	18
P2RY8_HUMAN	99.90%	3
ESYT1_HUMAN	100.00%	5
STT3B_HUMAN	99.90%	1
ARRD1_HUMAN	100.00%	6
GBG5_HUMAN	100.00%	42
GMFG_HUMAN	100.00%	17
ENV_HV1MA	100.00%	176
ENV_HV1LW	99.60%	398
EIF3F_HUMAN	100.00%	7
LASP1_HUMAN	100.00%	28
ANXA2_HUMAN	99.90%	2
ENV_HV1JR	100.00%	325
ROR2_HUMAN	100.00%	12
NHRF1_HUMAN	100.00%	338
LAIR1_HUMAN	95.00%	3
NNTM_HUMAN	100.00%	24
TCPB_HUMAN	100.00%	162
DCTP1_HUMAN	95.00%	1
STIP1_HUMAN	100.00%	17
IMB1_HUMAN	100.00%	57
SCRIB_HUMAN	100.00%	17
CUL3_HUMAN	100.00%	4
PSA4_HUMAN	100.00%	8
RADI_HUMAN	100.00%	811
SRSF7_HUMAN	100.00%	20
AGFG1_HUMAN	99.40%	2
DAD1_HUMAN	95.00%	6
ITA6_HUMAN	100.00%	105
ECH1_HUMAN	100.00%	53
TMX1_HUMAN	100.00%	30
IF4A1_HUMAN	100.00%	148
NUDC_HUMAN	100.00%	2
PLSL_HUMAN	100.00%	610
DHE3_HUMAN	100.00%	52
AIFM1_HUMAN	95.00%	1
CXCR4_HUMAN	100.00%	15
ENV_HV196	100.00%	89
RSSA_HUMAN	100.00%	81
FA49B_HUMAN	100.00%	35
YBOX1_HUMAN	100.00%	164
ATPG_HUMAN	100.00%	64

ARF6_HUMAN	100.00%	113
ACTN4_HUMAN	100.00%	109
CLH1_HUMAN	100.00%	4231
TMED7_HUMAN	100.00%	2
DSRAD_HUMAN	95.00%	2
COX2_HUMAN	100.00%	15
EPN4_HUMAN	95.00%	11
CCR5_HUMAN	100.00%	4
EHD4_HUMAN	100.00%	100
SRSF1_HUMAN	100.00%	19
ARPC3_HUMAN	100.00%	61
TMC8_HUMAN	95.00%	1
EIF3I_HUMAN	100.00%	3
ACPM_HUMAN	97.40%	1
C1TC_HUMAN	100.00%	94
COPG1_HUMAN	99.90%	1
MYDGF_HUMAN	95.00%	6
GANAB_HUMAN	100.00%	196
RL35A_HUMAN	99.20%	3
BACH_HUMAN	100.00%	14
SSRD_HUMAN	100.00%	17
CD1E_HUMAN	99.40%	34
LIS1_HUMAN	100.00%	2
RL36A_HUMAN,RL36L_HUMAN,gnl|unk|TRINITY_DN498_c0_g1_i1_4	100.00%	9
RCD1_HUMAN	100.00%	37
TSP1_HUMAN	100.00%	34
RHG17_HUMAN	100.00%	18
gnl|unk|TRINITY_DN557_c0_g2_i1_7	95.10%	39
H1X_HUMAN	94.60%	1
ERO1A_HUMAN	100.00%	21
S12A2_HUMAN	95.00%	3
AIMP2_HUMAN	95.00%	4
TCPZ_HUMAN	100.00%	97
TEST_HUMAN	100.00%	14
MCM3_HUMAN	100.00%	3
RUVB1_HUMAN	100.00%	16
S4A7_HUMAN	100.00%	27
M2OM_HUMAN	100.00%	40
VAX2_HUMAN	98.30%	1
GTR14_HUMAN	95.40%	25
AATM_HUMAN	100.00%	48
A2MG_HUMAN	100.00%	270

MDHM_HUMAN	100.00%	169
RAP1B_HUMAN	100.00%	291
NIF3L_HUMAN	95.00%	1
K1C10_HUMAN	100.00%	48
CC50A_HUMAN	100.00%	17
HCDH_HUMAN	100.00%	54
AP2A2_HUMAN	99.00%	19
EMB_HUMAN	95.00%	2
EFNB2_HUMAN	95.00%	7
EIF3A_HUMAN	100.00%	7
PRS6A_HUMAN	95.00%	2
TBB5_HUMAN	100.00%	1380
RL34_HUMAN	99.30%	14
GILT_HUMAN	95.00%	2
DCK_HUMAN	96.20%	1
TB10A_HUMAN	100.00%	25
BCAT2_HUMAN	100.00%	5
YBOX2_HUMAN	98.60%	41
PYRG1_HUMAN	100.00%	10
MUC18_HUMAN	100.00%	50
SIT1_HUMAN	100.00%	54
CYFP2_HUMAN	100.00%	76
CLIC1_HUMAN	100.00%	267
PEBP1_HUMAN	100.00%	12
CJ088_HUMAN	100.00%	9
NED4L_HUMAN	95.00%	1
ODO2_HUMAN	100.00%	11
ERP29_HUMAN	100.00%	14
PDC10_HUMAN	100.00%	43
H2AY_HUMAN	100.00%	31
ARK72_HUMAN	100.00%	18
DOC11_HUMAN	100.00%	8
ILK_HUMAN	98.10%	13
VTNC_HUMAN	95.00%	74
CUX1_HUMAN	100.00%	3
AP2B1_HUMAN	99.90%	29
VAMP2_HUMAN,VAMP3_HUMAN	95.00%	12
RL22_HUMAN,gnl|unk|TRINITY_DN567_c1_g1_i1_6	100.00%	30
ATPO_HUMAN	100.00%	81
LST8_HUMAN	95.00%	1
ATPB_HUMAN	100.00%	558
ERF3A_HUMAN	100.00%	17
SYDC_HUMAN	100.00%	41

EF1A1_HUMAN	100.00%	1128
ANXA5_HUMAN	100.00%	61
KPYM_HUMAN	100.00%	566
FLOT1_HUMAN	100.00%	172
SNP23_HUMAN	100.00%	32
SYRC_HUMAN	95.00%	8
TBA4A_HUMAN	100.00%	882
CALX_HUMAN	100.00%	146
GLYC_HUMAN	96.80%	32
IMPA1_HUMAN	99.90%	3
CSN1_HUMAN	99.50%	1
ACPH_HUMAN	95.00%	2
SCOT1_HUMAN	97.00%	3
MYH10_HUMAN	100.00%	132
EHD1_HUMAN	100.00%	169
ITM2C_HUMAN	100.00%	14
RL26L_HUMAN,RL26_HUMAN	100.00%	19
ACSL3_HUMAN	99.80%	9
CHM2B_HUMAN	99.10%	1
RAB4B_HUMAN	96.50%	51
EF1G_HUMAN	100.00%	70
LGUL_HUMAN	100.00%	13
H2A1B_HUMAN,H2A1C_HUMAN,H2A3_HUMAN	100.00%	272
CDK6_HUMAN	100.00%	45
ETFA_HUMAN	100.00%	5
RL35_HUMAN	100.00%	24
VIPR2_HUMAN	100.00%	12
MB12B_HUMAN	100.00%	112
RL18_HUMAN	100.00%	95
ILF2_HUMAN	100.00%	13
RPN1_HUMAN	100.00%	129
H31_HUMAN	100.00%	77
RB22A_HUMAN	100.00%	52
FDFT_HUMAN	100.00%	26
H14_HUMAN	100.00%	295
HABP2_HUMAN	95.00%	1
UB2L3_HUMAN	100.00%	25
TIPRL_HUMAN	95.00%	3
TPM3_HUMAN	100.00%	22
PDIA6_HUMAN	100.00%	79
EPHB6_HUMAN	100.00%	97
HS90B_HUMAN	100.00%	566
RAB5A_HUMAN	100.00%	68

MPZL1_HUMAN	100.00%	60
GAPR1_HUMAN	100.00%	30
CLCA_HUMAN	100.00%	71
TIF1B_HUMAN	100.00%	7
RYDEN_HUMAN	99.90%	3
APT_HUMAN	100.00%	106
RD23B_HUMAN	100.00%	1
TTC7A_HUMAN	95.00%	1
TBB4A_HUMAN	100.00%	1029
SNX18_HUMAN	95.00%	1
RAB10_HUMAN	100.00%	200
XRCC6_HUMAN	100.00%	8
RTN3_HUMAN	95.00%	2
FABP5_HUMAN	100.00%	31
RL27_HUMAN	100.00%	34
IDH3G_HUMAN	100.00%	5
RASN_HUMAN	100.00%	111
PPIL3_HUMAN	95.00%	4
VDAC3_HUMAN	100.00%	79
FLOT2_HUMAN	100.00%	112
C1QBP_HUMAN	100.00%	29
ARP5L_HUMAN	100.00%	20
BROX_HUMAN	100.00%	95
RUXE_HUMAN	95.00%	13
LDHA_HUMAN	100.00%	266
LAT3_HUMAN	95.00%	2
TMIG2_HUMAN	100.00%	17
CH60_HUMAN	100.00%	496
ACSL4_HUMAN	100.00%	16
XRP2_HUMAN	100.00%	22
CD2AP_HUMAN	100.00%	50
NRN1_HUMAN	95.00%	1
ENV_HV1Y2	100.00%	284
ABHEB_HUMAN	99.90%	4
DHB4_HUMAN	100.00%	23
RL21_HUMAN	100.00%	32
CD9_HUMAN	100.00%	71
IDH3A_HUMAN	100.00%	43
GNA13_HUMAN	100.00%	153
HBA_HUMAN	100.00%	152
PTPRC_HUMAN	100.00%	605
ETFB_HUMAN	100.00%	21
PROF2_HUMAN	95.00%	6

6PGL_HUMAN	100.00%	16
RL19_HUMAN	100.00%	2
SAM50_HUMAN	100.00%	1
CDC42_HUMAN	100.00%	331
H15_HUMAN	100.00%	191
1A24_HUMAN	100.00%	771
ARP2_HUMAN	100.00%	70
LIN7C_HUMAN	95.00%	1
AT1A3_HUMAN	100.00%	433
PZP_HUMAN	100.00%	158
LKHA4_HUMAN	95.00%	2
SERC3_HUMAN	100.00%	45
CD59_HUMAN	100.00%	108
K2C1_HUMAN	100.00%	103
AT11C_HUMAN	95.00%	4
UBE2N_HUMAN	100.00%	73
KPRB_HUMAN	100.00%	7
DYN3_HUMAN	99.90%	26
FSHR_HUMAN	98.30%	1
RUVB2_HUMAN	100.00%	29
RL30_HUMAN	96.30%	39
GRP75_HUMAN	100.00%	143
RL13_HUMAN	100.00%	66
CALM_HUMAN	100.00%	4
RS25_HUMAN	100.00%	45
PP1A_HUMAN	100.00%	22
APOC3_HUMAN	98.90%	8
GDIR2_HUMAN	100.00%	210
ICAM3_HUMAN	100.00%	25
AATC_HUMAN	100.00%	3
SEPT9_HUMAN	100.00%	25
MDHC_HUMAN	100.00%	71
PDIA1_HUMAN	100.00%	47
SAHH2_HUMAN	100.00%	12
SYVC_HUMAN	100.00%	2
ATX2L_HUMAN	100.00%	21
FBLN1_HUMAN	95.00%	1
ATX10_HUMAN	95.00%	1
ABCF1_HUMAN	95.00%	1
PI42A_HUMAN	100.00%	13
HMCS1_HUMAN	99.00%	4
PSMD2_HUMAN	100.00%	9
HNRC1_HUMAN,HNRC2_HUMAN,HNRC3_HUMAN,HNR	97.40%	1

C4_HUMAN		
CNOT3_HUMAN	100.00%	1
GDIB_HUMAN	100.00%	479
RAB8B_HUMAN	100.00%	308
RS8_HUMAN	100.00%	86
RENT1_HUMAN	100.00%	97
SRGP2_HUMAN	100.00%	7
IDH3B_HUMAN	100.00%	3
AT2A3_HUMAN	100.00%	132
RS17_HUMAN	100.00%	20
PIPNB_HUMAN	100.00%	24
NB5R3_HUMAN	100.00%	65
PP2BA_HUMAN	99.70%	4
RS15A_HUMAN	100.00%	44
SH3L3_HUMAN	95.00%	10
CD8A_HUMAN	100.00%	56
ARP3_HUMAN	100.00%	160
CYTB_HUMAN	100.00%	5
TRBC1_HUMAN,TRBC2_HUMAN	100.00%	4
RFA3_HUMAN	95.00%	5
FLNA_HUMAN	100.00%	2
AP2M1_HUMAN	100.00%	4
RL10A_HUMAN	100.00%	53
RAB2A_HUMAN	100.00%	46
RABP1_HUMAN	100.00%	65
GLU2B_HUMAN	100.00%	58
CD4_HUMAN	100.00%	110
COPB_HUMAN	100.00%	9
2B17_HUMAN	95.00%	9
DYHC1_HUMAN	100.00%	3
URP2_HUMAN	100.00%	329
IF4A3_HUMAN	99.40%	11
RGS19_HUMAN	100.00%	3
RS11_HUMAN	100.00%	47
RAF1_HUMAN	95.00%	5
RL14_HUMAN	100.00%	65
GPC1_HUMAN	100.00%	123
H10_HUMAN	100.00%	7
DNJA1_HUMAN	100.00%	62
PRDX5_HUMAN	100.00%	58
THIC_HUMAN	100.00%	28
NIPS1_HUMAN	100.00%	22
ZCHC3_HUMAN	95.00%	5

VANG1_HUMAN	95.00%	2
PABP4_HUMAN	100.00%	207
DPB1_HUMAN	95.00%	1
EFR3A_HUMAN	100.00%	11
SPTB2_HUMAN	100.00%	15
IPYR_HUMAN	100.00%	49
HS105_HUMAN	100.00%	5
HNRPD_HUMAN	100.00%	35
ELOB_HUMAN	99.80%	1
SF3B6_HUMAN	95.00%	1
RL9_HUMAN	100.00%	39
YKT6_HUMAN	100.00%	22
PSMD3_HUMAN	100.00%	9
PSB5_HUMAN	95.00%	1
RS9_HUMAN	100.00%	96
UBA1_HUMAN	100.00%	157
GNA15_HUMAN	100.00%	31
RS20_HUMAN	100.00%	25
VAPB_HUMAN	98.30%	4
ENOG_HUMAN	100.00%	251
FUBP2_HUMAN	100.00%	2
RSMB_HUMAN	100.00%	9
NASP_HUMAN	100.00%	10
R4RL2_HUMAN	99.90%	1
HN1_HUMAN	95.00%	1
DECR_HUMAN	97.60%	1
MOGS_HUMAN	100.00%	4
CPPED_HUMAN	100.00%	5
RL27A_HUMAN	100.00%	24
SC5A3_HUMAN	100.00%	3
SODC_HUMAN	100.00%	12
DX39B_HUMAN	100.00%	9
AHSA1_HUMAN	99.80%	10
DBNL_HUMAN	100.00%	20
ACTC_HUMAN	100.00%	762
PLCL1_HUMAN	100.00%	9
RUXGL_HUMAN	95.00%	5
PARK7_HUMAN	100.00%	54
ADA10_HUMAN	100.00%	52
TCPE_HUMAN	100.00%	71
CAPZB_HUMAN	100.00%	71
QCR2_HUMAN	100.00%	31
PPIB_HUMAN	100.00%	117

RS3_HUMAN	100.00%	100
DOPD_HUMAN	100.00%	27
G3P_HUMAN	100.00%	1064
CD99_HUMAN	100.00%	12
PSA7_HUMAN	100.00%	12
ZNRF1_HUMAN	95.00%	1
RS12_HUMAN	100.00%	8
TCTP_HUMAN	100.00%	32
EIF3E_HUMAN	100.00%	2
MYL6_HUMAN	100.00%	89
ADA_HUMAN	100.00%	433
ARF1_HUMAN	100.00%	305
SORT_HUMAN	95.00%	2
MIF_HUMAN	100.00%	157
DNJA2_HUMAN	100.00%	22
PRDX6_HUMAN	100.00%	100
SYSC_HUMAN	100.00%	20
LFA3_HUMAN	100.00%	14
F234A_HUMAN	100.00%	15
DHX9_HUMAN	100.00%	15
DDB1_HUMAN	95.00%	2
ROA2_HUMAN	100.00%	32
TERA_HUMAN	100.00%	71
KTHY_HUMAN	100.00%	9
3BP1_HUMAN	98.70%	4
APOB_HUMAN	99.90%	4
IF2A_HUMAN	100.00%	8
PCBP1_HUMAN	100.00%	195
BZW2_HUMAN	95.00%	2
CTL1_HUMAN	100.00%	10
MCA3_HUMAN	100.00%	2
SYFB_HUMAN	100.00%	5
ITIH3_HUMAN	100.00%	54
VPS4A_HUMAN	100.00%	18
PP2AA_HUMAN	100.00%	20
S39AA_HUMAN	95.00%	7
PTK7_HUMAN	100.00%	58
KAD2_HUMAN	100.00%	16
RASL3_HUMAN	100.00%	45
ROAA_HUMAN	100.00%	24
SF3B1_HUMAN	100.00%	7
RL4_HUMAN	100.00%	136
CECR5_HUMAN	95.00%	1

AMPL_HUMAN	99.90%	3
HMGB1_HUMAN	100.00%	23
ATPD_HUMAN	100.00%	19
LAMP1_HUMAN	100.00%	27
NLGNY_HUMAN	100.00%	28
RAB6A_HUMAN	100.00%	86
STABP_HUMAN	100.00%	16
ALDOA_HUMAN	100.00%	304
ENOB_HUMAN	100.00%	251
PACN1_HUMAN	100.00%	13
RAC1_HUMAN	100.00%	361
TOLIP_HUMAN	95.00%	2
RU2B_HUMAN	96.90%	1
NONO_HUMAN	97.10%	5
F120A_HUMAN	100.00%	9
gnl|unk|TRINITY_DN1340_c0_g1_i1_4	95.00%	9
TMM8A_HUMAN	99.80%	1
T106B_HUMAN	100.00%	6
PA1B2_HUMAN	100.00%	10
TS101_HUMAN	100.00%	345
CTR3_HUMAN	100.00%	35
RAB35_HUMAN	100.00%	303
ATPK_HUMAN	100.00%	11
VAT1_HUMAN	100.00%	78
SCAM3_HUMAN	100.00%	5
CLIC4_HUMAN	100.00%	37
ABCE1_HUMAN	99.10%	1
CD28_HUMAN	100.00%	34
AAAT_HUMAN	100.00%	107
SORCN_HUMAN	100.00%	21
RS3A_HUMAN	100.00%	128
IDHP_HUMAN	100.00%	84
PRS7_HUMAN	100.00%	13
SMD3_HUMAN	100.00%	22
PCBP2_HUMAN	100.00%	175
NTF2_HUMAN	100.00%	39
RAB5C_HUMAN	100.00%	108
SERA_HUMAN	100.00%	124
PACN2_HUMAN	100.00%	313
ESTD_HUMAN	100.00%	20
STAT1_HUMAN	99.90%	1
PRDX1_HUMAN	100.00%	169
LC7L2_HUMAN	95.00%	4

CTR1_HUMAN	100.00%	29
PDCD6_HUMAN	100.00%	20
RL29_HUMAN	100.00%	15
CAP1_HUMAN	100.00%	23
SRP14_HUMAN	100.00%	38
KC1G1_HUMAN	99.70%	3
ITIH4_HUMAN	100.00%	4
ARF4_HUMAN	100.00%	172
IF5AL_HUMAN	100.00%	28
MK01_HUMAN	100.00%	4
PTPRK_HUMAN	100.00%	10
H4_HUMAN	100.00%	554
KPCA_HUMAN	100.00%	191
MIA2_HUMAN	95.00%	1
TMC6_HUMAN	100.00%	10
UB2V1_HUMAN	99.10%	17
GOGA7_HUMAN	100.00%	19
GBB1_HUMAN	100.00%	353
PRDX3_HUMAN	100.00%	59
CHM4B_HUMAN	100.00%	102
CSK21_HUMAN	100.00%	85
CHMP5_HUMAN	100.00%	13
NICA_HUMAN	100.00%	42
S10A6_HUMAN	95.00%	1
DDX6_HUMAN	100.00%	67
CO9_HUMAN	100.00%	7
RAC2_HUMAN	100.00%	370
CYB5B_HUMAN	95.00%	10
GLGB_HUMAN	100.00%	6
NDKA_HUMAN	100.00%	91
DDX17_HUMAN	100.00%	34
STK24_HUMAN	99.70%	12
TXND5_HUMAN	100.00%	19
FNBP1_HUMAN	100.00%	204
TCPA_HUMAN	100.00%	143
MARCS_HUMAN	100.00%	39
KAP0_HUMAN	95.00%	4
DHB12_HUMAN	100.00%	30
DPM3_HUMAN	95.00%	4
SUMO2_HUMAN	95.00%	11
EF1D_HUMAN	100.00%	12
ITA5_HUMAN	100.00%	12
IFM1_HUMAN	100.00%	37

PACN3_HUMAN	95.00%	1
OSBP1_HUMAN	100.00%	2
MPU1_HUMAN	100.00%	6
CD3D_HUMAN	100.00%	12
ABHDA_HUMAN	100.00%	2
VP37B_HUMAN	100.00%	17
DRA_HUMAN	100.00%	29
SDHA_HUMAN	100.00%	16
NLTP_HUMAN	99.80%	5
COF1_HUMAN	100.00%	466
RLA2_HUMAN	100.00%	43
ARF5_HUMAN	100.00%	186
ECHA_HUMAN	99.80%	1
FAM3C_HUMAN	95.00%	5
ACADV_HUMAN	99.80%	1
TYB4_HUMAN	99.90%	2
SURF4_HUMAN	100.00%	4
MIC60_HUMAN	100.00%	17
TMM33_HUMAN	95.00%	11
PDPK2_HUMAN	95.00%	2
CH10_HUMAN	100.00%	90
LEUK_HUMAN	100.00%	105
MYO1C_HUMAN	100.00%	12
MRP_HUMAN	100.00%	61
IGF1R_HUMAN	100.00%	14
RL18A_HUMAN	100.00%	31
gnl|unk|TRINITY_DN565_c0_g3_i1_5	100.00%	51
gnl|unk|TRINITY_DN201_c0_g2_i1_4	99.90%	627
OST48_HUMAN	100.00%	50
1433F_HUMAN	100.00%	45
EFTU_HUMAN	100.00%	161
TMED2_HUMAN	100.00%	6
SEM7A_HUMAN	100.00%	521
FA10_HUMAN	100.00%	54
RL24_HUMAN	100.00%	31
CD3E_HUMAN	100.00%	18
HNRPR_HUMAN	100.00%	60
MOES_HUMAN	100.00%	1638
STK10_HUMAN	100.00%	23
NDKB_HUMAN	100.00%	91
PTPRF_HUMAN	100.00%	30
DOCK2_HUMAN	100.00%	13
LRC59_HUMAN	100.00%	10

TBB6_HUMAN	99.80%	418
PFD2_HUMAN	99.90%	1
RL10_HUMAN	100.00%	79
CO4A_HUMAN,CO4B_HUMAN	100.00%	12
NDUAD_HUMAN	95.00%	3
PYR1_HUMAN	100.00%	13
B2MG_HUMAN	100.00%	149
CD81_HUMAN	100.00%	203
GNAS1_HUMAN	100.00%	214
K1C9_HUMAN	100.00%	8
RSU1_HUMAN	98.80%	1
CHM2A_HUMAN	99.90%	14
1433B_HUMAN	100.00%	54
RAP1A_HUMAN	100.00%	232
ACON_HUMAN	100.00%	30
MARK2_HUMAN	100.00%	10
TKT_HUMAN	100.00%	67
ARPC2_HUMAN	100.00%	94
PTCA_HUMAN	100.00%	23
TMM43_HUMAN	95.00%	1
gnl|unk|TRINITY_DN4399_c0_g1_i1_3	95.00%	2
ALDR_HUMAN	100.00%	16
KIF23_HUMAN	95.00%	1
FUS_HUMAN	95.00%	1
AP2A1_HUMAN	100.00%	20
DDX3Y_HUMAN	97.50%	14
ACLY_HUMAN	100.00%	38
EVL_HUMAN	100.00%	12
MYH9_HUMAN	100.00%	557
GRP78_HUMAN	100.00%	376
SDHB_HUMAN	100.00%	6
RCC2_HUMAN	100.00%	6
CISY_HUMAN	100.00%	36
RS28_HUMAN	100.00%	5
SC11A_HUMAN	95.00%	7
RAB14_HUMAN	100.00%	96
TRAT1_HUMAN	95.00%	4
PTPRA_HUMAN	99.80%	4
SLIT1_HUMAN	100.00%	14
TBA8_HUMAN	95.10%	548
PUR8_HUMAN	100.00%	25
ECHB_HUMAN	97.00%	1
gnl|unk|TRINITY_DN655_c0_g1_i1_5	95.00%	4

THRB_HUMAN	100.00%	50
PARP1_HUMAN	97.00%	1
CDC37_HUMAN	100.00%	24
PDIA4_HUMAN	100.00%	140
PDC6I_HUMAN	100.00%	600
PAK4_HUMAN	100.00%	17
STRAP_HUMAN	100.00%	6
SMD2_HUMAN	100.00%	8
CHM1B_HUMAN	98.20%	17
ZCCHV_HUMAN	100.00%	132
RTCB_HUMAN	100.00%	11
C2D1A_HUMAN	100.00%	2
1433G_HUMAN	100.00%	92
GTR1_HUMAN	100.00%	55
SPP24_HUMAN	95.00%	2
PA2G4_HUMAN	100.00%	53
FRIH_HUMAN	98.40%	3
NACAM_HUMAN	100.00%	32
MARE1_HUMAN	95.00%	11
ATPA_HUMAN	100.00%	454
SDCB1_HUMAN	100.00%	313
PPIL1_HUMAN	100.00%	54
HEXA_HUMAN	100.00%	7
S38A2_HUMAN	99.90%	9
SH3G3_HUMAN	100.00%	5
PUR9_HUMAN	100.00%	86
NLGN2_HUMAN	98.70%	13
SCAM1_HUMAN	95.00%	3
CD82_HUMAN	100.00%	12
THIL_HUMAN	100.00%	12
PRP8_HUMAN	100.00%	12
AN32A_HUMAN	100.00%	13
BOLA2_HUMAN	95.00%	5
FINC_HUMAN	100.00%	3
DYN2_HUMAN	100.00%	22
MFGM_HUMAN	100.00%	387
LPPRC_HUMAN	100.00%	36
DDX1_HUMAN	100.00%	2
CD7_HUMAN	100.00%	31
HNRPM_HUMAN	95.00%	5
RU17_HUMAN	95.00%	4
ODPA_HUMAN	100.00%	28
TLN1_HUMAN	100.00%	78

FKBP4_HUMAN	100.00%	31
MB12A_HUMAN	99.80%	25
RL17_HUMAN	100.00%	64
FETUA_HUMAN	99.90%	2
H13_HUMAN	99.10%	263
CN37_HUMAN	100.00%	421
LMAN2_HUMAN	100.00%	53
FUMH_HUMAN	98.10%	2
TGON2_HUMAN	95.00%	1
PPIA_HUMAN	100.00%	1660
FAS_HUMAN	100.00%	123
AT1A1_HUMAN	100.00%	739
HS90A_HUMAN	100.00%	652
BAP31_HUMAN	100.00%	18
CNN2_HUMAN	100.00%	21
SRC_HUMAN	100.00%	4
HINT1_HUMAN	100.00%	6
COR1C_HUMAN	100.00%	27
PSMD6_HUMAN	100.00%	4
VPS25_HUMAN	100.00%	14
6PGD_HUMAN	100.00%	54
RL11_HUMAN	100.00%	49
TOM70_HUMAN	99.40%	1
DREB_HUMAN	100.00%	12
PP1G_HUMAN	99.80%	10
RS23_HUMAN	100.00%	33
XRCC5_HUMAN	100.00%	14
NOTC3_HUMAN	100.00%	39
CCND3_HUMAN	95.00%	3
CAN1_HUMAN	100.00%	7
HEXB_HUMAN	100.00%	19
VDAC2_HUMAN	100.00%	102
SELPL_HUMAN	95.00%	1
EIF3L_HUMAN	100.00%	5
PRAX_HUMAN	96.70%	1
CLH2_HUMAN	99.80%	789
NDUS8_HUMAN	95.00%	1
MBLC2_HUMAN	100.00%	16
HP1B3_HUMAN	100.00%	1
SR140_HUMAN	97.40%	1
CAND1_HUMAN	100.00%	22
CIB1_HUMAN	100.00%	11
LMNB1_HUMAN	100.00%	13

THIM_HUMAN	100.00%	7
HSP7C_HUMAN	100.00%	1380
USMG5_HUMAN	95.00%	1
TCPH_HUMAN	100.00%	69
MTCH2_HUMAN	100.00%	25
CLDN1_HUMAN	95.00%	3
UBC12_HUMAN	95.00%	8
PTMA_HUMAN	95.00%	6
RS6_HUMAN	100.00%	36
ABI1_HUMAN	99.80%	1
RHOF_HUMAN	100.00%	19
HNRH2_HUMAN	100.00%	6
TSN14_HUMAN	100.00%	12
TECR_HUMAN	95.00%	3
NP1L1_HUMAN	100.00%	40
CD1D_HUMAN	100.00%	29
PTBP1_HUMAN	100.00%	21
STXB3_HUMAN	100.00%	49
ODPB_HUMAN	100.00%	56
RS15_HUMAN	98.50%	8
TOM40_HUMAN	100.00%	16
PROF1_HUMAN	100.00%	397
TXD12_HUMAN	100.00%	2
DJB11_HUMAN	96.70%	2
HYOU1_HUMAN	100.00%	94
CALR_HUMAN	100.00%	150
VPS35_HUMAN	100.00%	202
SYNC_HUMAN	100.00%	23
RCN2_HUMAN	100.00%	8
NOMO3_HUMAN	99.00%	1
PEDF_HUMAN	100.00%	62
IPYR2_HUMAN	95.00%	5
SO3A1_HUMAN	95.00%	3
S29A1_HUMAN	100.00%	178
SYPL1_HUMAN	95.00%	17
CD2_HUMAN	95.00%	1
PTN23_HUMAN	99.90%	2
P4K2A_HUMAN	99.90%	3
HCLS1_HUMAN	95.00%	3
APOE_HUMAN	100.00%	40
SERC_HUMAN	100.00%	22
CATD_HUMAN	99.90%	4
WDR1_HUMAN	100.00%	185

RL12_HUMAN	100.00%	11
CR2_HUMAN	100.00%	40
ROA3_HUMAN	100.00%	18
RS24_HUMAN	100.00%	13
LUM_HUMAN	100.00%	18
GDIR1_HUMAN	100.00%	103
ICAM2_HUMAN	100.00%	67
TPP1_HUMAN	95.00%	2
PCNA_HUMAN	100.00%	37
UBP14_HUMAN	100.00%	12
CHLE_HUMAN	97.00%	5
CKAP4_HUMAN	100.00%	6
EIF3M_HUMAN	95.00%	3
CAZA2_HUMAN	100.00%	40
GNAI2_HUMAN	100.00%	469
TTYH3_HUMAN	100.00%	24
NCKPL_HUMAN	100.00%	30
HSP74_HUMAN	100.00%	17
PUR6_HUMAN	100.00%	90
ACTG_HUMAN	100.00%	2270
SNAG_HUMAN	100.00%	29
1433Z_HUMAN	100.00%	326
1A68_HUMAN	100.00%	733
THBG_HUMAN	95.00%	14
KCY_HUMAN	95.00%	2
RAB1A_HUMAN	100.00%	242
RL7_HUMAN	100.00%	80
TALDO_HUMAN	95.00%	6
TBCB_HUMAN	95.00%	4
CYC_HUMAN	99.90%	1
ADHX_HUMAN	100.00%	4
ARL8B_HUMAN	100.00%	18
RS7_HUMAN	100.00%	40
GLOD4_HUMAN	95.00%	7
FKB1A_HUMAN	100.00%	16
ESYT2_HUMAN	100.00%	20
ACADM_HUMAN	100.00%	6
AT2A2_HUMAN	100.00%	54
RS16_HUMAN	100.00%	91
MOV10_HUMAN	100.00%	402
STX4_HUMAN	100.00%	21
PIPNA_HUMAN	95.00%	5
RASA2_HUMAN	100.00%	28

NDUS3_HUMAN	95.00%	2
LYPA1_HUMAN	100.00%	2
BAHC1_HUMAN	98.40%	2
STK26_HUMAN	100.00%	17
1433T_HUMAN	100.00%	81
H2B1K_HUMAN,H2BFS_HUMAN	100.00%	266
ZCCHL_HUMAN	95.00%	7
MPRD_HUMAN	100.00%	43
POL_HV1Z2	100.00%	4176
POL_HV1YF	100.00%	1796
FETA_HUMAN	100.00%	21
CD44_HUMAN	100.00%	76
RM12_HUMAN	95.00%	1
1C14_HUMAN	99.90%	390
TM41A_HUMAN	95.00%	2
POL_HV1V9	100.00%	1617
RHOA_HUMAN	100.00%	798
PEF1_HUMAN	100.00%	34
POL_HV1U4	100.00%	1911
CD97_HUMAN	100.00%	21
TM9S4_HUMAN	95.00%	4
S38A5_HUMAN	99.90%	1
PSA5_HUMAN	100.00%	11
COPA_HUMAN	100.00%	14
SRSF8_HUMAN	95.00%	12
POL_HV1S2	100.00%	1619
POL_HV1RH	100.00%	4887
GSTP1_HUMAN	100.00%	210
SAP_HUMAN	100.00%	35
IF4A2_HUMAN	99.90%	98
TAGL2_HUMAN	100.00%	85
K2C79_HUMAN	96.10%	9
POL_HV1MV	99.90%	398
POL_HV1N5	100.00%	5527
TADBP_HUMAN	95.00%	3
POL_HV1MP	99.90%	2224
SYAC_HUMAN	100.00%	63
POL_HV1MN	100.00%	6829
POL_HV1MA	100.00%	2780
NUCB2_HUMAN	100.00%	30
POL_HV1LW	100.00%	7666
POL_HV1M2	100.00%	2061
NUCL_HUMAN	100.00%	11

RACK1_HUMAN	100.00%	90
BAIP2_HUMAN	100.00%	72
PRDX4_HUMAN	99.40%	28
POL_HV1JR	100.00%	7922

Table 4c. All proteins identified for the HIV-1 ADA/SUPT1-CCR5 CL.30.

Chapter 4: Micropeptidomics of Mouse CNS by ribosome profiling and mass spectrometry

Introduction

Neuropeptides are small signaling molecules in the CNS of many species, and play important roles in the regulation of behavior and many other physiological processes(Burbach, 2011; Nathoo, Moeller, Westlund, & Hart, 2001; L. S. Nelson, Rosoff, & Li, 1998; Zhang, Buchberger, Muthuvel, & Li, 2015). In the past two decades, many novel neuropeptides have been discovered by untargeted approaches(Hori et al., 2001; Kojima et al., 1999; Meunier et al., 1995; Sakurai, Amemiya, Ishii, Matsuzaki, Chemelli, Tanaka, Williams, Richardson, et al., 1998; Tatemoto et al., 1998). Some of these novel neuropeptides and their receptors, in particular nociceptin and orexin A and B, have since gone on to clinical trials as drugs or drug targets(Coleman & Renger, 2010; Lambert, 2008), which have recently produced the drug suvorexant(Patel, Aspesi, & Evoy, 2015). Thus, the discovery of novel neuropeptides may allow novel approaches to pharmacologic intervention in psychiatric disorders. However, in the past decade, no novel neuropeptides have been discovered, and new approaches to novel neuropeptide discovery may be needed.

A recently developed technique for studying translational regulation, ribosomal profiling, has uncovered that there may be many short, unannotated open reading frames (sORFs) in mammalian genomes(Brar & Weissman, 2015; Ingolia, 2014; Ingolia et al., 2014; Kondo et al., 2010; Slavoff, Heo, Budnik, Hanakahi, & Saghatelian, 2014). The translated products of these sORFs are very short peptides (<100 amino acids), and have been named micropeptides. Several of these have been found to be functional in human tissue systems such as skeletal muscle and the cardiovascular system(Anderson et al., 2015; C. Lee et al., 2015; Magny et al., 2013). In particular, the Toddler peptide has been found to be a secreted ligand for a G-protein coupled receptor (GPCR)(Pauli et al., 2014). Since nearly all known neuropeptides are ligands for GPCRs(Burbach, 2011;

Zhang, Wang, Parks, & Civelli, 2011), these recent discoveries motivate the hypothesis that some of these sORF-encoded peptides could be undiscovered neuropeptides.

In Chapters 2 and 3, I have developed and applied a novel method for profiling cell and tissue samples for micropeptides by mass spectrometry(Tharakan, Tao, Ubaida-Mohien, Dinglasan, & Graham, 2015). This micropeptidomics method can be easily adapted to the CNS to perform neuropeptidomics(Romanova & Sweedler, 2015), which is an approach that entails extraction of all neuropeptides from brain cells or brain tissue samples and then sequencing all neuropeptides by mass spectrometry. The method I have developed can increase neuropeptide discovery rates by several fold over traditional mass spectrometry-based neuropeptidomics techniques(Tharakan et al., 2015). Therefore, a combination of my neuropeptidomics method with ribosomal profiling of mouse brain allows novel sORF-encoded neuropeptide discovery in the mammalian CNS.

In this Chapter, we apply the same micropeptidomics methods to the mouse brain, in an attempt to apply the methods to a more constrained system and gain biological insights. While biochemical detection of these micropeptides proves that the micropeptides are translated, but this does not necessarily mean that they are functional, as they may be translational byproducts. We hypothesized in this Chapter that micropeptides which are functional in the brain will be expressed in a regulated manner during adolescent development. Thus, in order to validate the micropeptide targets thus discovered, we quantified these micropeptides by mass spectrometry, by time and mass tag quantitative profiling. Thus, the goals of this Chapter are, first, the discovery of translated micropeptides in the mammalian brain; with the hypothesis that the mammalian brain will have functional micropeptides. We approach this hypothesis by discovering sORFs that have ribosomal content in mouse brain by ribosomal profiling

(RP) and by mass spectrometry-based neuropeptidomics, using RP-derived sequences as databases for MS analysis. Second, we validate the novel CNS micropeptides by examining their regulation in development, with the hypothesis that micropeptides which are functional in the mammalian brain will change their abundance over the course of development. We approach this hypothesis by performing a screen for regulated micropeptides over the course of adolescence.

Methods

Mouse brain peptide extraction. A protease inhibitor solution was prepared by dissolving 1 Sigma Protease Inhibitor Tablet in 50 mL of Phosphate-buffered Saline, for a final concentration of AEBSF, 2 mM, Aprotinin, 0.3 μM, Bestatin, 130 μM, EDTA, 1 mM, E-64, 14 μM, and Leupeptin, 1 μM. This buffer was then used to perfuse the animals according to standard protocols after deep anesthetization, with perfusion being accomplished at a rate of 4 mL per minute for 5 minutes, until liver was visibly cleared of blood. Whole brains were then dissected out by standard protocols, and brains were heat inactivated by the Denator laser-guided heat inactivation system according to published protocols(Svensson et al., 2009), in the procedure for fresh frozen tissue without tissue structure preservation. The brains were then flash-frozen on liquid nitrogen and stored at -80C. Brains were then immersed into cold .5% acetic acid (pH ~2) to thaw, with 7.5 uL/mg tissue, minced, and triturated with a 21G needle, then transferred to a 5 mL Duall tissue grinder, to be homogenized with 20 strokes left and right. To shear DNA to reduce viscosity, samples were then treated with sonication with a 10 second burst at level 4, with a 20 second pause on ice, for 5 cycles. The homogenates were then cleared by centrifuging at 20,000xg at 4C for 20 minutes. The supernatant was then collected and loaded onto 30 kDa molecular weight cutoff filters, and centrifuged through them to

remove high molecular weight components, by centrifugation at 14,000xg for 10 minutes, at room temperature so as not to disrupt the chemistry of the filter. Flowthrough of the filtration was then collected and desalted by solid-phase extraction. Briefly, C18 SepPaks (Waters) were preconditioned with 10 mL of a buffer of 5% acetonitrile, 94.9% water, with .1% formic acid. The flowthrough sample was then loaded on these columns. Flowthrough of the filtration was then loaded onto the column. The sample was then desalted by washing with 20 mL of the preconditioning buffer, then eluted with a buffer of 70% acetonitrile, 29.9% water, with .1% formic acid. This elution was then evaporated to dryness under vacuum.

Database construction from ribosome profiling data. Ribosome profiling data was obtained from two published datasets, a cerebellum ribosome profiling dataset(Ishimura et al., 2014) and a frontal lobe ribosome profiling dataset(Hornstein et al., 2016). Briefly, in the former dataset, three cerebella were pooled for each library preparation, with brain tissues homogenized in a polysome buffer with DNase I, 100 ug/ml cycloheximide, and 2 ug/ml harringtonine, blocking both ribosome elongation and ribosome initiation(Ingolia et al., 2011). Samples were treated with RNase I and pelleted into a 1M sucrose cushion, as previously described(Ingolia, Brar, Rouskin, McGeachy, & Weissman, 2012). Upon gel purification, 26-34 nucleotide length fragments were purified, and library preparation proceeded according to standard protocols. In the latter dataset, the frontal lobe of the mice was dissected by standard protocols, and the ribosome footprints were isolated and purified in the standard manner. However, the ligation step was then omitted and a small RNA library preparation kit was used to produce the final library (smRNA-Seq Kit for Illumina). Finally, a ribosome profiling dataset was generated from mouse brain using published protocols(Ingolia et al., 2012). From these sequencing data, proteome

databases were constructed using a novel method by Olexiouk (Olexiouk, Menschaert, et al, forthcoming).

Mass spectrometry-based peptidomics analysis and TMT labelling, *database searching and publication re-analysis*. Datasets used for this study were the peptidomics study generated above, and the Sharma et al. mouse brain proteome(Sharma et al., 2015). In that study, brain regions were dissected from coronal sections from P60 mice. We used datasets only from the pre-frontal cortex experiments, and microglial and neuronal primary cell cultures. From this, the database searching was performed as in Chapter 3, with the ribosome profiling-based datasets concatenated as described and searched with the previously described settings.

Results

In these experiments, we performed peptidomics and proteogenomics analyses on the mouse brain in order to discover novel neuropeptides. In one experiment, we extracted neuropeptides from 6 mouse brains, one from each of three adolescent timepoints, at 4 weeks, 5 weeks and 6 weeks old, with two replicates per timepoint. The samples were labelled with TMT and for quantification. This experiment produced a dataset, at 1% FDR, of 368 proteins in 311 clusters, with the highest abundant protein being Immunoglobulin at 651 spectra followed by Ubiquitin at 617 spectra (Table 1). This is to be expected for a neuropeptides extraction, which extracts only soluble proteins. Of the 601 clustered proteins, 15 were known neuropeptides or their precursors (Table 2). We note that this workflow cannot differentiate between neuropeptides and their precursors, since a tryptic digest was done. The substantial number of neuropeptides

detected shows that the protocol is sensitive enough to observe neuropeptides, which are generally thought to be low abundance as signaling molecules.

Sixteen spectra mapped to the transcript 2210013O21Rik, which is a transcript without an annotated function. The peptide sequence thus determined maps to exon 1 of the corresponding transcript, with a canonical start and stop codon, defining a short ORF. This sORF contains 5 tryptic cleavage sites, producing 6 tryptic peptides, or 5 if one proline-blocked tryptic site is ignored(Olsen, Ong, & Mann, 2004). Of these, 3 tryptic peptides were detected by mass spectrometry, with high probabilities for all peptides (Table 3). An example spectrum and mass table from the peptide is shown in Figure 1. We also examined the translation of the protein by ribosome profiling. All three mouse brain ribosome profiling datasets showed substantial coverage of this locus by ribosome profiling reads (Figure 2).

To further examine the expression of this peptide, we also attempted to study its regulation over the course of adolescent development. We utilized the TMT labelling data to look for quantitative changes in the expression of the peptide over the course of adolescence, from 4 weeks development, 5 weeks development, and 6 weeks development. However, no substantial change was found in the abundance of the peptide over this timecourse (Figure 3). It is possible that, since whole brains were used in this experiment, there may be more region-specific changes which could not be found. Unlike embryonic development, the mouse brain undergoes only subtle changes during the course of adolescent development, although specific regions may change more substantially.

To further examine this peptide and its function, we searched for the expression of the underlying transcript in the database BioGPS, which has microarray-based datasets detailing expression of all known transcripts. These results are summarized in

Figure 4. The transcript is found to have highest expression in mouse brain out of all tissues in mouse, in particular in dorsal root ganglia, hypothalamus, and amygdala. The latter two regions are involved in regulation of behavior, indicating that this peptide is likely to be a behavior regulating neuropeptide.

In order to rule out contamination from the periphery in our sample, we re-analyzed datasets from Sharma et al (see Methods), using proteomics data from cultured primary neurons and microglia. These datasets also contained the novel peptide, albeit at a lower intensity, likely because they were not targeted toward soluble peptide extractions. Thus, our bioinformatics framework allows us to find a novel micropeptide in published datasets, as well. Since these proteomics datasets were derived from cultured primary neurons and microglia, we can conclude that the peptide is produced locally, rather than crossing from the periphery as a secreted hormone.

Finally, we further utilized this published dataset to attempt to find brain region-specific micropeptides. We used published datasets from dissected pre-frontal cortex, a region known to undergo changes during adolescence. While these datasets were derived from P60 mice, which are adult mice, the targets thus derived may be interesting candidates for future work on adolescent development, since they are expressed in the pre-frontal cortex. Analyzing these datasets using the cerebellum-derived database generated a dataset of 7,309 proteins in 5,312 clusters. Of these, 61 were potential micropeptide hits. These were subjected to the screening by BLAST searches as described in Chapter 3. Twelve micropeptides were found to be translated from 5' untranslated regions of known transcripts. Of these, 11 were found to map ambiguously to another isoform of a known gene, leaving one putative micropeptide. Twenty-six micropeptides were found to be translated from annotated long non-coding RNAs. Of these, homology screening rules out all but one. Thirteen micropeptides were found to

be alternately encoded from known exons. As we argued in Chapter 1, these cannot be unambiguously identified from mass spectrometry data. Ten micropeptides were found to be translated from transcripts expected to be degraded by nonsense-mediated decay; of these, one survived homology screening.

Discussion

In this chapter, we have developed a new proteogenomics framework utilizing ribosome profiling data, rather than RNAseq data, for generating databases for proteogenomics analyses. While no direct comparison between the two methods is within the scope of the work here, we suggest that this method appears to be more effective, since the search space is decreased by considering only ORFs which have substantial ribosomal content. As discussed in the introduction to this thesis, the ribosome profiling data should, in theory, match almost exactly to the proteomics data. However, it has been widely observed that ribosome profiling data and proteomics data mismatch to a large extent. Thus, allowing the two techniques to complement each other by orthogonally confirming results is a proteogenomics technique that allows the search space of the analysis to be decreased while nevertheless allowing dual confirmation of the novel protein identifications. Thus, in the case of searching the mouse brain for novel proteins, the ribosome profiling-based proteogenomics technique was successful, discovering indeed a new peptide.

Short open reading frames (sORFs) are sequences of nucleotides in the human genome containing a start and an in-frame stop codon separated by less than 300 nucleotides(Andrews & Rothnagel, 2014). The gene products of these sORFs are necessarily very short proteins of less than 100 amino acids. While there are many more

sORFs in most genomes than there are known genes [for example, the mouse genome has ~25,000 known genes, but ~47 million sORFs(Brown & Hancock, 2006; Crappe et al., 2013)], these very short genes have historically been understudied in all species, because of common bioinformatic, biochemical and genetic assumptions. First, since peptides generated from these sORFs would be very short, it was thought that they were unlikely to fold into stable structures which would allow them to be functional(Ingolia et al., 2014). Second, it is difficult to detect evolutionary conservation of these ORFs(Couso, 2015), and in classical random mutagenesis experiments, a shorter gene is less likely to be 'hit' than a longer one, leading to few phenotypes from these genes(Basrai et al., 1997). Finally, in a randomly-generated genome, there is a very high rate of occurrence of ORFs of <100 amino acids by random chance(Frith et al., 2006). All these lines of thinking led to the assumption that sORFs were non-functional, an assumption which has turned out to be wrong.

The assumption has been disproven in the following ways. First, it has recently been recognized that intrinsically disordered proteins have many biological functions(Dyson & Wright, 2005; Wright & Dyson, 2015). Second, if homology detection is adjusted for the small length of these genes, a great deal of conservation can be found(Bazzini et al., 2014; Mackowiak et al., 2015). Finally and most importantly, next generation sequencing techniques such as RNA sequencing and ribosome profiling have shown that many of these sORFs are both transcribed and translated(Ingolia et al., 2014; Ingolia et al., 2011). In particular, several significant novel genes, with likely roles in human disease, have been found recently. The peptide Myoregulin, which regulates the sarco/endoplasmic reticulum calcium ATPase (SERCA) pump in human skeletal muscle, was recently found by a bioinformatic screen(Anderson et al., 2015). This peptide is a fundamental discovery for the understanding of skeletal muscle physiology.

Similarly, the peptides MOTS-c (mitochondrial open reading frame of the 12S rRNA-c), discovered bioinformatically(C. Lee et al., 2015), and Toddler, discovered by ribosome profiling(Pauli et al., 2014), are involved in regulation of insulin metabolism in mouse and cardiovascular regulation in human, respectively(Yang, Maguire, & Davenport, 2015).

Neuropeptides have long been recognized to be involved in regulation of behavior of human and other species(Burbach, 2011; Nathoo et al., 2001; L. S. Nelson et al., 1998; Zhang et al., 2015), and their involvement has been suggested in mental illness as well(Bissette et al., 1986; Caceda, Kinkead, & Nemeroff, 2007). In recent decades, the discovery, by various biochemical approaches, of novel neuropeptides has provided insights into the molecular regulation of behavior(Civelli et al., 2013; Hori et al., 2001; Kojima et al., 1999; Meunier et al., 1995; Sakurai, Amemiya, Ishii, Matsuzaki, Chemelli, Tanaka, Williams, Richarson, et al., 1998; Tatemoto et al., 1998). For example, discovery of the orexin system, the peptides orexin A and orexin B and orexin receptor 1 and 2, has increased our understanding of sleep homeostasis, as well as pain and fear expression (de Lecea & Sutcliffe, 1999; Flores, Saravia, Maldonado, & Berrendero, 2015; Nunez, Rodrigo-Angulo, Andres, & Garzon, 2009). In this way, discovery of novel neuropeptides may provide insights into mental illness, for example, in the dysregulation of emotional expression. Furthermore, these discoveries have also yielded productive drug targets(Patel et al., 2015). Indeed, neuropeptides almost entirely signal through G-protein coupled receptors (GPCRs), which are the class of cell-surface molecules most commonly targeted by existing drugs(Civelli et al., 2013). Thus, discovery of novel neuropeptides is likely to produce new modes of pharmacological intervention in psychiatry. By discovering and validating novel sORF encoded peptides in the mammalian brain, novel neuronal signaling systems can be discovered; and by

studying these novel genes in the context of schizophrenia novel approaches for intervention in psychiatry can be produced.

In this chapter, we have implemented a novel method for discovery of neuropeptides, which can easily be applied to any biological system. Here, we apply this system to the mouse brain. Here we combine novel neuropeptidomics techniques by mass spectrometry-based peptidomics with novel bioinformatics methods to discover micropeptides. Neuropeptidomics by mass spectrometry has been performed for many years, and standard techniques that have developed have been solubilization of brain extracts into acetic acid as a preservative against neuropeptide degradation. The novel neuropeptidomics methods we incorporate here are the heat-inactivation of brain samples by laser-guided heat delivery to the sample to a specific temperature for a specific time, immediately after dissection of the brain, in order to block neuropeptidases whose targets are unknown; simultaneously, we use microfiltration techniques, based on the highly successful FASP protocols, to purify the neuropeptides after heat-inactivation, preservation by acid, and extraction. We also combine these methods with novel techniques developed to discover micropeptides from mass spectrometry data. These techniques utilize ribosome profiling data with statistical methods to generate lists of all potentially translated ORFs in a transcriptome. By applying trypsin digestion to the neuropeptidomics extracts described above, we can use the databases thus generated to find micropeptides which act as neuropeptides, which is to say, secreted signaling molecules. As a proof of concept, in this chapter we describe a novel peptide translated from a short ORF, which is abundantly detected in our neuropeptidomics extracts. While we detect many cytosolic proteins which are not neuropeptides in our mass spectrometry data, and therefore cannot say with certainty that our novel peptide is a neuropeptide, the enrichment of such a peptide in the hypothalamus and amygdala

suggests that it may be involved in behavioral regulation, and a publication in peripheral T cells shows that activation by the peptide can occur by treatment in cell culture media, suggesting that it acts as a signaling peptide. Thus, we can show that our platform is indeed able to find novel micropeptides, and we have a strong suggestion that the peptide we discovered is a novel neuropeptide. We suggest, therefore, that our platform can find novel neuropeptides, and constitute a significant contribution to the field of neuropsychiatry.

Figures and Tables.

A0A0N4SUI7_MOUSE (100%), 7,026.1 Da
Protein 2210013O21Rik OS=Mus musculus GN=2210013O21Rik PE=4 SV=1
3 exclusive unique peptides, 6 exclusive unique spectra, 16 total spectra, 44/68 amino acids (65% coverage)

MGDQPCASGR **STLPPGNTR**E PKPPKKRCVL APR**WDYPEGT** **PSGGSSTLPS**
APPPASAGLK **SHPPPPEK**

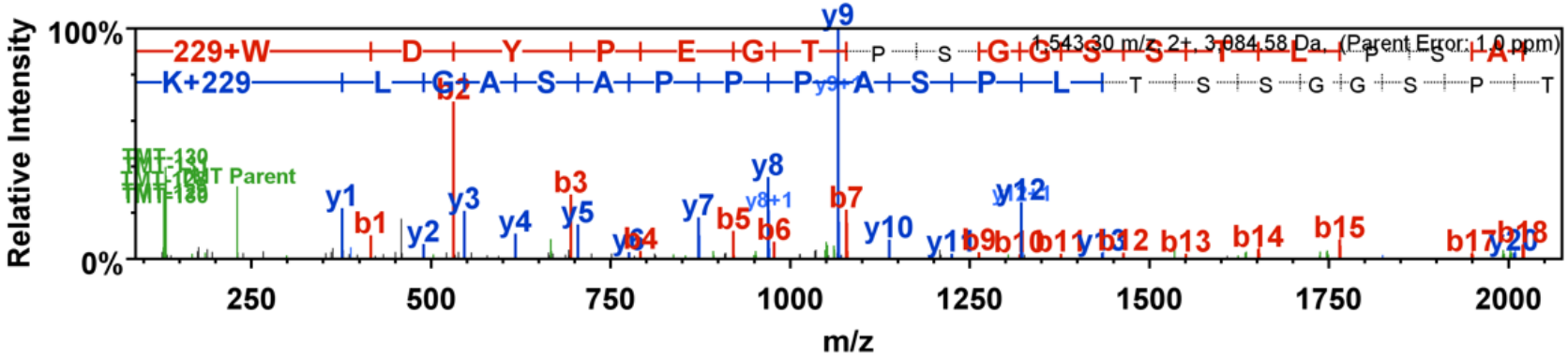

Figure 1. Micropeptide hit in mouse brain from peptidomics experiment. Transcript name is 2210013O21Rik. The protein produces 16 total spectra, and has 65% coverage. An example spectrum is shown.

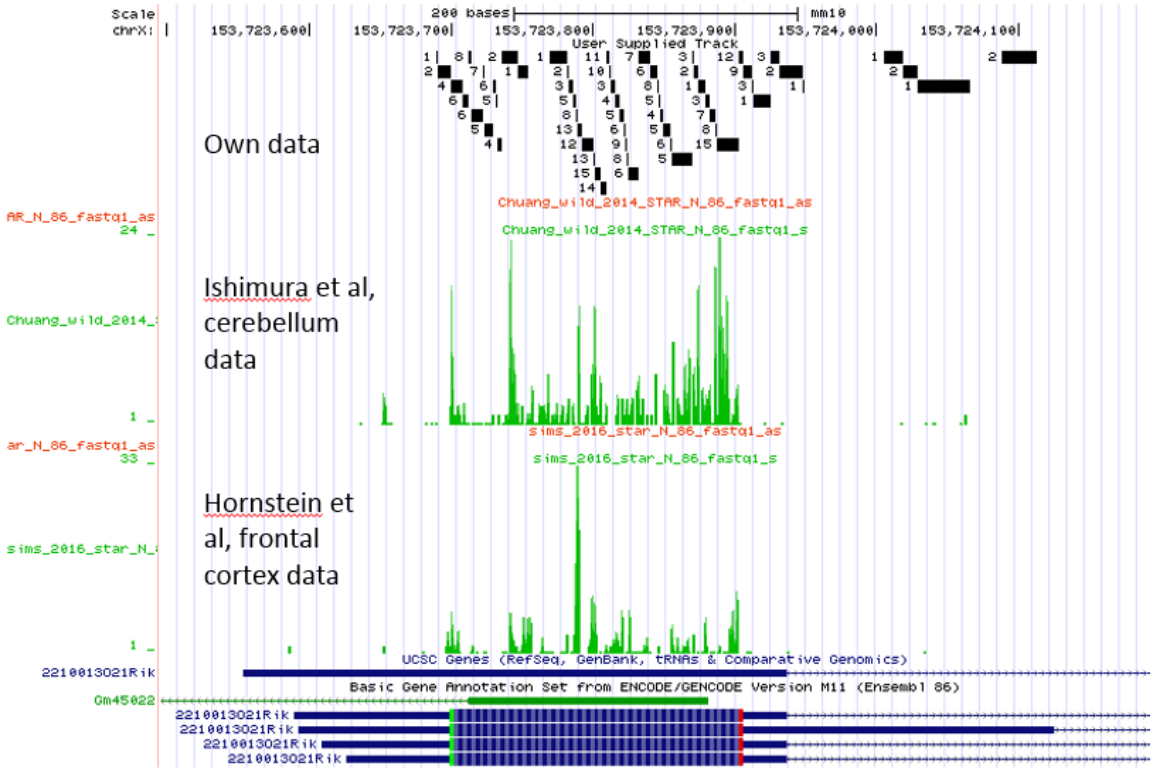

Figure 2. Ribosome profiling data showing translation of novel sORF. Bottom, genomic locus and transcript structure of sORF transcript. Four transcript isoforms of varying length and exon structure can be seen, but all four have a single ORF within the first exon. Above, an alternative transcript on the opposite genomic strand is shown in green. Above, overall exon structure of transcript. Above, ribosome profiling reads mapping to sORF from frontal lobe data (see Methods). Above, ribosome profiling reads mapping to sORF from cerebellum data (see Methods). Above, ribosome profiling reads mapping to sORF from whole brain ribosome profiling data.

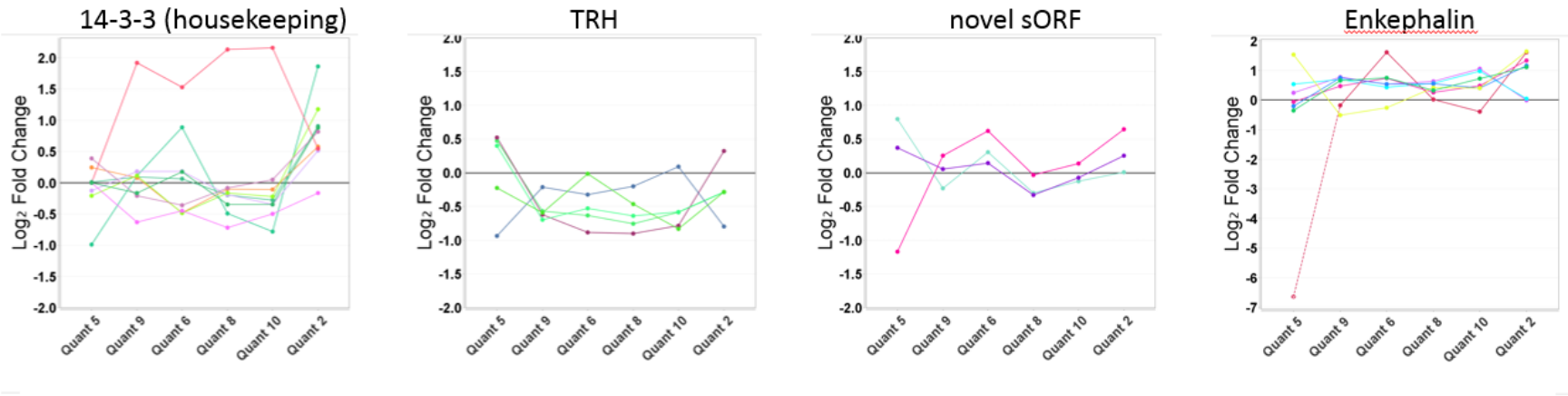

Figure 3. TMT labeling experiment for timecourse quantitation over mouse adolescence. Sample labels for each panel from left to right: 2 mice, 4 weeks old, 2 mice, 5 weeks old, 2 mice 6 weeks old. Panels from left to right: 14-3-3 scaffold protein, the TRH peptide hormone, the novel sORF found in this study, and the enkephalin protein. No clear differences in any protein. Each timecourse if for one representative tryptic peptide.

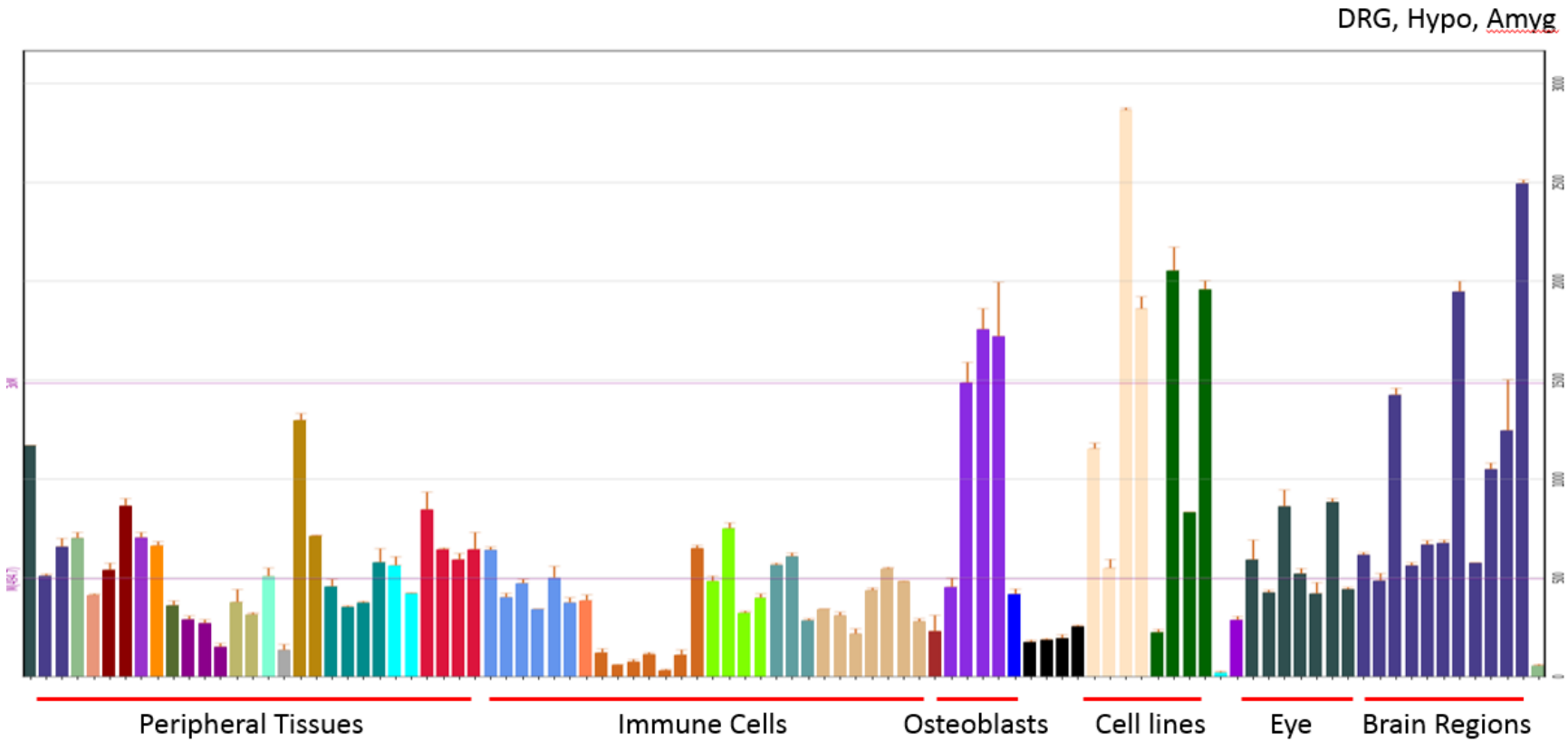

Figure 4. Analysis of novel sORF through BioGPS transcript expression data. Expression levels are organized into peripheral tissues, immune cells, osteoblasts, cell lines, eye tissue, and brain regions. Expression is highest in cell lines, specifically the NIH 3T3 line. However, among tissues expression is highest in brain, specifically in the dorsal root ganglion, hypothalamus, and amygdala.

Protein accession numbers	Protein identification probability	Total spectrum count
sp|P62814|VATB2_MOUSEV-type proton ATPase subunit B, brain isoform OS=Mus musculus GN=Atp6v1b2 PE=1 SV=1	100.00%	3
G3UW55_MOUSE	100.00%	16
E0CX65_MOUSE,Q2M4I8_MOUSE,Q6P6I8_MOUSE	100.00%	3
A0A0A0MQA8_MOUSE,Q149W7_MOUSE,TKN1_MOUSE	100.00%	8
D3YYN7_MOUSE,Q3UHK5_MOUSE,Q6ZQ49_MOUSE,sp|Q6PIE5|AT1A2_MOUSESodium /potassium-transporting ATPase subunit alpha-2 OS=Mus musculus GN=Atp1a2 PE=1 SV=1	98.20%	3
D3YXH0_MOUSE,PCP4_MOUSE	100.00%	651
sp|P56375|ACYP2_MOUSEAcylphosphatase-2 OS=Mus musculus GN=Acyp2 PE=1 SV=2	100.00%	18
Q9Z1R9_MOUSE	100.00%	13
D6REF3_MOUSE,Q5SS40_MOUSE,sp|P62259|1433E_MOUSE14-3-3 protein epsilon OS=Mus musculus GN=Ywhae PE=1 SV=1	99.80%	4
B2RTP7_MOUSE,K22E_MOUSE	100.00%	12
QCR6_MOUSE	100.00%	33
sp|Q3UNH4|GRIN1_MOUSEG protein-regulated inducer of neurite outgrowth 1 OS=Mus musculus GN=Gprin1 PE=1 SV=2	100.00%	118
F7BNZ5_MOUSE,Q8C0B4_MOUSE	100.00%	4
B9EIV5_MOUSE,E9PZM8_MOUSE,F7BX42_MOUSE,Q3UH37_MOUSE,Q3UH69_MOUSE, sp|Q99J85|NPTXR_MOUSENeuronal pentraxin receptor OS=Mus musculus GN=Nptxr PE=1 SV=1	100.00%	5
sp|Q60829|PPR1B_MOUSEProtein phosphatase 1 regulatory subunit 1B OS=Mus musculus	100.00%	4

GN=Ppp1r1b PE=1 SV=2		
sp|P63040|CPLX1_MOUSEComplexin-1 OS=Mus musculus GN=Cplx1 PE=1 SV=1	100.00%	22
IF4B_MOUSE,Q3TDD8_MOUSE,Q3THB0_MOUSE,Q3TSY9_MOUSE	100.00%	6
7B2_MOUSE,Q3TT51_MOUSE	100.00%	5
452333,sp|Q91VW3|SH3L3_MOUSESH3 domain-binding glutamic acid-rich-like protein 3 OS=Mus musculus GN=Sh3bgrl3 PE=1 SV=1	100.00%	48
Q564F6_MOUSE,sp|P56812|PDCD5_MOUSEProgrammed cell death protein 5 OS=Mus musculus GN=Pdcd5 PE=1 SV=3	100.00%	36
sp|P46414|CDN1B_MOUSECyclin-dependent kinase inhibitor 1B OS=Mus musculus GN=Cdkn1b PE=1 SV=2	100.00%	26
sp|Q32M26|CK087_MOUSEUncharacterized protein C11orf87 homolog OS=Mus musculus PE=2 SV=1	100.00%	3
sp|Q9WVA2|TIM8A_MOUSEMitochondrial import inner membrane translocase subunit Tim8 A OS=Mus musculus GN=Timm8a1 PE=1 SV=1	100.00%	4
323714,328814,DTD1_MOUSE	100.00%	17
MYL6_MOUSE,Q3TIG9_MOUSE,Q642K0_MOUSE	99.90%	2
D3Z0Y2_MOUSE,Q53ZU7_MOUSE,Q6A0D0_MOUSE,Q6GT24_MOUSE,sp|O08709|PRDX 6_MOUSEPeroxiredoxin-6 OS=Mus musculus GN=Prdx6 PE=1 SV=3	100.00%	2
Q0VGU4_MOUSE	100.00%	54
Q569X3_MOUSE,RU1C_MOUSE	100.00%	4
sp|Q6W8Q3|PC4L1_MOUSEPurkinje cell protein 4-like protein 1 OS=Mus musculus GN=Pcp4l1 PE=1 SV=1	100.00%	79
Q3THA6_MOUSE,sp|Q8BL97|SRSF7_MOUSESerine/arginine-rich splicing factor 7 OS=Mus musculus GN=Srsf7 PE=1 SV=1	99.80%	2
sp|Q9CRB6|TPPP3_MOUSETubulin polymerization-promoting protein family member 3 OS=Mus musculus GN=Tppp3 PE=1 SV=1	100.00%	10
sp|Q62048|PEA15_MOUSEAstrocytic phosphoprotein PEA-15 OS=Mus musculus GN=Pea15 PE=1 SV=1	100.00%	18
VATF_MOUSE	100.00%	5

CCKN_MOUSE	100.00%	9
sp|Q8BTE0|SDHF4_MOUSESuccinate dehydrogenase assembly factor 4, mitochondrial OS=Mus musculus GN=Sdhaf4 PE=3 SV=2	100.00%	18
B9EKJ7_MOUSE,sp|P58871|TB182_MOUSE182 kDa tankyrase-1-binding protein OS=Mus musculus GN=Tnks1bp1 PE=1 SV=2	100.00%	4
A6ZI44_MOUSE,Q5FWB7_MOUSE,Q6NY00_MOUSE,sp|P05064|ALDOA_MOUSEFructose-bisphosphate aldolase A OS=Mus musculus GN=Aldoa PE=1 SV=2	100.00%	5
MAP6_MOUSE	100.00%	77
A0A0A0MQ79_MOUSE,sp|Q3TLH4|PRC2C_MOUSEProtein PRRC2C OS=Mus musculus GN=Prrc2c PE=1 SV=3	100.00%	4
E9Q1Z0_MOUSE,Q148Q7_MOUSE,Q8BIS2_MOUSE	100.00%	8
B2RQ73_MOUSE,B7ZMZ9_MOUSE,E9Q4S3_MOUSE,NIN_MOUSE,Q3UR16_MOUSE,Q674R4_MOUSE	100.00%	7
sp|O35143|ATIF1_MOUSEATPase inhibitor, mitochondrial OS=Mus musculus GN=Atpif1 PE=1 SV=2	100.00%	14
ENOA_MOUSE,Q5FW97_MOUSE	100.00%	5
Q14C38_MOUSE,sp|Q8CCT4|TCAL5_MOUSETranscription elongation factor A protein-like 5 OS=Mus musculus GN=Tceal5 PE=1 SV=1	100.00%	69
COLI_MOUSE	100.00%	3
MIA3_MOUSE	99.90%	5
D0VYV7_MOUSE	100.00%	10
Q5I0U7_MOUSE,TBCA_MOUSE	100.00%	20
GUAD_MOUSE,Q3U0C4_MOUSE,Q548F2_MOUSE,Q69ZN0_MOUSE,Q6DFY1_MOUSE	99.70%	2
TKNK_MOUSE	100.00%	6
Q545V6_MOUSE,SMS_MOUSE	100.00%	9
K22O_MOUSE	99.80%	16
666324,E9Q827_MOUSE,sp|P56212|ARP19_MOUSEcAMP-regulated phosphoprotein 19 OS=Mus musculus GN=Arpp19 PE=1 SV=2	100.00%	69

sp|Q8BH93|MISSL_MOUSEMAPK-interacting and spindle-stabilizing protein-like OS=Mus musculus GN=Mapk1ip1l PE=2 SV=3	100.00%	4
CLCB_MOUSE	100.00%	7
Q543N3_MOUSE,sp|Q61792|LASP1_MOUSELIM and SH3 domain protein 1 OS=Mus musculus GN=Lasp1 PE=1 SV=1	100.00%	40
Q9D881_MOUSE,sp|P19536|COX5B_MOUSECytochrome c oxidase subunit 5B, mitochondrial OS=Mus musculus GN=Cox5b PE=1 SV=1	100.00%	8
A0A0A0MQF6_MOUSE,D2KHZ9_MOUSE,G3P_MOUSE,Q8CEV2_MOUSE,S4R1W1_MOUSE,S4R257_MOUSE	100.00%	3
sp|P50446|K2C6A_MOUSEKeratin, type II cytoskeletal 6A OS=Mus musculus GN=Krt6a PE=1 SV=3	100.00%	38
A0A0A6YW52_MOUSE,Q3UD53_MOUSE,Q5M9P7_MOUSE,sp|Q9CR86|CHSP1_MOUSE Calcium-regulated heat stable protein 1 OS=Mus musculus GN=Carhsp1 PE=1 SV=1	100.00%	4
Q3THQ5_MOUSE,sp|Q60864|STIP1_MOUSEStress-induced-phosphoprotein 1 OS=Mus musculus GN=Stip1 PE=1 SV=1	100.00%	2
IF4H_MOUSE,Q3TG58_MOUSE,Q564E5_MOUSE,Q80U88_MOUSE	100.00%	21
sp|O88852|TSYL1_MOUSETestis-specific Y-encoded-like protein 1 OS=Mus musculus GN=Tspyl1 PE=2 SV=1	100.00%	4
sp|Q8BK30|NDUV3_MOUSENADH dehydrogenase [ubiquinone] flavoprotein 3, mitochondrial OS=Mus musculus GN=Ndufv3 PE=1 SV=1	100.00%	35
EPN1_MOUSE	100.00%	8
AMD_MOUSE	100.00%	13
A2AJH3_MOUSE,NMT2_MOUSE,Q3THR4_MOUSE	100.00%	3
D3Z5R4_MOUSE,E9Q2D0_MOUSE,sp|P0C7L0|WIPF3_MOUSEWAS/WASL-interacting protein family member 3 OS=Mus musculus GN=Wipf3 PE=1 SV=1	100.00%	57
THIO_MOUSE	100.00%	42
sp|Q91YQ3|CSDC2_MOUSECold shock domain-containing protein C2 OS=Mus musculus GN=Csdc2 PE=1 SV=2	100.00%	8
Q54AC6_MOUSE,sp|P56394|COX17_MOUSECytochrome c oxidase copper chaperone	100.00%	23

OS=Mus musculus GN=Cox17 PE=1 SV=2		
ICLN_MOUSE,Q923F1_MOUSE	100.00%	2
sp|Q9DC07|LNEBL_MOUSELIM zinc-binding domain-containing Nebulette OS=Mus musculus GN=Nebl PE=1 SV=1	100.00%	27
HN1L_MOUSE,Q3TM10_MOUSE	100.00%	14
A0A0G2JDN7_MOUSE,E9PZ43_MOUSE	100.00%	2
sp|P38647|GRP75_MOUSEStress-70 protein, mitochondrial OS=Mus musculus GN=Hspa9 PE=1 SV=3	100.00%	3
A0A0A0MQC7_MOUSE,A2A5Y6_MOUSE,TAU_MOUSE	100.00%	56
sp|Q8R5H6|WASF1_MOUSEWiskott-Aldrich syndrome protein family member 1 OS=Mus musculus GN=Wasf1 PE=1 SV=2	100.00%	5
Q545B6_MOUSE,sp|P54227|STMN1_MOUSEStathmin OS=Mus musculus GN=Stmn1 PE=1 SV=2	100.00%	74
sp|Q99M71|EPDR1_MOUSEMammalian ependymin-related protein 1 OS=Mus musculus GN=Epdr1 PE=1 SV=1	100.00%	3
MTPN_MOUSE	100.00%	7
sp|P70349|HINT1_MOUSEHistidine triad nucleotide-binding protein 1 OS=Mus musculus GN=Hint1 PE=1 SV=3	100.00%	11
CEND_MOUSE	100.00%	114
A8IK50_MOUSE,PCP2_MOUSE	100.00%	69
A0A0G2JGX4_MOUSE,Q8VCE0_MOUSE,sp|Q6PIC6|AT1A3_MOUSESodium/potassium-transporting ATPase subunit alpha-3 OS=Mus musculus GN=Atp1a3 PE=1 SV=1	100.00%	5
A2ARP8_MOUSE,sp|Q9QYR6|MAP1A_MOUSEMicrotubule-associated protein 1A OS=Mus musculus GN=Map1a PE=1 SV=2	100.00%	28
E9PX89_MOUSE,E9Q705_MOUSE,Q14A77_MOUSE,sp|Q8CEI1|BOLA3_MOUSEBolA-like protein 3 OS=Mus musculus GN=Bola3 PE=1 SV=1	100.00%	5
KCRB_MOUSE	100.00%	4
UCRI_MOUSE	100.00%	25

ENSA_MOUSE	100.00%	246
sp|A2A8L1|CHD5_MOUSE-DECOY	99.80%	3
Q4FJU3_MOUSE,sp|Q9DCT8|CRIP2_MOUSECysteine-rich protein 2 OS=Mus musculus GN=Crip2 PE=1 SV=1	100.00%	4
sp|Q3U0V1|FUBP2_MOUSEFar upstream element-binding protein 2 OS=Mus musculus GN=Khsrp PE=1 SV=2	100.00%	14
SYN1_MOUSE	100.00%	45
Q3ULN5_MOUSE,sp|P26883|FKB1A_MOUSEPeptidyl-prolyl cis-trans isomerase FKBP1A OS=Mus musculus GN=Fkbp1a PE=1 SV=2	100.00%	14
sp|Q9D8Z2|TRIA1_MOUSETP53-regulated inhibitor of apoptosis 1 OS=Mus musculus GN=Triap1 PE=1 SV=1	100.00%	9
TPIS_MOUSE	100.00%	33
sp|Q9D1L0|CHCH2_MOUSECoiled-coil-helix-coiled-coil-helix domain-containing protein 2 OS=Mus musculus GN=Chchd2 PE=2 SV=1	81.90%	10
Q9D6F8_MOUSE	56.30%	5
Q059I1_MOUSE,RS28_MOUSE	100.00%	46
Q3TY66_MOUSE,SCG1_MOUSE	100.00%	72
WNK1_MOUSE	100.00%	4
B1AX78_MOUSE,Q99JH2_MOUSE	100.00%	8
NEU2_MOUSE,Q3UUQ5_MOUSE	100.00%	8
H7BX95_MOUSE,sp|Q6PDM2|SRSF1_MOUSESerine/arginine-rich splicing factor 1 OS=Mus musculus GN=Srsf1 PE=1 SV=3	100.00%	17
COA4_MOUSE	100.00%	14
sp|Q78J03|MSRB2_MOUSEMethionine-R-sulfoxide reductase B2, mitochondrial OS=Mus musculus GN=Msrb2 PE=1 SV=1	100.00%	8
AAK1_MOUSE	100.00%	15
Q3TJ52_MOUSE,Q3U041_MOUSE,Q3UQN3_MOUSE,Q6NVC3_MOUSE,sp|P54728|RD23B_MOUSEUV excision repair protein RAD23 homolog B OS=Mus musculus GN=Rad23b	100.00%	5

PE=1 SV=2		
Q8C6L4_MOUSE,RTN3_MOUSE	100.00%	4
sp|O08553|DPYL2_MOUSEDihydropyrimidinase-related protein 2 OS=Mus musculus GN=Dpysl2 PE=1 SV=2	100.00%	12
sp|Q9ERT9|PPR1A_MOUSEProtein phosphatase 1 regulatory subunit 1A OS=Mus musculus GN=Ppp1r1a PE=1 SV=1	100.00%	56
A2RTI3_MOUSE,LGMN_MOUSE,Q3UE99_MOUSE	100.00%	7
sp|Q6QWF9|CK2N1_MOUSECalcium/calmodulin-dependent protein kinase II inhibitor 1 OS=Mus musculus GN=Camk2n1 PE=1 SV=1	100.00%	12
ISCU_MOUSE	100.00%	7
sp|Q99JX1|TAF11_MOUSETranscription initiation factor TFIID subunit 11 OS=Mus musculus GN=Taf11 PE=2 SV=1	100.00%	5
DOPD_MOUSE,Q3UNI8_MOUSE	100.00%	7
C10_MOUSE	100.00%	3
493543,HOP_MOUSE	100.00%	10
K2C4_MOUSE	98.80%	7
A0A0N4SUN8_MOUSE,A0A0N4SUQ1_MOUSE,A0A0N4SV32_MOUSE,A0A0N4SWH2_MOUSE,Q3UEI6_MOUSE,Q3UJK2_MOUSE,Q3UMP4_MOUSE,Q3V274_MOUSE,sp|Q9CY58|PAIRB_MOUSEPlasminogen activator inhibitor 1 RNA-binding protein OS=Mus musculus GN=Serbp1 PE=1 SV=2	100.00%	2
NFH_MOUSE,Q80TQ3_MOUSE	100.00%	3
sp|P60879|SNP25_MOUSESynaptosomal-associated protein 25 OS=Mus musculus GN=Snap25 PE=1 SV=1	99.90%	2
sp|Q60865|CAPR1_MOUSECaprin-1 OS=Mus musculus GN=Caprin1 PE=1 SV=2	100.00%	2
539803,SYUA_MOUSE	100.00%	2
sp|P20357|MTAP2_MOUSEMicrotubule-associated protein 2 OS=Mus musculus GN=Map2 PE=1 SV=2	100.00%	26
Q8C9Y1_MOUSE,sp|O35188|X3CL1_MOUSEFractalkine OS=Mus musculus GN=Cx3cl1	100.00%	7

PE=1 SV=3		
E9QKI4_MOUSE,E9QKI5_MOUSE,sp|Q9D1F4|AKTS1_MOUSEProline-rich AKT1 substrate 1 OS=Mus musculus GN=Akt1s1 PE=1 SV=1	100.00%	3
Q3TD71_MOUSE,Q3UY11_MOUSE,sp|Q8K021|SCAM1_MOUSESecretory carrier-associated membrane protein 1 OS=Mus musculus GN=Scamp1 PE=1 SV=1	100.00%	2
sp|P52503|NDUS6_MOUSENADH dehydrogenase [ubiquinone] iron-sulfur protein 6, mitochondrial OS=Mus musculus GN=Ndufs6 PE=1 SV=2	100.00%	84
A0A0B4J1F2_MOUSE,A0A0B4J1M9_MOUSE,MAP4_MOUSE	100.00%	18
sp|Q6IFX2|K1C42_MOUSEKeratin, type I cytoskeletal 42 OS=Mus musculus GN=Krt42 PE=1 SV=1	99.90%	28
sp|Q8VED5|K2C79_MOUSEKeratin, type II cytoskeletal 79 OS=Mus musculus GN=Krt79 PE=1 SV=2	100.00%	20
DYL2_MOUSE	100.00%	2
PCNP_MOUSE,Q3UCC5_MOUSE	100.00%	35
SCG2_MOUSE	100.00%	53
Q8C1L7_MOUSE,RS21_MOUSE	100.00%	13
134381	100.00%	9
sp|P11087|CO1A1_MOUSECollagen alpha-1(I) chain OS=Mus musculus GN=Col1a1 PE=1 SV=4	100.00%	41
G3XA10_MOUSE,Q3TVV6_MOUSE,Q3TWN5_MOUSE,Q3TXW2_MOUSE,Q3ULH5_MOUSE,Q8C290_MOUSE,sp|Q8VEK3|HNRPU_MOUSEHeterogeneous nuclear ribonucleoprotein U OS=Mus musculus GN=Hnrnpu PE=1 SV=1	100.00%	2
YAP1_MOUSE	100.00%	4
A3KN68_MOUSE,sp|P80560|PTPR2_MOUSEReceptor-type tyrosine-protein phosphatase N2 OS=Mus musculus GN=Ptprn2 PE=1 SV=2	100.00%	12
685904,A0A0N4SUI7_MOUSE	100.00%	20
sp|Q9CPU2|NDUB2_MOUSENADH dehydrogenase [ubiquinone] 1 beta subcomplex subunit 2, mitochondrial OS=Mus musculus GN=Ndufb2 PE=1 SV=1	100.00%	2
Q3TG37_MOUSE,sp|P70441|NHRF1_MOUSENa(+)/H(+) exchange regulatory cofactor	100.00%	2

NHE-RF1 OS=Mus musculus GN=Slc9a3r1 PE=1 SV=3		
E0CZ08_MOUSE	95.80%	33
PENK_MOUSE,Q3UXY8_MOUSE	100.00%	13
sp|Q9CR98|F136A_MOUSEProtein FAM136A OS=Mus musculus GN=Fam136a PE=1 SV=1	100.00%	3
Q3U781_MOUSE,Q9D6W4_MOUSE,sp|P84104|SRSF3_MOUSESerine/arginine-rich splicing factor 3 OS=Mus musculus GN=Srsf3 PE=1 SV=1	100.00%	3
A0A087WNP6_MOUSE,CDV3_MOUSE	100.00%	72
sp|Q3UGS4|F195B_MOUSEProtein FAM195B OS=Mus musculus GN=Fam195b PE=1 SV=1	100.00%	6
sp|P13595|NCAM1_MOUSENeural cell adhesion molecule 1 OS=Mus musculus GN=Ncam1 PE=1 SV=3	6.70%	36
B2RRX2_MOUSE,sp|P63328|PP2BA_MOUSESerine/threonine-protein phosphatase 2B catalytic subunit alpha isoform OS=Mus musculus GN=Ppp3ca PE=1 SV=1	100.00%	8
ACTB_MOUSE,ACTG_MOUSE,B2RRX1_MOUSE,Q3U5R4_MOUSE,Q3U804_MOUSE,Q3U939_MOUSE,Q3UA89_MOUSE,Q3UAA9_MOUSE,Q3UAF7_MOUSE,Q3UCF8_MOUSE,Q4KL81_MOUSE,Q61276_MOUSE	100.00%	31
Q7TT20_MOUSE,Q8CHE0_MOUSE	100.00%	92
SCG3_MOUSE	100.00%	23
A2BI30_MOUSE,F6ZGR6_MOUSE	100.00%	7
sp|Q68ED7|CRTC1_MOUSECREB-regulated transcription coactivator 1 OS=Mus musculus GN=Crtc1 PE=1 SV=1	100.00%	8
V6BQR3_MOUSE	95.30%	10
R7RU63_MOUSE,R7RVD4_MOUSE	100.00%	2
33432	82.30%	334
BIN1_MOUSE,Q6P1B9_MOUSE	100.00%	5
Q3TCH2_MOUSE,sp|Q9R0P9|UCHL1_MOUSEUbiquitin carboxyl-terminal hydrolase isozyme L1 OS=Mus musculus GN=Uchl1 PE=1 SV=1	100.00%	4

Q3UI46_MOUSE,sp|P29595|NEDD8_MOUSENEDD8 OS=Mus musculus GN=Nedd8 PE=1 SV=2	100.00%	37
Q9D6K2_MOUSE,sp|Q9R1Q8|TAGL3_MOUSETransgelin-3 OS=Mus musculus GN=Tagln3 PE=1 SV=1	100.00%	3
E9QJT5_MOUSE,Q4VAF0_MOUSE,sp|P56376|ACYP1_MOUSEAcylphosphatase-1 OS=Mus musculus GN=Acyp1 PE=1 SV=2	100.00%	10
H2AX_MOUSE	100.00%	6
sp|Q80Y61|BI2L2_MOUSEBrain-specific angiogenesis inhibitor 1-associated protein 2-like protein 2 OS=Mus musculus GN=Baiap2l2 PE=1 SV=1	100.00%	2
sp|Q8C3W1|CA198_MOUSEUncharacterized protein C1orf198 homolog OS=Mus musculus PE=1 SV=1	100.00%	8
Q3TH99_MOUSE,sp|Q9JM96|BORG4_MOUSECdc42 effector protein 4 OS=Mus musculus GN=Cdc42ep4 PE=1 SV=1	100.00%	12
tr|E0CX45|E0CX45_MOUSE-DECOY	100.00%	13
sp|E9PUL5|PRRT2_MOUSEProline-rich transmembrane protein 2 OS=Mus musculus GN=Prrt2 PE=1 SV=1	100.00%	19
Q3TUB1_MOUSE,Q3U311_MOUSE,sp|Q03157|APLP1_MOUSEAmyloid-like protein 1 OS=Mus musculus GN=Aplp1 PE=1 SV=1	100.00%	4
HEXB_MOUSE,Q3TXR9_MOUSE	100.00%	3
J3QMK2_MOUSE	100.00%	2
Q561N4_MOUSE	100.00%	5
Q3TJA9_MOUSE,sp|Q99M87|DNJA3_MOUSEDnaJ homolog subfamily A member 3, mitochondrial OS=Mus musculus GN=Dnaja3 PE=1 SV=1	100.00%	9
sp|Q6PEV3|WIPF2_MOUSEWAS/WASL-interacting protein family member 2 OS=Mus musculus GN=Wipf2 PE=1 SV=1	100.00%	4
HN1_MOUSE	100.00%	38
Q3ULN7_MOUSE,sp|Q9DCP9|DAZP2_MOUSEDAZ-associated protein 2 OS=Mus musculus GN=Dazap2 PE=1 SV=1	100.00%	2
B1AQ77_MOUSE,sp|Q61414|K1C15_MOUSEKeratin, type I cytoskeletal 15 OS=Mus	99.90%	21

musculus GN=Krt15 PE=1 SV=2		
G3UZA7_MOUSE,sp|Q9Z172|SUMO3_MOUSESmall ubiquitin-related modifier 3 OS=Mus musculus GN=Sumo3 PE=1 SV=1	100.00%	53
sp|Q9CRD0|OCAD1_MOUSEOCIA domain-containing protein 1 OS=Mus musculus GN=Ociad1 PE=1 SV=1	100.00%	10
sp|Q9JHU4|DYHC1_MOUSECytoplasmic dynein 1 heavy chain 1 OS=Mus musculus GN=Dync1h1 PE=1 SV=2	99.50%	2
Q3TCR9_MOUSE,Q8CBM0_MOUSE,ZYX_MOUSE	100.00%	17
tr|A0A0G2JGW5|A0A0G2JGW5_MOUSE-DECOY	99.80%	5
sp|Q8CI43|MYL6B_MOUSEMyosin light chain 6B OS=Mus musculus GN=Myl6b PE=1 SV=1	100.00%	4
Q3TRX4_MOUSE,Q3UZP7_MOUSE,Q542N8_MOUSE	100.00%	26
BSN_MOUSE	100.00%	9
Q8BNA5_MOUSE,Q921L6_MOUSE,SRC8_MOUSE	100.00%	3
CATD_MOUSE,Q3TJN3_MOUSE,Q3TWD0_MOUSE,Q3TXL5_MOUSE,Q3U7I9_MOUSE,Q3U7P0_MOUSE,Q3U8W5_MOUSE,Q3UAQ1_MOUSE,Q3UCD9_MOUSE,Q3UCW4_MOUSE	100.00%	5
Q5GQ64_MOUSE,SYUG_MOUSE	100.00%	7
A2AL12_MOUSE,B2RXM2_MOUSE,E9Q7H5_MOUSE,J3QNY1_MOUSE,Q0VG47_MOUSE,Q3UZG3_MOUSE,Q5FB19_MOUSE,Q6P6I7_MOUSE,ROA3_MOUSE	99.80%	2
sp|Q80X50|UBP2L_MOUSEUbiquitin-associated protein 2-like OS=Mus musculus GN=Ubap2l PE=1 SV=1	100.00%	17
Q3U9A8_MOUSE,sp|Q9JJU8|SH3L1_MOUSESH3 domain-binding glutamic acid-rich-like protein OS=Mus musculus GN=Sh3bgrl PE=1 SV=1	100.00%	14
Q3UIL5_MOUSE	100.00%	9
Q3TU64_MOUSE,Q3TUE2_MOUSE,Q3TX57_MOUSE,sp|Q01149|CO1A2_MOUSECollagen alpha-2(I) chain OS=Mus musculus GN=Col1a2 PE=1 SV=2	100.00%	20
MT3_MOUSE,Q3USP9_MOUSE	100.00%	7
B0QZN5_MOUSE,O35619_MOUSE,Q8CHR4_MOUSE,sp|P63044|VAMP2_MOUSEVesicle-associated membrane protein 2 OS=Mus musculus GN=Vamp2 PE=1 SV=2	100.00%	13

Q3SYP5_MOUSE,Q3ZAW8_MOUSE,Q9EQD6_MOUSE,Q9EQD7_MOUSE,sp|Q9Z2K1|K1C16_MOUSEKeratin, type I cytoskeletal 16 OS=Mus musculus GN=Krt16 PE=1 SV=3	100.00%	27
B2RPU8_MOUSE,Q8CEW7_MOUSE	99.50%	10
Q6ZWX2_MOUSE	100.00%	115
D3Z1F7_MOUSE,sp|Q9DBN4|P33MX_MOUSEPutative monooxygenase p33MONOX OS=Mus musculus GN=P33monox PE=1 SV=1	100.00%	11
sp|Q9JMG7|HDGR3_MOUSEHepatoma-derived growth factor-related protein 3 OS=Mus musculus GN=Hdgfrp3 PE=1 SV=2	100.00%	8
Q3TGC5_MOUSE,Q5EBQ2_MOUSE,sp|P70296|PEBP1_MOUSEPhosphatidylethanolamine-binding protein 1 OS=Mus musculus GN=Pebp1 PE=1 SV=3	100.00%	92
A2AMY5_MOUSE,sp|Q91VX2|UBAP2_MOUSEUbiquitin-associated protein 2 OS=Mus musculus GN=Ubap2 PE=1...	100.00%	5
sp|Q9QZM0|UBQL2_MOUSEUbiquilin-2 OS=Mus musculus GN=Ubqln2 PE=1 SV=2	100.00%	19
Q3TFB1_MOUSE,Q3TIK8_MOUSE,Q3U7F3_MOUSE,Q3UK83_MOUSE,Q5EBP8_MOUSE,ROA1_MOUSE	99.80%	2
PLD3_MOUSE	100.00%	3
A0A0G2JEK2_MOUSE,Q6P3B4_MOUSE,sp|P63254|CRIP1_MOUSECysteine-rich protein 1 OS=Mus musculus GN=Crip1 PE=1 SV=2	100.00%	2
665268	100.00%	46
B7ZP22_MOUSE,ROA2_MOUSE	100.00%	6
TBB3_MOUSE	99.10%	14
sp|P56391|CX6B1_MOUSECytochrome c oxidase subunit 6B1 OS=Mus musculus GN=Cox6b1 PE=1 SV=2	100.00%	69
Q3U6L3_MOUSE,sp|Q9QUH0|GLRX1_MOUSEGlutaredoxin-1 OS=Mus musculus GN=Glrx PE=1 SV=3	100.00%	6
EF1B_MOUSE	100.00%	8
F6XIX0_MOUSE	99.80%	7
Q3TDY6_MOUSE,Q3U2Z6_MOUSE,Q8BNF3_MOUSE,TPP1_MOUSE	100.00%	4

K2C1_MOUSE	100.00%	22
Q3U7H9_MOUSE,Q3UWS9_MOUSE	100.00%	13
Q58E70_MOUSE	99.90%	2
DEST_MOUSE,Q4FK36_MOUSE	94.30%	2
ACTA_MOUSE,ACTC_MOUSE,ACTH_MOUSE,Q3U122_MOUSE,Q3UIJ3_MOUSE,Q3UJ36_MOUSE,Q497E4_MOUSE,Q61275_MOUSE,Q9CXK3_MOUSE	100.00%	24
EID2_MOUSE	100.00%	8
H7BWY8_MOUSE,TSR2_MOUSE,Z4YL87_MOUSE	100.00%	4
MDHC_MOUSE	100.00%	6
E9QAQ7_MOUSE,sp|A2BH40|ARI1A_MOUSEAT-rich interactive domain-containing protein 1A OS=Mus musculus GN=Arid1a PE=1 SV=1	100.00%	2
Q6NZC5_MOUSE	100.00%	612
sp|Q9QXV0|PCSK1_MOUSEProSAAS OS=Mus musculus GN=Pcsk1n PE=1 SV=2	100.00%	96
sp|Q8K039|K1143_MOUSEUncharacterized protein KIAA1143 homolog OS=Mus musculus PE=1 SV=1	100.00%	8
B2RQX9_MOUSE,B2RXV9_MOUSE	100.00%	2
A8IP69_MOUSE,sp|P61982|1433G_MOUSE14-3-3 protein gamma OS=Mus musculus GN=Ywhag PE=1 SV=2	100.00%	6
A6H6H4_MOUSE,sp|Q6ZWY8|TYB10_MOUSEThymosin beta-10 OS=Mus musculus GN=Tmsb10 PE=1 SV=3	100.00%	58
NEC2_MOUSE,Q3TT48_MOUSE,Q3TYM6_MOUSE,Q3UZV3_MOUSE,Q547J8_MOUSE	100.00%	3
E9PY90_MOUSE,E9Q3S2_MOUSE,H3BJI6_MOUSE,H3BJS0_MOUSE,H3BK44_MOUSE,H3BK48_MOUSE,H3BKH2_MOUSE,H3BKL6_MOUSE,H3BL19_MOUSE,Q3TZZ3_MOUSE,sp|Q8R311|CTGE5_MOUSEcTAGE family member 5 OS=Mus musculus GN=Ctage5 PE=1 SV=1	100.00%	2
A0A087WP98_MOUSE,A0A087WPN6_MOUSE,A0A087WQN2_MOUSE,PTMA_MOUSE,Q0VGU2_MOUSE,Q3U6E4_MOUSE,Q3U8X6_MOUSE,Q3UA54_MOUSE,Q8C2T3_MOUSE	100.00%	3
Q8BH80_MOUSE,VAPB_MOUSE	100.00%	7

A3KGA5_MOUSE,CMC4_MOUSE	100.00%	5
sp|Q9D8B3|CHM4B_MOUSECharged multivesicular body protein 4b OS=Mus musculus GN=Chmp4b PE=1 SV=2	100.00%	5
sp|Q6PGL7|FAM21_MOUSEWASH complex subunit FAM21 OS=Mus musculus GN=Fam21 PE=1 SV=1	100.00%	3
407588,412206,IPKA_MOUSE	100.00%	9
K2C5_MOUSE,Q32P04_MOUSE	100.00%	36
NEUG_MOUSE	100.00%	279
ENOG_MOUSE,Q3UJ20_MOUSE,Q545V3_MOUSE	100.00%	24
LYAG_MOUSE	100.00%	17
CH10_MOUSE,Q4KL76_MOUSE	100.00%	92
DPP2_MOUSE	100.00%	3
D3Z4A4_MOUSE	100.00%	2
sp|Q99JI1|MSTN1_MOUSEMusculoskeletal embryonic nuclear protein 1 OS=Mus musculus GN=Mustn1 PE=1 SV=1	100.00%	3
D3Z2Z1_MOUSE,F8WIA1_MOUSE,sp|Q922J3|CLIP1_MOUSECAP-Gly domain-containing linker protein 1 OS=Mus musculus GN=Clip1 PE=1 SV=1	100.00%	7
CART_MOUSE	100.00%	7
Q3URG1_MOUSE,TPPP_MOUSE	100.00%	18
sp|Q99JP4|CDC26_MOUSEAnaphase-promoting complex subunit CDC26 OS=Mus musculus GN=Cdc26 PE=1 SV=1	100.00%	15
sp|P63101|1433Z_MOUSE14-3-3 protein zeta/delta OS=Mus musculus GN=Ywhaz PE=1 SV=1	100.00%	10
SODC_MOUSE	100.00%	155
J3QK04_MOUSE	8.50%	587
CMGA_MOUSE	100.00%	6
Q3TWF2_MOUSE,Q3U6V3_MOUSE,Q3U9G2_MOUSE,Q9DC41_MOUSE,sp|P20029|GRP78_MOUSE78 kDa glucose-regulated protein OS=Mus musculus GN=Hspa5 PE=1 SV=3	100.00%	3

Q54A87_MOUSE,sp|Q9WTT4|VATG2_MOUSEV-type proton ATPase subunit G 2 OS=Mus musculus GN=Atp6v1g2 PE=1 SV=1	100.00%	7
DEMA_MOUSE	100.00%	19
A0A0H2UH17_MOUSE,Q812D4_MOUSE,Q8BJ53_MOUSE	95.90%	8
sp|Q61781|K1C14_MOUSEKeratin, type I cytoskeletal 14 OS=Mus musculus GN=Krt14 PE=1 SV=2	100.00%	35
sp|P68510|1433F_MOUSE14-3-3 protein eta OS=Mus musculus GN=Ywhah PE=1 SV=2	99.80%	4
sp|Q9Z1P6|NDUA7_MOUSENADH dehydrogenase [ubiquinone] 1 alpha subcomplex subunit 7 OS=Mus musculus GN=Ndufa7 PE=1 SV=3	100.00%	116
sp|P97450|ATP5J_MOUSEATP synthase-coupling factor 6, mitochondrial OS=Mus musculus GN=Atp5j PE=1 SV=1	100.00%	116
TERA_MOUSE	100.00%	3
sp|O09114|PTGDS_MOUSEProstaglandin-H2 D-isomerase OS=Mus musculus GN=Ptgds PE=1 SV=1	100.00%	8
PSB6_MOUSE	100.00%	34
F7D425_MOUSE	100.00%	33
C9K0Z8_MOUSE,HCN2_MOUSE	100.00%	2
Q6A090_MOUSE,sp|Q9Z0H8|CLIP2_MOUSECAP-Gly domain-containing linker protein 2 OS=Mus musculus GN=Clip2 PE=1 SV=2	100.00%	4
Q53YX2_MOUSE,THY1_MOUSE	100.00%	5
sp|P61957|SUMO2_MOUSESmall ubiquitin-related modifier 2 OS=Mus musculus GN=Sumo2 PE=1 SV=1	100.00%	69
Q3U422_MOUSE,Q3U4K3_MOUSE,Q91WP8_MOUSE	100.00%	23
A2AF33_MOUSE	100.00%	34
B1AWD9_MOUSE	100.00%	11
D3Z3A0_MOUSE,IPP2_MOUSE	100.00%	21
E9Q0F0_MOUSE	100.00%	10
HDGF_MOUSE	100.00%	9

AINX_MOUSE	100.00%	18
RT31_MOUSE	100.00%	2
NSG2_MOUSE,Q5SS02_MOUSE	100.00%	3
A0A0N4SUV3_MOUSE,D3YTU0_MOUSE,Q9CXX2_MOUSE,sp|Q62442|VAMP1_MOUSEVesicle-associated membrane protein 1 OS=Mus musculus GN=Vamp1 PE=1 SV=1	100.00%	10
Q3TYF2_MOUSE,Q543Y7_MOUSE,sp|Q61644|PACN1_MOUSEProtein kinase C and casein kinase substrate in neurons protein 1 OS=Mus musculus GN=Pacsin1 PE=1 SV=1	100.00%	5
A0A0A6YW88_MOUSE,sp|Q3UHL1|CAMKV_MOUSECaM kinase-like vesicle-associated protein OS=Mus musculus GN=Camkv PE=1 SV=2	100.00%	8
sp|Q9D8S9|BOLA1_MOUSEBolA-like protein 1 OS=Mus musculus GN=Bola1 PE=1 SV=1	100.00%	18
CALM_MOUSE,Q3UKW2_MOUSE	100.00%	14
RBP2_MOUSE	88.90%	16
MIF_MOUSE,Q545F0_MOUSE	100.00%	29
A0JLV3_MOUSE,B2RTK3_MOUSE,B2RVD5_MOUSE,Q8CBB6_MOUSE,Q921L4_MOUSE, sp|P10853|H2B1F_MOUSEHistone H2B type 1-F/J/L OS=Mus musculus GN=Hist1h2bf PE=1 SV=2,sp|P10854|H2B1M_MOUSEHistone H2B type 1-M OS=Mus musculus GN=Hist1h2bm PE=1 SV=2,sp|Q64478|H2B1H_MOUSEHistone H2B type 1-H OS=Mus musculus GN=Hist1h2bh PE=1 SV=3,sp|Q64524|H2B2E_MOUSEHistone H2B type 2-E OS=Mus musculus GN=Hist2h2be PE=1 SV=3,sp|Q64525|H2B2B_MOUSEHistone H2B type 2-B OS=Mus musculus GN=Hist2h2bb PE=1 SV=3,sp|Q6ZWY9|H2B1C_MOUSEHistone H2B type 1-C/E/G OS=Mus musculus GN=Hist1h2bc PE=1 SV=3,sp|Q8CGP0|H2B3B_MOUSEHistone H2B type 3-B OS=Mus musculus GN=Hist3h2bb PE=1 SV=3,sp|Q8CGP1|H2B1K_MOUSEHistone H2B type 1-K OS=Mus musculus GN=Hist1h2bk PE=1 SV=3,sp|Q8CGP2|H2B1P_MOUSEHistone H2B type 1-P OS=Mus musculus GN=Hist1h2bp PE=1 SV=3,sp|Q9D2U9|H2B3A_MOUSEHistone H2B type 3-A OS=Mus musculus GN=Hist3h2ba PE=1 SV=3	100.00%	5
AMPH_MOUSE	100.00%	2
Q3UAI4_MOUSE,Q3UBH2_MOUSE,Q3UJB0_MOUSE,Q80W39_MOUSE	100.00%	3

A3KML3_MOUSE,F6VW30_MOUSE,F6YY69_MOUSE,sp|P68254|1433T_MOUSE14-3-3 protein theta OS=Mus musculus GN=Ywhaq PE=1 SV=1	99.90%	7
D3YYZ2_MOUSE	100.00%	395
GLSK_MOUSE	100.00%	3
VIP_MOUSE	100.00%	2
F7D7A9_MOUSE	100.00%	16
EPN2_MOUSE,J3QNT7_MOUSE,Q5NCM5_MOUSE,Q5NCM6_MOUSE,Q5NCM7_MOUSE,Q69ZS5_MOUSE	100.00%	6
320707,325308,327798,339713,342196,344371,355946,355959,363275,365309,A2APX3_MOUSE,CYTC_MOUSE,Q3U5K7_MOUSE,Q9EPX9_MOUSE	100.00%	6
CYC_MOUSE,G3UWG1_MOUSE,Q56A15_MOUSE	100.00%	139
sp|Q91XV3|BASP1_MOUSEBrain acid soluble protein 1 OS=Mus musculus GN=Basp1 PE=1 SV=3	100.00%	192
Q8R3X4_MOUSE,sp|O35857|TIM44_MOUSEMitochondrial import inner membrane translocase subunit TIM44 OS=Mus musculus GN=Timm44 PE=1 SV=2	100.00%	5
Q3U7Z6_MOUSE,Q5NCI4_MOUSE,Q6NWV5_MOUSE,sp|O70250|PGAM2_MOUSEPhosphoglycerate mutase 2 OS=Mus musculus GN=Pgam2 PE=1 SV=3,sp|Q9DBJ1|PGAM1_MOUSEPhosphoglycerate mutase 1 OS=Mus musculus GN=Pgam1 PE=1 SV=3	100.00%	6
NFM_MOUSE	100.00%	19
sp|P52760|UK114_MOUSERibonuclease UK114 OS=Mus musculus GN=Hrsp12 PE=1 SV=3	100.00%	50
D3YZV2_MOUSE,E9QKI2_MOUSE	100.00%	4
D3YZD8_MOUSE,D3Z442_MOUSE,sp|Q8R0P4|AAMDC_MOUSEMth938 domain-containing protein OS=Mus musculus GN=Aamdc PE=1 SV=1	100.00%	10
Q9CVR0_MOUSE,sp|P68372|TBB4B_MOUSETubulin beta-4B chain OS=Mus musculus GN=Tubb4b PE=1 SV=1	100.00%	19
sp|Q9QWL7|K1C17_MOUSEKeratin, type I cytoskeletal 17 OS=Mus musculus GN=Krt17 PE=1 SV=3	100.00%	32

NEUM_MOUSE	100.00%	240
E9Q7S0_MOUSE,F7BQW7_MOUSE,sp|Q8CHC4|SYNJ1_MOUSESynaptojanin-1 OS=Mus musculus GN=Synj1 PE=1 SV=3	100.00%	16
691526,Q8C0W0_MOUSE	100.00%	53
B2RXL5_MOUSE,sp|Q78WH7|CK2N2_MOUSECalcium/calmodulin-dependent protein kinase II inhibitor 2 OS=Mus musculus GN=Camk2n2 PE=1 SV=1	99.90%	8
MRP_MOUSE	100.00%	33
PGP_MOUSE	100.00%	4
NPY_MOUSE	100.00%	32
Q9D6T9_MOUSE,RT36_MOUSE	100.00%	36
Q545F4_MOUSE,sp|P14602|HSPB1_MOUSEHeat shock protein beta-1 OS=Mus musculus GN=Hspb1 PE=1 SV=3	100.00%	4
sp|Q9CQ75|NDUA2_MOUSENADH dehydrogenase [ubiquinone] 1 alpha subcomplex subunit 2 OS=Mus musculus GN=Ndufa2 PE=1 SV=3	100.00%	3
D3Z5K8_MOUSE,D3Z5K9_MOUSE	100.00%	2
sp|Q59J78|MIMIT_MOUSEMimitin, mitochondrial OS=Mus musculus GN=Ndufaf2 PE=1 SV=1	100.00%	10
Q497I3_MOUSE,sp|Q05816|FABP5_MOUSEFatty acid-binding protein, epidermal OS=Mus musculus GN=Fabp5 PE=1 SV=3	100.00%	21
EPN4_MOUSE,Q3TJF5_MOUSE,Q3UPG6_MOUSE,Q5SUH6_MOUSE,Q5SUH7_MOUSE	100.00%	3
Q8C2K3_MOUSE	100.00%	605
MCH_MOUSE,Q80ZR6_MOUSE	100.00%	8
A0A0A6YY91_MOUSE	100.00%	42
D3YYE1_MOUSE,D3Z7M9_MOUSE,F6UFG6_MOUSE,sp|O35381|AN32A_MOUSEAcidic leucine-rich nuclear phosphoprotein 32 family member A OS=Mus musculus GN=Anp32a PE=1 SV=1	100.00%	7
Q08EK4_MOUSE,Q08EK5_MOUSE,sp|Q6IFZ6|K2C1B_MOUSEKeratin, type II cytoskeletal 1b OS=Mus musculus GN=Krt77 PE=1 SV=1	100.00%	13

TYB4_MOUSE	100.00%	113
CATB_MOUSE,Q3TVS6_MOUSE	100.00%	34
TRH_MOUSE	100.00%	16
PCLO_MOUSE	100.00%	6
Q3TIR0_MOUSE	5.80%	4
sp|Q9R0H5|K2C71_MOUSEKeratin, type II cytoskeletal 71 OS=Mus musculus GN=Krt71 PE=1 SV=1	100.00%	12
sp|Q9D727|CF226_MOUSEUncharacterized protein C6orf226 homolog OS=Mus musculus PE=1 SV=1	100.00%	4
Q5EBJ0_MOUSE,sp|P11404|FABPH_MOUSEFatty acid-binding protein, heart OS=Mus musculus GN=Fabp3 PE=1 SV=5	100.00%	12
COF1_MOUSE,F8WGL3_MOUSE,Q544Y7_MOUSE	100.00%	12
COA6_MOUSE	100.00%	9
sp|Q8C419|GP158_MOUSEProbable G-protein coupled receptor 158 OS=Mus musculus GN=Gpr158 PE=1 SV=2	100.00%	2
PRVA_MOUSE,Q545M7_MOUSE	100.00%	191
A2AEC2_MOUSE	99.80%	61
B2RSN3_MOUSE,sp|Q7TMM9|TBB2A_MOUSETubulin beta-2A chain OS=Mus musculus GN=Tubb2a PE=1 SV=1,sp|Q9CWF2|TBB2B_MOUSETubulin beta-2B chain OS=Mus musculus GN=Tubb2b PE=1 SV=1	100.00%	14
Q8CCS7_MOUSE	100.00%	3
Q3TEK2_MOUSE,Q3TF16_MOUSE,Q3TH56_MOUSE,Q3TQ13_MOUSE,Q3TRH3_MOUSE,Q3TZJ3_MOUSE,Q3U9L2_MOUSE,Q3UBA6_MOUSE,Q504P4_MOUSE,sp|P63017|HSP7C_MOUSEHeat shock cognate 71 kDa protein OS=Mus musculus GN=Hspa8 PE=1 SV=1	100.00%	7
A2A513_MOUSE,sp|P02535|K1C10_MOUSEKeratin, type I cytoskeletal 10 OS=Mus musculus GN=Krt10 PE=1 SV=3	100.00%	50
A2AA85_MOUSE,sp|Q6NXN1|SZRD1_MOUSESUZ domain-containing protein 1 OS=Mus musculus GN=Szrd1 PE=1 SV=1	100.00%	11

D3Z3F1_MOUSE,D3Z4V2_MOUSE,D3Z619_MOUSE,FIP1_MOUSE	100.00%	3
F6VME3_MOUSE	100.00%	26
ACBP_MOUSE,Q548W7_MOUSE	100.00%	336
A2ATI6_MOUSE,A2ATI9_MOUSE,Q3TG07_MOUSE,Q3TIK1_MOUSE,Q3TX06_MOUSE,Q3V458_MOUSE,sp|Q99JX3|GORS2_MOUSEGolgi reassembly-stacking protein 2 OS=Mus musculus GN=Gorasp2 PE=1 SV=3	100.00%	3
sp|Q9CPQ1|COX6C_MOUSECytochrome c oxidase subunit 6C OS=Mus musculus GN=Cox6c PE=1 SV=3	100.00%	6
E9QM38_MOUSE	100.00%	12
PPIA_MOUSE,Q3UAJ1_MOUSE,Q5SVY2_MOUSE	100.00%	121

Table 1. All proteins identified in the peptidomics experiment.

Identified Protein	Spectral Count
ProSAAS	96
Chromogranin B	72
Secretogranin-2	53
Pro-neuropeptide Y	32
Secretogranin-3	23
Proenkephalin-A	13
Pro-thyrotropin-releasing hormone	16
Cholecystokinin	9
Somatostatin	9
Protachykinin-1	8
Chromogranin-A	6
Pro-opiomelanocortin	3
Prothymosin alpha	3
VIP peptides	2

Table 2. Known neuropeptides or their precursors identified in the peptidomics experiment.

Sequence	Prob	Mascot Ion score	Mascot Identity score	Mascot Delta Ion Score	X! Tandem	Retention Time	TIC	Start	Stop
(R)sTLPPGNTR(E)	100%	23.33	51.21688	9	3.677781	954.262	3751070	11	19
(R)sTLPPGNTR(E)	100%	18.8	51.82865	5.16	3.853872	931.776	3011470	11	19
(R)sTLPPGNTR(E)	100%	23.23	51.21688	9.04	2.823909	976.649	3960360	11	19
(R)sTLPPGNTR(E)	100%	18.29	51.47157	8.08	2.39794	1,021.70	4191230	11	19
(R)sTLPPGNTR(E)	100%	20.71	51.21688	5.87	1.958607	999.38	3601380	11	19
(R)sTLPPGNTR(E)	97%	14.22	51.70115	1.77	1.568636	909.745	2100740	11	19
(R)wDYPEGTPSGGSSTLPSAPPPASAGLk(S)	100%	72.61	61.42182	60.14		3,080.42	5.16E+07	34	60
(R)wDYPEGTPSGGSSTLPSAPPPASAGLk(S)	100%	86.01	61.44331	80.14		3,102.32	9276140	34	60
(R)wDYPEGTPSGGSSTLPSAPPPASAGLk(S)	100%	33.45	61.41948	24.26		3,086.67	1.51E+07	34	60
(R)wDYPEGTPSGGSSTLPSAPPPASAGLk(S)	100%	34.41	61.44419	29.08		3,107.08	6640180	34	60
(K)sHPPPPEk(-)	100%	25.47	53.67378	19.48	1.148742	485.259	1.95E+08	61	68
(K)sHPPPPEk(-)	100%	21.42	53.67378	20.15	1	497.769	6.16E+07	61	68
(K)sHPPPPEk(-)	100%	28.68	53.64467	12.56	1.677781	501.231	6046330	61	68
(K)sHPPPPEk(-)	100%	20.83	53.70718	16.34	0.552842	613.344	519783	61	68
(K)sHPPPPEk(-)	100%	26.46	53.67378	18.15	2.113509	486.507	2.23E+07	61	68
(K)sHPPPPEk(-)	100%	18.64	53.70311	14.55	1.356547	637.989	387991	61	68
(K)sHPPPPEk(-)	99%	16.48	53.6895	16.48	0.537602	674.166	346576	61	68
(K)sHPPPPEk(-)	98%	24.19	53.64467	12.76		497.292	6.37E+07	61	68
(K)sHPPPPEk(-)	98%	23.84	53.70539	21.05		567.396	893007	61	68
(K)sHPPPPEk(-)	97%	21.7	53.64468	15.85		520.693	3597110	61	68

Table 3. All peptides detected from novel sORF, and PeptideProphet probability, Mascot, and X!Tandem score for each.

Bibliography

Altschul, S. F., Gish, W., Miller, W., Myers, E. W., & Lipman, D. J. (1990). Basic local alignment search tool. *J Mol Biol, 215*(3), 403-410. doi:10.1016/S0022-2836(05)80360-2

Anderson, D. M., Anderson, K. M., Chang, C. L., Makarewich, C. A., Nelson, B. R., McAnally, J. R., . . . Olson, E. N. (2015). A micropeptide encoded by a putative long noncoding RNA regulates muscle performance. *Cell, 160*(4), 595-606. doi:10.1016/j.cell.2015.01.009

Anderson, D. M., Makarewich, C. A., Anderson, K. M., Shelton, J. M., Bezprozvannaya, S., Bassel-Duby, R., & Olson, E. N. (2016). Widespread control of calcium signaling by a family of SERCA-inhibiting micropeptides. *Sci Signal, 9*(457), ra119. doi:10.1126/scisignal.aaj1460

Andreev, D. E., O'Connor, P. B., Fahey, C., Kenny, E. M., Terenin, I. M., Dmitriev, S. E., . . . Baranov, P. V. (2015). Translation of 5' leaders is pervasive in genes resistant to eIF2 repression. *Elife, 4*, e03971. doi:10.7554/eLife.03971

Andrews, S. J., & Rothnagel, J. A. (2014). Emerging evidence for functional peptides encoded by short open reading frames. *Nat Rev Genet, 15*(3), 193-204. doi:10.1038/nrg3520

Aspden, J. L., Eyre-Walker, Y. C., Phillips, R. J., Amin, U., Mumtaz, M. A., Brocard, M., & Couso, J. P. (2014). Extensive translation of small Open Reading Frames revealed by Poly-Ribo-Seq. *Elife, 3*, e03528. doi:10.7554/eLife.03528

Basrai, M. A., Hieter, P., & Boeke, J. D. (1997). Small open reading frames: beautiful needles in the haystack. *Genome Res, 7*(8), 768-771.

Baumgartner, D., Kopf, M., Klahn, S., Steglich, C., & Hess, W. R. (2016). Small proteins in cyanobacteria provide a paradigm for the functional analysis of the bacterial micro-proteome. *BMC Microbiol, 16*(1), 285. doi:10.1186/s12866-016-0896-z

Bazzini, A. A., Johnstone, T. G., Christiano, R., Mackowiak, S. D., Obermayer, B., Fleming, E. S., . . . Giraldez, A. J. (2014). Identification of small ORFs in vertebrates using ribosome footprinting and evolutionary conservation. *EMBO J, 33*(9), 981-993. doi:10.1002/embj.201488411

Bissette, G., Nemeroff, C. B., & MacKay, A. V. (1986). Neuropeptides and schizophrenia. *Prog Brain Res, 66*, 161-174.

Blankenberg, D., Taylor, J., Schenck, I., He, J., Zhang, Y., Ghent, M., . . . Nekrutenko, A. (2007). A framework for collaborative analysis of ENCODE data: making large-scale analyses biologist-friendly. *Genome Res, 17*(6), 960-964. doi:10.1101/gr.5578007

Brar, G. A., & Weissman, J. S. (2015). Ribosome profiling reveals the what, when, where and how of protein synthesis. *Nat Rev Mol Cell Biol, 16*(11), 651-664. doi:10.1038/nrm4069

Brar, G. A., Yassour, M., Friedman, N., Regev, A., Ingolia, N. T., & Weissman, J. S. (2012). High-resolution view of the yeast meiotic program revealed by ribosome profiling. *Science, 335*(6068), 552-557. doi:10.1126/science.1215110

Brown, S. D., & Hancock, J. M. (2006). The mouse genome. *Genome Dyn, 2*, 33-45. doi:10.1159/000095091

Buckenmaier, S., Vollmer, M., Trojer, L., & Emotte, C. (2008). Ultra-high capacity small molecule chips for the quantification of pharmaceuticals using triple-quadrupole mass spectrometry. *Agilent Technologies Application Note, 5989-7967EN*.

Burbach, J. P. (2011). What are neuropeptides? *Methods Mol Biol, 789*, 1-36. doi:10.1007/978-1-61779-310-3_1

Cabili, M. N., Dunagin, M. C., McClanahan, P. D., Biaesch, A., Padovan-Merhar, O., Regev, A., . . . Raj, A. (2015). Localization and abundance analysis of human lncRNAs at single-cell and single-molecule resolution. *Genome Biol, 16*, 20. doi:10.1186/s13059-015-0586-4

Caceda, R., Kinkead, B., & Nemeroff, C. B. (2007). Involvement of neuropeptide systems in schizophrenia: human studies. *Int Rev Neurobiol, 78*, 327-376. doi:10.1016/S0074-7742(06)78011-4

Calviello, L., Mukherjee, N., Wyler, E., Zauber, H., Hirsekorn, A., Selbach, M., . . . Ohler, U. (2016). Detecting actively translated open reading frames in ribosome profiling data. *Nat Methods, 13*(2), 165-170. doi:10.1038/nmeth.3688

Chattopadhyay, R., de la Vega, P., Paik, S. H., Murata, Y., Ferguson, E. W., Richie, T. L., & Ooi, G. T. (2011). Early transcriptional responses of HepG2-A16 liver cells to infection by Plasmodium falciparum sporozoites. *J Biol Chem, 286*(30), 26396-26405. doi:10.1074/jbc.M111.240879

Chew, G. L., Pauli, A., Rinn, J. L., Regev, A., Schier, A. F., & Valen, E. (2013). Ribosome profiling reveals resemblance between long non-coding RNAs and 5' leaders of coding RNAs. *Development, 140*(13), 2828-2834. doi:10.1242/dev.098343

Choi, H., Fermin, D., & Nesvizhskii, A. I. (2008). Significance analysis of spectral count data in label-free shotgun proteomics. *Mol Cell Proteomics, 7*(12), 2373-2385. doi:10.1074/mcp.M800203-MCP200

Civelli, O., Reinscheid, R. K., Zhang, Y., Wang, Z., Fredriksson, R., & Schioth, H. B. (2013). G protein-coupled receptor deorphanizations. *Annu Rev Pharmacol Toxicol, 53*, 127-146. doi:10.1146/annurev-pharmtox-010611-134548

Clements, J. E., Mankowski, J. L., Gama, L., & Zink, M. C. (2008). The accelerated simian immunodeficiency virus macaque model of human immunodeficiency

virus-associated neurological disease: from mechanism to treatment. *J Neurovirol, 14*(4), 309-317. doi:10.1080/13550280802132832

902188749 [pii]

Coleman, P. J., & Renger, J. J. (2010). Orexin receptor antagonists: a review of promising compounds patented since 2006. *Expert Opin Ther Pat, 20*(3), 307-324. doi:10.1517/13543770903567085

Couso, J. P. (2015). Finding smORFs: getting closer. *Genome Biol, 16*, 189. doi:10.1186/s13059-015-0765-3

Crappe, J., Van Criekinge, W., Trooskens, G., Hayakawa, E., Luyten, W., Baggerman, G., & Menschaert, G. (2013). Combining in silico prediction and ribosome profiling in a genome-wide search for novel putatively coding sORFs. *BMC Genomics, 14*, 648. doi:10.1186/1471-2164-14-648

Crowe, M. L., Wang, X. Q., & Rothnagel, J. A. (2006). Evidence for conservation and selection of upstream open reading frames suggests probable encoding of bioactive peptides. *BMC Genomics, 7*, 16. doi:10.1186/1471-2164-7-16

de Lecea, L., & Sutcliffe, J. G. (1999). The hypocretins/orexins: novel hypothalamic neuropeptides involved in different physiological systems. *Cell Mol Life Sci, 56*(5-6), 473-480.

Del Prete, G. Q., Haggarty, B., Leslie, G. J., Jordan, A. P., Romano, J., Wang, N., . . . Hoxie, J. A. (2009). Derivation and characterization of a simian immunodeficiency virus SIVmac239 variant with tropism for CXCR4. *J Virol, 83*(19), 9911-9922. doi:10.1128/JVI.00533-09

Deutsch, E. W., Csordas, A., Sun, Z., Jarnuczak, A., Perez-Riverol, Y., Ternent, T., . . . Vizcaino, J. A. (2017). The ProteomeXchange consortium in 2017: supporting the

cultural change in proteomics public data deposition. *Nucleic Acids Res, 45*(D1), D1100-D1106. doi:10.1093/nar/gkw936

DiMaio, D. (2014). Viral miniproteins. *Annu Rev Microbiol, 68*, 21-43. doi:10.1146/annurev-micro-091313-103727

Dinoso, J. B., Rabi, S. A., Blankson, J. N., Gama, L., Mankowski, J. L., Siliciano, R. F., . . . Clements, J. E. (2009). A simian immunodeficiency virus-infected macaque model to study viral reservoirs that persist during highly active antiretroviral therapy. *J Virol, 83*(18), 9247-9257. doi:10.1128/JVI.00840-09

JVI.00840-09 [pii]

Djebali, S., Davis, C. A., Merkel, A., Dobin, A., Lassmann, T., Mortazavi, A., . . . Gingeras, T. R. (2012). Landscape of transcription in human cells. *Nature, 489*(7414), 101-108. doi:10.1038/nature11233

Dujon, B., Alexandraki, D., Andre, B., Ansorge, W., Baladron, V., Ballesta, J. P., . . . Mewes, H. W. (1994). Complete DNA sequence of yeast chromosome XI. *Nature, 369*(6479), 371-378. doi:10.1038/369371a0

Dyson, H. J., & Wright, P. E. (2005). Intrinsically unstructured proteins and their functions. *Nat Rev Mol Cell Biol, 6*(3), 197-208. doi:10.1038/nrm1589

Eng, J. K., McCormack, A. L., & Yates, J. R. (1994). An approach to correlate tandem mass spectral data of peptides with amino acid sequences in a protein database. *J Am Soc Mass Spectrom, 5*(11), 976-989. doi:10.1016/1044-0305(94)80016-2

Fenyo, D., & Beavis, R. C. (2003). A method for assessing the statistical significance of mass spectrometry-based protein identifications using general scoring schemes. *Anal Chem, 75*(4), 768-774.

Flores, A., Saravia, R., Maldonado, R., & Berrendero, F. (2015). Orexins and fear: implications for the treatment of anxiety disorders. *Trends Neurosci, 38*(9), 550-559. doi:10.1016/j.tins.2015.06.005

Frith, M. C., Forrest, A. R., Nourbakhsh, E., Pang, K. C., Kai, C., Kawai, J., . . . Grimmond, S. M. (2006). The abundance of short proteins in the mammalian proteome. *PLoS Genet, 2*(4), e52. doi:10.1371/journal.pgen.0020052

Goebel, S. J., Johnson, G. P., Perkus, M. E., Davis, S. W., Winslow, J. P., & Paoletti, E. (1990). The complete DNA sequence of vaccinia virus. *Virology, 179*(1), 247-266, 517-263.

Grabherr, M. G., Haas, B. J., Yassour, M., Levin, J. Z., Thompson, D. A., Amit, I., . . . Regev, A. (2011). Full-length transcriptome assembly from RNA-Seq data without a reference genome. *Nat Biotechnol, 29*(7), 644-652. doi:10.1038/nbt.1883

Gruenbaum, Y., Wilson, K. L., Harel, A., Goldberg, M., & Cohen, M. (2000). Review: nuclear lamins--structural proteins with fundamental functions. *J Struct Biol, 129*(2-3), 313-323. doi:10.1006/jsbi.2000.4216

Guo, B., Zhai, D., Cabezas, E., Welsh, K., Nouraini, S., Satterthwait, A. C., & Reed, J. C. (2003). Humanin peptide suppresses apoptosis by interfering with Bax activation. *Nature, 423*(6938), 456-461. doi:10.1038/nature01627

Guttman, M., Russell, P., Ingolia, N. T., Weissman, J. S., & Lander, E. S. (2013). Ribosome profiling provides evidence that large noncoding RNAs do not encode proteins. *Cell, 154*(1), 240-251. doi:10.1016/j.cell.2013.06.009

Hackett, P. B., Petersen, R. B., Hensel, C. H., Albericio, F., Gunderson, S. I., Palmenberg, A. C., & Barany, G. (1986). Synthesis in vitro of a seven amino acid peptide encoded in the leader RNA of Rous sarcoma virus. *J Mol Biol, 190*(1), 45-57.

Hanyu-Nakamura, K., Sonobe-Nojima, H., Tanigawa, A., Lasko, P., & Nakamura, A. (2008). Drosophila Pgc protein inhibits P-TEFb recruitment to chromatin in primordial germ cells. *Nature, 451*(7179), 730-733. doi:10.1038/nature06498

Hart, R. P., & Goff, L. A. (2016). Long noncoding RNAs: Central to nervous system development. *Int J Dev Neurosci, 55*, 109-116. doi:10.1016/j.ijdevneu.2016.06.001

Hashimoto, Y., Niikura, T., Tajima, H., Yasukawa, T., Sudo, H., Ito, Y., . . . Nishimoto, I. (2001). A rescue factor abolishing neuronal cell death by a wide spectrum of familial Alzheimer's disease genes and Abeta. *Proc Natl Acad Sci U S A, 98*(11), 6336-6341. doi:10.1073/pnas.101133498

Hemm, M. R., Paul, B. J., Miranda-Rios, J., Zhang, A., Soltanzad, N., & Storz, G. (2010). Small stress response proteins in Escherichia coli: proteins missed by classical proteomic studies. *J Bacteriol, 192*(1), 46-58. doi:10.1128/JB.00872-09

Hemm, M. R., Paul, B. J., Schneider, T. D., Storz, G., & Rudd, K. E. (2008). Small membrane proteins found by comparative genomics and ribosome binding site models. *Mol Microbiol, 70*(6), 1487-1501. doi:10.1111/j.1365-2958.2008.06495.x

Hinnebusch, A. G. (2014). The scanning mechanism of eukaryotic translation initiation. *Annu Rev Biochem, 83*, 779-812. doi:10.1146/annurev-biochem-060713-035802

Hori, A., Honda, S., Asada, M., Ohtaki, T., Oda, K., Watanabe, T., . . . Fujino, M. (2001). Metastin suppresses the motility and growth of CHO cells transfected with its receptor. *Biochem Biophys Res Commun, 286*(5), 958-963. doi:10.1006/bbrc.2001.5470

Hornstein, N., Torres, D., Das Sharma, S., Tang, G., Canoll, P., & Sims, P. A. (2016). Ligation-free ribosome profiling of cell type-specific translation in the brain. *Genome Biol, 17*(1), 149. doi:10.1186/s13059-016-1005-1

Hosokawa, Y., Suzuki, H., Toda, H., Nishikimi, M., & Ozawa, T. (1989). Complementary DNA encoding core protein II of human mitochondrial cytochrome bc1 complex. Substantial diversity in deduced primary structure from its yeast counterpart. *J Biol Chem, 264*(23), 13483-13488.

Hughes, A. L., Becker, E. A., Lauck, M., Karl, J. A., Braasch, A. T., O'Connor, D. H., & O'Connor, S. L. (2012). SIV genome-wide pyrosequencing provides a comprehensive and unbiased view of variation within and outside CD8 T lymphocyte epitopes. *PLoS One, 7*(10), e47818. doi:10.1371/journal.pone.0047818

Ingolia, N. T. (2014). Ribosome profiling: new views of translation, from single codons to genome scale. *Nat Rev Genet, 15*(3), 205-213. doi:10.1038/nrg3645

Ingolia, N. T., Brar, G. A., Rouskin, S., McGeachy, A. M., & Weissman, J. S. (2012). The ribosome profiling strategy for monitoring translation in vivo by deep sequencing of ribosome-protected mRNA fragments. *Nat Protoc, 7*(8), 1534-1550. doi:10.1038/nprot.2012.086

Ingolia, N. T., Brar, G. A., Stern-Ginossar, N., Harris, M. S., Talhouarne, G. J., Jackson, S. E., . . . Weissman, J. S. (2014). Ribosome profiling reveals pervasive translation outside of annotated protein-coding genes. *Cell Rep, 8*(5), 1365-1379. doi:10.1016/j.celrep.2014.07.045

Ingolia, N. T., Ghaemmaghami, S., Newman, J. R., & Weissman, J. S. (2009). Genome-wide analysis in vivo of translation with nucleotide resolution using ribosome profiling. *Science, 324*(5924), 218-223. doi:10.1126/science.1168978

Ingolia, N. T., Lareau, L. F., & Weissman, J. S. (2011). Ribosome profiling of mouse embryonic stem cells reveals the complexity and dynamics of mammalian proteomes. *Cell, 147*(4), 789-802. doi:10.1016/j.cell.2011.10.002

Ishida, N., Yoshioka, S., Chiba, Y., Takeuchi, M., & Kawakita, M. (1999). Molecular cloning and functional expression of the human Golgi UDP-N-acetylglucosamine transporter. *J Biochem, 126*(1), 68-77.

Ishimura, R., Nagy, G., Dotu, I., Zhou, H., Yang, X. L., Schimmel, P., . . . Ackerman, S. L. (2014). RNA function. Ribosome stalling induced by mutation of a CNS-specific tRNA causes neurodegeneration. *Science, 345*(6195), 455-459. doi:10.1126/science.1249749

Kageyama, Y., Kondo, T., & Hashimoto, Y. (2011). Coding vs non-coding: Translatability of short ORFs found in putative non-coding transcripts. *Biochimie, 93*(11), 1981-1986. doi:10.1016/j.biochi.2011.06.024

Kastenmayer, J. P., Ni, L., Chu, A., Kitchen, L. E., Au, W. C., Yang, H., . . . Basrai, M. A. (2006). Functional genomics of genes with small open reading frames (sORFs) in S. cerevisiae. *Genome Res, 16*(3), 365-373. doi:10.1101/gr.4355406

Keller, A., Nesvizhskii, A. I., Kolker, E., & Aebersold, R. (2002). Empirical statistical model to estimate the accuracy of peptide identifications made by MS/MS and database search. *Anal Chem, 74*(20), 5383-5392.

Kislinger, T., Gramolini, A. O., MacLennan, D. H., & Emili, A. (2005). Multidimensional protein identification technology (MudPIT): technical overview of a profiling method optimized for the comprehensive proteomic investigation of normal and diseased heart tissue. *J Am Soc Mass Spectrom, 16*(8), 1207-1220. doi:10.1016/j.jasms.2005.02.015

Kojima, M., Hosoda, H., Date, Y., Nakazato, M., Matsuo, H., & Kangawa, K. (1999). Ghrelin is a growth-hormone-releasing acylated peptide from stomach. *Nature, 402*(6762), 656-660. doi:10.1038/45230

Kondo, T., Plaza, S., Zanet, J., Benrabah, E., Valenti, P., Hashimoto, Y., . . . Kageyama, Y. (2010). Small peptides switch the transcriptional activity of Shavenbaby during

Drosophila embryogenesis. *Science, 329*(5989), 336-339. doi:10.1126/science.1188158

Koskinen, V. R., Emery, P. A., Creasy, D. M., & Cottrell, J. S. (2011). Hierarchical clustering of shotgun proteomics data. *Mol Cell Proteomics, 10*(6), M110 003822. doi:10.1074/mcp.M110.003822

Lambert, D. G. (2008). The nociceptin/orphanin FQ receptor: a target with broad therapeutic potential. *Nat Rev Drug Discov, 7*(8), 694-710. doi:10.1038/nrd2572

Lee, C., Zeng, J., Drew, B. G., Sallam, T., Martin-Montalvo, A., Wan, J., . . . Cohen, P. (2015). The mitochondrial-derived peptide MOTS-c promotes metabolic homeostasis and reduces obesity and insulin resistance. *Cell Metab, 21*(3), 443-454. doi:10.1016/j.cmet.2015.02.009

Lee, S., Liu, B., Lee, S., Huang, S. X., Shen, B., & Qian, S. B. (2012). Global mapping of translation initiation sites in mammalian cells at single-nucleotide resolution. *Proc Natl Acad Sci U S A, 109*(37), E2424-2432. doi:10.1073/pnas.1207846109

Lluch-Senar, M., Delgado, J., Chen, W. H., Llorens-Rico, V., O'Reilly, F. J., Wodke, J. A., . . . Serrano, L. (2015). Defining a minimal cell: essentiality of small ORFs and ncRNAs in a genome-reduced bacterium. *Mol Syst Biol, 11*(1), 780. doi:10.15252/msb.20145558

Ma, K., Vitek, O., & Nesvizhskii, A. I. (2012). A statistical model-building perspective to identification of MS/MS spectra with PeptideProphet. *BMC Bioinformatics, 13 Suppl 16*, S1. doi:10.1186/1471-2105-13-S16-S1

Mackowiak, S. D., Zauber, H., Bielow, C., Thiel, D., Kutz, K., Calviello, L., . . . Obermayer, B. (2015). Extensive identification and analysis of conserved small ORFs in animals. *Genome Biol, 16*, 179. doi:10.1186/s13059-015-0742-x

Magny, E. G., Pueyo, J. I., Pearl, F. M., Cespedes, M. A., Niven, J. E., Bishop, S. A., & Couso, J. P. (2013). Conserved regulation of cardiac calcium uptake by peptides

encoded in small open reading frames. *Science, 341*(6150), 1116-1120. doi:10.1126/science.1238802

Mankowski, J. L., Clements, J. E., & Zink, M. C. (2002). Searching for clues: tracking the pathogenesis of human immunodeficiency virus central nervous system disease by use of an accelerated, consistent simian immunodeficiency virus macaque model. *J Infect Dis, 186 Suppl 2*, S199-208. doi:10.1086/344938

Marino-Ramirez, L., Kann, M. G., Shoemaker, B. A., & Landsman, D. (2005). Histone structure and nucleosome stability. *Expert Rev Proteomics, 2*(5), 719-729. doi:10.1586/14789450.2.5.719

Mebius, R. E., & Kraal, G. (2005). Structure and function of the spleen. *Nat Rev Immunol, 5*(8), 606-616. doi:nri1669 [pii]

10.1038/nri1669

Mersch-Sundermann, V., Knasmuller, S., Wu, X. J., Darroudi, F., & Kassie, F. (2004). Use of a human-derived liver cell line for the detection of cytoprotective, antigenotoxic and cogenotoxic agents. *Toxicology, 198*(1-3), 329-340. doi:10.1016/j.tox.2004.02.009

Meunier, J. C., Mollereau, C., Toll, L., Suaudeau, C., Moisand, C., Alvinerie, P., . . . et al. (1995). Isolation and structure of the endogenous agonist of opioid receptor-like ORL1 receptor. *Nature, 377*(6549), 532-535. doi:10.1038/377532a0

Milne, S. B., Mathews, T. P., Myers, D. S., Ivanova, P. T., & Brown, H. A. (2013). Sum of the parts: mass spectrometry-based metabolomics. *Biochemistry, 52*(22), 3829-3840. doi:10.1021/bi400060e

Nathoo, A. N., Moeller, R. A., Westlund, B. A., & Hart, A. C. (2001). Identification of neuropeptide-like protein gene families in Caenorhabditiselegans and other

species. *Proc Natl Acad Sci U S A, 98*(24), 14000-14005. doi:10.1073/pnas.241231298

Neckelmann, N., Warner, C. K., Chung, A., Kudoh, J., Minoshima, S., Fukuyama, R., . . . et al. (1989). The human ATP synthase beta subunit gene: sequence analysis, chromosome assignment, and differential expression. *Genomics, 5*(4), 829-843.

Nelson, B. R., Makarewich, C. A., Anderson, D. M., Winders, B. R., Troupes, C. D., Wu, F., . . . Olson, E. N. (2016). A peptide encoded by a transcript annotated as long noncoding RNA enhances SERCA activity in muscle. *Science, 351*(6270), 271-275. doi:10.1126/science.aad4076

Nelson, L. S., Rosoff, M. L., & Li, C. (1998). Disruption of a neuropeptide gene, flp-1, causes multiple behavioral defects in Caenorhabditis elegans. *Science, 281*(5383), 1686-1690.

Nesvizhskii, A. I. (2014). Proteogenomics: concepts, applications and computational strategies. *Nat Methods, 11*(11), 1114-1125. doi:10.1038/nmeth.3144

Nesvizhskii, A. I., Keller, A., Kolker, E., & Aebersold, R. (2003). A statistical model for identifying proteins by tandem mass spectrometry. *Anal Chem, 75*(17), 4646-4658.

Nunez, A., Rodrigo-Angulo, M. L., Andres, I. D., & Garzon, M. (2009). Hypocretin/Orexin neuropeptides: participation in the control of sleep-wakefulness cycle and energy homeostasis. *Curr Neuropharmacol, 7*(1), 50-59. doi:10.2174/157015909787602797

Oliver, S. G., Winson, M. K., Kell, D. B., & Baganz, F. (1998). Systematic functional analysis of the yeast genome. *Trends Biotechnol, 16*(9), 373-378. doi:S0167-7799(98)01214-1 [pii]

Olsen, J. V., Ong, S. E., & Mann, M. (2004). Trypsin cleaves exclusively C-terminal to arginine and lysine residues. *Mol Cell Proteomics, 3*(6), 608-614. doi:10.1074/mcp.T400003-MCP200

Ott, D. E., Nigida, S. M., Jr., Henderson, L. E., & Arthur, L. O. (1995). The majority of cells are superinfected in a cloned cell line that produces high levels of human immunodeficiency virus type 1 strain MN. *J Virol, 69*(4), 2443-2450.

Patel, K. V., Aspesi, A. V., & Evoy, K. E. (2015). Suvorexant: a dual orexin receptor antagonist for the treatment of sleep onset and sleep maintenance insomnia. *Ann Pharmacother, 49*(4), 477-483. doi:10.1177/1060028015570467

Patti, G. J., Yanes, O., & Siuzdak, G. (2012). Innovation: Metabolomics: the apogee of the omics trilogy. *Nat Rev Mol Cell Biol, 13*(4), 263-269. doi:10.1038/nrm3314

Pauli, A., Norris, M. L., Valen, E., Chew, G. L., Gagnon, J. A., Zimmerman, S., . . . Schier, A. F. (2014). Toddler: an embryonic signal that promotes cell movement via Apelin receptors. *Science, 343*(6172), 1248636. doi:10.1126/science.1248636

Pauli, A., Valen, E., Lin, M. F., Garber, M., Vastenhouw, N. L., Levin, J. Z., . . . Schier, A. F. (2012). Systematic identification of long noncoding RNAs expressed during zebrafish embryogenesis. *Genome Res, 22*(3), 577-591. doi:10.1101/gr.133009.111

Peabody, D. S. (1989). Translation initiation at non-AUG triplets in mammalian cells. *J Biol Chem, 264*(9), 5031-5035.

Perkins, D. N., Pappin, D. J., Creasy, D. M., & Cottrell, J. S. (1999). Probability-based protein identification by searching sequence databases using mass spectrometry data. *Electrophoresis, 20*(18), 3551-3567. doi:10.1002/(SICI)1522-2683(19991201)20:18<3551::AID-ELPS3551>3.0.CO;2-2

Ratner, L., Haseltine, W., Patarca, R., Livak, K. J., Starcich, B., Josephs, S. F., . . . et al. (1985). Complete nucleotide sequence of the AIDS virus, HTLV-III. *Nature, 313*(6000), 277-284.

Rice, P., Longden, I., & Bleasby, A. (2000). EMBOSS: the European Molecular Biology Open Software Suite. *Trends Genet, 16*(6), 276-277.

Romanova, E. V., & Sweedler, J. V. (2015). Peptidomics for the discovery and characterization of neuropeptides and hormones. *Trends Pharmacol Sci, 36*(9), 579-586. doi:10.1016/j.tips.2015.05.009

Ropers, F., Derivery, E., Hu, H., Garshasbi, M., Karbasiyan, M., Herold, M., . . . Rajab, A. (2011). Identification of a novel candidate gene for non-syndromic autosomal recessive intellectual disability: the WASH complex member SWIP. *Hum Mol Genet, 20*(13), 2585-2590. doi:10.1093/hmg/ddr158

Rossio, J. L., Esser, M. T., Suryanarayana, K., Schneider, D. K., Bess, J. W., Jr., Vasquez, G. M., . . . Lifson, J. D. (1998). Inactivation of human immunodeficiency virus type 1 infectivity with preservation of conformational and functional integrity of virion surface proteins. *J Virol, 72*(10), 7992-8001.

Sakurai, T., Amemiya, A., Ishii, M., Matsuzaki, I., Chemelli, R. M., Tanaka, H., . . . Yanagisawa, M. (1998). Orexins and orexin receptors: a family of hypothalamic neuropeptides and G protein-coupled receptors that regulate feeding behavior. *Cell, 92*(4), 573-585.

Sakurai, T., Amemiya, A., Ishii, M., Matsuzaki, I., Chemelli, R. M., Tanaka, H., . . . Yanagisawa, M. (1998). Orexins and orexin receptors: a family of hypothalamic neuropeptides and G protein-coupled receptors that regulate feeding behavior. *Cell, 92*(5), 1 page following 696.

Salter, R. D., Howell, D. N., & Cresswell, P. (1985). Genes regulating HLA class I antigen expression in T-B lymphoblast hybrids. *Immunogenetics, 21*(3), 235-246.

Samarakoon, S. R., Thabrew, I., Galhena, P. B., & Tennekoon, K. H. (2012). Modulation of apoptosis in human hepatocellular carcinoma (HepG2 cells) by a standardized herbal decoction of Nigella sativa seeds, Hemidesmus indicus roots and Smilax glabra rhizomes with anti- hepatocarcinogenic effects. *BMC Complement Altern Med, 12*, 25. doi:10.1186/1472-6882-12-25

Sana, T., & Fischer, S. (2007). Maximizing Metabolite Extraction for Comprehensive Metabolomics Studies of Erythrocytes. *Agilent Technologies Application Note, 5989-7407EN*.

Schulz-Knappe, P., Schrader, M., & Zucht, H. D. (2005). The peptidomics concept. *Comb Chem High Throughput Screen, 8*(8), 697-704.

Sharma, K., Schmitt, S., Bergner, C. G., Tyanova, S., Kannaiyan, N., Manrique-Hoyos, N., . . . Simons, M. (2015). Cell type- and brain region-resolved mouse brain proteome. *Nat Neurosci, 18*(12), 1819-1831. doi:10.1038/nn.4160

Slavoff, S. A., Heo, J., Budnik, B. A., Hanakahi, L. A., & Saghatelian, A. (2014). A human short open reading frame (sORF)-encoded polypeptide that stimulates DNA end joining. *J Biol Chem, 289*(16), 10950-10957. doi:10.1074/jbc.C113.533968

Starck, S. R., Tsai, J. C., Chen, K., Shodiya, M., Wang, L., Yahiro, K., . . . Walter, P. (2016). Translation from the 5' untranslated region shapes the integrated stress response. *Science, 351*(6272), aad3867. doi:10.1126/science.aad3867

Stern-Ginossar, N., Weisburd, B., Michalski, A., Le, V. T., Hein, M. Y., Huang, S. X., . . . Weissman, J. S. (2012). Decoding human cytomegalovirus. *Science, 338*(6110), 1088-1093. doi:10.1126/science.1227919

Sun, L., Goff, L. A., Trapnell, C., Alexander, R., Lo, K. A., Hacisuleyman, E., . . . Rinn, J. L. (2013). Long noncoding RNAs regulate adipogenesis. *Proc Natl Acad Sci U S A, 110*(9), 3387-3392. doi:10.1073/pnas.1222643110

Svensson, M., Boren, M., Skold, K., Falth, M., Sjogren, B., Andersson, M., . . . Andren, P. E. (2009). Heat stabilization of the tissue proteome: a new technology for improved proteomics. *J Proteome Res, 8*(2), 974-981. doi:10.1021/pr8006446

Tao, D., King, J. G., Tweedell, R. E., Jost, P. J., Boddey, J. A., & Dinglasan, R. R. (2014). The acute transcriptomic and proteomic response of HC-04 hepatoma cells to Hepatocyte Growth Factor and its implications for Plasmodium falciparum sporozoite invasion. *Mol Cell Proteomics*. doi:M113.035584 [pii]

Tatemoto, K., Hosoya, M., Habata, Y., Fujii, R., Kakegawa, T., Zou, M. X., . . . Fujino, M. (1998). Isolation and characterization of a novel endogenous peptide ligand for the human APJ receptor. *Biochem Biophys Res Commun, 251*(2), 471-476. doi:10.1006/bbrc.1998.9489

Tautenhahn, R., Cho, K., Uritboonthai, W., Zhu, Z., Patti, G. J., & Siuzdak, G. (2012). An accelerated workflow for untargeted metabolomics using the METLIN database. *Nat Biotechnol, 30*(9), 826-828. doi:10.1038/nbt.2348

Tharakan, R., Edwards, N., & Graham, D. R. (2010). Data maximization by multipass analysis of protein mass spectra. *Proteomics, 10*(6), 1160-1171. doi:10.1002/pmic.200900433

Tharakan, R., Tao, D., Ubaida-Mohien, C., Dinglasan, R. R., & Graham, D. R. (2015). Integrated microfluidic chip and online SCX separation allows untargeted nanoscale metabolomic and peptidomic profiling. *J Proteome Res, 14*(3), 1621-1626. doi:10.1021/pr5011422

The UniProt, C. (2017). UniProt: the universal protein knowledgebase. *Nucleic Acids Res, 45*(D1), D158-D169. doi:10.1093/nar/gkw1099

Ubaida Mohien, C., Hartler, J., Breitwieser, F., Rix, U., Remsing Rix, L., Winter, G. E., . . . Colinge, J. (2010). MASPECTRAS 2: An integration and analysis platform for proteomic data. *Proteomics, 10*(14), 2719-2722. doi:10.1002/pmic.201000075

Ulitsky, I., & Bartel, D. P. (2013). lincRNAs: genomics, evolution, and mechanisms. *Cell, 154*(1), 26-46. doi:10.1016/j.cell.2013.06.020

Vanderperre, B., Lucier, J. F., Bissonnette, C., Motard, J., Tremblay, G., Vanderperre, S., . . . Roucou, X. (2013). Direct detection of alternative open reading frames translation products in human significantly expands the proteome. *PLoS One, 8*(8), e70698. doi:10.1371/journal.pone.0070698

Wandinger, S. K., Richter, K., & Buchner, J. (2008). The Hsp90 chaperone machinery. *J Biol Chem, 283*(27), 18473-18477. doi:10.1074/jbc.R800007200

Wild, C. P. (2012). The exposome: from concept to utility. *Int J Epidemiol, 41*(1), 24-32. doi:10.1093/ije/dyr236

Wright, P. E., & Dyson, H. J. (2015). Intrinsically disordered proteins in cellular signalling and regulation. *Nat Rev Mol Cell Biol, 16*(1), 18-29. doi:10.1038/nrm3920

Yang, P., Maguire, J. J., & Davenport, A. P. (2015). Apelin, Elabela/Toddler, and biased agonists as novel therapeutic agents in the cardiovascular system. *Trends Pharmacol Sci, 36*(9), 560-567. doi:10.1016/j.tips.2015.06.002

Yang, P., Read, C., Kuc, R. E., Buonincontri, G., Southwood, M., Torella, R., . . . Davenport, A. P. (2017). Elabela/Toddler is an Endogenous Agonist of the Apelin APJ Receptor in the Adult Cardiovascular System, and Exogenous Administration of the Peptide Compensates for the Downregulation of its Expression in Pulmonary Arterial Hypertension. *Circulation*. doi:10.1161/CIRCULATIONAHA.116.023218

Zanet, J., Benrabah, E., Li, T., Pelissier-Monier, A., Chanut-Delalande, H., Ronsin, B., . . . Plaza, S. (2015). Pri sORF peptides induce selective proteasome-mediated protein processing. *Science, 349*(6254), 1356-1358. doi:10.1126/science.aac5677

Zanet, J., Chanut-Delalande, H., Plaza, S., & Payre, F. (2016). Small Peptides as Newcomers in the Control of Drosophila Development. *Curr Top Dev Biol, 117*, 199-219. doi:10.1016/bs.ctdb.2015.11.004

Zhang, Y., Buchberger, A., Muthuvel, G., & Li, L. (2015). Expression and distribution of neuropeptides in the nervous system of the crab Carcinus maenas and their roles in environmental stress. *Proteomics*. doi:10.1002/pmic.201500256

Zhang, Y., Wang, Z., Parks, G. S., & Civelli, O. (2011). Novel neuropeptides as ligands of orphan G protein-coupled receptors. *Curr Pharm Des, 17*(25), 2626-2631.

Ravi Tharakan Curriculum Vitae

Home Address: 3925 Beech Ave #415, Baltimore, MD 21211
Office Address: Meyer 4-157, 600 N. Wolfe Street, Baltimore, MD 21205
Date of Birth: 1/1/1984, Arlington, VA

EDUCATION

JOHNS HOPKINS UNIVERSITY — Baltimore, MD
PhD, Cellular and Molecular Medicine — *May 2017*
- Dissertation supervised by Dr. Akira Sawa, Department of Psychiatry
- Focus: Proteogenomics Approaches to Micropeptide Discovery

WESTERN MICHIGAN UNIVERSITY — Kalamazoo, MI
Master of Arts, Philosophy — *May 2011*
- GPA: 3.95

JOHNS HOPKINS UNIVERSITY — Baltimore, MD
Bachelor of Arts, Philosophy — *May 2007*
- GPA in major: 3.81/4.0

Bachelor of Sciences, Biomedical Engineering — *May 2007*
- Concentration: Computer Science

RESEARCH EXPERIENCE

JOHNS HOPKINS MEDICAL INSTITUTIONS
Baltimore, MD

PhD Candidate, Sawa Lab, Psychiatry, *March 2015-Present*
- Discovery of sORF-encoded micropeptides by proteomics and ribosome profiling.

PhD Candidate, Graham Lab, Molecular and Comparative Pathobiology, *May 2012-March 2015*
- Peptidomic, metabolomic and lipidomic profiling of innate immune response to acute HIV infection in an SIV macaque model.

Rotation Student, Huganir Lab, Neuroscience, *March 2012-May 2012*
- Interactome of C-terminal 3Y peptide of AMPA receptor.

Rotation Student, Sawa Lab, Psychiatry, *Jan 2012-March 2012*
- Direct conversion of adult human fibroblasts to neurons.

Rotation Student, Zink Lab, Molecular and Comparative Pathobiology, *Sept 2012-Dec 2012*
- Mechanism of immunomodulation of minocycline by lipid raft localization in T cell lines.

Bioinformatician, Johns Hopkins NHLBI Proteomics Center, *May 2007-September 2009*
- Data analysis of mass spectrometric proteomics data.

PUBLICATIONS (*INDICATES JOINT PRIMARY):

1. **Ravi Tharakan***, Lennart Martens*, Jennifer Van Eyk, David Graham. *OMSSAGUI: an open-source user interface component to configure and run the OMSSA search engine.* Proteomics. 2008 Jun; 8(12):2376-8.

2. **Ravi Tharakan,** Nathan Edwards, David Graham. *Data maximization by multipass analysis of protein mass spectra.* Proteomics. 2010 Jan; 10(6):1160-1171. (Cited 30 times.)
3. Jürgen Hartler, Harald C Köfeler, Christopher JO Baker, **Ravi Tharakan**, Gerhard G Thallinger. "Lipidomics, Mass Spectrometry and Bioinformatics." In Zlatko Trajanoski, ed., *Computational Medicine.* Springler-Verlag, 2012.
4. Jürgen Hartler, **Ravi Tharakan**, Harald C Köfeler, David R Graham, Gerhard G Thallinger. *Bioinformatics tools and challenges in structural analysis of lipidomics MS/MS data.* Briefings in Bioinformatics. 2013 May; 14(3):375-90.
5. **Ravi Tharakan**, Dingyin Tao, Ceereena Ubaida-Mohien, Rhoel Dinglasan, David Graham. *Integrated Microfluidic Chip and Online SCX Separation Allows Untargeted Nanoscale Metabolomic and Peptidomic Profiling*. Journal of Proteome Research. 2015 Mar; 14(3):1621-6.
6. Ceereena Ubaida-Mohien, Ben Lamberty, Alex Dickens, Michelle Mielke, Thomas Marcotte, Ned Sacktor, Igor Grant, Scott Letendre, Pavel Ciborowski, Hui Pan, **Ravi Tharakan**, Justin McArthur, Howard Fox, Norman Haughey. *Informatic Interrogation of CSF Proteomic Profiles from HIV-infected Subjects Implicates Acute Phase and Complement Systems in Shifting Cognitive Status.* AIDS. Under revision.
7. Ubaida-Mohien CM, **Tharakan R.** *Informatics and Systems Biology as applied to HIV-1.* Review. In process.

PROFESSIONAL ACTIVITY AND AWARDS:

Honors:

- **Young Investigator's Award**, 12th Annual International Society for Neurovirology Symposium, Nov 2nd, 2013.
- **AAAS/Science Program for Excellence in Science**, 2013-15. Sponsored by Dr. Rajini Rao.
- **Abstract Invitation,** Keystone Symposia, "HIV Pathogenesis – Virus vs. Host," 2014.

Reviewer:

- Invited by Editor Joshua Sheetz, *Yale Journal of Biology and Medicine*, 2017.
- Invited by Editor Royston Goodacre, *Metabolomics*, 2016.
- *Ad hoc* peer review for 6 manuscripts with David Graham, *Proteomics*.
- Invited by Editor Lennart Martens, *Proteomics*, 2009.
- *Ad hoc* peer review with David Graham, Wellcome Trust Grant Application, 2008.

Selected Presentations:

- Oral Presentation: "Discovering Novel Neuropeptide Genes in the Human Genome." Cellular and Molecular Medicine Program Retreat, Baltimore, MD, Sept 15th, 2016.
- Poster Presentation: "Proteomics of HIV-1 Viral Isoforms: Studying Viral Protein Evolution
  by Mass Spectrometry." 62nd Annual American Society for Mass Spectrometry, Baltimore, MD, June 14th-19th, 2014.

- Poster Presentation: “Multiomic Profiling of Peripheral Immune Response in an SIV Macaque Model of HIV-Associated Neurological Disease.” 12th Annual International Society for Neurovirology, Washington, DC, Oct 12th–Nov 2nd, 2013.
- Poster Presentation: Cellular and Molecular Medicine Program Retreat, Baltimore, MD, Sept 12th, 2013.
- Oral Presentation: “Investigating Minocycline's Mechanism of Immunomodulation.” Cellular and Molecular Medicine Program Rotation Presentations, Baltimore, MD, Dec 9th, 2011.
- Poster Presentation: “When every spectrum counts: An integrated grid and cloud enabled software pipeline for identification of elusive proteins.” 59th Annual American Society for Mass Spectrometry, Denver, CO, June 5th-9th 2011.
- Oral Presentation: Van Eyk Lab Retreat, “Redundancy Removal by Homology Graph Clustering.” Baltimore, MD, May 9, 2008.

Professional Activity:

- Attended Conference: 63rd Annual American Society for Mass Spectrometry, St. Louis, MO, June 1st-5th, 2015.
- Attended Course: “Case Studies in Quantitative Proteome Bioinformatics,” American Society for Mass Spectrometry, St. Louis, MO, May 29th-30th, 2015.
- Attended Course: “Stable and Transient Protein-Protein Interactions: Discovery, Quantification and Validation,” American Society for Mass Spectrometry, St. Louis, MO, June 14th-15th, 2014.
- Attended Training Course: Society of Nuclear Medicine, In Vivo Preclinical Imaging: Introductory Workshop. Johns Hopkins University, March 20-21, 2012.
- **Co-organizer (Submissions and Program Coordinator),** 4th Annual Western Michigan Graduate Philosophy Conference, Kalamazoo, MI, Dec 3rd-5th 2010.
- Attended Conference: 3rd Conference on Integrated History and Philosophy of Science, Indiana University, Bloomington, IN, Sept 23rd-26th, 2010.
- **Visiting Scientist**: Institute for Genomics and Bioinformatics of the Technical University of Graz, Graz, Austria, March-August 2009.
- Attended Course: “Proteomics Informatics,” Institute for Systems Biology, Seattle, WA, Nov 1st-8th, 2008.

Teaching Experience:

- **Instructor**, Biomedical Ethics; designed and taught course: Western Michigan University, Spring Semester, 2010.
- **Instructor**, Critical Reasoning (Introductory Logic Course); designed and taught course: Western Michigan University, Summer Sessions 1 and 2, Fall Semester, 2010.
- **Teaching Assistant**, Introduction to Ethics, Spring Semester 2010, and Critical Reasoning (Introductory Logic Course), Western Michigan University, Fall Semester 2010.